Summer 2022

Synthesis and process optimization of colloidal unimolecular polymer, cup, particle formation, and its interfacial surface tension behavior

Ashish Zore

Department: Chemistry

SYNTHESIS AND PROCESS OPTIMIZATION OF COLLOIDAL UNIMOLECULAR POLYMER, CUP, PARTICLE FORMATION, AND ITS INTERFACIAL SURFACE TENSION BEHAVIOR

by

ASHISH SHANTARAM ZORE

A DISSERTATION

Presented to the Graduate Faculty of the

MISSOURI UNIVERSITY OF SCIENCE AND TECHNOLOGY

In Partial Fulfillment of the Requirements for the Degree

DOCTOR OF PHILOSOPHY

in

CHEMISTRY

2022

Approved by:

Dr. Michael R. Van De Mark, Advisor
Dr. Chariklia Sotiriou-Leventis
Dr. Thomas Schuman
Dr. Jeffrey Winiarz
Dr. Melanie Mormile

PUBLICATION DISSERTATION OPTION

This dissertation consists of five papers, formatted in the style used by the Missouri University of Science and Technology:

Paper I, found on pages 11–99, is a book chapter in "Single-Chain Polymer Nanoparticles: Synthesis, Characterization, Simulations, and Applications" published in Wiley.

Paper II, found on pages 100–137, has been submitted to *Polymers Journal*.

Paper III, found on pages 138–176, is published in *Polymers Journal*.

Paper IV, found on pages 177–214, is intended for submission to *Polymers Journal*.

Paper V, found on pages 215–235, is published in *CoatingsTech*.

ABSTRACT

Colloidal Unimolecular Polymer (CUP) particles are 3-9 nm size single-chain polymer nanoparticles that are made from amphiphilic acrylic co-polymers using the process of water reduction. The formation of CUP particles was driven by the polymer-polymer interactions being greater than polymer-solvent interactions as well as the charge-charge repulsion due to the increasing dielectric of the medium. CUPs provide a surfactant or additive-free nanoparticle system that was useful for studying the interfacial behavior of pure aqueous nanoparticles using a maximum bubble pressure tensiometer. The equilibrium surface tension shows a dependence on concentration and the charge density of the CUP particle. The equilibrium surface tension becomes constant at higher concentrations due to the counterion condensation effect. The dynamic surface tension is dominated by the rate of diffusion of CUP particles to the interface. The water reduction process which transforms a single polymer chain into a particle was observed using viscosity measurements on a vibration viscometer. Changing the hydrophobic and hydrophilic ratios in the co-polymer, changed the THF-water composition required to cause the collapse or self-organization of the polymer chain. The design of the CUP polymer was optimized by defining the charge density limits for stable and spheroidal CUP particle formation. It was found that the charge density (ions/nm^2) of the particle must be between 0.32 to 0.85 to form a stable and spheroidal particle. When the Charge density (ions/nm^2) is higher than 0.85, it would result in non-spheroid conformation (like dumbbell, pearl necklace, etc.) whereas when it is lower than 0.32, it would result in aggregation of the particles due to poor stability.

ACKNOWLEDGMENTS

I would like to thank my advisor, Prof. Dr. Michael Van De Mark for his continuous support, guidance, and financial backing in the pursuit of my graduate studies at Missouri S&T. His passion for science and research and critical thinking has helped me become an academically successful person and a better human being.

I would like to thank my committee members Dr. Thomas Schuman, Dr. Chariklia Sotiriou-Leventis, Dr. Jeffrey Winiarz, and Dr. Melanie Mormile for their support throughout the completion of my graduate degree. I would like to thank the Department of Chemistry and Missouri coatings institute for funding my research endeavors. I want to acknowledge my fellow researcher Dr. Peng Geng, Dr. Sagar Gade, Dr. Minghang Chen, Dr. Ameya Natu, Ms. Abbie Braden, and Mr. Fei Zhang for their help in my research.

Finally, I would like to express my sincere gratitude and respect to my parents for their unconditional love and care. I would like to thank my friends for their support in my graduation journey.

TABLE OF CONTENTS

LIST OF ILLUSTRATIONS

SECTION Page

PAPER V

LIST OF TABLES

PAPER I Page

PAPER II

PAPER III

PAPER IV

PAPER V

1. INTRODUCTION

1.1. SINGLE CHAIN NANOPARTICLE (SCNP)

Over the past two decades research in Single-Chain Polymer Nanoparticles (SCNPs), which are polymer nanoparticles made from individual polymer chains, has seen remarkable growth [1,2]. SCNPs are sub-20 nm range polymer nanoparticles that are made by intramolecular collapsing/folding of the polymer chain. One example developed in Van De Mark's group is Colloidal Unimolecular Polymers, CUP, which are made by self-assembly or collapse of single polymer chains into spheroidal particles on a nanoscale level. The ability of the CUPs to be tailor-made of the desired size and charge density with relative ease while being free of VOCs or additives makes them ideal for studying structure-property effects in nanoparticles and as well as beneficial for applications like coating, catalysis, drug delivery, etc.

Past studies with SCNPs, have shown the collapse or folding of the polymer chains accomplished by covalent crosslinking of functional groups on the precursor polymer or by self-assembly [3]. In 2001, Mecerreyes' et. al. [4] introduced the concept of SCNPs obtained by intramolecular cross-linking of individual linear polymer chains which contained pendant acryloyl and methacryloyl groups as reactive precursors. Aliphatic polyesters with acryloyl pendant group were made by living ring-opening co-polymerization of 4-acryloyloxy caprolactone with ε-caprolactone. The polystyrene copolymers with methacryloyl pendant groups were prepared by modifying poly(styrene-co-hydroxyethyl methacrylate) copolymers. These reactive precursor polymers were then radically polymerized in ultra-dilute concentrations using initiators such as

azobisisobutyronitrile (AIBN) to obtain a single chain nanoparticle of diameter 3.8-13.1 nm. When the polymerization was carried out in higher concentrations, it showed the formation of a 3-Dimensional polymer network instead of particles. The growing interest in SCNP have been evident by the continuous introduction of new intrachain crosslinking chemistries for synthesizing SCNPs such as Diels–Alder (DA) reaction [5], cross-metathesis [6], quinodimethane formation [7], copper(I)-catalyzed azide–alkyne cycloaddition [8] (CuAAC), amide formation [9], urea formation [10], benzoxazine ring-opening polymerization [11] (ROP), Bergman cyclization [12], nitrene cross-linking [13], alkyne homocoupling [14], oxidative polymerization [15], thiol–ene coupling [16], Michael addition [17], epoxide ROP [18], tetrazine–norbornene reaction [19], nitrile–imine ligation [20] and thiol–yne coupling [21].

The collapse or folding by self-organization of amphiphilic polymer chains to form a nanoparticle is analogous to that of micelle formation in surfactants. The coil to globule transition can be triggered by changing the solvent quality like solvent composition, dielectric, or pH. Li [22] made a self-assembled multi-chain polymeric micelle (dia. 50-120 nm) as a drug delivery system using an amphiphilic copolymer that was prepared by grafting the hydrophobic blocks of the anticancer drug paclitaxel onto blocks of a hydrophilic polyether ester. In an aqueous environment with adjusted pH, the block copolymer orients its hydrophilic polyether ester out in the aqueous phase and the hydrophobic paclitaxel in the interior domain. Sawamoto et. al. [23] reported the single chain self-folding of neutral amphiphilic random methacrylate copolymers, consisting of PEG and alkyl side groups. The copolymer undergoes reversible self-assembly where the chain folds in the presence of water and unfolds with the addition of methanol. SCNPs

were stabilized by the PEG side-groups acting as efficient steric stabilizers. Morishima demonstrated the single chain collapse in polyelectrolytes [24] using a random copolymer of a 1:1 monomer ratio of hydrophilic and hydrophobic monomers. The chains were collapsed into single chain polymer particles (dia. 5.5 nm) by dissolving the co-polymer at a very low concentration in aqueous NaOH.

Colloidal unimolecular polymer (CUP) particles, although similar in concept to Morishima's single chain polymer micelles are still unique because of their method of synthesis. In the case of CUPs, the collapse the of chain occurs because the solvent composition is slowly changed from solvent to non-solvent.

1.2. COLLOIDAL UNIMOLECULAR POLYMER (CUP)

Colloidal unimolecular polymers or CUPs [25] are nanoscale size charge stabilized, single chain nanoparticles made from a polymer chain having a well-balanced number of hydrophobic and hydrophilic (anionic or cationic) units. The polymer chain is collapsed into a CUP particle by a simple process called water reduction which is depicted in Figure 1.1. The water reduction process begins by dissolving the polymer in a low boiling, water-miscible solvent like THF and forming the ionic group by neutralizing in this case the carboxylic acid groups with a base like sodium hydroxide, triethylamine, ammonia, etc. Then in the next step water is added very slowly until the composition of the solvent reaches a point where the polymer-polymer interactions become stronger than polymer-solvent interactions which cause the chain to collapse. The THF is then removed to provide a zero VOC, stable suspension of CUP particles in water. The collapse of the

chain is such that the hydrophobic segments fold in to form the interior of the particle and the charged groups are present on the surface of the particle as shown in Figure 1.2.

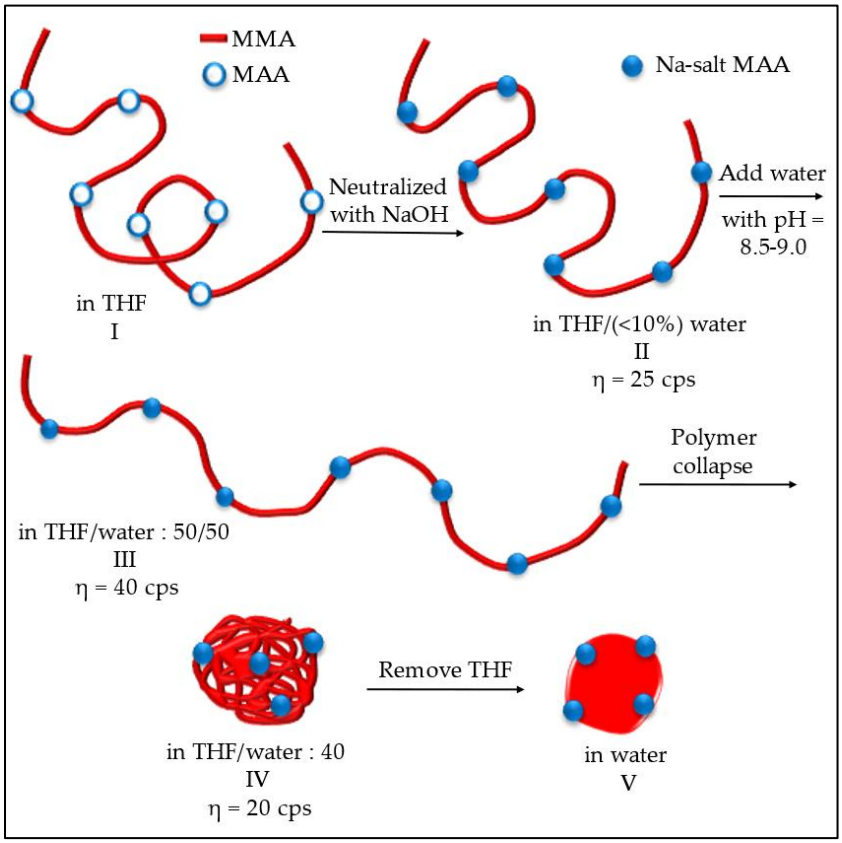

Figure 1.1. Schematics of the water reduction process, viscosity behavior, and CUP formation.

CUPs can be a good model for studying proteins as they are formed by a single strand of a polymer chain with surface ionizable groups which are similar to the conformation of globular proteins. CUPs are free of any impurities like surfactants which are otherwise present in other nanoparticles like latex. CUPs are inexpensive and relatively easy to make while providing control over particle size and surface charge

density. The surface functional groups of the particle are readily available for further modification or reaction.

Due to the large surface area of the CUP particles as compared to latex and PUD (polyurethane dispersions), they have a higher volume ratio of surface/bound water. This

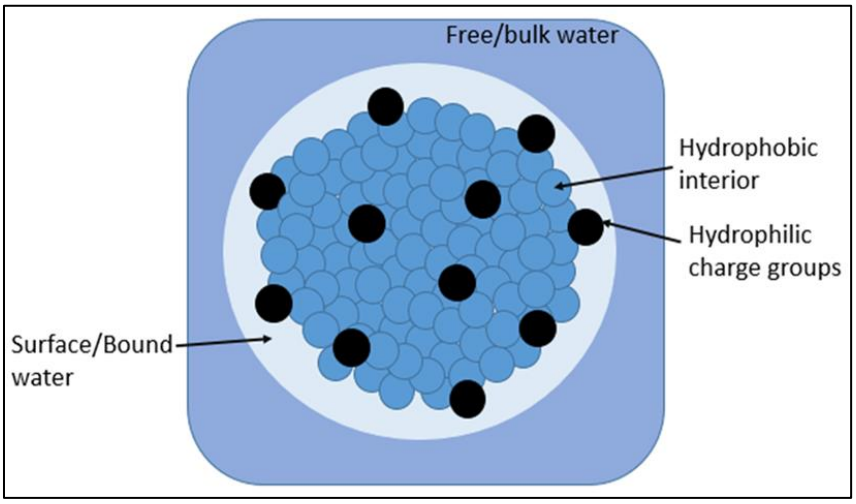

Figure 1.2. Structure of CUP particle suspended in water.

makes CUP particles extremely useful in studying the properties of bound/surface water [26,27]. CUPs also have a lot of utility in applications such as a resin [28,29], an additive for freeze-thaw stability [30], or as a catalyst [31]. A brief history of the previous research done with CUPs is provided in Paper 1.

1.3. WATER REDUCTION PROCESS AND COLLAPSE POINT

During the process of water reduction, the polymer chain undergoes conformational changes which lead to the viscosity behavior as shown in Figure 1.1. At stage I, the polymer chains in THF are in a random coil conformation. After neutralizing

the acid groups, the chain associates slightly due to the salt associations in the low dielectric medium, THF. As the water is being added the dielectric of the solvent mixture increases and the carboxylate anions start repelling each other. This elongates the polymer chains and increases the viscosity as more water gets added. This trend will continue until the composition of the water-THF mixture reaches the ratio where the polymer chain transitions from an elongated coil to a globule which is called the collapse point or collapse composition. The collapse of the chain leads to a drop in viscosity. Riddles et al. [25] have demonstrated the viscosity behavior by measuring the viscosity at different stages of the water reduction process. Aseyev [32] has also reported similar viscosity behavior with polymethacryloyl ethyl trimethyl ammonium methyl sulfate (PMETMMS) in a water acetone mixture where the collapse of the polymer chains occurs at 0.80 mass fraction of acetone in aqueous solution as observed by the decrease of the reduced viscosity, radius of gyration and hydrodynamic radius.

Non-unimolecular collapse can also be observed in some cases of the water reducible resin systems for example polyurethane dispersions where the polymer is synthesized in acetone and then followed by the addition of water [33]. When the acetone is removed from the solution, the polymer chain collapses into multi-chain aggregates particles of approximately 25 nm in diameter. This aggregated collapse is likely due to the use of relatively high concentrations. During the water reduction of CUPs, the concentration of polymer in the solution is low enough to prevent chain overlapping or entangling thereby ensuring that the collapse is unimolecular/single chain. Also, the particle size distribution measured by dynamic light scattering (DLS) overlaps with the

distribution of particle size calculated from the absolute molecular weight measurements on GPC which validates the unimolecular collapse.

1.4. SURFACE TENSION OF NANOPARTICLES

Understanding the contribution to the surface tension behavior by charge stabilized particles has been stifled due to the difficulty in obtaining colloidal suspensions free of surface-active ingredients or any contaminants. Removing impurities often involves time-consuming and complicated processes like dialysis, ultrafiltration cell and ion exchange resin [34], etc. The air-water surface tension of [34] charge stabilized suspensions was first reported by Okubo using monodispersed polystyrene latex particles (38-460 nm) with a strongly hydrophobic surface and silica particles (6-184 nm) which have a hydrophilic surface. The particle's suspensions were turbid and milky at low concentrations whereas at higher concentrations the suspension form a crystal-like structure in which brilliant iridescent colors from Bragg's diffraction and glittering single crystals were observed with the naked eye. In general, there was a decrease in surface tension as the particle volume fraction increased but the drop was more when the suspension formed a crystal-like structure. Polystyrene showed higher surface activity than silica due to the high hydrophobicity of the surface of polystyrene. Dong and Johnson [35,36] studied the surface activity of TiO_2 and SiO_2 (pH =10 and 11) based charge-stabilized aqueous colloidal dispersions that were large size (average size much greater than 30 nm) and broad distribution. The surface tension first decreases reaching a minimum at 5-7% solids and then rises back as the particle concentration increases. The author attributes the increase in surface tension to strong capillary forces between the

particles at the interface causing resistance to deformation. Surface tension studies of sub 20 nm size charge stabilized particles nm have rarely been reported. Surface tension of 2.5 nm and 10.4 nm bismuth telluride nanofluids have been successfully studied to gain insight regarding their surface tension behavior. They observed a decrease in surface energy and attributed it to the electrostatic repulsion between the nanoparticles at the air-water interface.

The use of CUP suspensions allows the study of interfacial tension without the effect of additives, surfactants, volatile organic compounds (VOCs), or any form of impurities. CUP suspension contains only charged particles, water, and counter-ions, and a relatively small amount of base to keep the pH (8.5-9.0) basic. The ease of control over particle size and charge density helps understand their effect on air interface behavior. Equilibrium and dynamic surface tension of CUPs having carboxylate, sulfonate, and QUAT-based ionized groups were done in a previous study where the surface tension behavior of these CUP particles was also compared against large size colloids like polyurethane dispersions (PUDs) and latex [37]. The study showed sulfonates to have lower surface tension as compared to QUATs which was followed by carboxylates. Latex and PUDs, on the other hand, due to their large particle size have slow diffusion and therefore take longer to reach equilibrium than CUPs.

The maximum bubble pressure tensiometer allows for the measurement of both equilibrium and dynamic surface tension. The instrument creates a new surface by creating bubbles in the solution. Figure 1.3 shows the dynamic and equilibrium behavior of surfactant/particles observed with maximum bubble pressure tensiometer by varying the surface age of the bubble. The surfactant/particles migrating to the newly created

interface can provide information about the diffusion behavior of particles. Equilibrium surface tension is measured in the equilibrium region of the curve where the surface tension becomes constant with surface age. For obtaining the dynamic curve, surface tension is measured with increasing surface age. The dynamic interfacial study can be more useful in practical applications with non-equilibrium/dynamic conditions like spraying, printing, foaming, or coating. The maximum bubble pressure method mitigates the effects of humidity, air turbulence, and contamination of carbon dioxide.

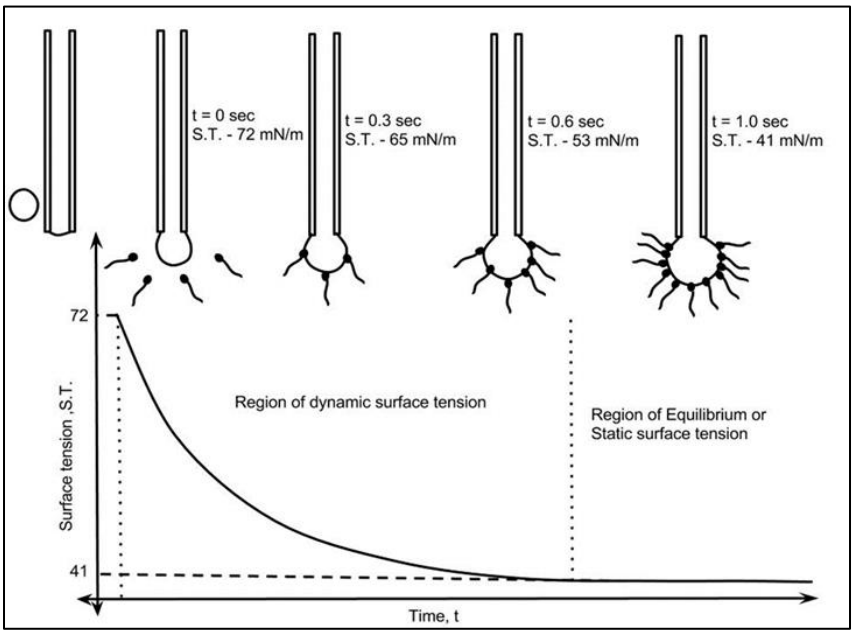

Figure 1.3. Equilibrium and dynamic behavior observed using maximum bubble pressure tensiometer.

In this study, CUP particles with carboxylate charge groups were used for studying air interfacial tension and to understand the collapse behavior.

1. Paper I will introduce the CUPs and summarize the past research done to understand their properties and explore their application.

2. Paper II will address the equilibrium and dynamic interfacial behavior of CUP particles by investigating CUPs with different particle sizes and charge densities. A model for CUP particles at the air-water interface will be developed. The interfacial behavior at high concentration and the effect of counterion condensation will be discussed.
3. Paper III will address the need for a better survey method to define the optimum amount of solvent and water at the collapse point. A more rapid, accurate, and less labor-intensive method will be presented. The effect of polymer structure (hydrophobicity and hydrophilicity) on the solvent composition required for the collapse will be presented.
4. Paper IV defines the limits of CUP formation for a carboxylate-based polymer using the charge density parameter. Rules for designing the CUP polymer using any type of hydrophobic and carboxylate-based hydrophilic monomer will be presented.
5. Paper V addresses the equilibrium and dynamic interfacial behavior of CUP particles when compared against latex and Polyurethane dispersions used in the coating industry.

PAPER

I. COLLOIDAL UNIMOLECULAR POLYMER PARTICLES: CUP

Michael R. Van De Mark, Ashish Zore, Peng Geng, and Fei Zheng

Department of Chemistry, Missouri University of Science and Technology, Rolla, MO 65409

ABSTRACT

Colloidal unimolecular polymer (CUP) particles can be made with any hydrophobic backbone as long as it has sufficient hydrophilic pendent groups to stabilize the particle and the backbone flexibility to conform to a spheroidal shape. This chapter covers the synthesis, characterization, and application of CUPs. It covers the driving force for the formation and the effect of CUPs as a function of concentration. The formation of CUPs particles involves both soap theory and Flory-Huggin's theory. Soap theory is mainly due to the hydrophobic effect, and Flory-Huggin's theory is introduced in the chapter regarding the polymer-solvent interaction. CUPs can be considered as charged nanoparticles. The CUPs behave like ions in an ionic crystal positioning at equal distance from the nearby particles. The gel point behavior study gives an idea of the packing CUPs can undergo and also the properties of the bound water on the surface of the particle.

1. INTRODUCTION

Colloidal unimolecular polymers (CUPs) are a new class of unimolecular polymer particles. They are formed by the effect of hydrophilic/hydrophobic interaction of hydrophilic pendant groups and a hydrophobic backbone as the solvent composition is changed [1, 2]. The formation of CUP particles is driven by the polymer–polymer interaction being greater than that of the polymer–solvent and is entropically favored by release of water molecules surrounding the backbone, analogous to micelle formation [3, 4]. The spheroidal shape is derived from the repulsive interaction of the ionic groups or the hydrophilic group's steric effects. The formation is analogous to the globular folding of a protein or the formation of a micelle. Figure 1 illustrates the process of formation of CUP particles.

The process of the CUP particle formation is very analogous to that of water-reducible coating resins. The resin is dissolved in a water-miscible solvent such as THF or as in water-reducible coatings ethylene glycol mono-butyl ether. The organic solvent must dissolve the polymer and have a boiling point below water so it can be removed easily. It is important to keep the solution dilute enough to avoid chain–chain entanglement during collapse to avoid multichain particles. The resin is treated with acid or base to form a salt and then water is added. At a critical ratio of solvent to water, the polymer collapses into a single molecule particle. Once the water has been added, the solvent is stripped off – in the case of CUP – but remains for water-reducible coatings. Thus, CUPs are zero VOC and have no stabilizer chemicals added. Unlike other methods of unimolecular particle production, the CUP process is not limited to single chemistry.

CUP particles can be made with any hydrophobic backbone as long as it has sufficient hydrophilic pendent groups to stabilize the particle and the backbone flexibility to conform to a spheroidal shape [1, 2].

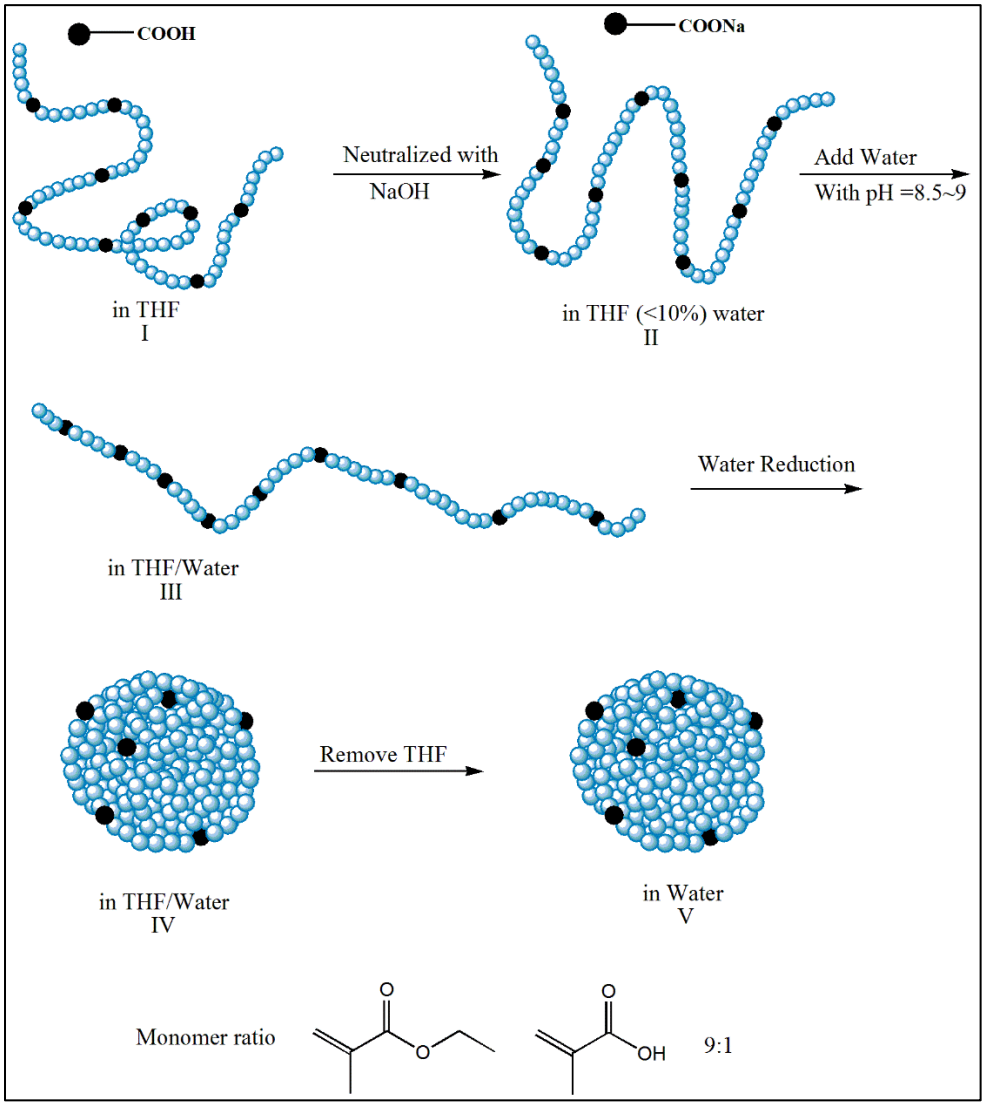

Figure 1. Process of forming CUP particles from poly(ethyl methacrylate-co-methacrylic acid) copolymers: (I) random coil configuration in tetrahydrofuran (THF), (II) random coil intimate ion pair, (III) extended coil solvent separated ion pair, (IV) collapsed coil, and (V) hard-sphere. (Riddles et al. 2014 [1]. Reproduced with permission of Elsevier.)

This paper covers the synthesis, characterization, and application of CUPs. The driving force for the formation and the effect of CUPs as a function of concentration will be covered in detail. Emphasis will also be given to the determination and characterization of the water on the surface of CUPs due to its dominance over their properties.

2. SYNTHESIS

CUP particles can be made from any hydrophobic backbone polymer with the correct number of hydrophilic groups. Alkyds, urethanes, polyesters, phenolic, epoxy, and many other building blocks and functionality can be used to make CUP resins. Most of the work to date has concentrated on acrylic polymers due to the number of monomers available. These monomers lend themselves to radical polymerization and yield little chain branching. Table 1 gives the monomer composition for polymers that have been demonstrated to form CUP particles. All the polymers were made by free-radical polymerization in solution. The molecular weights were determined by size exclusion chromatography (SEC) with refractive index, light scattering, and viscosity detector to yield absolute molecular weight for all but the sulfonate and QUAT polymers. The diameters were determined by backscattered light scattering using the solution viscosity [1, 2]. The molecular weight and the total number of hydrophilic groups must be high enough to form and stabilize the particle. For a methyl methacrylate (MMA)/methacrylic acid (MAA) 9 : 1 copolymer, the molecular weight needed to be over about 13 000 g mol^{-1}, which gives the polymer approximately 13 acid groups per particle. Since 13K is

the average, some chains are in the order of 10K that would only have 10 groups. It is the smaller chains that would have a tendency to not be stable and aggregate [8, 12].

2.1. MONOMERS AND RATIO, MOLECULAR WEIGHT, GLASS TRANSITION, CUP SIZE AND FUNCTIONALITY

The procedure for the synthesis of the polymers in Table 1 relies on AIBN as the initiator and a thiol as a chain transfer agent to control the molecular weight. The polymers were all purified by precipitation to remove residual monomers and dried. All the molecular weight and its distribution were absolute since the size of the CUP is based upon the molecular weight and the polymer density, as explained in Section 2.4. It is important to note that since this is a unimolecular particle, the molecular weight of each polymer molecule defines its size. Once purified all were characterized by SEC, functionality (by titration using the appropriate ASTM method), differential scanning calorimetry (DSC) for the glass transition temperature (Tg) of the polymer, and gas displacement pycnometer for density measurement of the polymer [1, 2].

2.2. REDUCTION AND CUP FORMATION

The formation of the cup particle is through a process known as water reduction. The polymer is dissolved in a water-miscible solvent such as THF, dimethyl ether, acetone, methyl, or ethyl alcohol, and then water is added slowly with stirring. It is critical that water be added very slowly to avoid too rapid an environmental change that could precipitate or aggregate the polymer. The water must also be of the correct pH and free of polyvalent cations such as calcium, which may aggregate the resin, especially for carboxylate-containing resins. The concentration of the polymer must be kept in a

Table 1.List of polymers synthesized for CUP study.

#	Polymer	Ratio	M_n (g mol^{-1})	M_w (g mol^{-1})	T_g (°C)	Hydrophilic groups [a]	Acid value	Diameter (nm)	References
1	MMA/MAA	9:1	111K	174K		122.5	62.2	6.5	[5-7]
2	MMA/QUAT	9:1		36K				4.3	[8, 9]
3	MMA/QUAT	9:1		55K				5.6	[8, 9]
4	MMA/QUAT	9:1		94K				6.3	[8, 9]
5	EMA/BMA/MAA	2.5:5.5:1	19K		55	16	48.7	4.0	[10, 11]
6	EMA/BMA/MAA	2.5:5.5:1	50K		55	43	48.7	4.5	[10, 11]
7	BMA/EA/2-EHMA/MAA	1.5:1.5:4:1	21K		21	19	50.9	3.1	[10, 11]
8	BMA/EA/2-EHMA/MAA	1.5:1.5:4:1	51K		21	46	50.9	4.7	[10, 11]
9 [b]	MMA/MAA	9:1	3.5K			3.5	57.7	4.6	[6, 8, 12]
10 [b]	MMA/MAA	9:1	4.5K			5	57.1	4.4	[6, 8, 12]
11 [b]	MMA/MAA	9:1	8.5K			9	58.4	3.2	[6, 8, 12]
12	MMA/MAA	9:1	13K			13	58.2	3.3	[6, 8, 12]

Table 1.List of polymers synthesized for CUP study (cont.).

#	Polymer	Ratio	M_n (g mol^{-1})	M_w (g mol^{-1})	T_g (°C)	Hydrophilic groups [a]	Acid value	Diameter (nm)	References
13	MMA/MAA	9:1	15K			15	57.3	3.6	[6, 8, 12]
14	MMA/MAA	9:1	20K			21	57.3	3.9	[6, 8, 12]
15	MMA/MAA	9:1	72K			74	57.8	5.8	[6, 8, 12]
16	MMA/MAA	9:1	90K			92	57.1	5.9	[6, 8, 12]
17	MMA/MAA	9:1	153K			157	58.4	7.8	[6, 8, 12]
18	MMA/MAA	9:1	28K			29	59.1	4.2	[1, 6, 13]
19	MMA/MAA	9:1	36K			37	57.7	4.5	[1, 2, 6, 13]
20	MMA/AMPS	10:1	80K		123		48.1	5.7	[8, 14]
21	MMA/AMPS	9:1	28K				47.1	4.2	[8, 14]
22	MMA/AMPS	9:1	56K				46.9	5.3	[8, 14]
23	MMA/AMPS	9:1	80K				48.1	5.9	[8, 14]
24	BMA/MMA/MAA	6.4:1.6:1	22K		57		47.5		[15]

Table 1.List of polymers synthesized for CUP study (cont.).

#	Polymer	Ratio	M_n (g mol^{-1})	M_w (g mol^{-1})	T_g (°C)	Hydrophilic groups [a]	Acid value	Diameter (nm)	References
13	MMA/MAA	9:1	15K			15	57.3	3.6	[6, 8, 12]
14	MMA/MAA	9:1	20K			21	57.3	3.9	[6, 8, 12]
15	MMA/MAA	9:1	72K			74	57.8	5.8	[6, 8, 12]
16	MMA/MAA	9:1	90K			92	57.1	5.9	[6, 8, 12]
17	MMA/MAA	9:1	153K			157	58.4	7.8	[6, 8, 12]
18	MMA/MAA	9:1	28K			29	59.1	4.2	[1, 6, 13]
19	MMA/MAA	9:1	36K			37	57.7	4.5	[1, 2, 6, 13]
20	MMA/AMPS	10:1	80K		123		48.1	5.7	[8, 14]
21	MMA/AMPS	9:1	28K				47.1	4.2	[8, 14]
22	MMA/AMPS	9:1	56K				46.9	5.3	[8, 14]
23	MMA/AMPS	9:1	80K				48.1	5.9	[8, 14]
24	BMA/MMA/MAA	6.4:1.6:1	22K		57		47.5		[15]

Table 1.List of polymers synthesized for CUP study (cont.).

#	Polymer	Ratio	M_n (g mol^{-1})	M_w (g mol^{-1})	T_g (°C)	Hydrophilic groups [a]	Acid value	Diameter (nm)	References
25	BMA/MMA/MAA	6.4:1.6:1	118K		66		46.6		[15]
26	MMA/MAA	5:1	20K				96		[16]
27	MMA/MAA	16:1	17K				33		[16]
28	MMA/MAA	6:1	11.3K				82		[16]
29	MMA/MAA	10:1	9.7K				52		[16]
30	EA/AA	10:1	42K		-9		67.8		[17]
31	MMA/MAA	10:1	28.4K		113		49.4		[17]
32	MMA/MAA	9:1	58K				58		[1, 2]
33	MMA/MAA	9:1	106K				59.7		[1, 2]
34	MMA/MAA	9:1	122K				59.7		[1, 2]
35	MMA/BA/TFEMA/AA	6.3:2.5:0.3:1	26K		68		60	4.6	[2, 7]
36	EA/AA	9:1	10.5K		-16	10.5	56.4	4.2	[18]

Table 1.List of polymers synthesized for CUP study (cont.).

#	Polymer	Ratio	M_n (g mol^{-1})	M_w (g mol^{-1})	T_g (°C)	Hydrophilic groups [a]	Acid value	Diameter (nm)	References
37	EA/AA	9:1	37K		-17	37.5	56.8	4.3	[18]
38	EA/AA	9:1	31K		-16	31.8	56.4	4.1	[18]
39	MMA/MAA	12:1	16K		133		29.6		[19]
40	MMA/MAA	12:1	20K		111		37.8		[19]
41	MMA/MAA	12:1	31K		123		37.8		[19]
42	MMA/MAA	10:1	14K		124		48.7		[19]
43	MMA/MAA	10:1	22K		130		57		[19]
44	MMA/MAA	10:1	24K		125		42.7		[19]
45	MMA/MAA	8:1	21K		100		56		[19]
46	MMA/MAA	8:1	25K		100		65.8		[19]
47	MMA/MAA	8:1	21K		136		78.8		[19]

Table 1.List of polymers synthesized for CUP study (cont.).

#	Polymer	Ratio	M_n (g mol^{-1})	M_w (g mol^{-1})	T_g (°C)	Hydrophilic groups [a]	Acid value	Diameter (nm)	References
48	MMA/MAA	9:1	29K				59.1	4.1	[7]

AA, acrylic acid; MMA, methyl methacrylate; MAA, methacrylic acid; BMA, butyl methacrylate; EA, ethyl acrylate; EMA, ethyl methacrylate; 2-EHMA, 2 ethylhexyl methacrylate; QUAT, [2-(methacryloyloxy)ethyl] trimethylammonium chloride; AMPS, 2-acrylamido-2-methylpropane sulfonic acid; TFEMA, 2, 2, 2-trifluoroethyl methacrylate; BA, butyl acrylate.
a) Number of hydrophilic groups per CUP particle.
b) Does not form CUP particles cleanly.
Source: Chen et al. 2013 [5]. Reproduced with permission of Springer

dilute state to avoid aggregation. This polymer concentration, for THF, is typically 20% for less than 30K, 10% for 30–70K, and 5% for up to 150K polymer molecular weight. Slightly higher concentration will also produce reasonable results, but it will have some aggregate. For industrial processes this may not be an issue but for scientific research, the aggregation should be avoided.

As water is added to the polymer solution, the polymer exhibits many changes in conformation (Figure 1). Figure 2 illustrates the viscosity change as the water is added.

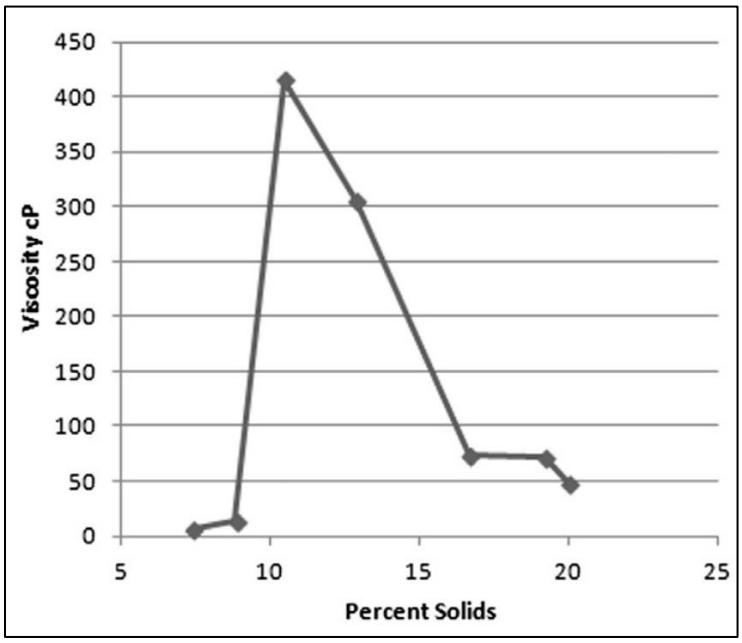

Figure 2. Viscosity of polymer 32 (Table 7.1) during water reduction of 20 g polymer in 80 g in THF with 160 g water being added. (Riddles et al. 2014 [1]. Reproduced with permission of Elsevier.).

At low water content the polymer is associated through the acid or ionic groups and in a random coil configuration. As water is added the dielectric of the solvent rises, allowing the ions to feel each other on the chain repelling each other. This causes the

polymer to extend its conformation. At the peak in viscosity, the polymer-polymer and polymer-solvent interactions are at a critical point. The addition, of a very small amount of water to the system, results in a collapse of the chain into a near-hard sphere conformation. At this point, the viscosity has dropped precipitously. The Mark–Houwink equation exponent for the THF only portion is typically 0.7, but at the peak, the value would be much larger with the value after collapse being close to zero. However, the Mark–Houwink value after the collapse will be different due to the charges on the particle that result in repulsion between particles. This area will be discussed in detail in the electroviscous effect in Section 6.

2.3. COLLAPSE POINT

The solvent composition when the polymer goes from basically a near ridged rod to a spherical collapsed state is a critical issue. Synthetic polymer chemists need to be able to relate structure to solvent composition at the critical collapse point. The maximum concentration of polymer and the minimum amount of both solvent and water governs the final concentration of the CUP suspension. For polymer 34 the collapse took place at water to THF ratio of 58 : 42 and the Hansen solubility parameters for the blend at the collapse were calculated and compared with two solvents, ethanol and methanol [1, 20], where δ_t is the total solubility parameter; δ_d, δ_p, δ_h are the parameters for the dispersion, polar and hydrogen bonding contributions; and φ_1 and φ_2 are the volume fractions for each solvent (Table 2):

$$\delta_t^2 = \delta_d^2 + \delta_p^2 + \delta_h^2 \quad (1)$$

$$\delta_d = \delta_{d1}\varphi_1 + \delta_{d2}\varphi_2 \quad (2)$$

$$\delta_p = \delta_{p1}\varphi_1 + \delta_{p2}\varphi_2 \quad (3)$$

$$\delta_h = \delta_{h1}\varphi_1 + \delta_{h2}\varphi_2 \quad (4)$$

The solubility parameter for the solvent blend was consistent with the polymer being insoluble in methanol and soluble in ethanol when heated. Current work is

Table 2. Solubility parameters of individual solvents and their blends with water at collapse point [20].

Solvent	δ_d	δ_p	δ_h	δ_t
THF	16.8	5.7	8.0	19.4
Water	15.6	16.0	42.3	47.8
Methanol	15.1	12.3	22.3	29.6
Ethanol	15.8	8.8	19.4	26.5
Blend (42% THF & 58% water)	16.1	11.7	27.9	34.3

underway to utilize continuous monitoring of viscosity as the pump delivers the water to have a method for the rapid determination of the collapse point. If the collapse point can be modeled and predicted based on structure, the synthetic polymer chemist can better design the CUP system.

2.4. CUP SIZE AND DISTRIBUTION CORRELATION TO MOLECULAR WEIGHT

To verify that the particles were truly unimolecular upon reduction, a comparison of the distribution curves obtained by SEC of the polymer to the distribution of diameters obtained from the dynamic light scattering (DLS) particle size on the CUP samples was

made [1, 2]. The weight fraction of polymer chains at each molecular weight was used to determine the diameter of the chains. It was assumed that the bulk density of the polymer, 1.2 ($g.cm^{-3}$), was equal to the density of the polymer chains inside the CUP particles. The volume of 1.0 g of polymer is, V_g,

$$V_g = \frac{1.0\ gram\ CUP\ polymer}{density\ of\ bulk\ polymer} \quad (5)$$

Next, the number of particles, P, at each weight fraction (from SEC) was determined by using Avogadro's number, N_A, and the number average molecular weight:

$$P = (Wt\ fraction * N_A\ )/M_n \quad (6)$$

From these two equations, the volume of the CUP particle, V_{CUP}, was calculated by

$$V_{CUP}\ = (\frac{V_{gram}}{P}) \quad (7)$$

The volume, V_{CUP}, was used in the equation of a sphere to get the diameter D_{CUP} of each particle at each molecular weight:

$$V_{CUP} = \frac{1}{6}\pi {D_{CUP}}^3 \quad (8)$$

Figure 3 illustrates the particle size by DLS and calculated from the SEC data and Equation (5–8) for polymer 32 from Table 1 [1, 2]. The fit between these two data sets is excellent for the systems studied. The utilization of this correlation aids the researcher in validating that the CUP is truly unimolecular. It should be noted that if the monomers used do not distribute the hydrophilic groups well, the resultant polymer formed early or late in the polymerization process may not reduce properly. Careful attention to the reactivity ratios is necessary to avoid this problem. Methods to produce block copolymers would avoid this but are usually time-consuming. If living polymerizations were to be

employed producing very narrow polydispersity, the resultant CUP particles would be nearly a single size.

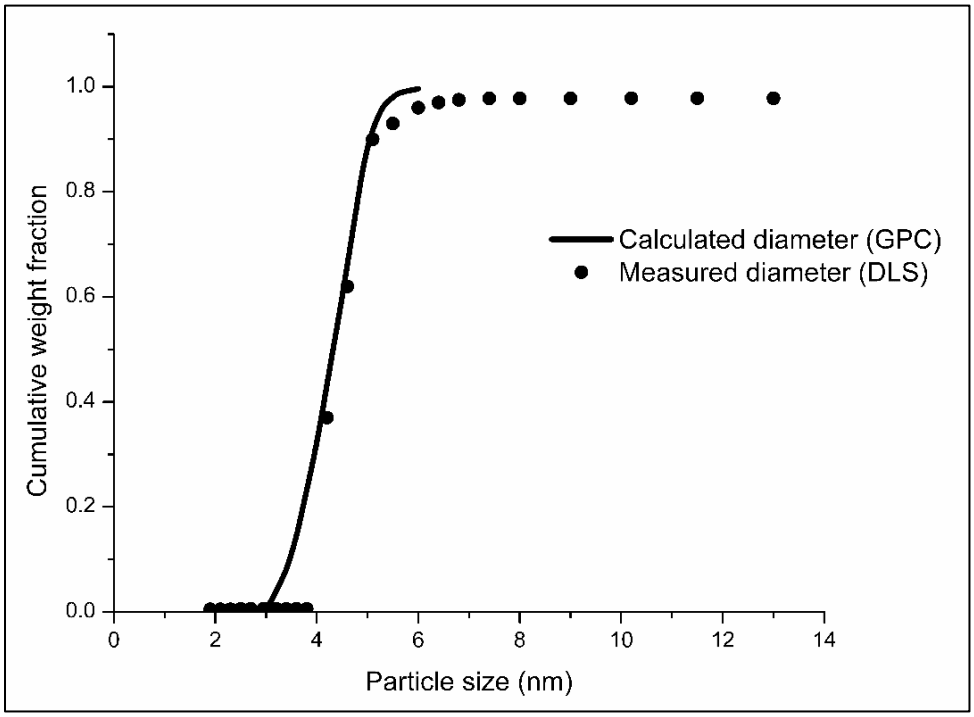

Figure 3. Particle size measured by dynamic light scattering (DLS) and calculated from SEC/GPC data. (Riddles et al. 2014 [1]. Reproduced with permission of Elsevier.).

After the reduction and removal of the solvent, the solution is clear with no aggregates. Typically, less than 0.05% aggregate is retained on a 0.2-micron filter [1, 2]. Figure 4 illustrates the solution clarity of a 4.2 nm CUP versus a 32 nm polyurethane dispersion (PUD) and a 100 nm latex resin.

3. FORMATION OF CUP PARTICLES

The formation of CUPs particles involves both soap theory and Flory–Huggins theory. Soap theory is mainly due to the hydrophobic effect, and Flory–Huggins's theory is introduced here regarding the polymer-solvent interaction.

3.1. ENTROPY EFFECT/SOAP THEORY

The CUP particles and micelles have some similarities, and the CUP particle formation process is analogous to that of micelle formation. Both micelle and CUP particles are composed of amphiphiles, forming a hydrophobic core and hydrophilic head groups oriented into the water phase. The particle size of micelles and CUP particles are both at the true nanoscale (<50 nm).

The entropy effect is one of the driving forces for micelle formation. It describes the disorder change of amphiphilic molecules to form micelles in an aqueous solution. This process can be understood using thermodynamics (Table 3) [21].

This table lists the thermodynamic parameters of some common surfactants forming micelles in water. According to this table, we note that $\Delta G°$ is always negative at room temperature, which means the formation of the micelle can occur spontaneously. However, for some surfactants, $\Delta H°$ is a positive value at low temperatures, which indicates the micelle formation is an endothermic process. It is the large gain in entropy that contributes to the negative change in Gibbs energy [21]. Micelle formation is entropy-driven at low temperatures [25]. Once surfactants dissolve or disperse in water, water molecules form in ordered iceberg structure around hydrocarbon groups [26].

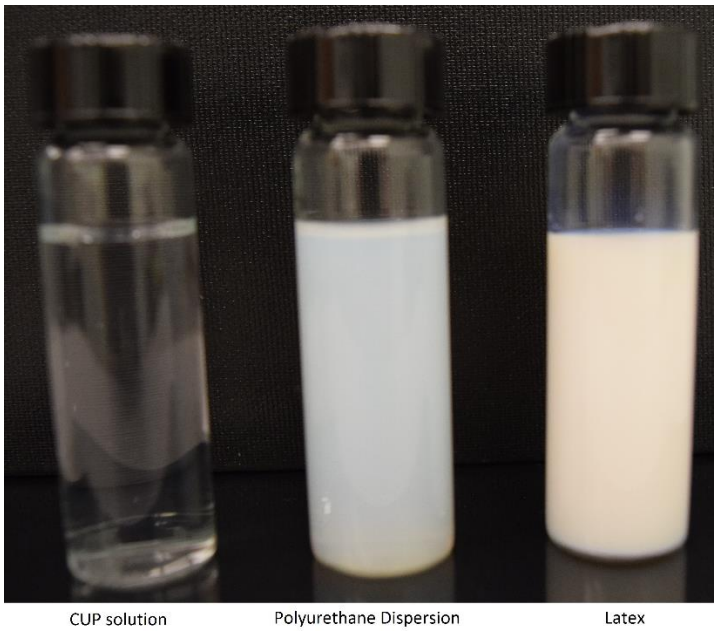

Figure 4. Solution clarity of a 4.2 nm CUP solution versus a 32 nm polyurethane dispersion, PUD, and a 100 nm latex resin.

Table 3. Thermodynamic parameters of micelle formation in some common surfactants [21–24].

Surfactant	**T (K)**	**CMC ($mol.l^{-1}$)**	**$\Delta G°$ ($kJ\ mol^{-1}$)**	**$\Delta H°$ ($kJ\ mol^{-1}$)**	**$T\Delta S°$ ($kJ\ mol^{-1}$)**	**$\Delta S°$ ($J\ mol^{-1}\cdot K$)**
SDBS	298	0.0015	-26.57	23.27	49.84	167.17
SDS	293	0.0087	-38.83	1.55	40.38	137.81
Triton X-100	298	0.0028	-20.28	9	29.22	98
Octyl glucoside	300	0.0026	-19.30	7.01	26.31	87.7

This ordered structure is destroyed when those hydrophobic hydrocarbon chains aggregate into a core. Thus, at room temperature, the entropy increase of micelle

formation is due to the release of structured water molecules in the hydration shell around the hydrophobic parts of the monomeric amphiphiles during the micelle formation process. The same thing happens during CUP formation, and as the water was added to the polymer/THF solution, water molecules are organized around the hydrophobic backbone. At the collapse point, the release of the organized water to the bulk increasing the entropy drives the CUP particle formation process [2].

3.2. HYDROPHILIC/LIPOPHILIC BALANCE (HLB)

Hydrophilic/lipophilic balance (HLB) is an important parameter of amphiphilic molecules, which indicates a surfactant's solubility in water. It is a fractional ratio of hydrophobic to hydrophilic part of a surfactant, and the value of HLB is usually between 0 and 20 (HLB of some ionic surfactants could be greater than 20). The higher a surfactant's HLB value, the more hydrophilic it is.

There are two common ways to estimate the HLB of a surfactant. One is Griffin's method [27, 28], and the other one is Davies' method [29]. We apply Griffin's method to estimate the HLB of CUPs. Griffin's method is described below:

$$HLB = 20 \times {}^{M_h}/_{M_w} \tag{9}$$

where M_h is the molecular weight of the hydrophilic portion of the molecule and M_w is the molecular weight of whole molecule.

In the case of CUPs, for an MMA/MAA, 9 : 1 copolymer, if we assume the repeat units ratio of MMA and MAA is also 9 : 1 in the copolymer and it was neutralized with ammonium hydroxide, then HLB of the copolymer can be calculated using the following method:

Hydrophilic part: -$COONH_4$ and -COO of the ester,

$M_h = 62\times1+44\times9 = 458$ g mol^{-1}

Molecular weight of average repeat unit: $M_w = 100\times9+103\times1 = 1003$ g mol^{-1}

HLB for MMA/MAA polymer = $(20\times458)/1003 = 9.1$

In this calculation, ammonium carboxylate and ester group in MMA units are considered hydrophilic contribution groups, and the rest of the groups are hydrophobic. HLB of CUP is 9.1, which falls in the range of 6–13 for oil in water (O/W) emulsifiers that are generally micelle forming materials [30].

CUPs are also amphiphilic molecules typically prepared from hydrophilic monomers such as MAA and hydrophobic monomers like methyl methacrylate or butyl methacrylate (BMA). The ratio of hydrophilic monomers and hydrophilic monomers on the polymer chain (HLB) plays an important role in the unimolecular collapse of the polymer chains during the process of water reduction [1]. A reasonable ratio of MMA and MAA to make a CUP would be 9∶1, and this is consistent with ratios reported in the literature for the formation of a micelle [31] that typical surfactants have approximately 16–22 carbon atoms comprising the hydrophobic portion of the chain to one hydrophilic group.

Other ratios of monomers slightly above or below 9 : 1 were found to water-reduce into CUP particles without any difficulties; however, increasing the MMA, above 12 produced coagulum. The reason is that the amount of hydrophilic groups is insufficient to stabilize the particles [12]. In that case, the particles may aggregate or simply precipitate. If the MAA fraction increases, the polymer may produce other

conformations or become water-soluble when reduced. As a result, collapse of the chains will not occur.

The hydrophobicity of the monomers also determines the ratio of monomers. For more hydrophobic monomers, such as n-BMA or n-butyl acrylate that have a long hydrophobic tail, the ratio of hydrophobic/hydrophilic monomer should decrease to 5 : 1 or 6 : 1 in order to make sure HLB value still falls above 6. For BMA/MMA, 5 : 1, the HLB would be 6.9.

3.3. FLORY-HUGGINS THEORY

Many of the thermodynamic properties of polymer solutions that depend on the composition of the mixture can be explained by means of a polymer–solvent interaction parameter, χ. It is the most important thermodynamic theory for understanding polymer solutions, which was first investigated by Paul Flory [32] and Maurice Huggins [33] independently in 1940s. It was employed for solvent–solvent and polymer–solvent mixtures. An enthalpy change can be observed when adding polymeric solute into a solvent, since polymer–polymer interactions are replaced by solvent–polymer interactions. At a given temperature, the free energy change is directly related to the enthalpy and entropy:

$$\Delta G = \Delta H - T\Delta S \tag{10}$$

The Flory–Huggins model assumes that when mixing the polymer segments into a solution, if the solution is dilute, the polymer segments are randomly mixed with the solution molecules. In a good solvent, the polymer segments seem to “repel” each other, since they prefer to interact with the solvent instead of the polymer. This means that there

exists a strong driving force for keeping each polymer segment apart so that they do not overlap, and there are no other segments in between each two polymer segments. The mixture can be considered, to a first approximation, as many small segments are separated and suspended in the solution. In terms of the Flory–Huggins model, the change in free energy upon mixing a polymer with solvent molecules is given by

$$\frac{\Delta Fm}{kT} = 1ln\phi_p + n_s ln\phi_s + n_s\phi_p\chi \quad (11)$$

From Equation (11), the change in free energy accompanying the mixing process can be estimated if the value of χ is known [34].

The CUP particles function very similar to what Flory described, in which at theta condition, the polymer should act as an ideal chain, and polymer–polymer interactions are balanced with polymer–solvent interaction. Because of the decrease in polymer–solvent interaction and the increasing of the polymer–polymer interaction, any change in the solution of the system from organic solvent to the mixture of organic solvent and water will result in changing the polymer's conformation. The polymer chain tends to swell in a good solvent or collapse in a bad solvent, such as water, and in this case, the charged groups of the CUP prevent particles from aggregation, and their repulsion drives the conformation into a spheroidal shape [1].

4. CONFORMATION OF THE CUP PARTICLES

Theoretically, polymers with ionic groups can form many conformations depending on the charge density along the chain. De Gennes and Pfuety first developed a widely accepted theoretical model that was further reviewed by Dobryinin [35]. It was

based on an electrostatic blob and the scaling theory. According to scaling theory, a polyelectrolyte takes on a pearl necklace shape in a poor solvent, with the “pearls” being electrostatic blobs. A neutral polymer will collapse into a spheroid globule in a poor solvent such as water. With the presence of charges, the globule becomes an elongated electrostatic blob followed by the formation of the pearl necklace shape. These transformations depend on the fraction of charges in the blob, the dielectric of the solvent, and the temperature. A theoretical model shows a polyelectrolyte undergoing several conformations from an electrostatic blob to a dumbbell and to a necklace of three pearls [36]. This model considers a dilute solution of a polyelectrolyte of uniform charge having a degree of polymerization N, monomer size b, and fraction of charged monomers f in a poor solvent having a dielectric constant ϵ. The following predictions are made for a polyelectrolyte of N =200 monomers at three different charge densities (f): (i) a polymer without any charge will collapse into a spherical globule, (ii) an electrostatic blob containing a fraction of charged monomers equal to 0.125 will separate into a dumbbell shape, and (iii) for a fraction of 0.15, a necklace of three pearls will exist.

The CUP particles studied here are on the lower edge of the theoretical model for which the pearl necklace conformations are not observed. This could be due to the low charge fraction since the chains were 9 : 1 MMA:MAA, meaning 10% of the polymer chain would be ionizable. If all the acid groups were neutralized by the ammonium hydroxide, the resulting charge fraction would be 0.10. A coil-to-globule transition instead of a dumbbell or pearl necklace conformation was observed for a polycation polyelectrolyte by Aseyev [37]. The viscosity and the hydrodynamic radius and radius of gyration were measured as acetone was added to water. The authors observed a typical

polyelectrolyte behavior displayed by the viscosity of the solution when the mass fraction (γ) of acetone was below 0.80, but when γ >0.80, collapse of the polycation into a globular state occurred. The CUPs were not of the pearl necklace conformation. This was evidenced by the measured particle diameters being very close to the calculated diameters [1].

5. ELECTROKINETIC BEHAVIOR IN CUPS

Charged particles dispersed in high dielectric solvent like water exhibit electrokinetic behavior. CUPs can be considered charged nanoparticles. There are four common electrokinetic phenomena, namely, electrophoresis, electroosmosis, streaming potential, and sedimentation potential. For CUPs the phenomena of electrophoresis have been studied. Electrophoresis is defined as the migration of charge colloidal particles or molecules through a solution under influence of an applied electric field. The fundamental parameters in electrophoresis are the zeta potential, ζ Debye–Hückel parameter, κ and electrophoretic mobility, μ. An important parameter for colloid behavior is the effective charge that is related to rheology, surface tension, and stability in colloidal particles. The effective charges can be calculated from the electrophoretic mobility and the conductivity values that can be measured experimentally. After the effective charge is determined, the Debye–Hückel parameters and zeta potential can also be calculated.

5.1. ZETA POTENTIAL, DEBYE-HÜCKEL PARAMETER AND ELECTROPHORETIC MOBILITY

The zeta potential (ζ) is the potential at the surface of shear that is defined as the layer of liquid immediately to the particle and moves with the same velocity as the surface. In regular suspensions, ionic strength is dominated by added electrolyte, and the value of the Debye–Hückel parameter κ is expressed as Equation (12):

$$\kappa^2 = [\left(\frac{e^2}{\varepsilon k_B T}\right) \sum_i z_i^2 n_{i\infty}] \tag{12}$$

κ is also defined using the Debye–Hückel approximation:

$$\psi = \psi_0 \, exp(-\kappa x) \tag{13}$$

where ψ_0 is the surface potential of the particle and x is the distance from the particle surface. κ^{-1} has the unit of meter and is called the Debye length referring to the thickness of the electrical double layer. Electrophoretic mobility (μ) is the velocity of an ion per unit electric field with unit ms−1/Vm^{-1} or m^{2}V^{-1}s^{-1} [6].

5.2. DETERMINING THE EFFECTIVE NUCLEAR CHARGE

5.2.1. Nernst-Einstein Model. This model [38] assumes that the counterions surrounding the macro-ions have no interaction with the macro-ions. It can be expressed as Equation (14):

$$\mu = Q_{eff}/f \tag{14}$$

where μ is the electrophoretic mobility, Q_{eff} is the effective charge, and f is the friction coefficient. The Stokes–Einstein equation relates friction coefficient, f, to the diffusion coefficient, D, by Equation (15):

$$D = \frac{k_B T}{f} = \frac{k_B T}{6\pi\eta a} \tag{15}$$

Here, the particle can be treated as a sphere with radius a. k_B is the Boltzmann constant, T is absolute temperature, and η is the viscosity of the suspension medium. Combining the above two equations, we can express the relationship between electrophoretic mobility and the effective charge as Equation (16)

$$Q_{eff} = 6\pi\eta a\mu^{\infty} \tag{16}$$

where μ^{∞} is the electrophoretic mobility extrapolated to infinite dilution. There is, however, no available model to extrapolate the μ^{∞} for spherical particles and hence cannot be used.

5.2.2. Hessinger's Model. When a deionized suspension with low surface pK_a is neutralized by a strong base like NaOH, both the conductivity of the suspension and the electrophoretic mobility of the particle change. At complete neutralization of the protons, the relationship can be expressed as Equation (17) [39]:

$$\sigma = ne\left[Z_{eff}\left(\mu_p + \mu_{Na^+}\right) + M(\mu_{OH^-} + \mu_{Na^+})\right] + \sigma_b \tag{17}$$

where σ is the conductivity of the suspension; n is the number density of particles; Z_{eff} is the effective charge; μ_p and μ_{Na^+} are electrophoretic mobilities of the particles and sodium ion, respectively; M is the concentration of the small ions per particle defined as $M = 1000cN_A/n$ where c is the concentration of small ions in mol l^{-1}; and σ_b is the conductivity of the background. The conductivity and the electrophoretic mobility can be measured experimentally, and the effective charge can then be calculated

5.2.3. Charge Renormalization. Some counterions surrounding the macro-ions will bind or condense on the surface of the macro-ions due to minimization of electrostatic repulsion between the charges. This will cause the effective charge to be smaller than the bare charge of the colloidal particles [40]. Alexander et al. [41] proposed

a model based on the assumption that each colloidal particle occupies the center of a spherical Wigner Seitz cell [42] with the presence of counterions. This model works well for colloidal particles with known bare charges. However, if the spherical particles have weak acid or base groups on the surface, the bare charge is regulated by the dissociation equilibrium at the surface of the particle. Ninham and Parsegian [43] first proposed a model that goes with a basic idea that two electrical repulsive forces tend to minimize the total free energy. Following this theory, Belloni [44] developed a simple program to calculate the effective charge as long as the particle size, maximum bare charge, pK_a of the ionizable group, pH of the reservoir solution, and salinity of the reservoir are known

For CUPs, the Hessinger's model has been used since it does not involve calculating the Debye–Hückel parameter for determining μ^{∞} for the effective charge.

5.3. ELECTROKINETIC BEHAVIOR IN COO^- CUPS

The CUPs used for this study were a carboxylate functional with molecular weight, M_n =36K and M_w =45K, (polymer 19), particle size of 4.5 nm, and acid number of 57.7. The linear increase in conductivity with the number density (in the range 4–22 × 10^{23} m^{-3}) (Figure 5) indicates no significant counterion condensation at that concentration. The effective charges calculated using the Hessinger's model and the values predicted by Belloni's program show good agreement except for number density larger than 35 × 10^{23} m^{-3} (Figure 6). The electrophoretic mobility of the CUP decreases with increasing the number densities [6]. The electrophoretic mobility behavior is similar to the simulation of the charge particle with radius 4 nm and charge of 60 and also similar to experimental result of monodisperse latex [45].

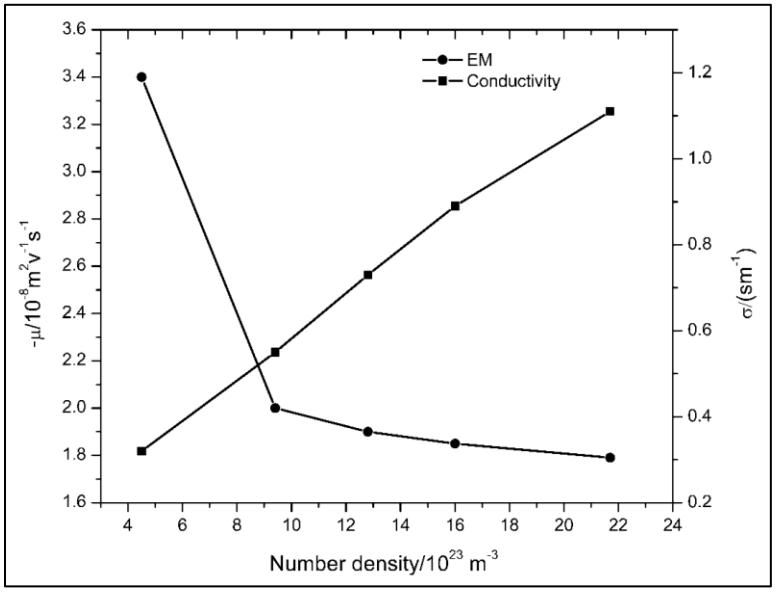

Figure 5. Electrophoretic mobility (μ) and conductivity (σ) versus number density. (Chen 2013 [6]. Reproduced with permission of Minghang Chen.).

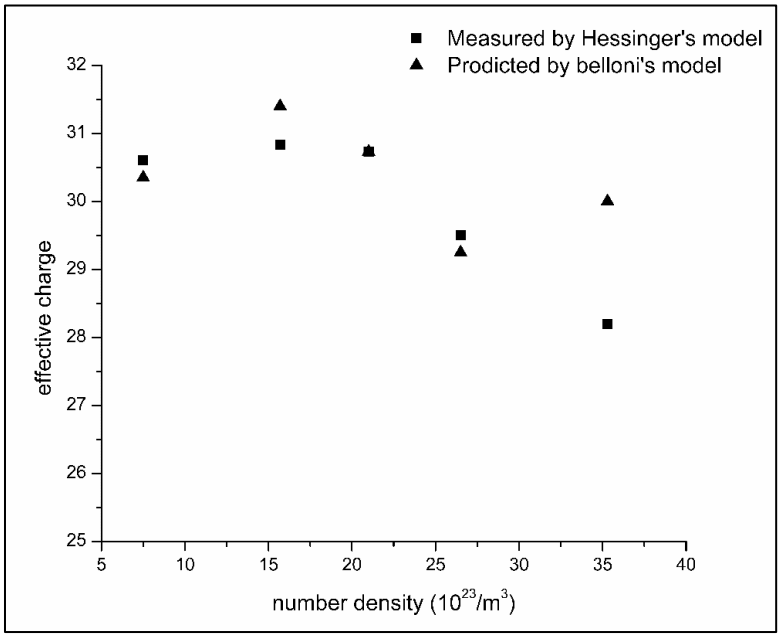

Figure 6. Effective charge (Zeff) measured by Hessinger's model and predicted by Belloni's model. (Chen 2013 [6]. Reproduced with permission of Minghang Chen.).

6. ELECTROVISCOUS EFFECT IN CUPS

The CUP particles have groups on the surface, which are hydrophilic and will adsorb a layer of water molecules to the surface of the particle. Many factors such as roughness, surface chemistry, charge density, etc., affect the structure of the surface water. The extent of hydration of the CUPs can be determined from the intrinsic viscosity of the suspension [46]. If the density and the molecular weight of the CUPs are known, the thickness of the water layer on the particle can be estimated. The particle size of latex is about 100 nm and that of a water molecule is 0.28 nm. Assuming that one layer of water molecule is bound to the surface, the ratio of volume of bound water to a 100 nm diameter latex particle is 0.0084 : 1. The effect of bound or surface water on rheology becomes negligible when the particle size is large. For small particles of size 3–9 nm, like CUPs, the ratio of bound water to particle increases up to 0.67 : 1. This high volume fraction of surface water in CUPs makes them excellent material to study the effect of surface water on rheological behavior [6, 13].

6.1. ELECTROVISCOUS EFFECT: THEORY

There are three types of electroviscous effect: primary (1EE), secondary (2EE), and tertiary (3EE).

6.1.1. Primary Electroviscous Effect. The distortion of the electrical double layer around the charged particles causes additional energy dissipation under shear. This effect is called the primary electroviscous effect (1EE). For 1EE, Smoluchowski [47]

related the intrinsic viscosity to primary electroviscous coefficient, p, by the Equation (18):

$$[\eta] = 2.5(1 + p) = 2.5[1 + \frac{4(\epsilon_r \epsilon_0 \zeta)^2}{(k\eta_0 R_s)^2}] \quad (18)$$

where ϵ_r is the dielectric constant of the solvent, ϵ_0 is the permittivity of a vacuum, k is the specific conductivity of the continuous phase, ζ is the zeta potential, and R_s is the radius of the spheres. The 1EE was further corrected by replacing the specific conductivity of the continuous phase with Debye length κ^{-1} [48, 49]. This relates the 1EE with the electrical double layer. The Debye length is calculated by Equation (19):

$$\kappa^{-1} = 1/[\left(\frac{1000e^2 N_A}{\epsilon_0 \epsilon_r k_B T}\right) \sum_i Z_i^2 M_i]^2 \quad (19)$$

where k_B is the Boltzmann constant, T is the temperature, N_A is the Avogadro's constant, Z_i is the valence of ions, and M_i is the concentration of the various ions with unit mol l^{-1}. The intrinsic viscosity was further corrected by Russel [50] for large distortion of the electrical double layer at high shear rate conditions by the Equation (20):

$$[\eta] = 2.5[1 + \frac{6(\epsilon_r \epsilon_0 \zeta)^2}{k\eta_0 R_s^2} \frac{1}{1+P_e^2}] \quad (20)$$

where P_e is the Peclet number defined as $P_e = \frac{R_s^2}{D}\dot{\gamma}$ where $\dot{\gamma}$ is the shear rate, D is the diffusion coefficient expressed as, $D = \frac{k_B T}{6\pi\eta_0 R_s}$.

The recent expression for primary electroviscous coefficient, p, given by Equation (21) was derived by Watterson and White [51]:

$$p \approx \frac{6\epsilon_0 \epsilon_r k_B T}{5\eta_0 e^2} \frac{\sum_{i=1}^{N} n_i^{\infty} z_i^2 \lambda_i}{\sum_{i=1}^{N} n_i^{\infty} z_i^2} L(\kappa R_s)(\frac{e\zeta}{k_B T})^2 \quad (21)$$

η_0 is the viscosity of water, Z_i is the valence of the ions, λ_i is the drag coefficient of the various ions in the solution expressed as $\lambda_i = \frac{e^2 N_A}{\Lambda_i^0}$, $\Lambda_i{}^0$ is the limiting equivalent conductance of each ion. $L(\kappa R_s)$ is a function of κR_s, expressed as

$$L(\kappa R_s) = \frac{10\pi}{3} Z(\kappa R_s)(1 + \kappa R_s) \tag{22}$$

Where,

$$Z(\kappa R_s) \approx (200\pi\kappa R_s)^{-1} + \left(\frac{11\kappa R_s}{3200\pi}\right) \; for\ thick\ double\ layers, i.e, small\ \kappa R_s,$$

or

$$Z(\kappa R_s) = \left(\frac{3}{2\pi}\right)(\kappa R_s)^{-4} \; for\ thin\ double\ layers, i.e., large\ \kappa R_s$$

In order to use Equation (21), we need to know the zeta potential that cannot be easily determined for CUPs without added electrolyte. However, the zeta potential can be related to the effective charge of particles by Equation (23) [51]. The calculation of the effective charge is shown in the electrokinetic section:

$$\zeta = \frac{Q_{eff}}{4\pi\epsilon_0\epsilon_r R_s(1+\kappa R_s)} \tag{23}$$

Equation (21) was used to estimate the primary electroviscous coefficient of CUPs [13].

6.1.2. Secondary Electroviscous Effect. When particles approach each other, the electrical repulsion between the electrical double layers increases the viscosity of the suspension. This effect is called the secondary electroviscous effect (2EE). The 2EE can be observed as the concentration of the suspension increases from dilute to semi-dilute range when the electrical double layer senses the presence of near particles. At low concentrations the 2EE is negligible and the 1EE dominates. The secondary electroviscous effect is related to the volume fraction.

Equation (24) relates the relative viscosity of the suspension to the volume fraction of the charged particles [52]:

$$\eta_{rel} = 1 + [\eta]\phi + \frac{2}{5}([\eta]\phi)^2 + \frac{3}{40} ln\left(\frac{\alpha}{ln\,(\alpha)}\right)(\kappa L)^4 \frac{\phi^2}{(\kappa R_S)^5} + B(\phi)^3 \quad (24)$$

where $[\eta]$ is the intrinsic viscosity including 1EE and α represents the ratio of electro-repulsion force to Brownian motion and is defined as

$$\alpha = A(4\pi\epsilon_0\epsilon_r\psi_s^2 R_s^2\kappa)\, exp(2)\, /k_B T \quad (25)$$

where ψ_s is the surface potential of the charged particle, A is a complicate function of κR_s and interparticle distance and varies from 0.6 to 1 with increasing interparticle distance [53], and L is the effective collision diameter defined as

$$L = \kappa^{-1} ln\,[\frac{\alpha}{ln\left(\frac{\alpha}{ln(\alpha)}\right)}] \quad (26)$$

The surface potential of the CUPs cannot be determined without adding salt and needs to be calculated. For high surface potential values, Equation (27) can be used to estimate the value [54]:

$$\psi_s = \frac{k_B T}{ze} ln\left[\frac{1}{6\phi\, ln\left(\frac{1}{\phi}\right)}\left(\frac{ze}{k_B T}\right)^2 \left(\frac{Q_{eff}}{4\pi\epsilon_0\epsilon_r R_s}\right)^2\right] \quad (27)$$

If $\frac{Q}{4\pi\epsilon_0\epsilon_r R_s} . \frac{ze}{k_B T} > \ln\,(\frac{1}{\phi})$

6.1.3. Tertiary Electroviscous Effect. The tertiary electroviscous effect (3EE) is referring to the expansion or contraction of particles due to change of conformation especially to polyelectrolytes [55, 56]. CUPs have a volume fraction occupied by the surface water layer that is the only possible conformational change and contribute to the tertiary electroviscous effect. Volume fraction can be expressed as

$$\phi_{eff} = \phi(1 + \frac{\delta}{R_s})^3 \quad (28)$$

where δ is the thickness of the surface water layer (see Section 6.3 for surface water determination).

6.2. INTRINSIC VISCOSITY DETERMINATION

For uncharged polymer, the intrinsic viscosity can be determined by extrapolating the reduced viscosity to infinite dilution. However, the intrinsic viscosity of polyelectrolyte solution cannot be determined without adding electrolyte. At dilute concentrations, the reduced viscosity of polyelectrolytes does not approach a set value; instead, it may increase sharply or give a maximum value. To determine the intrinsic viscosity, the relative viscosity, η_{rel}, can be related with volume, φ, by Equation (29) at dilute concentration [57]:

$$\ln(\eta_{rel}) = [\eta]_{\varphi}\varphi \tag{29}$$

where $[\eta]_{\varphi}$ is the intrinsic viscosity in term of volume fraction. η_{rel} can be determined experimentally. The slope of ln (η_{rel}) versus volume fraction gives the intrinsic viscosity.

6.3. SURFACE WATER DETERMINATION

The associated water fraction, β, is defined as the ratio of surface water to CUPs by weight. It is measured in grams of water per gram of CUPs. The value can be semi-quantitatively calculated by Equation (30) [51]:

$$\beta = \frac{\rho_1}{\rho_2}\left(\frac{[\eta]}{2.5} - 1\right) \tag{30}$$

where ρ_1/ρ_2 is the density ratio of water to CUPs (ρ_1 is 0.997 at 25° C). Further assumption can be made that the CUP particle is spherical and surrounded by a uniform layer of water molecules with thickness, δ, which can be expressed as

$$\delta = R_s[\left(\frac{\beta\rho_2}{\rho_1}\right)^{\frac{1}{3}} - 1] \quad (31)$$

6.4. ELECTROVISCOUS EFFECT IN CUPS

The relative viscosity was determined experimentally for CUPs of different molecular weights at different volume fractions. The intrinsic viscosity is determined from the slope of ln(η_{rel}) versus volume fraction plot. Further, associated water fraction and thickness of water layer were calculated using the intrinsic viscosity values. The values are presented in the Table 4 [6, 8, 9, 13].

Table 4. Associated water fraction, β, and surface water thickness, δ, for CUPs with different functional groups.

CUPs	**Polymer Composition**	**Molecular Weight (Mn/Mw)**	**Intrinsic Viscosity, [η]**	**Associated Water fraction, β**	**Surface water thickness, δ**
COO^- [10, 13]	Polymer 18	28K/35K	9.61	2.3	0.88
	Polymer 19	36K/45K	9.97	2.4	1.02
	Polymer 1	111K/175K	12.37	3.2	1.9
SO_3^- [6]	Polymer 21	28K	9.9	2.47	0.92
	Polymer 22	56K	12.4	3.29	1.55
	Polymer 23	80K	12.8	3.31	1.78
QUAT [6, 8]	Polymer 2	36K	15.8	4.5	1.6
	Polymer 3	55K	17.2	5.0	2.3
	Polymer 4	94K	20.0	5.9	2.9

6.4.1. Electroviscous Effect in COO^- CUPs. There is an increase in the thickness of the surface water layer with the molecular weight and the radius of the particles. This can be explained by bare surface charge density of the CUPs. The bare surface charge density is roughly linear with the cube root of the molecular weight of the polymer. The radius of the particle is also proportional to its molecular weight. Thus, the bare surface charge density is proportional to the particle size. The larger the particle size, the higher the surface charge density is, that is, more carboxylate groups are present on the surface, which forms thicker electrical double layers. This will attract more water molecules to the surface causing thicker water layers and increase in the viscosity [6].

6.4.2. Electroviscous Effect in SO_3^- CUPs. It was experimentally observed that the intrinsic viscosity is higher for the sulfonate-functional CUPs as compared with the carboxylate-functional CUPs of the similar molecular weight (28K) (polymer 21) [8]. This increase is due to high surface water being present, which increases the contribution of tertiary electroviscous effect to the overall viscosity. For similar charge density, the sulfonate group has higher hydration number (i.e., the number of water molecules in the hydration shell) (8–14) than the carboxylate group (5–7) because of higher number of oxygen atoms with which the water molecules can hydrogen bond [58]. For a given volume fraction, the sulfonate functional CUPs have higher effective charge (calculated using Belloni's program [13, 41]) than the carboxylate functional CUPs. The associated water fraction in sulfonate CUPs was found to be higher than the carboxylate CUPs, and this is attributed to the higher effective charge and hydrogen-bonding capability of the sulfonate CUPs [13]. The secondary amide group in AMPS monomer also interacts strongly with water and contributes to the viscosity [59, 60].

6.4.3. Electroviscous Effect in QUAT CUPs. The QUAT CUPs-36K (polymer 2) has higher viscosity than the carboxylate CUPs-36K (polymer 19), which is due to the higher surface water fraction that contributes to tertiary electroviscous effect [8, 9]. The bound water fraction for QUAT CUPs-36K is 4.5 (g of water/g of CUPs) and that of carboxylate CUPs-36K is 2.4 (g of water/g of CUPs) [8, 9]. The counterion in the QUAT CUPs, that is, Cl^-, and the counterion in the carboxylate CUPs, that is, Na^+, both have similar number of associated water molecules in the first hydration shell [61, 62]. The higher viscosity caused by the presence of higher amount bound water fraction is, therefore, attributed to the QUAT groups. Monte Carlo simulations show two hydration shells with a cage-like structuring of the water molecule around the tetramethylammonium (TMA) cation [63, 64]. Molecular simulation dynamics show the hydration number for TMA cation to be 23 [65], which is much higher than that of carboxylate ion (5–7) [66, 67].

6.5. EFFECTS OF SALT ON RHEOLOGY

The ionic atmosphere around the charged particles governs the surface charge density and thus affects the primary and secondary electroviscous effect. It is expected that adding similar electrolytes to the CUPs suspension will screen the ionic repulsion between the charged particles and reduce the viscosity. At higher electrolyte concentration, the associated water on the sodium and chloride ions will associate with the surface water on the CUPs. Thus, an increase in viscosity is expected. The specific viscosities of CUPs (polymer 1) were measured at different concentrations and different level of NaCl (see Figure 7). CUP concentration lower than 7.5% is not affected by

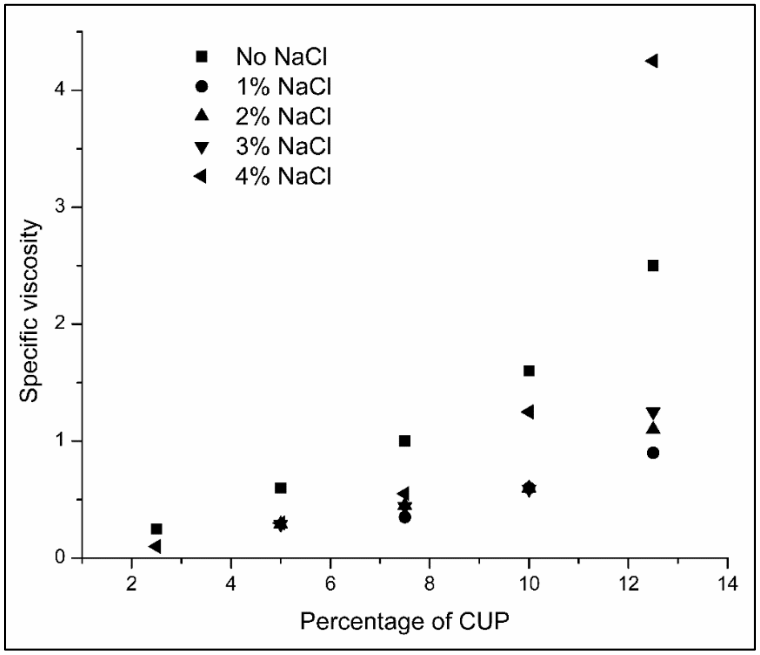

Figure 7. Specific viscosity of CUPs at different concentrations and different levels of NaCl. (Chen 2013 [6]. Reproduced with permission of Minghang Chen.).

addition of salt [6]. When the concentration is 10%, the viscosity drops due to the addition of salt. This is due to the screening effects of the added sodium ions as explained in the previous paragraph. The screening effect compresses the electrical double layer around the CUP particles and reduces the effective surface charge of the particle. This will cause the viscosity to drop. However, at salt concentration of more than 3% and CUP concentration of 12.5%, there was an increase in viscosity. This is due to the associated water molecules around the sodium and chloride ions, which is less mobile than the bulk water. Calculations show the amount of associated water on sodium and chloride ions in a 12.5% CUP solution containing 4% NaCl to be 19% of the total volume. The water can also hydrogen bond with surface water of the CUPs [6].

7. GEL POINT BEHAVIOR

The CUPs are charged particles and stable, even at high concentration, due to the electrostatic repulsion between the particles. The CUPs behave like ions in an ionic crystal positioning at equal distance from the nearby particles. The gel point behavior study gives an idea of the packing CUPs can undergo and also the properties of the bound water on the surface of the particle [5].

7.1. PACKING IN CUPS

The Kepler conjecture states that no arrangement of equally sized spheres filling a space has a greater average density than that of the cubic close packing (face-centered cubic) and hexagonal close packing arrangements. The maximum packing density for a sphere is 0.7405 which means 74.05% of the volume is occupied by the spheres [68]. When the particles in the suspension reach the maximum packing density of 0.7405, it will reach the maximum density as a solid, that is, the viscosity will reach infinity. This type of packing is called regular packing. Other types of regular packing include tetrahedral lattice, cubic lattice, and hexagonal lattice that have maximum packing densities of 0.3399, 0.5233, and 0.6043, respectively. The maximum packing volume fraction for the irregular packing is random close packing (RCP). Recent analytical and experimental work shows the RCP to be not more than 0.634 [69]. The CUPs due to electrostatic repulsion between the particles tend to arrange themselves at equal distance from each other like ions in ionic crystals. One can hypothesize the final structure of CUPs solid to be face-centered cubic, which is the most stable ionic structure. However,

the CUPs do not have a single particle size but a range. Hence, the maximum packing volume fraction for CUPs could be between RCP, 0.634, and hexagonal close packing, 0.7405 [6].

7.2. GEL POINT STUDY

7.2.1. Determination of Gel Point. The gel point of the CUPs suspension can be reached by evaporating the water in a vacuum desiccator with sodium hydroxide as the drying agent. Solid-like material can be obtained after several days of drying. However, this method has several issues. The evaporation is not homogenous as the suspension is not being stirred. The water molecules will evaporate slowly when the suspension is close to the gel point making it difficult to tell whether the suspension has reached the true gel point. This method cannot be used for accurately measuring the gel point. Instead, the gel point is determined using the viscosity increase with volume fraction [1].

The relative viscosity of suspension in the high-volume fraction range usually follows the Krieger–Dougherty equation [57]:

$$\eta_r = [1 - \frac{\phi}{\phi_{max}}]^{-[\eta]\phi_{max}} \quad (32)$$

where ϕ_{max} is the packing volume fraction when the viscosity of the suspension diverges and $[\eta]$ is the dimensionless intrinsic viscosity of the suspension. The relative viscosity at different volume fractions can be fit to the Krieger–Dougherty equation with $[\eta]$ and ϕ_{max} as fitting parameters. When the effective volume fraction of particles, including the bound layer of surface water, reaches the RCP value of 0.634, the viscosity of the suspension reaches infinity. With this assumption, the thickness of the water layer, δ, can be calculated using Equation (33):

$$\phi_{max}(1 + \delta/r)^3 = 0.634 \quad (33)$$

The volume fraction is calculated by $\phi = \rho_s f / \rho_p$ where ρ_s is the density of suspension, f is the mass fraction of the CUP in suspension, and ρ_p is the density of the CUP

7.2.2. Viscosity measurements. The shear viscosity of CUPs (polymer 1) measured at different volume fractions show that shear thinning behavior increases as the volume fraction of the CUPs increase. This increase is due to the balance between Brownian motion and repulsive force among the CUP particles [70]. At low volume fractions, the Brownian motion is dominant, and the suspension is in a random disordered state. The distance between the CUPs is so large that the repulsive force interactions are Electroviscous Effect in COO^- CUPs. There is an increase in the thickness of the surface weak. The repulsive forces begin to dominate as the volume fraction increased, and the CUPs form a pseudo-lattice structure, which is unstable under shear.

The shear thinning can be explained by fitting the data with Casson's model [71]:

$$\sqrt{\tau} = \sqrt{\tau_0} + \sqrt{\eta_c \dot{\gamma}} \quad (34)$$

where τ_0 is the yield stress, that is, the minimum stress to flow, η_c is the plastic viscosity, $\dot{\gamma}$ is the shear rate, and τ is the shear stress. Data from Ref. [5] showed zero yield stress for low volume fractions ($\leq$0.062) implying Newtonian behavior of the suspension. The yield stress increases as the volume fraction increases ($\geq$0.062), indicating a rise in shear thinning behavior. CUPs with volume fraction 0.083 to 0.288 (more than 0.062) that show shear thinning behavior by Casson's model were further studied using Cross's semiempirical model [72]. The zero-shear viscosity and the limiting high shear viscosity were estimated using Equation (35):

$$\eta_r = \eta_{r\infty} + (\eta_{r0} - \eta_{r\infty})/[1 + (b\tau)^m] \quad (35)$$

where η_r is the relative viscosity of the suspension, $\eta_{r\infty}$ is the limiting high shear relative viscosity, η_{r0} is the zero-shear relative viscosity, τ is shear stress, and b and m are fitting parameters. The relative viscosity and shear rate (for volume fraction 0.083 to 0.288) were fitted using Equation (35) to get the zero-shear viscosity and limiting high shear viscosity. The fitting results showed significant shear thinning behavior for volume fractions higher than 0.171. This volume fraction (0.171) for CUPs is significantly lower than that observed for the charge stabilized poly(styrene-co-ethylacrylate) 250 nm particles [73] in water, which show shear thinning for volume fractions higher than 0.34. This difference can be explained by long-range charge–charge interactions. The charge densities for CUPs that vary between 0.01 and 0.02 C m^{-2} was similar to that of normal latex particle, which is normally in the range of 0.01–0.07 C m^{-2} [6, 74]. However, at the same volume fraction, the interparticle between the CUPs was much smaller than that of the latex particles. The interparticle distance was proportional to the diameter of the particles. CUPs have very small diameter (3–7 nm) as compared with size of latex particles. CUPs can, therefore, readily form a pseudo-lattice structure, which is not shear stable, and show shear thinning behavior.

For studying the gel point, the zero-shear viscosities of suspensions with a volume fraction higher than 0.171 were fitted to Cross's model. The viscosities of the suspension with a volume fraction lower than 0.171 were measured using Ubbelohde capillary viscometer. These suspensions were treated as Newtonian fluids as they do not show significant shear thinning behavior and are closer to Newtonian fluids than to shear thinning fluids.

7.2.3. Maximum Packing Volume Fraction, Density and Thickness of Surface Water.

The Krieger–Dougherty equation can be used to fit the viscosities and determine the maximum packing volume fraction at the gel point [5, 57]. This equation also applies to zero-shear viscosities of the CUP suspension with high volume fraction. The fitting results of the viscosities of the CUP (polymer 1) (M_n =111K and M_w =174K) suspensions against volume fraction give the fitting parameters ϕ_{max} =0.394 and [η]=14.1. The value of intrinsic viscosity was similar to spherical polyelectrolytes that are highly charged, which indicates that surface of the CUPs was also highly charged. The maximum packing volume fraction of 0.394 was low due to the large amount of bound or surface water being present [75]. Further calculations were done with two assumptions: First, the shape of CUPs was spherical and the layer of surface water around the sphere was homogenous; second, CUPs along with the surface water reach an RCP (0.634) even though the actual volume fraction of CUP was 0.394. The thickness of the water layer can then be calculated from Equation (36) as

$$\delta = \left(\sqrt[3]{\frac{0.634}{0.394}} - 1\right) \times 3.3 = 0.57nm \tag{36}$$

Assuming the RCP in CUPs with bound or surface water being present, the volume fraction of surface water will be 0.634−0.394=0.24. The volume fraction of free water between the particles is 1−0.634=0.366. Assuming 1 ml suspension of the CUP, the densities can be related as follows:

$$\rho_p\phi_p + \rho_{H_2O,B}\phi_{H_2O,B} + \rho_{H_2O,S}\phi_{H_2O,S} = \rho_s \tag{37}$$

where ρ_s is the density of suspension, ρ_p is the density of the CUP, $\rho_{H2O,S}$ is the density of the surface water, ϕ_p is the volume fraction of the CUP, $\phi_{H2O,S}$ is the volume fraction of

surface water, and $\phi_{H2O,B}$ is the volume fraction of the bulk water. The density of the CUP suspension at the gel point was 1.1077 g ml^{-1} , which was obtained by extrapolating densities measured at different volume fractions (from 0 to 0.1). The density of surface water calculated using Equation (37) was 1.0688 g ml^{-1}, which was 7.19% larger than that of bulk water at 25° C. This implies that the water on the surface of the particles is more compact than bulk water.

The density and the water layer thickness values can be validated by simple arithmetic calculation based on the relationship between surface water, bulk water, and particle volume fraction. Now, the summation of volume fraction of CUP particle, surface water, and bulk water is one, as shown in Equation (38):

$$\phi_p + \phi_{H_2O,B} + \phi_{H_2O,S} = 1 \tag{38}$$

There exists a conservation of mass of total material as given by Equation (39):

$$m_s = m_p + m_{H_2O,B} + m_{H_2O,S} \tag{39}$$

Where,

$$m_p = \rho_s f \tag{40}$$

$$m_{H_2O,S} = \rho_{H_2O,S}\phi_{H_2O,S} \tag{41}$$

$$m_{H_2O,B} = \rho_{H_2O,B}\phi_{H_2O,B} \tag{42}$$

and m denotes mass of each material. Using Equation (39) through (42), along with the relation between volume fraction of particle and surface water, which is Equation (43), Equation (38) can be solved, and we get

$$\frac{1}{\rho_s} = kf + b \; where \; b = \frac{1}{\rho_{H_2O,B}} \; amd \; k = \frac{(1+\frac{\delta}{r})^3}{\rho_p} - \frac{1}{\rho_{H_2O,B}} - \frac{\rho_{H_2O,S}}{\rho_p \rho_{H_2O,B}}\left[\left(1+\frac{\delta}{r}\right)^3 - 1\right]$$

$$\phi_{H_2O,S} = \left[\left(1 + \frac{\delta}{r}\right)^3 - 1\right]\phi_p \quad (43)$$

The densities (ρ_s) measured at various mass fractions (f) of CUP (M_n =111K and M_w =174K) (polymer 1) suspension were plotted as $1/\rho_s$ against f. The plot was linear, and the slope was k = −0.2282. Thus,

$$k = \frac{(1+\frac{\delta}{r})^3}{\rho_p} - \frac{1}{\rho_{H_2O,B}} - \frac{\rho_{H_2O,S}}{\rho_p \rho_{H_2O,B}}\left[\left(1 + \frac{\delta}{r}\right)^3 - 1\right] = -0.2282 \quad (44)$$

If the values of δ =0.57 nm and $\rho_{H2O,B}$ =1.0688 g ml^{-1} calculated before are plugged in the left side of the Equation (44), we get the value −0.22845, which is just 0.11% off from the measured value −0.2282. This verifies that the thickness, 0.57 nm, and density of bound water, 1.0688 g ml^{-1}, were good estimates from the Krieger–Dougherty equation.

The hydrophobic part of the CUPs can only adsorb up to 2% w/w of water, which accounts for 2.46% increased volume in CUPs [76, 77]. This increase is very small as compared with the increase in volume fraction by surface water, which is 61% of the CUP volume for a CUP particle of 3.3 nm radius. This gives conclusive evidence that most of the bound water is located on the surface of the CUPs.

7.3. COMPARISON WITH COMMERCIAL RESIN LIKE LATEX AND POLYURETHANE DISPERSION

For a large particle like a latex resin with radius of 100 nm, assuming the thickness of surface water to be same as CUPs, the ratio of surface water to latex by volume is only 1.72% [5]. The particle size and thickness of bound water layer have a significant effect on maximum volume fraction, ϕ_{max}. This can be understood from Figure 7.8, showing a plot of calculated volume fraction at gel point as a function of

particle size and thickness of bound water layer. For particles with same bond water thickness, ϕ_{max} drops with particle size, especially for thicker water layers. For particles of same size, the ϕ_{max} decreases as the bound water layer gets thicker, especially in smaller particles.

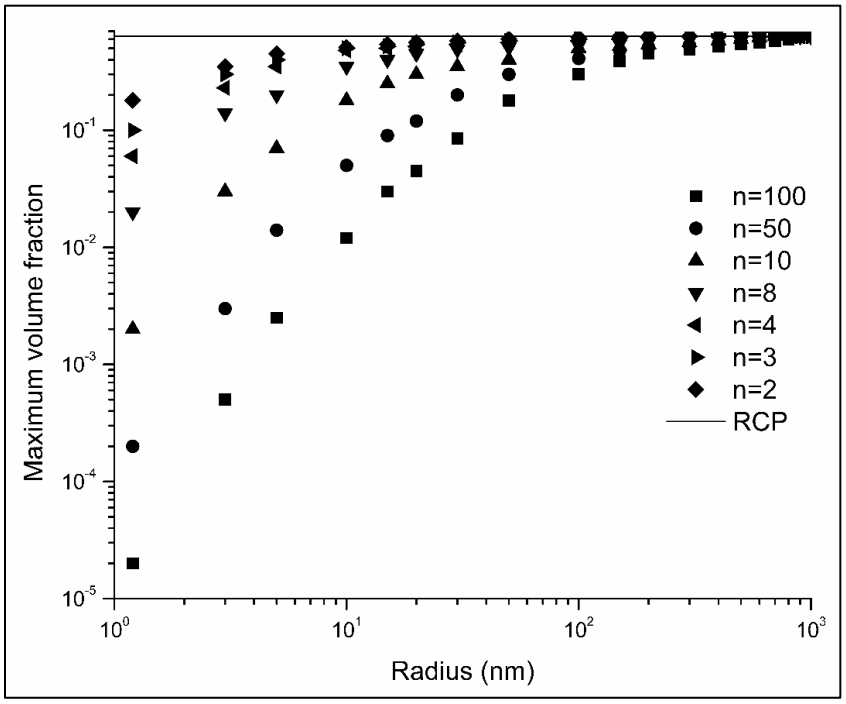

Figure 8. Calculated volume fraction at gel point as function of particle size and thickness of bound water layer (n is the number of water layers, RCP is random closed packing). (Chen et al. 2013 [5]. Reproduced with permission of Springer.).

The effect of particles can be observed in the viscosity behavior of waterborne polyurethane (25 nm) and latex (77 nm) particles. The relative viscosities at different volume fractions were measured, and the intrinsic viscosity was determined to be 8.0 and 5.5 for urethane and latex, respectively [57]. If we assume the thickness of the surface water layer to be 0.57 nm for both urethane and latex, then using Equation (33) the ϕ_{max}

are 0.55 and 0.6 for urethane and latex, respectively. The Krieger–Dougherty's equation can be used to predict theoretical relative viscosities of the urethane and latex as shown in Equation (45) and (46):

$$\eta_{r1} = \left(1 - \frac{\phi}{0.55}\right)^{-[\eta]_1 \times 0.55} \quad for\ waterborne\ urethane \tag{45}$$

$$\eta_{r2} = \left(1 - \frac{\phi}{0.60}\right)^{-[\eta]_2 \times 0.60} \quad for\ latex \tag{46}$$

The data of relative viscosities at different volume fractions show that the viscosity of CUPs was larger than waterborne urethanes and latex at a given volume fraction (Figure 9).

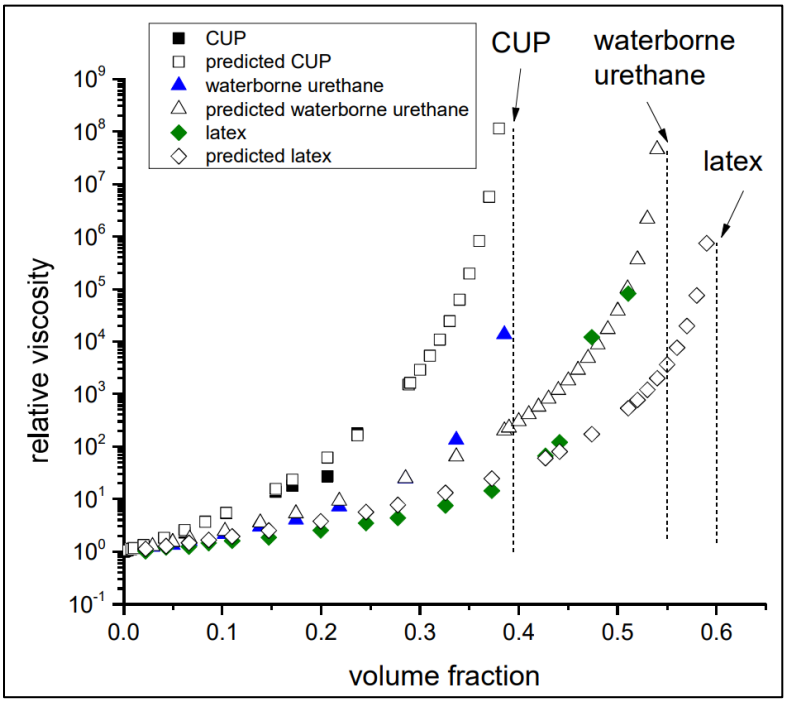

Figure 9. Relative viscosities at different volume fraction. (Chen et al. 2013 [5]. Reproduced with permission of Springer.).

This confirms the hypothesis that surface water has more effect on rheology in smaller particles as compared with that in larger particles for same thickness of water layer. The deviation of the experimental results from the predictions in case of latex and urethanes at high concentrations can be due to residual surfactants or rheology modifiers that are not present in CUPs. The absence of interfering residuals is a major advantage of using CUPs as model material for studying the gel point behavior of charged particles [5, 6].

8. SURFACE TENSION BEHAVIOR

Surface tension is the energy required to increase the surface area of a liquid. There are several methods of measuring surface tension, such as ring method, drop methods, oscillating jet method, and maximum bubble pressure method [78]. The maximum bubble pressure method was used to evaluate the surface tension of CUPs suspensions [8, 14].

The maximum bubble pressure method can measure both equilibrium and dynamic surface tension of suspension as long as the surface age is properly controlled. The surface age is the time interval between the beginning of bubble growth and the moment of maximum bubble pressure. As surface age is increased, the bubble rate is reduced, which gives CUP particles more time to migrate to the air (bubble)–water interface and change the surface tension [79].

8.1. EQUILIBRIUM SURFACE TENSION BEHAVIOR

8.1.1. Effect of Concentration on Equilibrium Surface Tension. Figure 10 shows a plot of equilibrium surface tension behavior of three sulfonate-functional CUPs versus concentrations [8]. For comparison, surface tension of carboxylate-functional CUP with molecular weight of 28K is also shown in the graph.

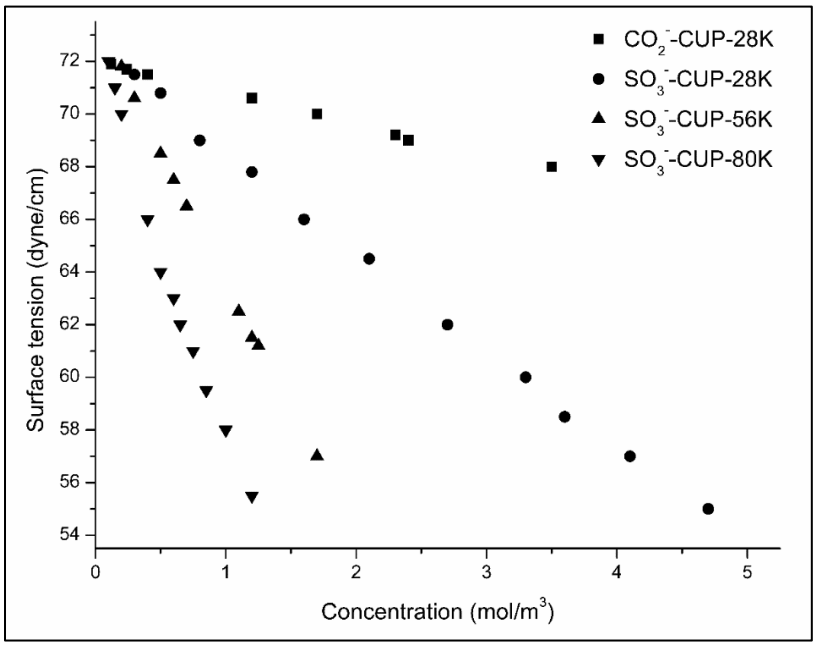

Figure 10. Equilibrium surface tension behavior of different CUPs versus concentration. (Natu 2015 [8]. Reproduced with permission of Ameya M. Natu.).

The equilibrium surface tension of all the four CUP suspensions decreased linearly with increasing concentration of the CUPs. The reduction in surface tension was similar to that observed for typical surfactants; the higher the concentration of surface-active groups, the lower the surface tension will be. Typical surfactants show a critical micelle concentration (CMC), above which the surface tension does not change;

however, no such point was observed in our CUP suspensions in the concentration range of 1–5 mol m^{-3}.

The relationship between concentration of surface-active groups and surface tension is expressed by the equation below [8]:

$$\gamma - \gamma_w = k(^{d\gamma}/_{dc}) \quad (47)$$

where γ_w is the surface tension of pure water, k is the slope, and c is the concentration (mol m^{-3}). Since k is a negative value, as the concentration c goes up, γ will decrease linearly.

This can be explained by Manning condensation [41]. Increasing the CUPs concentration also increases the counterion concentration, some of which condenses on the surface of CUP particles reducing its effective charge. The counterion condensation makes effective charge lower than bare surface charge and allows more CUP particles with better packing at air–water interface. As a result, the total number of charged groups at the air–water interface increases. Therefore, the electrostatic repulsion also increases and then reduces the surface energy of the system. Thus, less work is required to distort the surface and the surface tension becomes lower [80].

8.1.2. Effect of Molecular Weight on Equilibrium Surface Tension. The equilibrium surface tension of sulfonate-functional CUPs decreased with increasing molecular weight [8]. The decrease in surface tension was due to the increase in the number of charged groups on the surface of CUP particle as molecular weight increased. The individual polymer chain was composed of 9 : 1 ratio of MMA:AMPS on an average. Polymer with molecular weight of 28, 56, and 80K (polymer 21, polymer 22, polymer 23) had on average 25, 51, and 72 sulfonate groups on the surface of particle,

respectively. Large amount of charged surface active groups reduced the surface energy via electrostatic repulsion and therefore reduced the surface tension.

8.1.3. Effect of Surface-Active Groups on Equilibrium Surface Tension. The sulfonate-functional CUPs showed higher surface activity than the carboxylate-functional CUPs [8]. As shown in Figure 10, for similar molecular weight (28K) (polymer 21), the slope k of SO_3^- CUPs was more negative than CO_2^- CUPs (polymer 18). Compared with CO_2^- CUPs, SO_3^- CUPs are more efficient in decreasing the surface tension to a degree. The reason is that SO_3^- CUPs have higher effective charge than CO_2^- CUPs at each volume fraction due to which the surface energy, and the surface tension is reduced to a greater extent.

Another reason could be the contact angle reduction caused by the particles at the interface. Typically, as the surface tension decreases, the contact angle of the adsorbed particle at the air–water interface becomes smaller [81, 82]. Cooper [83] had demonstrated that the sulfonate group, being more hydrophilic and polar than carboxylate one, gave lower contact angle at the air water interface. Therefore, the sulfonate-functional CUPs gave lower surface tension than carboxylate-functional CUPs.

Unlike sulfonate-functional CUPs, the quaternary ammonium-functional CUPs showed similar surface activity to the carboxylate-functional CUPs. This was possible because the similar polarities and effective charge of the hydrophilic quaternary ammonium and carboxylate groups resulted in similar reduction of surface energy via electrostatic repulsion.

8.2. DYNAMIC SURFACE TENSION BEHAVIOR

Figure 11 shows a plot of dynamic surface tension behavior of three sulfonate-functional CUPs versus surface age at a concentration of 0.5 mol m^{-3}. For comparison, surface tension of carboxylate-functional CUP with molecular weight of 28K was also shown in the graph [8].

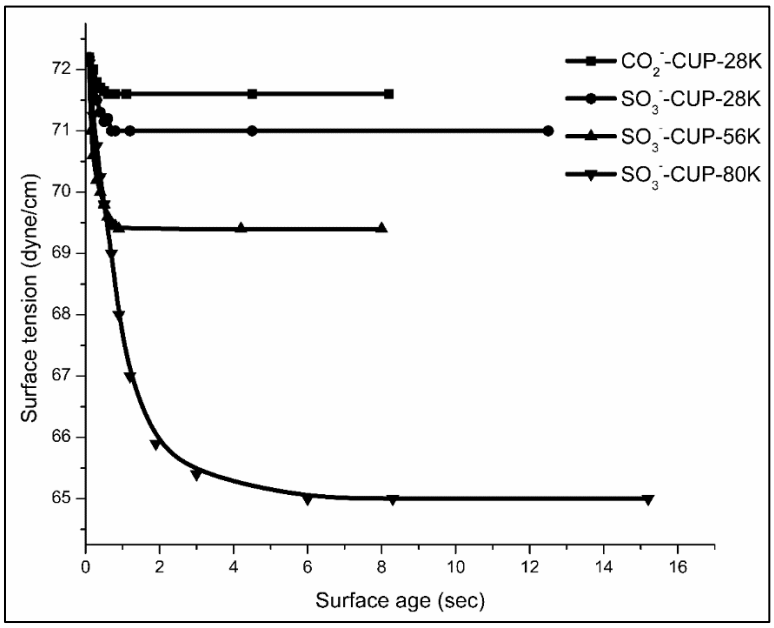

Figure 11. Dynamic surface tension behavior of different CUPs versus surface age at a concentration of 0.5 mol m−3. (Natu 2015 [8]. Reproduced with permission of Ameya M. Natu.).

The data gave a good exponential fit represented by the Equation (48):

$$\gamma - \gamma_e = A * exp\left(-\frac{t}{\tau_k}\right) \tag{48}$$

where γ_e is the equilibrium surface tension, A and τ_k (the kinetic relaxation time) are the fitting parameters, and τ_k is the half-life for the surfactant to reach equilibrium surface tension. It indicates the barrier to surface adsorption via electrostatic repulsion.

8.2.1. Effect of Molecular Weight on Kinetic Relaxation Time. Table 5 indicated that the kinetic relaxation time, τ_k, increased with increasing molecular weight, which means that CUP particles with high molecular weight took longer time to reach the equilibrium surface tension [8].

Table 5. Relaxation time (τ_k) for three sulfonate CUPs at various concentrations [8].

SO_3^- CUP	**Concentration (mol m^{-3})**	**τ_k (s)**	**R^2**
28K	0.50	0.084	0.995
28K	1.01	0.234	0.999
28K	1.48	1.324	0.992
28K	1.97	1.431	0.993
56K	0.25	0.083	0.997
56K	0.50	0.136	0.999
56K	1.04	0.242	0.999
56K	1.76	1.007	0.997
80K	0.25	0.527	0.998
80K	0.50	0.990	0.980
80K	1.01	2.436	0.996
80K	1.25	3.135	0.993

This can be explained by the diffusion coefficient D expressed by the Stokes–Einstein equation mentioned below [84]:

$$D = \frac{k_b T}{6\pi\eta r} \quad (49)$$

where k_b is the Boltzmann constant, T is the absolute temperature, η is the viscosity of the solvent, and r is the radius of the particle. The radius r of the particle can be related to the molecular weight of polymer, M_n:

$$r = \frac{1}{2}\sqrt[3]{\frac{6Mn}{\pi\rho_p N_A}} \quad (50)$$

where M_n is the number-average molecular weight, N_A is the Avogadro constant, and ρp is the bulk density of polymer. As molecular weight of polymer goes up, the radius of the CUP particle increases, which results in lower diffusion coefficient. Therefore, the SO_3^- CUP-80K having greater value of τ_k could be explained by a slower diffusion of the higher molecular weight CUP to the air–water interface [8].

8.2.2. Effect of Concentration on Kinetic Relaxation Time. Table 5 also indicated that τ_k increases with increasing concentration. CUPs of higher concentration took longer time to reach the equilibrium surface tension [8]. Viscosity plays an important role in this phenomenon. The viscosity of CUP solution increases with increasing concentration, which lowers the diffusion coefficient D. According to the Stokes–Einstein equation (Equation 49), diffusion coefficient $D \propto 1/\eta$. Therefore, slower diffusion of CUP particles leads to larger kinetic relaxation time τ_k. Although increasing the concentration could also increase the probability of a CUP particle getting adsorbed at the air–water interface and decreases the distance required to travel in order to reach the interface, the overall effect was an increase in the relaxation time to reach the equilibrium surface tension

8.2.3. Effect of Molecular Weight on Dynamic Surface Tension. The dynamic surface tension γ decreased with increasing molecular weight as shown in Figure 11. High molecular weight CUPs cause greater reduction in dynamic surface tension because they have more surface-active groups per unit area. This increased charge density causes a greater drop in the surface energy and therefore a drop in the surface tension.

8.2.4. Effect of Concentration on Dynamic Surface Tension. Figure 12 shows the effect of concentration on dynamic surface tension for SO_3^- CUPs-28K. The dynamic surface tension decreases with increasing concentration, which was attributed to a greater reduction in surface energy due to the higher number of surface-active groups at the air–water interface. The mechanism is same as the effect of concentration on equilibrium surface tension.

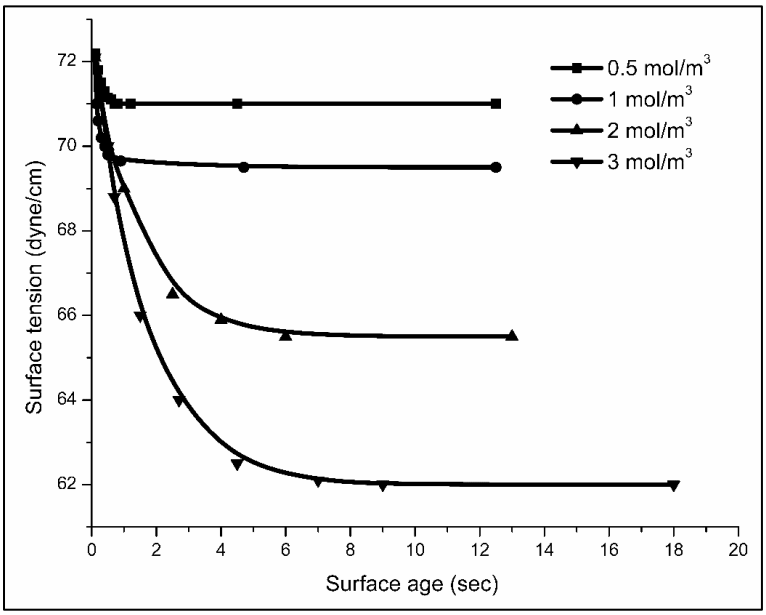

Figure 12. Effect of concentration on dynamic surface tension for SO_3^- CUPs-28K. (Natu 2015 [8]. Reproduced with permission of Ameya M. Natu.).

9. CUP SURFACE WATER

CUPs have hydrophilic functional groups on their surface, which can associate with water and produce a “bound or surface water layer” on it. This layer and any charges keep the polymer from aggregation and also affect many of the CUP properties. The term “bound water” was first raised by Newton and Gortner [85] in 1922 that there is certain amount of water existing in close proximity to constituent particles in hydrophilic colloids. The bulk water is not bounded to the colloidal particles, instead, bulk waters exist freely in solution. These molecules are considered to be freely moving in the solution media. Since the particle size of CUPs is very small, ranges from 3 to 9 nm, the surface area is relatively large. Therefore, many properties of the CUP system are dominated by the associated surface water. It is important to define its science.

9.1. ELECTROVISCOUS EFFECT AND GEL POINT

The previously discussed electroviscous effect and gel point defined the higher density and an estimate of the thickness of the water layer. These studies were good evidence of the surface layer, but the use of other analytical approaches is needed to confirm the bound water layer.

9.2. DIFFERENTIAL SCANNING CALORIMETRY

Surface water has been investigated in many systems [86, 87] with the finding that bulk water freezes near 0° C, but surface water does not freeze until below −40° C with some bound water not freezing until below −100° C [88, 89]. Examples of this bulk and bound water have been found in proteins [90] and hydrogels [91]. In DSC, for the

CUP system, there are potentially three forms of water: (i) bulk or free water, which freezes conventionally at around 0° C, (ii) bound non-freezing water, and (iii) bound water that freeze at very low temperature. It has been very difficult to determine the existence of bound water in biological and colloidal systems. In the past, many studies have been made; DSC has the potential to measure the heat of fusion of the water system, which gives the possibility of distinguishing the types of water present in the samples. Based on the heat of fusion of the free water versus total water present, the amount of the surface water in each CUP (W_b) could be determined from Equation (51) and (52):

$$W_f = {}^{\Delta H_c}\Big/_{\Delta H_f} \tag{51}$$

$$R_1 = W_t(1 - c) - W_f \tag{52}$$

where W_f is the weight fraction of freezable water, ΔH_c is the heat absorbed during the melting procedure with CUP (as measured from the area of the endothermic peak in the DSC scan), ΔH_f is the heat of fusion of the standard solution (pH modified water), W_t is the weight fraction of total sample, and C is the weight percent CUP of the sample.

DSC scans were used to determine the enthalpy of the freezing transition of water in CUP samples. The DSC of water without CUP was used to define the maximum enthalpy of free water during the melt cycle (ΔH_f) (Figure 13, continuous line). The heat of fusion of the tested CUP sample (ΔH_c) was obtained from the area under the peak of the corresponding DSC scan (Figure 13, dotted line).

Figure 14 shows that upon increasing the CUP concentration, the area of the DSC peak decreases, which indicates that less free water is present in the samples. The results obey Raoult's law producing a linear relationship between the heat of fusion and the concentration of the CUP over the range studied (0–20%).

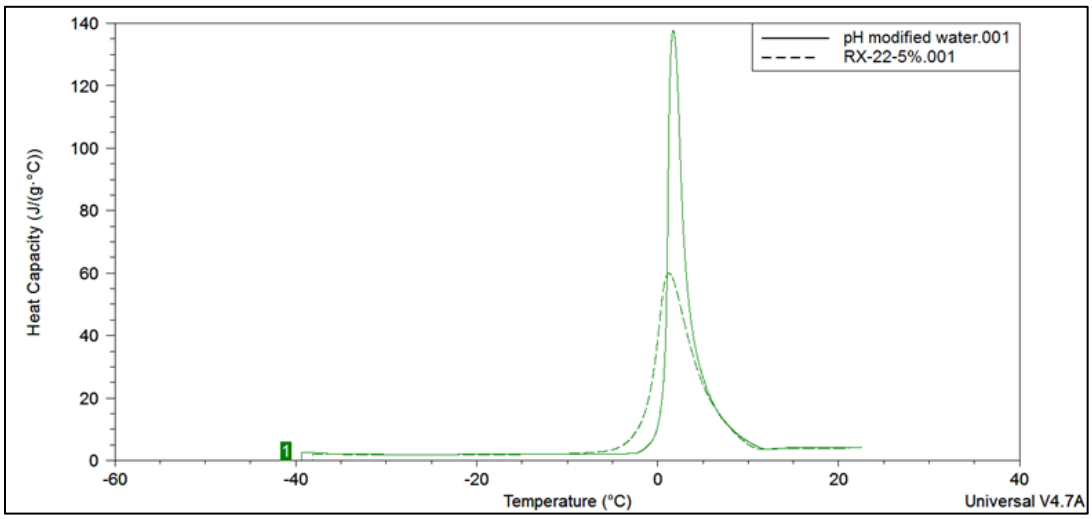

Figure 13. The heat of fusion of water (continuous line) and CUPs from polymer 1 (dotted line).

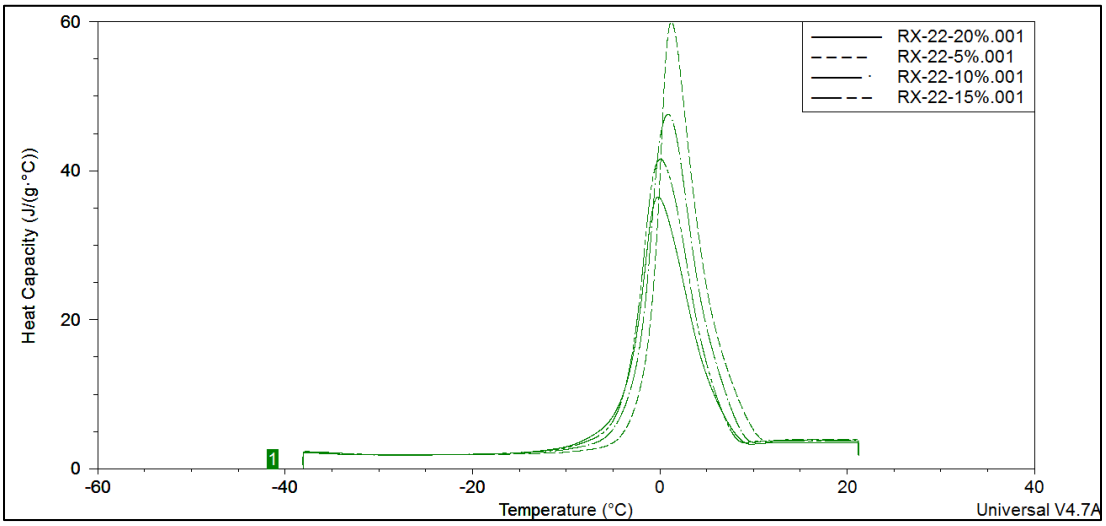

Figure 14. The specific enthalpy of CUPs from polymer 1 at different concentrations: 5, 10, 15 and 20%, respectively.

Figure 15 illustrates the weight fraction of the surface water versus concentration of the suspension for CUPs prepared from different polymers (1, 33, and 34; see Table 1).

If we assume that each polymer chain collapse into a dense sphere and the density was the same as the bulk polymer, we can calculate the thickness of the surface water by knowing the amount of the weight fraction of the surface water and the diameter of the particles. The bare surface charge density is proportional to particle size; the bigger the size, the higher the charge density, which associates more water on the surface.

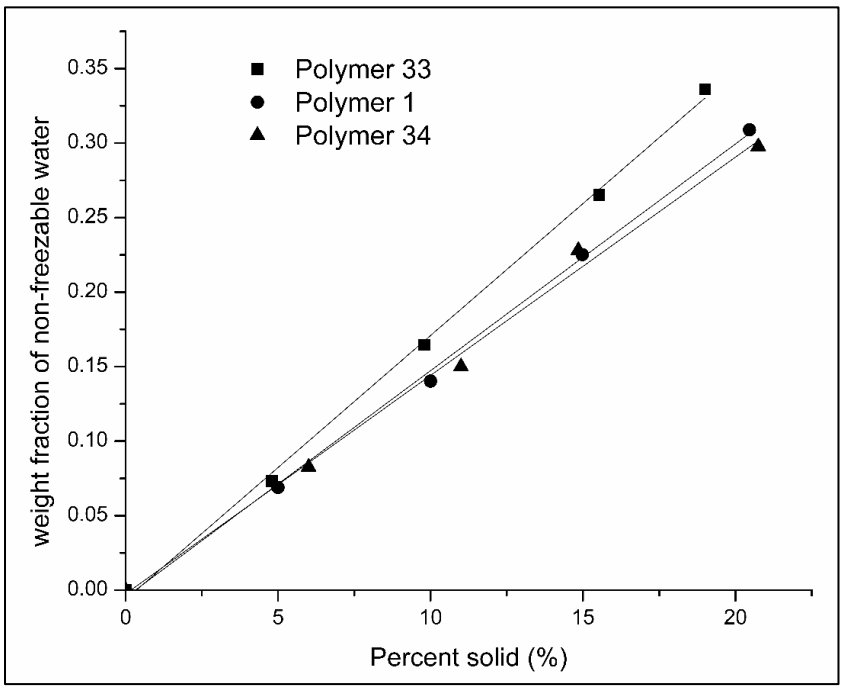

Figure 15. Comparison of weight fraction of non-freezable water versus percent solid for CUPs prepared from different polymers (see Table 7.1).

9.3. NMR RELAXATION STUDY

The spin–lattice relaxation is the heat transfer process of the nuclear spin transition energy to the surrounding. The time constant, T_1, describes how the

longitudinal M_z component of the magnetization vector returns to its equilibrium value M_0 according to Equation (53):

$$M_z = M_o \left[1 - 2\, exp\left(-\frac{t}{T_1}\right)\right] \tag{53}$$

The CUP surface water and the free water have different H^1 NMR relaxation rates that are due to the difference in their mobilities. Bound water has lower mobility than free bulk water [91, 92]. The protons in bound water have lower spin–lattice relaxation time constants (T_{1b}) than the proton in free water molecules (T_{1f}). The proton NMR spin–lattice relaxation time constant, T_1, in water solvent was studied at different concentration and different temperatures.

9.3.1. Proton NMR Spin-Lattice Relaxation Time Constant Versus CUP Concentration. The NMR study shows decrease in T_1 values with increase in CUP concentration indicating an inversely proportional relation between T_1 and CUP concentration [7]. The measured T_1 values from the mono-exponential analysis are the weighted average value of the spin–lattice relaxation time constant for protons in bound water (T_{1b}) and in free water molecule (T_{1f}). However, the lowering of the T_1 with increasing concentration is due to the different contribution from each phase (T_{1b} and T_{1f}) in lowering the T_1 values. The experimental data in Figure 16 indicates the decrease in T_1 due to the increase in the contribution of T_{1b}. The T_1 should therefore be analyzed on the basis of a bi-exponential recovery model given by Equation (54)

$$\frac{1}{T_1} = \frac{\phi}{T_{1b}} + \frac{1-\phi}{T_{1f}} \tag{54}$$

where ϕ is the fraction of bound water molecules and is given by

$$\phi = \frac{N_b}{N_b + N_f} \tag{55}$$

where N_b is the number of bound water molecules and N_f the number of free water molecules.

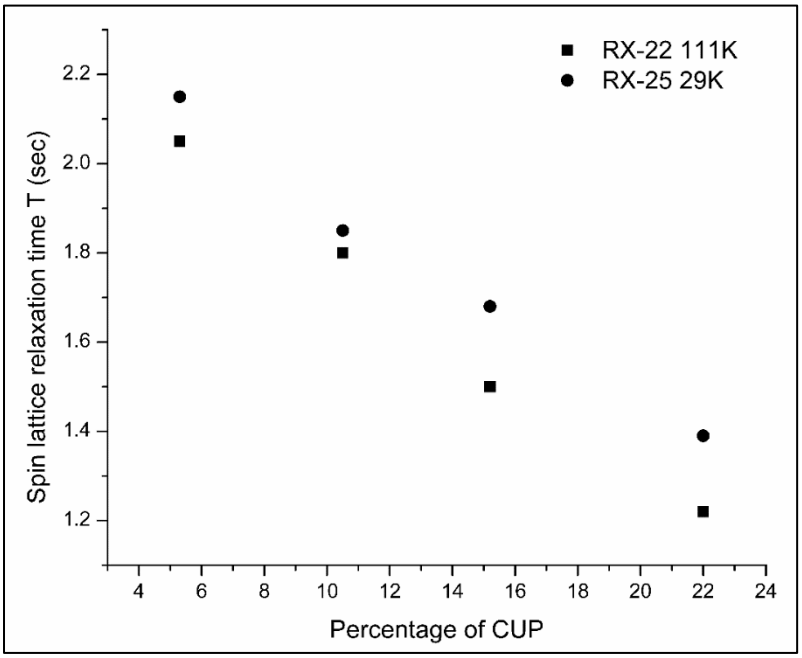

Figure 16. Spin–lattice relaxation time at 18 ∘C for high and low molecular weight CUPs at different concentrations. (Dawib 2015 [7]. Reproduced with permission of Y A Dawib.).

At the same CUP concentration, the spin-lattice relaxation time constant, T_1, for high molecular weight CUP (polymer 1, 111K) is smaller than that of lower molecular weight CUP (polymer 48, 29K). This is because high molecular weight CUP particles have a large amount of bound water associated due to the greater surface charge density per unit area, they have than the lower molecular weight CUP particles. The difference is more pronounced at higher concentrations of CUP again likely due to Manning condensation effects.

9.3.2. Proton NMR Spin-Lattice Relaxation Time Constant Versus Temperature.

With an increase in temperature, the rate of molecular motion of waters increases and so does the T_1 values (Figure 17). The increase is linear for pure water but deviates slightly from linearity for CUP solution, which is probably due to two types, bound and free water, being present. The temperature has influence on the diffusion coefficient, D, of the bulk water, which can be represented by Stokes–Einstein equation (see Section 5.2.1).

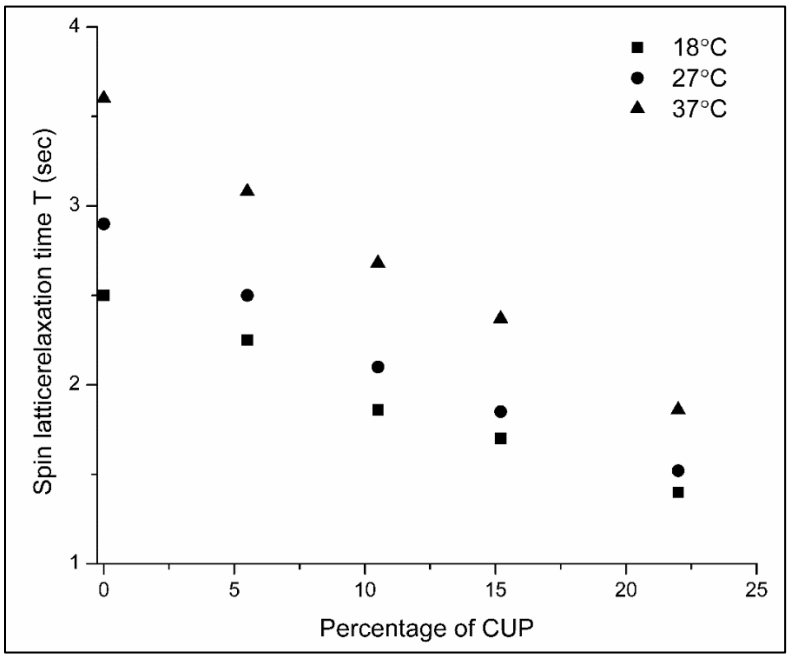

Figure 17. Spin–lattice relaxation time for low molecular weight CUPs at different concentration and at different temperatures. (Dawib 2015 [7]. Reproduced with permission of Y A Dawib.).

The diffusion coefficient of water molecules is directly proportional to temperature and inversely proportional to the viscosity. The viscosity of the CUP increases with increase in concentration and so the diffusion constant decreases. The

proton NMR spin–lattice relaxation time constant, T_1, is related to the diffusion coefficient, viscosity, and temperature by the following equation:

$$T_1 \propto D \propto \frac{T}{\eta} \propto exp\left(\frac{-E}{RT}\right) \quad (56)$$

where E is the activation energy and R is gas constant. The increase in the T_1 values with increasing temperature can be attributed to the increase in the diffusion coefficient of water molecules

9.3.3. Calculation of Bound Water Amount. To calculate the amount of bound and free water in the CUP system as well as the T_{1b} and T_{1f}, the proton spin inversion recovery data was analyzed by the following model equation [93]:

$$F(t) = \sum_{i=1}^{n} A_i(1 - 2exp^{-t/T_{1i}}) \quad (57)$$

The calculation shows that the bound water fraction varies linearly with CUP concentration up to 15% but deviates at higher concentration due to deviation in surface charge density. CUPs have negative charges on their surface due to the carboxylate groups. According to Manning counterion condensation [40], high concentration of ions causes the counterion condensation. There are two types of counterion condensation: short-range condensation due to the repulsion between the neighboring charges on the same particle and long-range condensation due to charge repulsion between the two particles. The long-range counterion condensation is more pronounced at high concentration. Calculations using the Belloni program [13] show decrease in effective charge with increase in CUP concentration [6]. The counterion condensation at high concentration results in shortening of the electrical double layer due to accumulation of ions. This reduces the thickness of the bound water layer.

Table 6. Bound water layer thickness calculated for high and low molecular weight CUPs at different temperatures and different concentrations [7].

Approximate concentration (%)	**Bound water layer thickness in nm for low molecular weight polymer (29K) at different temperatures**			**Bound water layer thickness in nm for low molecular weight polymer (111K) at different temperatures**		
	18° C	**27° C**	**37° C**	**18° C**	**27° C**	**37° C**
5	0.45	0.48	0.52	0.63	0.67	0.69
10	0.41	0.43	0.46	0.56	0.60	0.63
15	0.34	0.36	0.39	0.52	0.55	0.57
22	0.23	0.21	0.19	0.53	0.33	0.30

The thickness of the bound water layer can be calculated by relating the results to a microscopic model of the CUP system. The weight of the bound water can be calculated by using Equation (58):

$$\phi = \frac{m_{bound}}{100 - m_{cup}} \tag{58}$$

where m_{bound} is the weight of bound water and m_{cup} is the weight of CUP (the total weight of CUP solution was 100 g). The total volume of bound water is calculated by dividing the weight of bound water by the density of bound water, which is equal to 1.0688 g cm^{-3} [5]. The diameter of a single CUP spheroid is measured by DLS, which can be used to calculate the surface area of the particle. Finally, the water layer thickness can be calculated by dividing the total volume of bound water by the total surface area of the CUP particles.

At same concentrations and temperature, high molecular weight CUP (111K) has higher bound water layer (0.45 nm) thickness than low molecular weight (29K) CUP (0.63 nm) due to high surface charge density. Considering the diameter of the water molecule to be 0.27–0.28 nm, high molecular weight CUP holds 2.3 bound water layers, whereas the low molecular weight CUP holds about 1.7 bound water layers. The bonding is via hydrogen bonding by the acid and ester groups on the CUP particles. The results from this study agree well with the rheology study (Table 6) [5, 6, 13].

The thickness of water layer increases with molecular weight because the bare surface charge density is proportional to particle size. The bigger the particle, the higher the surface charge density. In other words, there will be more carboxylate groups at the surface per unit area, which forms a thicker electrical double layer. The larger charge densities of larger CUPs cause thicker surface water layer. These observations correlate well with the other approaches with NMR and DSC.

10. STUDY OF CORE ENVIRONMENT OF CUPS

The polymer chain undergoes a lot of structural changes during the reduction process. One of them is the transformation of an extended chain polymer to spherical globule at the collapse point. There are two structural properties of CUPs that need to be analyzed. First, whether the hydrophobic moiety along the polymer chain ends up in the interior of the CUP particle after the water reduction process. The presence of the hydrophobic moiety in the interior of the particles confirms the similarity of CUPs to that of micelles [1]. Second, whether the CUP particles behave as bulk polymer or are

plasticized due to water penetrating into the particles. Water penetration into the particle's interior will create more free volume and reduce the T_g of the particles relative to the bulk polymer

10.1. F^{19} NMR T_2 RELAXATION EXPERIMENT

The interior of the CUPs was studied by introducing fluorine into the interior of the CUP (polymer 35) using 2, 2, 2-trifluoroethyl methacrylate (TFEMA) as one of the monomers [2]. F^{19} spin–lattice (T_1) and spin–spin (T_2) relaxation was used to get information about the structural location and mobility of the fluorine after the collapse of the particle. The collapse of the CUP particles is supposed to be similar to micelles where the hydrophilic pendant groups get oriented in the water phase and the hydrophobic group forms the interior. Fluorine being hydrophobic in nature is expected to be located in the interior of the CUP particle.

The T_2 relaxation plotted in the temperature range 25–70° C shows a linear trend until the temperature gets close to T_g where it starts to deviate from linearity and later becomes linear again as the temperature increases further (Figure 19). This deviation in T_2 relaxation at T_g shows increase in the mobility of fluorine at T_g and not below it. Since fluorine is in the interior of the CUP particle, we can say that the interior of the CUPs behaves similar to a bulk polymer and does not exhibit hydro-plasticization.

The trend in the Figure 18 can be explained as follows. As the temperature increases, there is increase in the energy due to tumbling of the actual particles, which can be evidenced by increase in the relaxation time. As the temperature gets close to the

T_g, there is deviation from linearity, which can be attributed to the tumbling of the particle and the fluorine atom being able to spin more freely in the glass transition phase.

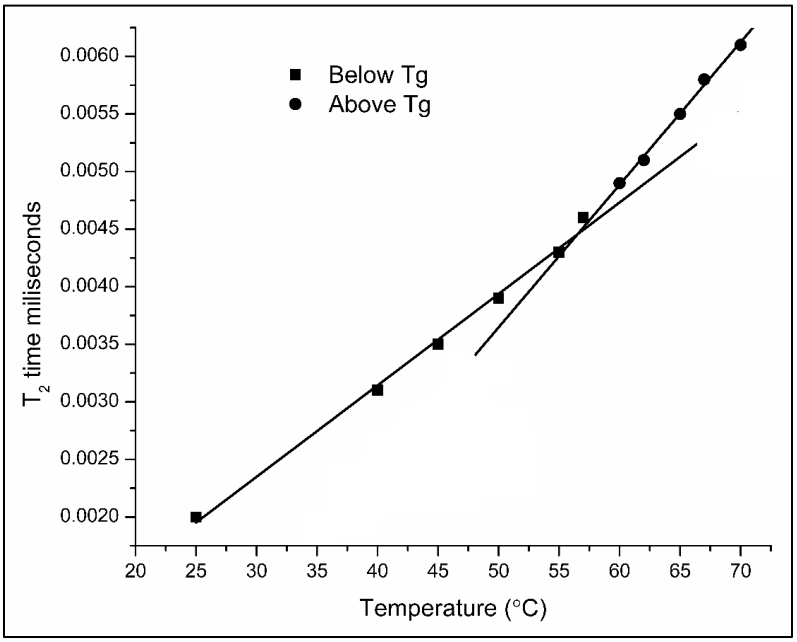

Figure 18. T_2 relaxation of CUPs plotted in the temperature range 25–70° C. (Riddles 2015 [2]. Reproduced with permission of Cynthia J. Riddles.).

The plot becomes linear again because the polymer is not passing through any other phase. If the fluorine atom had been present outside the particle in the water phase, the change observed in the T_2 times would be smaller. The T_g measured by the T_2 relaxation was found to be around 56° C (Figure 18), which was also confirmed by CP-TOSS experiment that showed T_g of 56.9° C. The DSC of polymer 35 showed the onset of T_g at the same point.

11. APPLICATIONS: USE OF CUPS IN COATINGS

CUP solutions can be made VOC-free since all the solvent is being stripped off after the water reduction process. They also do not require a coalescent aid and freeze–thaw agent that are the common VOCs present in waterborne coatings provided the CUP T_g is below the application or cure temperature and since CUPs are freeze–thaw stable. The nanoscale particle size of CUP particles makes them thermodynamically stable through Brownian motion. So, the CUP particles do not settle/aggregate unlike the large latex particles that settle with time. These properties of CUPs make them suitable for use in many coating application as well as adhesives and many other uses.

11.1. ACRYLIC CUP COATING LACQUERS

Latex and dispersed resins have been utilized as the binder for coatings applications for over 60 years. CUP resins offer many advantages in that they are VOC-free nanoscale, which increases the amount of pigment that can be incorporated. The CUP system is shear stable and they are freeze–thaw stable. Latex produces pigment to pigment gaps of about 80 nm due to their size, while the CUP being about 5 nm in size would yield a gap of less than 5 nm (Figure 19). Also, the dry time for film formation was expected to be much shorter. It is well known that all solid particles coalesce via reptational motion of the resin diffusing together to form a film. The rate of motion is inversely proportional to the molecular weight. The larger the particle, the further the resin must diffuse to fill the voids and form a film. Therefore, CUP particles being small will only need to diffuse about 1 nm to form a film, but latex resins must flow in about 40

nm. Since the rate of the diffusion of the same molecular weight polymer is the same, the latex will take many times longer to form a film than CUPs [94].

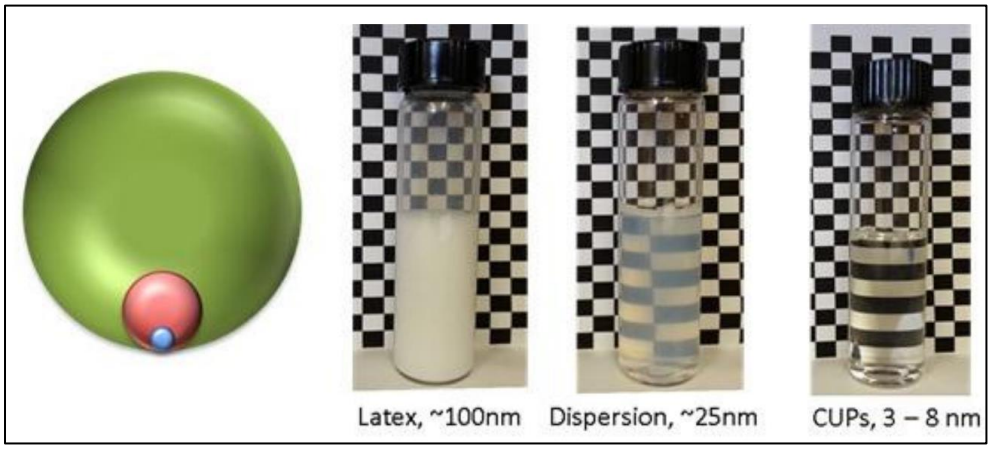

Figure 19. Latex of 100 nm, dispersion of 25 nm, and CUP of 3–8 nm in size. (Gade 2015 [18]. Reproduced with permission of S.V. Gade.

Two CUP systems were synthesized based upon n-BMA, one of high molecular weight and the other low polymers 24 and 25 from Table 1 [15]. Both resins were high T_g of 57 and 66° C, respectively. Since the T_g was above ambient, a coalescing aid was added similar to that used in a latex paint to allow film formation at ambient. The VOC level as tested was 0.23 and 0.42 lbs gal^{-1}, respectively. A white paint was formulated from each and a variety of tests were performed. The hardness was 2H and 4H, respectively. The 60° gloss was 61 and 65, respectively. The adhesion and flexibility were both the same. The abrasion resistance of the two were 120 mg/100 cycles and 112 mg/100 cycles, respectively, indicating the higher molecular weight resin is more abrasion resistant than the lower one. All the data are similar to that found with comparable latex systems. Both latex and CUP systems drying by evaporation are

lacquers. Other CUP systems with T_g at or below room temperature will form a film at ambient temperature, but since they are below their T_g, they will potentially have block resistance issues. If the above resins are dried at elevated temperature – above the T_g – no added coalescent aid is necessary, and the system becomes zero VOC.

Unlike conventional water-reducible resins and latex, CUPs resins are free of surfactant and can be formulated to zero VOC. The carboxylic acid groups on the surface of the CUP can act to improve adhesion to both the substrate and pigment. These groups are also available to react with melamine or aziridine cross-linkers, which will be discussed separately. Thus, the resin can be useful for both architectural and original equipment manufacturer (OEM) coatings.

11.2. AZIRIDINE-CURED ACRYLIC CUPS RESIN

Acrylic CUPs have also been explored for use as an aziridine-cured resin. Its potential application as clear floor finishes and clear topcoats has been studied [10].

Some acid-rich copolymers were synthesized from MAA, BMA, ethyl acrylate (EA), ethyl methacrylate (EMA), and 2-ethylhexyl methacrylate (2-EHMA). The ratio of acrylate monomers to acrylic acid was 8 : 1 or 7 : 1 (polymers 5, 6 or 7, 8), which were slightly lower than ratio used in the previous experiments. This was because more acrylic acid groups gave higher cross-linking density when CUPs are applied as the resin. CX-100, a commercially available aziridine with a functionality of 3, was chosen as a cross-linker. The cured coatings were evaluated for their organic solvent resistance, adhesion, hardness, gloss, flexibility, wet adhesion, and abrasion [10, 11].

Organic solvent resistance, hardness, and abrasion improved after being cured with the aziridine cross-linker. Testing results showed that the optimum ratio of aziridine:acid for the effective cure of acrylic CUPs resin was about 1.25 : 1. If the ratio was greater than 1.25 : 1, some of the excess aziridine cross-linker will only be able to react one of its three aziridine groups with a CUP carboxylate group thus, decreasing the cross-link density. However, insufficient cross-linker would render the coating a lacquer, thus resulting in poor solvent resistance and hardness. At the aziridine:acid ratio of 1.25 : 1, the slight excess of aziridine made sure that even if one of the three aziridine groups was hydrolyzed, the other two will be available for cross-linking, thus giving a highly cross-linked coating with excellent performance. In the CUP system, the reactive group carboxylates is on the surface of the particle and thus is easily accessible to aziridine. The CUP particles do not need extensive reptational motion to access the aziridine, or to coalesce, as would a latex or a water dispersion resin such as a urethane [10].

The hard dry time of this aziridine-cured acrylic CUPs resin was around 3 h, which was similar to commercial waterborne urethane clear floor coatings. The cured coatings also have high flexibility and impact resistance. This indicated that these polymers had high tensile strength and cross-linked films were not brittle. Wet adhesion test was done on this coating. No significant change was observed on the films nor was there any hazing or change in pencil hardness. This indicated that negligible free carboxylic acid groups were present in the cured resin. These film performances were similar to commercial waterborne polyurethane resins but with less VOC. Aziridine-cured acrylic CUP coatings produced well-cross-linked films. These zero-VOC resins

offer a potentially high-performance technology option for future coatings for both OEM and architectural applications.

11.3. USE OF CUPS WITH MELAMINE RESIN CROSS-LINKING

The CUPs can be used as a coating resin cured with melamine cross-linker via the reaction of carboxyl groups on the CUPs and the methylol group of the melamine. The carboxylic groups should be neutralized with trimethylamine or a similar kind of volatile amine. Ammonium hydroxide can react with free formaldehyde present in melamine during the curing process and can result in gelation [11].

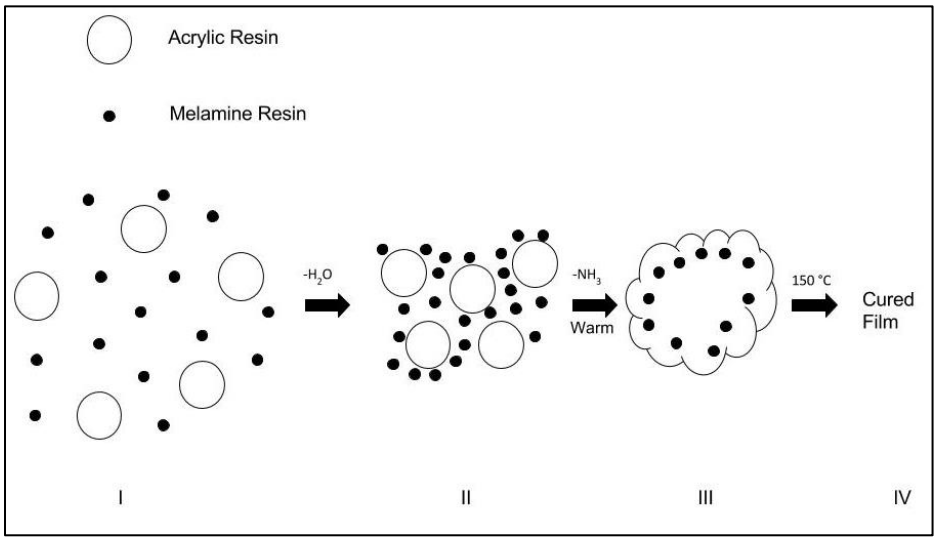

Figure 20. Steps involved in the cross-linking of the acrylic–melamine resin.

Figure 20 shows a model for the steps involved in the cross-linking of the acrylic–melamine resin. Stage I is where the coating is applied to the panel. The water is evaporated at stage II and the particles come in contact with each other and melamine. In stage III, the diffusion of melamine into the latex particle and interdiffusion of latex

particles begin. The cross-linking occurs at stage IV. For uniform cross-linking, the melamine diffusion should be faster than the cross-linking reaction. Slower diffusion will result in cross-link on the surface of the latex or particle. Due to the small size of CUPs and the presence of all the acid groups on the surface, the diffusion of melamine is not required. The cross-link is better and more uniform in CUP particle as compared with a latex particle [8, 14].

Various optimization experiments were carried out using the CUP resin, melamine cross-linker (Cymel 373 with assumed functionality of 4.5), and p-TSA catalyst (Na-Cure 2547) to optimize the curing time, curing temperature, catalyst amount, and cross-linker amount. Pencil hardness and methyl ethyl ketone (MEK) double rub tests were used for evaluating the performance. Pencil hardness is the measure of hardness of the coating, while MEK double rub test is a measure of solvent resistance that is related to the cross-link density of the coating. Determining the optimum amount of catalyst is important because the acid catalyst can cause corrosion or polymer degradation with time. The best coating performance was at 0.25% dosage of active catalyst (based on resin solids) at temperature 150° C for curing time of 30 min. and using the equivalent amount of melamine such that its functionality is assumed to be 4.5. The melamine-cured CUP clear coat has good hardness characteristics. The CUP coating has excellent flexibility and impact resistance that can be attributed to the true nanoscale size of the CUPs yielding good cross-linking efficiency. The small size makes easy access for the cross-linking agent without having to penetrate, which reduces the diffusion time. The adhesion (ASTM D-4541) to the substrate is excellent and water permeability is also very low [11].

11.4. USE OF SULFONATE CUPS AS CATALYST FOR MELAMINE CURE SYSTEMS

Acrylic resin cross-linked with amino resins is widely used in OEMs and automotive industry, and this system often requires an acid catalyst like p-TSA to speed up the curing [95]. CUPs being nano-sized particles (3–9 nm) have a high surface availability that makes them suitable for application in catalysis. CUPs made from copolymer of MMA and AMPS (polymer 20 or 23) will have active sulfonic acid group on the surface, which can be used in catalyzing the curing of acrylic and melamine resin. The CUP catalyst was studied with an acrylic melamine ratio of 75 : 25 and with catalyst concentration of 0.5% (wt/wt on resin solids) at a curing temperature of 150° C [8, 14]. When cured for 30 min the indentation hardness for both the catalyzed coatings (the commercial p-TSA and CUP catalyst) was close but higher than the uncatalyzed, which indicates the cross-linking reaction taking place. The CUP catalyst is equally effective in catalysis of acrylic–melamine reaction as the commercial p-TSA catalyst as implied by the similar values of pencil and indentation hardness. Both catalysts perform well in MEK double rub test (more than 200), which confirms the effectiveness of the CUPs catalyst [8, 14].

The catalysis in CUPs is affected by two factors, the diffusion of the catalyst and the catalyst surface activity. For linear polymers $D \alpha M_w^{-2}$, where D is the diffusion coefficient and M_w is the molecular weight [96]. Polymers have high molecular weight and therefore slow diffusion rates. The CUP catalyst will also diffuse slower through the film than the commercial p-TSA catalyst, which is comparatively a small molecule. The CUPs, however, are nano-sized particles with all the active groups, that is, the sulfonate groups present on the surface of the particles, which enhance the availability of the CUPs

toward the curing reaction. For commercial catalyst like p-TSA that has a high diffusion rate, the separation of charges in the media is the critical factor. It is the proton that does the catalysis, while the sulfonate is the counterion [97]. For shorter cure times, the cross-link density (MEK double rub test result) for both the catalysts is similar because the surface availability of the CUP catalyst dominates the chemistry. At longer cure times, the diffusion effect becomes more pronounced, which is lower for CUPs than the commercial catalyst. This can be seen from the cross-link density (MEK double rub test result), which is lower for the CUP catalyst system.

The number of mole equivalents of acid present in 0.5% (wt/wt on resin solids as used for the above experiment) of the CUP catalyst is 4.16×10^{-6} per gram of resin solid and in commercial catalyst is 2.91×10^{-5} per gram of resin solid. On mole basis the amount of commercial catalyst used was seven times more than the CUP catalyst. When using the same molar equivalents of both catalysts, the pencil hardness and MEK double rubs results for CUP catalyst (H and 225) were far better than the commercial catalyst (B and 20). This indicates that higher surface availability in the CUP catalyst greatly enhances the catalytic activity toward the cross-linking reaction. This higher efficiency could also be due to greater separation of proton and sulfonate group because the sulfonic acid group is present in the interstitial areas that have higher dielectric. For CO_2H-latex and CO_2H-CUP resin systems, the sulfonate CUP catalyst is as effective as the commercial blocked p-TSA catalyst [8, 14].

The NMR results from the water leaching experiment show CUP catalyst that do not leach out of the coating in water like the commercial blocked catalysts. This could be due to the transesterification reaction of the CUP catalyst with the melamine component

that makes it immobile and prevents the leaching to the surface [98, 99]. The commercial catalyst is also water soluble, which would cause it to leach out in water, whereas the CUP catalyst is water insoluble.

11.5. EPOXY

Today, solvent-borne epoxy systems are being switched to waterborne systems due to increasing environmental regulations. Waterborne epoxy resins can be an emulsifiable amino resin or an emulsifiable epoxy or both an emulsifiable amino resin and epoxy [100–103]. There are two fundamental types of the waterborne epoxy coatings.

Type I epoxy systems are based on liquid bisphenol A or bisphenol F chemistry with an epoxy equivalent weight (EEW) of less than 250. In this system the curing agent cross-links acts as an emulsifier in the liquid state. Thus, the curing agent and epoxy resin both are present in the emulsion particles, and the phase separation is reduced. Low molecular weight gives a high diffusion rate, giving good coalescence without addition of any coalescent aid. Near-zero VOC formulations can be made using this system [104].

Type II epoxy systems are based on solid higher molecular weight dispersed resins. They are pre-dispersed using an emulsifier in water along with a co-solvent. Glycol ether has to be added to improve the flow and coalescence of solid epoxies, which adds to VOC in the formulations. The curing agent has to migrate from the aqueous phase into the dispersed solid epoxy resin particles in order to cross-link. This leads to development of heterogeneous film morphology with unreacted epoxy resin in the particle cores and amine-rich particle boundaries [104].

To make the amine-based CUP cross-linker, first EA–AA copolymer was synthesized followed by the reaction of carboxyl groups of acrylic acid with 2-methylaziridine in order to introduce the amino functionality. The reaction of acid group and the 2-methylaziridine involves protonation of the nitrogen atom of the basic 2-methylaziridine, followed by nucleophilic attack by the carboxylate anion through a six-membered transition state, forming an ester linkage that yields a terminal amine group (Figure 21) [105, 106].

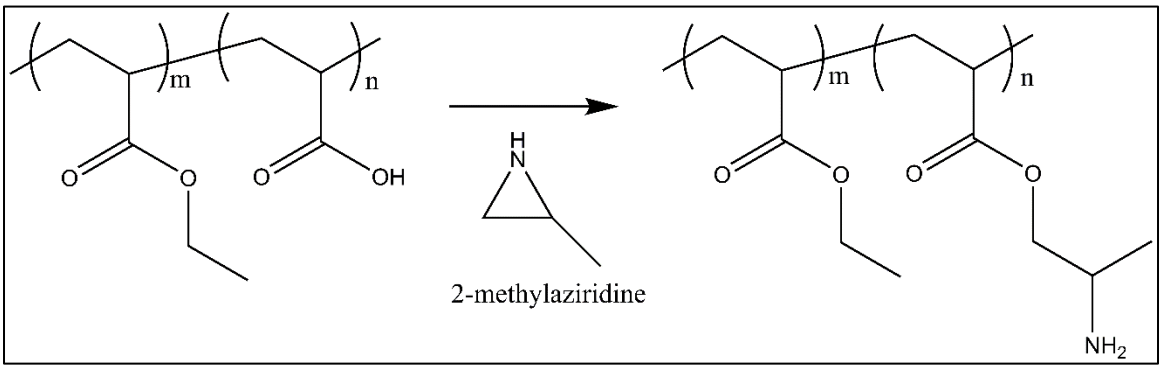

Figure 21. Functionalization of EA–AA copolymer with 2-methylazidirine to give an amino functional copolymer.

The covalent attachment of the aziridine gives a polyfunctional amine copolymer that is an efficient cross-linker for epoxy. The EA–AAZ (methylaziridine adduct) amino functional copolymer is then reduced by the water reduction process using acetic acid for neutralizing the amino groups to form EA–AAZ CUP particles. These EA–AAZ CUPs can be used as a new approach for cross-linking the waterborne epoxy systems to produce no/low VOC clear coats. Apart from 2-methylaziridine, other aziridine derivatives like n-butyl aziridine can also be used to get amino functionality in the copolymer [18].

In the epoxy–CUP system, after the water has evaporated CUP (4 nm in size) cross-linker particles diffuse by reptational motion to the core of the 200 nm solid epoxy particles plasticized with 2-propoxyethanol to give improved residual cross-linking, two different molecular weight polymers were used. The polymer 36 (M_n=10.5K) polymer chains will have higher reptation diffusion compared with polymer 37 (M_n=37K) polymer chains during curing, due to lower molecular weight. The EA–AAZ 1 CUP (polymer 36) and EA–AAZ 2 CUP (polymer 37) have about 20 and 70 amine hydrogens per chain separated by about 9 units of EA monomers, which give more mobility during cross-linking but at the same time such high number of amine functionalities may hinder the residual cross-linking.

The test results from Table 7 show the performance of EA–AAZ 1 CUP (polymer 36) and EA–AAZ 2 CUP (polymer 37) cross-linker in the epoxy system compared with the conventional waterborne epoxy amine system using EPI-REZ resin 5522-wy-55 epoxy resin and EPIKURE 8290-Y-60 cross-linker.

The properties of epoxy coatings cured using CUP cross-linker are close to the properties of the conventional system, that is, Coating 3 in Table 7 [18]. The conventional EPIKURE 8290-Y-60 cross-linker has a coalescing solvent 2-propoxyethanol that helps yielding better film during curing, whereas EA–AAZ CUP cross-linker has a lower glass transition temperature and does not require any solvent. This is because all the amine groups are on the surface, and reaction is rapid since diffusion is over a short distance with the nano-size resin. The minimum film forming temperature (MFFT) of the CUPs is lower [18] due to small size of CUPs, since the MFFT is proportional to the number average particle diameter of the particles [107]. The

Table 7. Gloss, flexibility, impact resistance, dry and wet adhesion resistance, minimum film forming temperature (MFFT), pencil hardness, and indentation hardness of the epoxy clear coats [18].

		Coating 1	**Coating 2**	**Coating 3**
Crosslinker		EA-AAZ 1 CUP	EA-AAZ 2 CUP	EPIKURE 8290-Y-60
Gloss	20°	88.5 ± 1.0	88.2 ± 1.2	87.9 ± 2.2
	60°	104.4 ± 0.1	101.0 ± 0.2	99.9 ± 0.0
Flexibility	¼ inch Mandrel	Pass	Pass	Pass
Impact resistance	Forward (extrusion)	100 in.lbs	100 in.lbs	100 in.lbs
	Reverse (intrusion)	140 in.lbs	140 in.lbs	140 in.lbs
Adhesion	ASTM D3359	5B	5B	4B
Wet adhesion		5B	5B	2B
Puck adhesion	ASTM D4541	1041PSI	1033PSI	1108PSI
	Failiure mode: a/b [a]	80%/20%	80%/20%	80%/20%
Pencil Hardness	ASTM D3363	HB	HB	HB
Microindenter Hardness	ASTM E2546	193 $N.mm^{-2}$	200 $N.mm^{-2}$	233 $N.mm^{-2}$
Indentation Modulus	ASTM E2546	7605 MPa	6072 MPa	5331 MPa

a) Failure mode: a – cohesive coating failure; b – adhesive substrate to coating failure.

rate of cross-linking also depends on mobility of the resin and cross-linker. For CUPs the higher mobility of the particles gives better cross-linking compared with the conventional cross-linker.

11.6. USE OF CUPS AS ADDITIVES FOR FREEZE-THAW STABILITY AND WET EDGE RETENTION

Waterborne coating formulations utilize co-solvents that are VOCs to improve properties like freeze–thaw stability, wet edge retention, coalescence, etc. Glycols are commonly used as antifreeze, that is, depress the freezing point of the water and prevent the gelation and aggregation due to freezing in waterborne coatings. They also evaporate slowly during drying, inhibiting film formation that helps in wet edge retention. However, glycols being a VOC are becoming undesirable for this purpose. The CUP particles are nanoscale in size and therefore have a large surface area (16 600 m^2 g^{-1} for 3 nm diameter particles). The particles are suspended in water with a large amount of "surface water," which is nonfreezing. The large surface area per gram yields a higher weight fraction of nonfreezing surface water around these particles compared with latex systems. The surface water of the CUP could control the evaporation and coalescence rates and therefore improve the freeze–thaw stability and the wet edge retention.

The evaluation of EA–AA CUPs (polymer 38) as an additive was studied by adding different concentration of CUP solution to a latex paint formulation and subjecting to freeze–thaw cycles according to ASTM 2243-95. The paint with the lowest level (20 lbs) of CUP failed on the 2nd freeze–thaw, the medium level (30 lbs) remained stable up to 3rd freeze–thaw cycle, and the highest level (40 lbs) remained stable through all 5 freeze–thaw cycles. Negatively charged CUP particles space the coating due to

repulsion between them. The CUP particles keep the latex particles from coming into contact through this spacing effect and the nonfreezing bound water layer. It should be noted that the CUP replaced an equal weight of latex resin solids

When the paint is applied on a substrate, the water starts evaporating, and at the edge of the paint film near the paint–air interface, the latex particles come closer and start to coalesce. This process makes it difficult to rework after first few minutes of drying. Using high boiling solvents can delay the evaporation to give good wet edge retention and open time. When CUPs are used as additive, the latex particles along with the CUP particle come closer together at the surface of the paint film near the paint–air interface during the initial stage of evaporation of the water. The CUPs delay the process of coalescence because these nanoparticles with bound water on the surface act as spacers between the latex particles. Due to the smaller particle size and large amount of bound water of the CUPs compared with the latex particles, the viscosity of the paint increases because the gel point is reached at much lower solids content [5]. The increase in the viscosity at interface reduces the water diffusion and slows down the evaporation, thereby keeping the latex particles within the drying paint layer separated for a larger time. The use of CUP technology can therefore improve the wet edge retention and open time while substantially reducing the VOC of the paint formulation.

Tinting in the stores often produce miss tints. This error is due to use of hair dryer to accelerate the drying of a test smear of paint. The cause is the osmotic flow driven differential mobility of the pigments in a paint. The use of CUP as a mobility inhibitor increases the viscosity rapidly as water is removed due to gel point formation. Tests

reported show that at the same concentration needed to prevent freeze–thaw instability, the tint problem became negligible.

REFERENCES

1. Riddles, C.J., Zhao, W., Hu, H.-J., Chen, M., and Van De Mark, M.R. (2014) Self-assembly of water insoluble polymers into colloidal unimolecular polymer (CUP) particles of 3–9 nm. Polymer, 55, 48–57.

2. Riddles, C.J. (2015) The synthesis and characterization of water-reducible nanoscale colloidal unimolecular polymer (CUP) particles. Doctoral Dissertations. Paper 2457.

3. Zhao, M. and Zheng, L. (2011) Micelle formation by N-alkyl-N-methylpyrrolidinium bromide in aqueous solution. Phys. Chem. Chem. Phys., 13, 1332–1337.

4. Rusdi, M. (2009) Micelle formation and surface adsorption of sodium 4-octyl benzene sulfonate (S4OBS) in water solvent. J. Mat. Sains, 14, 57–61.

5. Chen, M., Riddles, C., and Van De Mark, M. (2013) Gel point behavior of colloidal unimolecular polymer (CUP) particles. Colloid Polym. Sci., 291, 2893–2901.

6. Chen, M. (2013) Fundamental properties of colloidal unimolecular polymer particles. Doctoral Dissertations. Paper 2058.

7. Dawib, Y.A. (2015) NMR T1 studies of colloidal unimolecular polymer (CUP) surface water. Doctoral Dissertations. Paper 2406.

8. Natu, A.M. (2015) Synthesis, characterization and application of acrylic colloidal unimolecular polymer (CUP). Doctoral Dissertations. Paper 2391.

9. Natu, A.M., Wiggins, M., and Van De Mark, M.R. (2015) Synthesis and characterization of cationic colloidal unimolecular polymer (CUP) particles. Colloid Polym. Sci., 293, 1191–1204.

10. Mistry, J.K. and Van De Mark, M.R. (2013) Aziridine cure of acrylic colloidal unimolecular polymers (CUPs). J. Coat. Tech. Res., 10, 453–463.

11. Mistry, J.K. (2012) Chelating compounds as potential flash rust inhibitors and melamine and aziridine cure of acrylic colloidal unimolecular polymers (CUPs). Doctoral Dissertations. Paper 2027.

12. Van De Mark, M.R., Natu, A.M., Gade, S.V., Chen, M., Hancock, C., and Riddles, C. (2013) Molecular weight (Mn) and functionality effects on CUP formation and stability. J. Coat. Tech. Res., 11, 111–122.

13. Chen, M., Riddles, C.J., and Van De Mark, M.R. (2013) Electroviscous contribution to the rheology of colloidal unimolecular polymer (CUP) particles in water. Langmuir, 29, 14034–14043.

14. Natu, A.M. and Van De Mark, M.R. (2015) Synthesis and characterization of an acid catalyst for acrylic-melamine resin systems based on colloidal unimolecular polymer (CUP) particles of MMA-AMPS. Prog. Org. Coat., 81, 35–46.

15. Jones, J.A. (2001) The effects of variable molecular weight and solvents, in water-reducible acrylic resins. Masters theses. Paper 5991.

16. Hu, H.-J. (1995) Synthesis and characterization of water reducible MMA-MMA copolymers. Masters theses. Paper 5990.

17. Bhave, M.R. (2000) Synthesis of crosslinkable water reducible acrylic copolymers for coatings. Masters theses. Paper 1938.

18. Gade, S.V. (2015) Application of colloidal unimolecular polymer (CUP) particles in coatings. Doctoral Dissertations. Paper 2446.

19. Zhao, W.I. (2003) Ultrasonic microscopy analysis of corrosion – a nondestructive evaluation of paint weathering effects and synthesis and characterization of nanoscale water-reducible polymer particles. Doctoral Dissertations. Paper 87.

20. Allan, F.B. and Barton, P.D. (1983) CRC Handbook of Solubility Parameters and Other Cohesion Parameters, CRC, Boca Raton, Florida.

21. Paula, S., Sues, W., Tuchtenhagen, J., and Blume, A. (1995) Thermodynamics of micelle formation as a function of temperature: a high sensitivity titration calorimetry study. J. Phys. Chem., 99, 11742–11751.

22. Chauhan, S. and Sharma, K. (2014) Effect of temperature and additives on the critical micelle concentration and thermodynamics of micelle formation of sodium dodecyl benzene sulfonate and dodecyltrimethylammonium bromide in aqueous solution: a conductometric study. J. Chem. Thermodyn., 71, 205–211.

23. Majhi, P.R. and Blume, A. (2001) Thermodynamic characterization of temperature-induced micellization and demicellization of detergents studied by differential scanning calorimetry. Langmuir, 17, 3844–3851.

24. Jha, R. and Ahluwalia, J.C. (1991) Thermodynamics of micellization of Triton X-100 in aqueous ethylene glycol solutions. J. Phys. Chem., 95, 7782–7784.

25. Kralchevsky, P., Miller, R., and Ravera, F. (2013) Colloid and Interface Chemistry for Nanotechnology, CRC Press, Boca Raton, Florida.

26. Hepler, L.G. (1969) Thermal expansion and structure in water and aqueous solutions. Can. J. Chem., 47, 4613–4617.

27. Griffin, W.C. (1946) Classification of surface-active agents by "HLB". J. Soc. Cosmet. Chem., 1, 311–326.

28. Griffin, W.C. (1954) Calculation of HLB values of nonionic surfactants. J. Soc. Cosmet. Chem., 5, 249–256.

29. Davies, J. (1957) A quantitative kinetic theory of emulsion type, I. Physical chemistry of the emulsifying agent, in Gas/Liquid and Liquid/Liquid Interface. Proceedings of the International Congress of Surface Activity, pp. 426–438.

30. Americas, I. (1984) The HLB System: A Time-Saving Guide to Emulsifier Selection, ICI Americas, Incorporated.

31. Myers, D. (2005) Surfactant Science and Technology, John Wiley & Sons.

32. Flory, P.J. (1941) Thermodynamics of high polymer solutions. J. Chem. Phys., 9, 660.

33. Huggins, M.L. (1942) Some properties of solutions of long-chain compounds. J. Phys. Chem., 46, 151–158.

34. Mark, J.E. (2007) Physical Properties of Polymers Handbook, Springer.

35. Dobrynin, A.V. and Rubinstein, M. (2005) Theory of polyelectrolytes in solutions and at surfaces. Prog. Polym. Sci., 30, 1049–1118.

36. Dobrynin, A.V., Rubinstein, M., and Obukhov, S.P. (1996) Cascade of transitions of polyelectrolytes in poor solvents. Macromolecules, 29, 2974–2979.

37. Aseyev, V.O., Tenhu, H., and Klenin, S.I. (1998) Contraction of a polyelectrolyte upon dilution. Light-scattering studies on a polycation in saltless water-acetone mixtures. Macromolecules, 31, 7717–7722.

38. Grass, K. and Holm, C. (2009) Polyelectrolytes in electric fields: measuring the dynamical effective charge and effective friction. Soft Matter, 5, 2079–2092.

39. Hessinger, D., Evers, M., and Palberg, T. (2000) Independent ion migration in suspensions of strongly interacting charged colloidal spheres. Phys. Rev. E, 61, 5493.

40. Manning, G.S. (1975) Limiting law for the conductance of the rod model of a salt-free polyelectrolyte solution. J. Phys. Chem., 79, 262–265.

41. Alexander, S., Chaikin, P.M., Grant, P., Morales, G.J., Pincus, P., and Hone, D. (1984) Charge renormalization, osmotic pressure, and bulk modulus of colloidal crystals: theory. J. Chem. Phys., 80, 5776–5781.

42. Girifalco, L.A. (2003) Statistical Mechanics of Solids, OUP, USA.

43. Ninham, B.W. and Parsegian, V.A. (1971) Electrostatic potential between surfaces bearing ionizable groups in ionic equilibrium with physiologic saline solution. J. Theor. Biol., 31, 405–428.

44. Belloni, L. (1998) Ionic condensation and charge renormalization in colloidal suspensions. Colloids Surf. A: Physicochem. Eng. Asp., 140, 227–243.

45. Lobaskin, V., Dünweg, B., Medebach, M., Palberg, T., and Holm, C. (2007) Electrophoresis of colloidal dispersions in the low-salt regime. Phys. Rev. Lett., 98, 176105.

46. Oncley, J.L. (1941) Evidence from physical chemistry regarding the size and shape of protein molecules from ultra-centrifugation, diffusion, viscosity, dielectric dispersion, and double refraction of flow. Ann. N. Y. Acad. Sci., 41, 121–150.

47. Smoluchowski, M.V. (1916) Theoretische bemerkungen über die viskosität der kolloide. Colloid Polym. Sci., 18, 190–195.

48. Booth, F. (1950) The electroviscous effect for suspensions of solid spherical particles, in Proceedings of the Royal Society of London A: Mathematical, Physical and Engineering Sciences, The Royal Society.

49. Watterson, I.G. and White, L.R. (1981) Primary electroviscous effect in suspensions of charged spherical particles. J. Chem. Soc. Faraday Trans. 2: Mol. Chem. Phys., 77, 1115–1128.

50. Russel, W.B. (1978) Bulk stresses due to deformation of the electrical double layer around a charged sphere. J. Fluid Mech., 85, 673–683.

51. Hiemenz, P.C. and Rajagopalan, R. (eds) (1997) Principles of Colloid and Surface Chemistry, Revised and Expanded, CRC Press.

52. Russel, W.B. (1978) The rheology of suspensions of charged rigid spheres. J. Fluid Mech., 85, 209–232.

53. Verwey, E.J.W., Overbeek, J.T.G., and Overbeek, J.T.G. (1999) Theory of the Stability of Lyophobic Colloids, Courier Corporation.

54. Ohshima, H. (2002) Surface charge density/surface potential relationship for a spherical colloidal particle in a salt-free medium. J. Colloid Interface Sci., 247, 18–23.

55. Vaynberg, K.A. and Wagner, N.J. (2001) Rheology of polyampholyte (gelatin)-stabilized colloidal dispersions: the tertiary electroviscous effect. J. Rheol., 45, 451–466.

56. Jiang, L. and Chen, S.B. (2001) Electroviscous effect on the rheology of a dilute solution of flexible polyelectrolytes in extensional flow. J. NonNewton. Fluid, 96, 445–458.

57. Krieger, I.M. (1972) Rheology of monodisperse latices. Adv. Colloid Interface Sci., 3, 111–136.

58. Yan, H., Guo, X.L., Yuan, S.L., and Liu, C.B. (2011) Molecular dynamics study of the effect of calcium ions on the monolayer of SDC and SDS surfactants at the vapor/liquid interface. Langmuir, 27, 5762–5771.

59. Karlsson, L.E., Wesslén, B., and Jannasch, P. (2002) Water absorption and proton conductivity of sulfonated acrylamide copolymers. Electrochim. Acta, 47, 3269–3275.

60. Fedotova, M.V. and Kruchinin, S.E. (2011) Hydration of acetic acid and acetate ion in water studied by 1D-RISM theory. J. Mol. Liq., 164, 201–206.

61. Powell, D.H., Barnes, A.C., Enderby, J.E., Neilson, G.W., and Salmon, P.S. (1988) The hydration structure around chloride ions in aqueous solution. Faraday Discuss. Chem. Soc., 85, 137–146.

62. Mähler, J. and Persson, I. (2011) A study of the hydration of the alkali metal ions in aqueous solution. Inorg. Chem., 51, 425–438.

63. Hribar-Lee, B., Dill, K.A., and Vlachy, V. (2010) Receptacle model of salting-in by tetramethylammonium ions. J. Phys. Chem. B, 114, 15085–15091.

64. Babiaczyk, W.I., Bonella, S., Guidoni, L., and Ciccotti, G. (2010) Hydration structure of the quaternary ammonium cations. J. Phys. Chem. B, 114, 15018–15028.

65. Garcia-Tarres, L. and Guardia, E. (1998) Hydration and dynamics of a tetramethylammonium ion in water: a computer simulation study. J. Phys. Chem. B, 102, 7448–7454.

66. Jorgensen, W.L. and Gao, J. (1986) Monte Carlo simulations of the hydration of ammonium and carboxylate ions. J. Phys. Chem., 90, 2174–2182.

67. Markham, G.D., Bock, C.L., and Bock, C.W. (1997) Hydration of the carboxylate group: anab initio molecular orbital study of acetate-water complexes. Struct. Chem., 8, 293–307.

68. Hales, T.C. (2005) A proof of the Kepler conjecture. Ann. Math., 162, 1065–1185.

69. Song, C., Wang, P., and Makse, H.A. (2008) A phase diagram for jammed matter. Nature, 453, 629–632.

70. Barnes, H.A., Hutton, J.F., and Walters, K. (1989) An Introduction to Rheology, Elsevier.

71. Mill, C.C. (1959) Rheology of disperse systems (Proceedings of a conference), in Symposium Publications Division, Pergamon Press.

72. Cross, M.M. (1965) Rheology of non-Newtonian fluids: a new flow equation for pseudoplastic systems. J. Colloid Sci., 20, 417–437.

73. Laun, H.M. (1984) Rheological properties of aqueous polymer dispersions. Die Angew. Makromol. Chem., 123, 335–359.

74. Ohsawa, K., Murata, M., and Ohshima, H. (1986) Zeta potential and surface charge density of polystyrene-latex; comparison with synaptic vesicle and brush border membrane vesicle. Colloid Polym. Sci., 264, 1005–1009.

75. de Kruif, C.D., Van Iersel, E.M.F., Vrij, A., and Russel, W.B. (1985) Hard sphere colloidal dispersions: viscosity as a function of shear rate and volume fraction. J. Chem. Phys., 83, 4717–4725.

76. McCabe, J.F. and Rusby, S. (2004) Water absorption, dimensional change and radial pressure in resin matrix dental restorative materials. Biomaterials, 25, 4001–4007.

77. Kusy, R.P., Whitley, J.Q., and Kalachandra, S. (2001) Mechanical properties and interrelationships of poly (methyl methacrylate) following hydration over saturated salts. Polymer, 42, 2585–2595.

78. Christensen, T.C., Teichmann, A.F., and Janule, V.P. (2000) US Patent. 6,085,577.

79. Fainerman, V.B., Miller, R., and Joos, P. (1994) The measurement of dynamic surface tension by the maximum bubble pressure method. Colloid Polym. Sci., 272, 731–739.

80. Tanvir, S. and Qiao, L. (2012) Surface tension of nanofluid-type fuels containing suspended nanomaterials. Nanoscale Res. Lett., 7, 226.

81. Chaudhuri, R.G. and Paria, S. (2009) Dynamic contact angles on PTFE surface by aqueous surfactant solution in the absence and presence of electrolytes. J. Colloid Interface Sci., 337, 555–562.

82. Bernett, M.K. and Zisman, W.A. (1959) Wetting of low-energy solids by aqueous solutions of highly fluorinated acids and salts. J. Phys. Chem., 63, 1911–1916.

83. Okkema, A.Z. and Cooper, S.L. (1991) Effect of carboxylate and/or sulphonate ion incorporation on the physical and blood-contacting properties of a polyetherurethane. Biomaterials, 12, 668–676.

84. Edward, J.T. (1970) Molecular volumes and the Stokes-Einstein equation. J. Chem. Educ., 47, 261.

85. Newton, R. and Gortner, R.A. (1922) A method for estimating hydrophilic colloid content of expressed plant tissue fluids. Bot. Gaz., 74, 442–446.

86. Moran, T. (1930) The frozen state in mammalian muscle. R. Soc. Lond. Ser. B: Containing Papers of a Biological Character, 107, 182–187.

87. Hill, A.V. (1930) The state of water in muscle and blood and the osmotic behaviour of muscle. R. Soc. Lond. Ser. B: Containing Papers of a Biological Character, 106, 477–505.

88. Cooke, R. and Kuntz, I.D. (1974) The properties of water in biological systems. Annu. Rev. Biophys. Bioeng., 3, 95–126.

89. Nandi, N. and Bagchi, B. (1997) Dielectric relaxation of biological water. J. Phys. Chem. B, 101, 10954–10961.

90. Buchanan, T.J., Haggis, G.H., Hasted, J.B., and Robinson, B.G. (1952) The dielectric estimation of protein hydration. R. Soc. Lond. Ser. A: Math. Phys. Eng. Sci., 213, 379–391.

91. Gortner, R.A. (1930) The state of water in colloidal and living systems. Trans. Faraday Soc., 26, 678–686.

92. Blinc, R., Rutar, V., Zupanciˆ c, I., Zidan ˆ sek, A., Lahajnar, G., and Slak, J. ˆ (1995) Proton NMR relaxation of adsorbed water in gelatin and collagen. Appl. Magn. Reson., 9, 193–216.

93. Rex, G.E. II, Chi, L., Zhang, H., and Woelk, K. (2011) Low-Field NMR Spin–Lattice Relaxation Time-Constant Distributions of Shale. 46th Midwest and 39th Great Lakes Regional Meeting of the American Chemical Society, 16, 19–22.

94. Steward, P.A., Hearn, J., and Wilkinson, M.C. (2000) An overview of polymer latex film formation and properties. Adv. Colloid Interface Sci., 86, 195–267.

95. Müller, B. and Poth, U. (2011) Coatings Formulation, Vincentz Network.

96. Westheimer, F.H. and Jones, W.A. (1941) The effect of solvent on some reaction rates. J. Am. Chem. Soc., 63, 3283–3286.

97. Fakirov, S., Baltá Calleja, F.J., and Krumova, M. (1999) On the relationship between microhardness and glass transition temperature of some amorphous polymers. J. Polym. Sci. Part B: Polym. Phys., 37, 1413–1419.

98. Tillet, G., Boutevin, B., and Ameduri, B. (2011) Chemical reactions of polymer crosslinking and post-crosslinking at room and medium temperature. Prog. Polym. Sci., 36, 191–217.

99. Mistry, J.K., Natu, A.M., and Mark, M.R. (2014) Synthesis and application of acrylic colloidal unimolecular polymers as a melamine thermoset system. J. Appl. Polym. Sci., 131.

100. Kojima, S., Moriga, T., and Watanabe, Y. (1993) Development of high performance, water-based emulsion coatings for can coatings application. J. Coat. Technol., 65, 25–38.

101. Walker, F.H. and Shaffer, O. (1996) Film formation and morphology in two-component, ambient-cured, waterborne epoxy coatings, in Film Formation in Waterborne Coatings, vol. 648, pp. 403–417.

102. Liqiang, Q.I.A.N. (1999) Study of fast drying two-component water borne epoxy resin coatings. Paint and Coatings Industry, 11, 011.

103. Jianying, L. and Sumin, L. (2009) Preparation of two-package water-borne epoxy anticorrosion coatings [J]. China Coat., 9, 017.

104. Rufo, M., Shah, D., Raymond, W., Walker, F.H., Lohe, M., Klippstein, A., and Cook, M. (2005) 2K Waterborne Epoxy Systems: Technology Overview and New Developments, Air Products and Chemicals, Inc.

105. Potyrailo, R.A. and Amis, E.J. (eds) (2012) High-Throughput Analysis: A Tool for Combinatorial Materials Science, Springer Science and Business Media.

106. Dermer, O. (1969) Ethylenimine and Other Aziridines: Chemistry and Applications, Academic Press Inc, New York.

107. Eckersley, S.T. and Rudin, A. (1990) Mechanism of film formation from polymer latexes. J. Coat. Technol., 62, 89–100.

II. EQUILIBRIUM AND DYNAMIC SURFACE TENSION BEHAVIOR IN COLLOIDAL UNIMOLECULAR POLYMERS (CUP)

Ashish Zore, Peng Geng, and Michael R. Van De Mark

Department of Chemistry, Missouri University of Science and Technology, Rolla, MO 65409

ABSTRACT

Studies of interfacial behavior of pure aqueous nanoparticles have been limited due to the difficulty in making contaminant-free nanoparticles while also providing narrow size distribution. Colloidal unimolecular polymers (CUPs) are a new type of single chain nanoparticles with a particle size range from 3 to 9 nm that can be made free of surfactants and VOCs. CUP particles of different size and surface charges were made. The surface tension behavior of these CUP particles in water was studied using a maximum bubble pressure tensiometer. The equilibrium surface tension decreased with increasing concentration and the number of charges present on the surface of the CUP particles influences the magnitude of the interfacial behavior. The effect of electrostatic repulsion between the particles on the surface tension was related. At higher concentrations, surface charge condensation starts to dominate the surface tension behavior. The dynamic surface tension of CUP particles shows the influence of diffusion of the particles to the interface on the relaxation time.

1. INTRODUCTION

Surface tension is a crucial property that has significance in many industries like the field of coatings, adhesives, inks, etc. The growing use of nanoparticles and colloidal suspensions in these industries also generates interest in understanding their contribution to the surface tension behavior by these charge stabilized particles in the absence of any surface-active ingredients. However, making charge stabilized colloidal suspensions free of surface-active ingredients or any contaminants has been difficult and often involves time-consuming and complicated processes like dialysis, ultrafiltration cell and ion exchange resin, etc. [1]. This purification issue makes studying the surface tension behavior of nanoparticles difficult as the presence of trace amounts of impurities can affect or dominate the measurements.

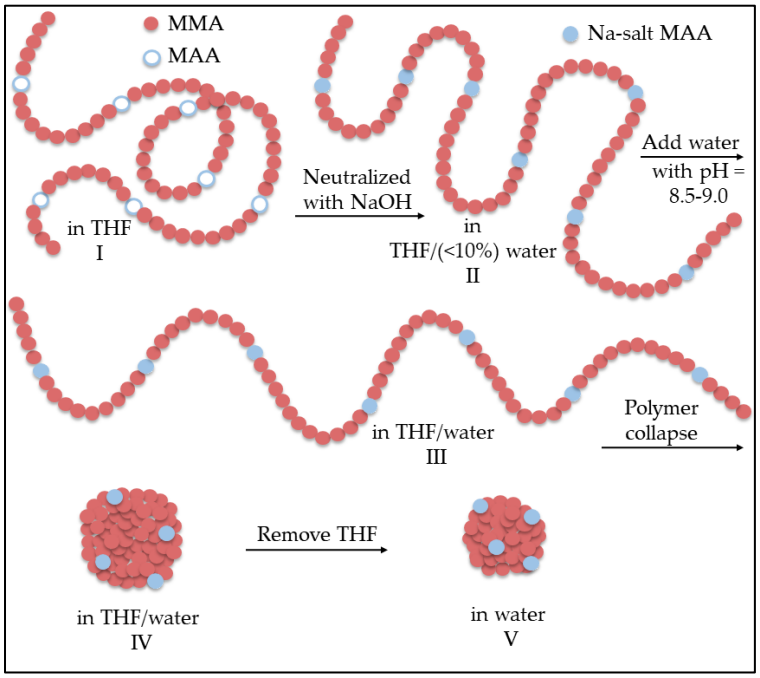

Figure 1. Schematics of the water reduction process and CUP formation

Colloidal unimolecular polymer or CUP particles are typically 3-9 nm size charge stabilized particles that are simple and easy to prepare [2]. These CUP particles are made from a single polymer chain, having a well-balanced number of hydrophobic and hydrophilic units, which collapses into a particle by a simple process called water reduction (Figure 1). The polymer chains collapse into a particle because the polymer-polymer interactions become stronger than the polymer-solvent interactions, similar to the formation of micelles. The charge groups repel each other, pushing them apart, which causes the chains to conform into a spheroid during the collapse. The charges will try to distribute evenly on the particle surface to minimize the charge-charge repulsion forces. The charged groups present on the surface of the particle prevent aggregation by providing stability through ionic repulsion. The water reduction process gives a stable colloidal dispersion, which is free of additives, surfactants, volatile organic compounds (VOCs) or any form of impurities. The CUP suspension thus prepared contains only charged particles, water and counter-ions and a relatively small amount of base to keep the pH (8.5-9.0) basic. It is easy to manipulate the physical parameters like particle size, charge density on the CUP surface and polymer composition of these CUP particles [3]. CUP particles can be a good model material for studying proteins and they can also have potential applications in the field of coatings, drug delivery, catalyst matrix and many others. These CUP particles have a layer of surface or bound water that has different properties like density, specific heat capacity, freezing point, NMR relaxation time, etc. as compared to regular/bulk water [4-6]. The charges present on the particles and the surface water also gives rise to electroviscous effects [7].

In the field of coatings, CUPs can be used as a coating resin and in conjunction with latex and polyurethane dispersions (PUDs) wherein they can also be cured with an aziridine [8] or a melamine [9] crosslinker. CUPs particles can be made with sulfonic acids as the charge stabilizing group [10] which can be used as a catalyst for waterborne acrylic-melamine systems [11]. CUP particles with cationic charged groups have been made using QUAT monomer ([2-(methacryloyloxy) ethyl] trimethylammonium chloride) [12] or amines with acetic acid to generate the cationic salt [13]. CUPs with amine functional charged groups have also been used as a crosslinker for waterborne epoxy coatings. CUP particles have also been proven to be a useful additive for freeze-thaw stability and wet edge retention due to the presence of non-freezable water around them [13].

Surface tension is one of the important properties of coatings and is controlled primarily using surface-active agents. CUP particles can alter the surface tension of water and it is, therefore, important to understand the interfacial behavior of these particles at the air-water interface. Surface tension studies [14,15] done with polyelectrolytes solutions show that surface activity is due to the orientation of hydrophobic and hydrophilic groups in the polymer chain at the air-water interface. The polyelectrolytes are present in the solution in a free moving open chain configuration which makes the orientation of hydrophobic groups at the interface possible. For a CUP particle, the polyelectrolyte chain is collapsed such that the hydrophobic groups are present mainly in the interior of the particle. The behavior of the CUP particle at the air-water interface is similar to solid charge stabilized colloidal particles rather than freely moving or flexible polyelectrolyte chains. When the glass transition temperature of the CUP polymer is high

(above ambient temperature), the hydrophobic groups present in the interior are not mobile. Studies have been done to understand the surface behavior of small charge stabilized particles like silica [16], TiO_2 [17], and polystyrene [1] at the air-water interface. A theoretical model was developed by Paunov [18] for understanding the adsorption of charged colloid particles at the air-water interface. The studies [16,17] done with TiO_2 and SiO_2 based charge stabilized colloidal particles were using large size particles (average size much greater than 30 nm) having very broad size distribution and they contained contaminants or supernatants present in the dispersion. Surface tension studies of charge stabilized particles of size less than 10 nm have rarely been reported. One of the difficulties has been to make a charge stabilized nano-particle free of any other ingredients. Nanoscale dispersions of inorganic particles like bismuth telluride, [19] aluminum oxide and boron nanoparticles [20] have been successfully studied to gain insight into their surface tension behavior. These studies attributed the electrostatic repulsion between the particles as a cause of a decrease in surface energy. A preliminary study on the equilibrium and dynamic surface tension was done using CUPs having carboxylate, sulfonate and QUAT-based ionized groups [21]. Sulfonates showed lower surface tension as compared to QUATs which was followed by carboxylates. The surface tension behavior of CUP particles was also compared against polyurethane dispersions (PUDs) and latex. Latex and PUDs due to their large particle size have slow diffusion and therefore take longer to reach equilibrium.

This study focuses on both equilibrium and dynamic surface tension behavior of CUP particles at the N_2-water interface. Air contains 78% N_2, and therefore, using pure N_2 helps understand the air interface behavior without any carbon dioxide contamination.

The effect of concentration, polymer structure, particle size and charge density (ions per nm^2) on the interfacial behavior was of primary interest in this evaluation. A recent investigation on the effect of CUP particles on the evaporation rate of water provided an important insight into the particle arrangement at the interface [22]. Since evaporation and surface tension both are interfacial phenomena, this investigation relates both studies to better understand the interfacial behavior of CUP particles. In dynamic surface tension, the bubble rate is varied from fast to slow in order to create a new surface of different surface ages. When a new surface is created the CUP particles migrate to the new interface and dynamic surface tension can provide information about the mechanism and the diffusion behavior of particles. The dynamic interfacial study can be more useful in practical applications like spraying, printing, foaming, or coating which occur under non-equilibrium or dynamic conditions. The maximum bubble pressure method, used in this study, allows the measurement of both dynamic and equilibrium surface tensions without the effects of humidity, air turbulence, and contamination by carbon dioxide.

2. MATERIALS AND METHOD

2.1. MATERIALS AND SYNTHESIS

The polymerization procedure, water reduction process to form CUP particles, characterization methods of polymers 1-8 and CUP particles are reported elsewhere [4]. The molar quantities of monomers - methyl methacrylate (MMA) and methacrylic acid (MAA), initiator (AIBN) and chain transfer agent (1-dodecanethiol) for making the two

new polymers used in this study are mentioned in Table 1. Heptanoic acid and octanoic acid were purchased from Sigma-Aldrich and used as received. Sodium heptanoate and

Table 1. Molar quantities of monomers, initiator (AIBN) and chain transfer agent (1-dodecanethiol) used for synthesis of polymer 7 & 8.

Polymer	**MMA (mol)**	**MAA (mol)**	**AIBN (mol)**	**1-Dodecanethiol (mol)**	**THF (mol)**
7	0.953	0.053	$7.04 * 10^{-4}$	$1.6 * 10^{-3}$	2.77
8	0.852	0.170	$7.16 * 10^{-4}$	$1.6 * 10^{-3}$	2.77

sodium octanoate was prepared by mixing equimolar quantities of the carboxylic acid with sodium hydroxide (0.1M solution). For surface tension measurements, solutions of sodium heptanoate and sodium octanoate were prepared in deionized water.

2.2. SURFACE TENSION MEASUREMENTS

Sensadyne PC-500 LV, a maximum bubble pressure method (MBPM) based instrument, was used to measure the surface tension of CUP suspensions. A constant temperature water bath was used to equilibrate the temperature of the suspension at 25 ± 0.1° C before making the equilibrium surface tension measurements and at 22 ± 0.1° C for dynamic surface tension. The tensiometer was calibrated with analytical reagent 100% absolute isopropyl alcohol and Milli-Q ultrapure water. The flow pressure of nitrogen gas was maintained at 40 psi. An average of three readings with less than 0.1

mN/m difference was reported. The surface age used for measuring the equilibrium surface tension was 3 sec.

2.3. THERMOGRAVIMETRIC ANALYSIS MEASUREMENTS

Thermogravimetric analysis at atmospheric pressure was performed on a TA instruments Q500 (TA Instruments, New Castle, DE, USA). Nitrogen was used as inert gas at a constant flow rate of 40 ml/min. Sample amount of approximately 30 μL was loaded to a tared platinum pan via a micro-pipette to maintain the same depth of solution. The platinum pans from TA instruments had a diameter of 9.4 mm. To minimize the evaporation before reaching temperature, the sample was heated to the experimental temperature 298.15 K at 100 K/min. The instrument has a built-in thermocouple placed aside the pan for measuring the temperature of the sample. The sample was held isothermally at 298.15 K for 360 min and the weight percent change of the sample was recorded as a function of time. Each CUP solution was run three times.

3. RESULTS AND DISCUSSION

3.1. POLYMER SYNTHESIS AND CHARACTERIZATION

Polymers were made such that they have different molecular weights, different monomer ratios of hydrophobic (MMA) and hydrophilic (MAA) monomers and a different number of charges per unit area on the surface, charge density, of the CUP particle. Polymers 1-3 have the same monomer ratio but different molecular weights which gives them different charge densities. Polymers 2, 4 and 5 have the same charge

density but different molecular weights. All polymers except for polymers 2, 4, and 5 have variations in charge density. Variations in molecular weight will result in CUP particles of different diameters. The relation between particle size and molecular weight is discussed later. Note, all molecular weights for the polymers are absolute number average since the real molecular weights define the collapsed size whereas the relative molecular weights would not. Table 2 shows the acid number, density and molecular weight of the copolymers used for this study. The molecular weight and density of the dry CUPs were used for calculating the particle size.

Table 2. Acid number, densities, molecular weight, and polydispersity index of the copolymers.

Sample ID	**M_W [b] (g/mol)**	**P.D.I. [c]**	**Monomer ratio (MMA: MAA)**	**AN (mg KOH/g) [d]**	**Density of dry CUP, ρ_p (g/ml)**
Polymer 1 [a]	28.9k	1.8	9:1	56.8	1.2246±0.0018
Polymer 2 [a]	59.8k	1.7	9:1	57.0	1.2311±0.0014
Polymer 3 [a]	122.5k	1.7	9:1	56.9	1.2342±0.0018
Polymer 4 [a]	25.4k	2.3	6.8:1	73.2	1.2243±0.0018
Polymer 5 [a]	73.5k	1.7	9.8:1	52.6	1.2315±0.0018
Polymer 6 [a]	49.7k	1.8	14:1	37.7	1.2307±0.0016
Polymer 7	45.4K	1.9	18:1	29.1	1.2290±0.0019
Polymer 8	50.1K	1.6	5:1	95.8	1.2300±0.0012

a) Data were taken from Ref [4].
b) Absolute number average molecular weight from GPC.
c) P.D.I – Polydispersity index
d) A.N. - Acid Number was measured using ASTM D974.

3.2. PARTICLE SIZE ANALYSIS AND CHARGE DENSITY

After water reduction and solvent stripping the CUP suspensions were filtered through a 0.45-μm Millipore membrane filter before performing particle size measurements using a dynamic light scattering (DLS) instrument as reported elsewhere [4]. Table 3 shows the measured particle size for the copolymers and calculated particle size from the absolute molecular weight from GPC data. The diameter of the CUP particles was calculated from its molecular weight using the following equation 1.

$$d = \sqrt[3]{\frac{6M_w}{\pi N_A \rho_p}} \quad (1)$$

where d is the diameter of the particle, M_W is the number average molecular weight of the CUPs, N_A is the Avogadro's number and ρ_p is the density of the dry polymer. As expected, the diameter of the CUP particle increases with an increase in molecular weight which was consistent with our previous work [3]. For a unimolecular collapse into a sphere, the measured size from DLS should be very close to the calculated size from the molecular weight as shown in Table 3.

Charge density is the number of charges present per unit area (nm^2) of the particle and is calculated using equation 2.

$$\rho_v = \frac{M_W}{4\pi r^2 (n \times M_{H1} + m \times M_{H2} + \ldots\ldots\ldots + M_i)} \quad (2)$$

where n and m are the statistical number of hydrophobic monomer 1 and 2 in a repeat unit and is also mentioned as monomer ratio, M_W is the molecular weight of the CUP, M_{H1} and M_{H2} is the molecular weight of hydrophobic monomer 1 and 2, M_i is the molecular weight of hydrophilic monomer, r is the radius of the CUP particle. The charge

density of the CUP particle can be easily manipulated by changing the molecular weight of the polymer/particle size and/or the composition (monomer ratio) of the polymer.

Table 3. Measured and calculated particle size (diameter) and charge density of the CUPs.

Sample ID	**d(DLS) [b] (nm)**	**d(GPC) [c] (nm)**	**charge density, ρ_v, (ions per nm^2)**
Polymer 1 [a]	4.22	4.25	0.52
Polymer 2 [a]	5.38	5.40	0.66
Polymer 3 [a]	6.83	6.80	0.85
Polymer 4 [a]	4.04	4.05	0.66
Polymer 5 [a]	5.76	5.80	0.66
Polymer 6 [a]	5.06	5.08	0.42
Polymer 7	4.90	4.92	0.32
Polymer 8	5.94	5.08[c]	1.04 [d], 0.83 [e]

a) Data were taken from Ref [4].
b) Diameters are measured by dynamic light scattering (DLS) instrument.
c) Diameters are calculated from average molecular weight measured using gel permeation chromatography (GPC) using equation 1.
d) Assuming sphere conformation.
e) Assuming dumbbell conformation.

3.3. EQUILIBRIUM SURFACE TENSION

The bubble tensiometer required a bubble rate slow enough to allow equilibrium to be established. The surface age of three seconds was long enough to allow the CUP particles to reach equilibrium at the interface. The equilibrium surface tension of all the

CUPs that were measured show linear decreases with increasing concentration and then curves and finally becomes constant at high concentrations as seen from Figure 2. This behavior of reduction in surface tension with increasing concentration was also observed for typical surfactants [23]. When comparing CUPs (see Table 4) against an ionic surfactant, like SDS, at the same concentration (0.001 M), all the CUP polymers show a smaller reduction in surface tension ($\Delta\gamma$) than SDS [23, 24]. Polymer 3 CUPs show the largest difference $\Delta\gamma = 4.2$. The slope $\Delta\gamma/\Delta c$ gives a better illustration of "the effectiveness" of the surface-active agent to reduce the surface tension. The surface tension value of QUAT [12] and sulphonate [10] CUPs of molecular weight 55K and 56K and charge density 0.52 and 0.58 ions/nm^2 respectively are shown in Table 4. The $\Delta\gamma/\Delta c$ value of carboxylate CUPs (Polymer 3) was closer to that of QUAT CUPs. The higher effectiveness of sulfonate CUPs as compared to carboxylates can be attributed to the strong electrostatic repulsion of the sulfonate groups. A comparison study done with sulfonate and carboxylate ionomers show stronger ionic interaction in sulfonates which was attributed to greater polarization [25]. Sodium salts of carboxylic acid (see Table 4) have also been known to show some surface activity in water [26,27]. Sodium formate shows increase in surface tension with concentration similar to that of NaCl which could be attributed to the absence of hydrophobic groups. In the case of sodium acetate and sodium benzoate, they show surface activity like surfactants but at much higher concentration. Sodium laurate (at pH = 8.5), however, shows a much high surface activity. The size of the hydrophobic group affects surface activity as seen from $\Delta\gamma/\Delta c$ vales of sodium acetate, sodium benzoate and sodium laurate. For the same concentration, the $\Delta\gamma/\Delta c$ value of CUPs had a larger effect than sodium acetate and

benzoate but less effect than sodium laurate. Unlike most surface-active agents, the molar concentration of CUPs may not be a simple relationship. The hydrophobic groups in the CUP particles are not free to move around or orient their chains at the interface as in carboxylate-based small molecules. The hydrophobic regions in CUPs are larger than the methyl/phenyl group of the carboxylates and are dominated by the ester groups and likely some of the methyl groups on the backbone.

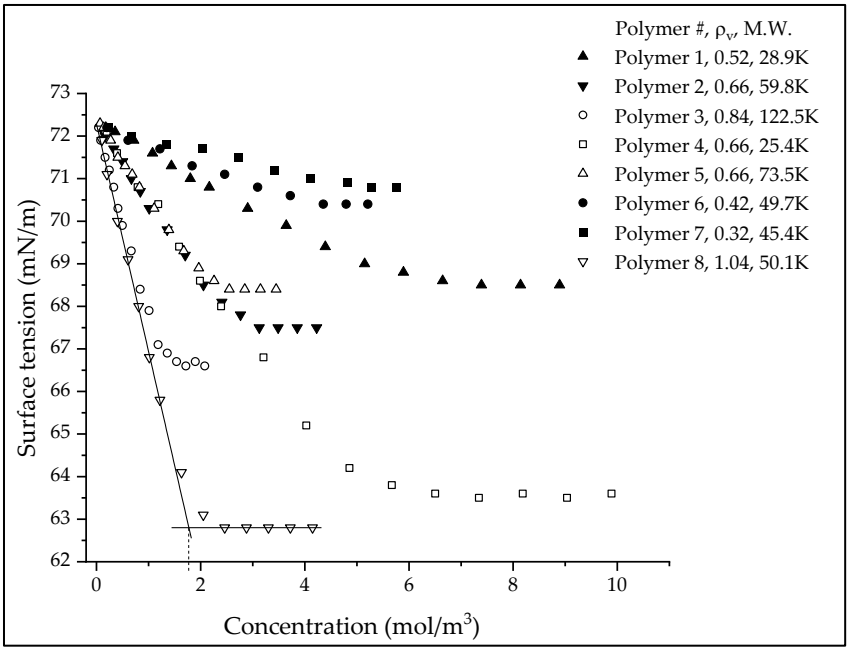

Figure 2. Equilibrium surface tension (mN/m) vs molar concentration (mol/m^3) of CUP solution made from polymer 1-8.

Okubo used monodispersed polystyrene latex particles with a strongly hydrophobic surface and silica particles which have a hydrophilic surface to study the surface tension behavior of colloids in deionized water without the addition of any

surfactant [1]. In general, there was a decrease in surface tension as the particle volume fraction increased. The particles suspensions were described to be liquid-like or gas-like

Table 4. Comparison of surface tension of CUPs surfactants, sodium chloride and sodium carboxylates.

	Concentration c/c* [b], mols/L	**Surface tension [a], γ, mN/m**	**Δγ**	**Δγ/Δc (Δγ/Δc*)**
Water	0	72.2	0.0	0
CUPs (Polymer 3)	0.001/0.0155 [b]	68.0	4.2	-4200 (-271)
CUPs (Polymer 2)	0.001/0.0114 [b]	70.3	1.9	-1900 (-166)
CUPs (Polymer 7)	0.001/0.0067 [b]	71.9	0.3	-300 (-45)
QUAT CUPs [c]	0.001	68.7	3.5	-3500
Sulphonate CUPs [c]	0.001	65.6	6.6	-6600
SDS [c]	0.001	65.0	7.2	-7200
Sodium Chloride	0.35	73.9	-1.7	4.86
Sodium Formate [c]	1	73.2	-1.0	1
Sodium Acetate [c]	1	70.2	2.0	-2
Sodium Benzoate [c]	0.26	68.2	4.0	-15.38
Sodium laurate [c]	0.001	63.6	8.6	-8600
Sodium heptanoate	0.005	70.5	1.7	-340
Sodium Octanoate	0.005	65.5	6.7	-1340

a) The surface tension values are below the CMC.
b) The concentration c* for CUP polymers 2,3 and 7 were calculated using equation 7.
c) Data taken from Ref [10,12,26].

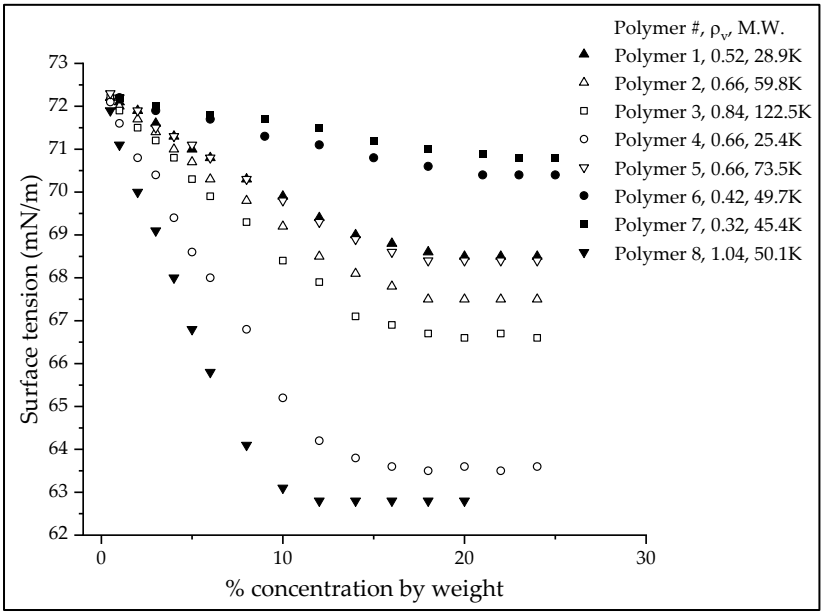

Figure 3. Equilibrium surface tension (mN/m) vs % solid of CUP solution made from polymer 1-8.

at low concentration due to the suspensions being turbid and milky. The decrease in the surface tension for the liquid-like or gas-like suspension was not very significant. However, at higher concentration, the surface tension significantly drops with concentration and the suspension form crystal-like structure in which brilliant iridescent colors from Bragg's diffraction and glittering single crystals were observed with the naked eye. The CUP suspensions were clear at all the concentrations measured in this study. The CUP particles being in the true nano-scale size of 4-7 nm and cannot scatter visible light, hence they look clear. At high concentrations, the CUP particles are sufficiently stable and don't aggregate. CUP solutions have been followed for over 10 years without a size change or any stability issue. The volume fraction concentration that was measured for the polystyrene and silica suspensions did not exceed 0.1 and the surface tension differed by $\Delta\gamma = 12$ for most polystyrene suspensions and $\Delta\gamma = 2$ for

silica suspensions. The difference in surface activity for polystyrene and silica is attributed to high hydrophobicity of the surface of polystyrene. Another study done by Dong and Johnson [16,17], shows the surface activity of TiO_2 and SiO_2 (pH =10 and 11) based charge-stabilized colloidal dispersions. The surface tension values of TiO_2 and SiO_2 decreased with increase in concentration of particles. The surface tension drops to the lowest value at 5% concentration by weight and then plateaus for a while before increasing as the concentration increases. The maximum surface tension difference of $\Delta\gamma = 3.5$ for SiO_2 suspension and $\Delta\gamma = 5.2$ for TiO_2 suspensions was observed at 5% concentration by weight. For CUPs at 5% concentration by weight (Figure 3) a difference of $\Delta\gamma = 1.9$ was observed for Polymer 3. However, the maximum difference of $\Delta\gamma = 5.5$ was observed for Polymer 3 CUPs at 18% solids which is higher than in SiO_2 and close to the TiO_2. One of the significant differences between CUPs and TiO_2 and SiO_2 particles is the size distribution. TiO_2 and SiO_2 particles used in the study had a very broad particle size distribution with the size ranging from 40 nm to 1,400 nm and 500 nm to 8,000 nm respectively. CUPs, on the other hand, have consistently shown much narrower particle size distributions [2,3]. Also, the particle shape of TiO_2 and SiO_2 particles in the suspension was irregular and not spheroidal like CUPs. Surface tension studies have been done with 2.5 nm and 10.4 nm bismuth telluride nanofluids [19] using contact angle measurements on silicon wafers and glass substrates. At 0.0003% concentration by weight, the 2.5 nm suspension shows a difference of $\Delta\gamma = 26.70$ and the 10.4 nm suspension show a difference of $\Delta\gamma = 18.67$. The surface tension reduction in the case of bismuth telluride was much higher when compared to the CUP, TiO_2 and SiO_2 particles. Bismuth telluride particles used in the study were modified using thioglycolic acid which

can interact with each other to form acid dimers at the interface. The amount of acid groups on the nanoparticle surface are unknown which makes it difficult to access the contribution of thioglycolic acid to surface tension reduction as compared to the actual bismuth telluride nanoparticle surface. The pH of the nanoparticle solution is unknown. The acid groups may also cause the particles to adsorb on the silicon and glass interface of the silicon wafer and glass substrates used in contact angle measurement. Furthermore, the bismuth telluride nanoparticles used were stable for a few hours to a couple days whereas CUP solution, as mentioned earlier, is stable for over 10 years if the pH is maintained basic (~8.5). Studies done with 18 nm aluminum oxide [20] and multiwall carbon nanotubes (D = 8-15 nm, L = 10-50 μm) measured using a pendent drop method only show an increase in surface tension with concentration of the particles in water and ethanol. This behavior was different from the bismuth telluride, TiO_2 and SiO_2. All the surface tension studies mentioned earlier do not consider a critical aspect, charge density of the nanoparticle, which can possibly influence the surface tension behavior. This could be due to the inability to precisely manipulate the number of charges on the surface of these nanoparticles to obtain a required charge density.

For CUPs, the effect of molecular weight on surface tension behavior can be understood from the data of polymers – 2, 4 & 5 (Figure 2) which have the same charge density but different molecular weights. They have a similar reduction in surface tension at the same molar concentration. This indicates a dependency of surface tension on the charge density of the polymer. Polymers 1 & 4 and Polymers 2, 6, 7 & 8 (Figure 2) which have similar molecular weight, but different surface charge densities show that higher charge density CUP particles have more reduction in surface tension. The data in Figure

2 can be fit using two lines, first for the initial decrease and the second for the constant region. The slope of the first fit can be considered as the "effectiveness of the CUP particles" at reducing the surface tension. The more negative the value of slope the higher is the effectiveness of the CUP particle at reducing the surface tension. The plot of slope or effectiveness of CUPs against the charge density is show in Figure 4. The data follows an exponential trend and later deviates at very high charge density.

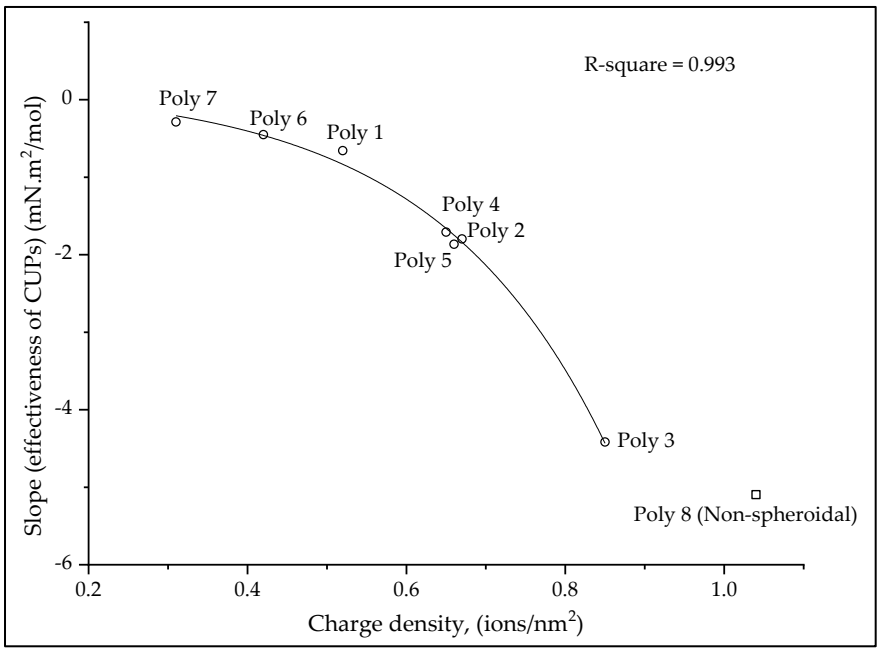

Figure 4. Slope or effectiveness of CUP against charge density (ions/nm^2) of the particle.

For polymers containing many ionic groups, a theoretical model for the conformation of the chain based on an electrostatic blob and the scaling theory was first developed by de Gennes and Pfuety and reviewed by Dobrynin [28]. Depending on the number of charges or ionic groups present on the chain, the conformation can range from an electrostatic blob to a pearl necklace. A theoretical model [29] has been developed for

a dilute solution of polyelectrolyte of uniform charge having a degree of polymerization N, monomer size b, and fraction of charged monomers f in a poor solvent having a dielectric of ε. The model predicts the following for a polyelectrolyte of N = 200 monomers: when the polymer chain is uncharged (f =0) it collapses into a spherical globule, at f = 0.125 the chain collapses into a dumbbell shape and at f = 0.150 the chain collapses into a pearl necklace with three beads. In the case of polymer 8 (f =0.17), the charge density of the polymer is high enough to cause the chain to collapse into a different conformation instead of spheroidal. The deviation in the surface tension behavior at higher charge density can be attributed to the change in conformation of the particle from a spheroidal to non-spheroidal shape. All the other polymers fall into spheroidal charge density region where f is between 0.05 and 0.128.

3.4. MODEL FOR CUP PARTICLES AT INTERFACE

A better understanding of the mechanism of reduction in surface tension caused by the CUP particles requires a model of these particles arranged at the N_2-water interface. In a study done on the evaporation rate of water for these CUP solutions, a model of CUP particles arranged at the N_2-water interface was presented [22]. Since both evaporation rate and surface tension are interfacial phenomena, the model should explain all the results. In a dilute solution at equilibrium, the particles are randomly distributed and stabilized by a combination of Brownian motion, solvation by water and electrostatic repulsion due to the presence of an electrical double layer around the particles. The particles present in the water phase are constantly experiencing charge repulsive force from all directions as they are surrounded by other particles. However, the particles at the

interface do not have any charge force exerted on them from the N_2 side. Thus, the other particles around it push the particles towards the N_2-interface and force them partially out of the N_2-water interface as shown in Figure 5a.

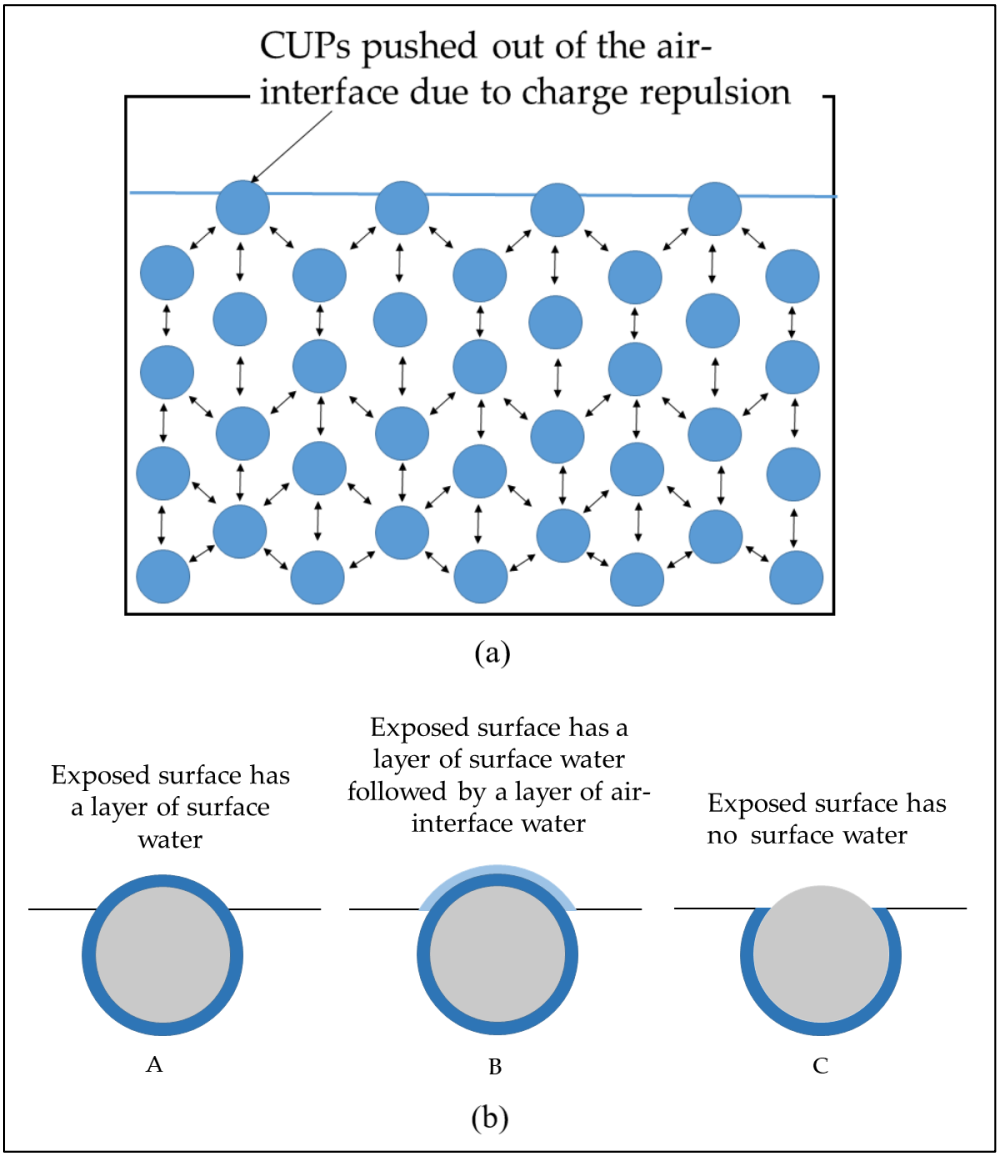

Figure 5. a) CUP particles pushed through the N_2 water interface due to charge repulsion from particles below. b) CUP particles pushed through the N_2 water interface due to charge repulsion can exist in three possible states A-C.

At the interface, the particles can exist in three different states (Figure 5b): A: CUP with a layer of surface water, B: CUP with a surface water layer followed by a layer of N_2-interface water, and C: Cup particle with no water. The CUP particle surface is highly hydrophilic and has a layer of strongly associated surface water. Hence, model C is less likely to exist. The particles at the N_2 interface are very likely to exist as shown in Model A or B. The results from evaporation rate study are in good agreement with Model A or B [22]. When the evaporation rates of dilute CUP solutions were measured, it showed an increase in evaporation rate of water from the solution over pure water. This increase in evaporation rate has been attributed to the increase in surface area caused by the particles when they deform the interface as shown in Model A & B. If Model C were to exit, then a decrease in the evaporation rate would be expected as it reduces the surface area at the interface.

3.5. RELATIONSHIP BETWEEN SURFACE TENSION AND CHARGE GROUP BASED ON MODEL A

Figure 6 shows a particle of radius r_{CUP} present at the N_2-water interface. The CUP particle extends above the N_2-water interface to a height, h. Since the increase in the evaporation rate is due to increase in the surface area, the height h for a given concentration can be estimated using the equation 3.

$$h = \sqrt{\frac{\Delta R}{R \times \pi}} \times \left(\sqrt[3]{\frac{M_W}{\rho \times X_{CUP}}} \right) \quad (3)$$

where h is the height of the interface water deformation, ΔR is the increased evaporation rate compared with water, R is the evaporation rate of the CUP solution, M_w is the molecular weight of CUP, ρ is the density of the CUP solution, X_{CUP} is the weight

fraction of CUP. There are two main assumptions in calculating the height (h) values using equation 3: 1) The increase in evaporation rate is solely due to an increase in area, thereby neglecting any other effects if present and 2) The evaporation rate of bulk water

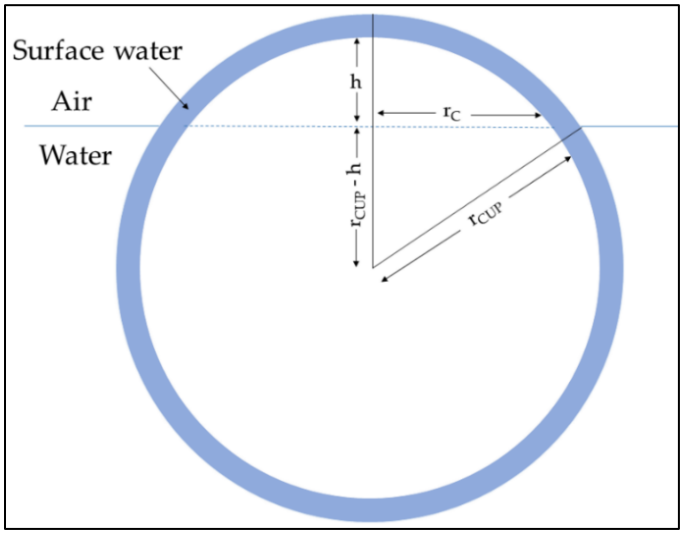

Figure 6. Deformation of surface by CUP particles at N_2-water interface.

is the same as surface water (model A) or N_2-interfacial water (model B). Surface water has been successfully studied and has been shown to have different properties like density, specific heat capacity and freezing point than bulk water. Hence, it is possible for the evaporation rate of surface and bulk water to be different as well. However, despite these assumptions, the height values can be crucial in better understanding the surface tension behavior. The evaporation rate data for Polymer 1-6 at different concentrations was borrowed from the evaporation rate study [22] and for polymer 7-8 was measured. Further, the height values were calculated using equation 3 and the circumference of CUP at the interface was calculated using equations 4 and 5.

$$r_c = \sqrt{{r_{cup}}^2 - (r_{cup} - h)^2} \quad (4)$$

$$circumference = c_{int} = 2\pi r_c \quad (5)$$

The circumference, c_{int} is the length of the interface created by N_2, water and CUP particle or surface water. The inverse of charge density (nm^2/ion) gives the area occupied

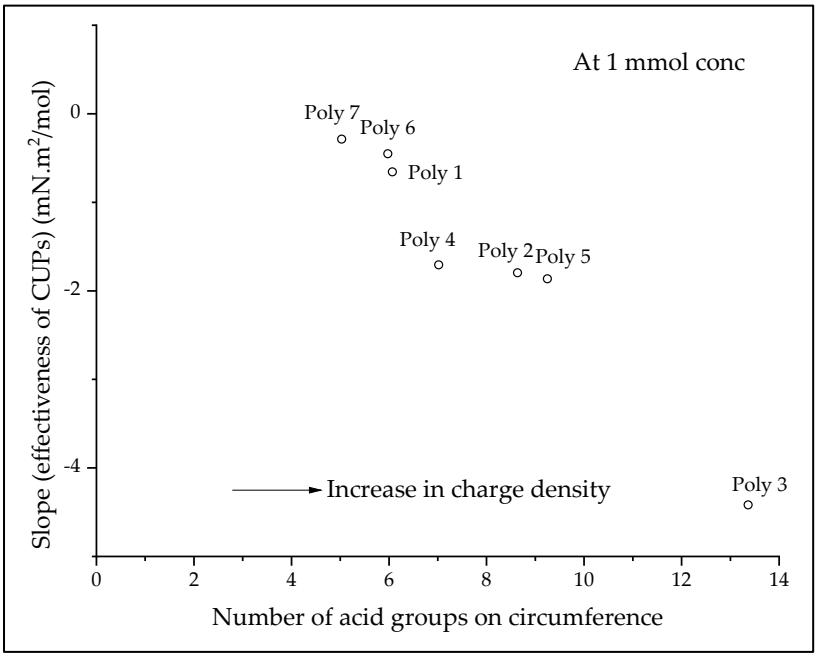

Figure 7. Slope or effectiveness of CUPs against Number of charges or acid groups (N_{charge}) present on the circumference (N_{charge}).

by each ion on the surface of the particle. Assuming each ion occupied a circular area on the surface, the diameter of the charge (d_c) can be calculated. Using the diameter of charge (d_c), we can calculate the number of charges or acid groups present on the circumference (N_{charge}) using the following equation 6,

$$N_{charge} = \frac{c_{int}}{d_c} \quad (6)$$

Figure 7 shows a plot of the number of charges or acid groups present on the circumference against the effectiveness of CUPs. As the number of charges or acid groups at the circumference increases, the CUP particles become more effective at reducing the surface tension. The charge on the circumference also explains the trend with charge density seen in Figure 4 because the number of charge groups at circumference is directly related charge density. Hence, CUPs with high charge density show lower surface tension.

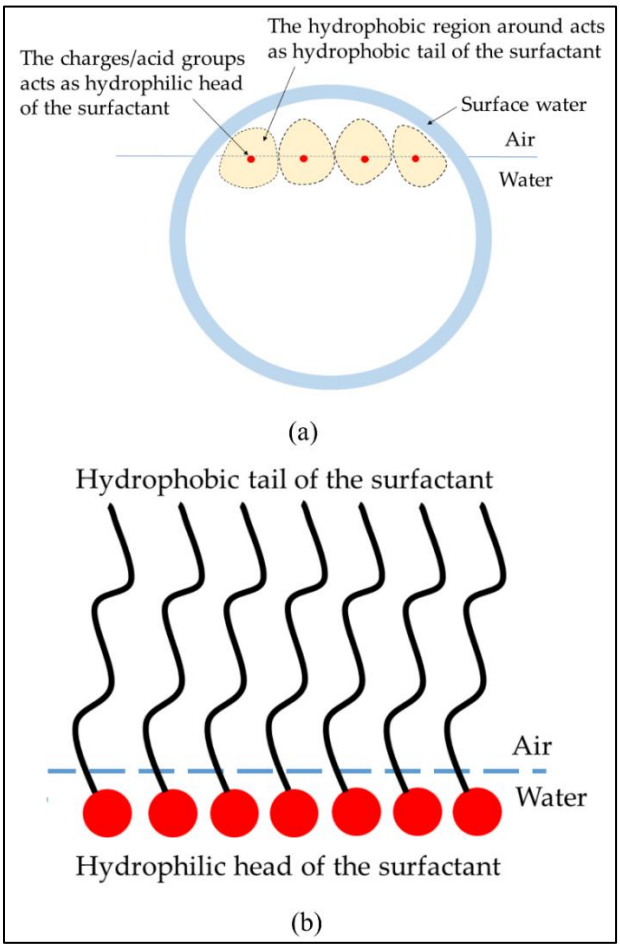

Figure 8. a) Model depiction of charge groups mimicking as a classic surfactant at the N_2-water interface. b) a Classic surfactant at the N_2-water interface [30].

A plausible explanation for the trend observed in Figure 7 is that the charges or acid groups present on the circumference, which is also the N_2-water interface, behave as a surfactant. This can be visualized from Figure 8a which shows a charge group acting as a surfactant where the charge or acid group is the hydrophilic head and the hydrophobic surface around it is the hydrophobic tail. When there are more acid groups present on the interfacial circumference, it corresponds to having more surfactant molecules at the interface and hence the surface tension becomes lower. The concentration (c*) of the charge groups present at the interface for CUP particle at a given concentration, c (mols/l) can be calculated using equation 7.

$$c^* = c \times N_{charge} \tag{7}$$

The c* for polymers 2,3 and 7 are shown in Table 4. The slope values show the effectiveness of CUP particles to be between that of sodium benzoate and sodium heptanoate. However, as shown in the depiction in Figure 8a, the hydrophobic region of the CUP is not a linear chain-like sodium heptanoate. Also, unlike sodium benzoate and heptanoate, the hydrophobic region is also comprised of ester groups, and it extends not only above the surface but also to the left, right and below.

3.6. SURFACE TENSION AT HIGHER CONCENTRATION

The surface tension deviates from linearity at high concentrations and eventually reaches a constant value (See Figure 2). Similar behavior was also observed in surfactants wherein, due to micelle formation, the surface tension becomes constant [24, 31]. Sodium acetate and sodium benzoate also show a constant surface tension at higher concentration which could be due to formation of loose aggregates instead of a proper micelle [26]. In

case of CUP particles, there is no micelle formation. The surface activity of TiO_2 and SiO_2 (pH =10 and 11) studied by Dong and Johnson at high concentration (above 5% solids) also showed a constant surface tension. However, as the particle concentration is increased further, the surface tension starts to increase. They explained this behavior by the presence of strong capillary forces between the particles at the interface. For colloidal particles stabilized by surface charges (ionic) when the concentration of particles becomes very high, the charges present on the surface can undergo intermolecular counter-ion condensation or Manning condensation where some of the charges or surface ions will recombine with its counter-ion. Intermolecular counterion condensation has been observed in CUP solutions and its effect on the surface water thickness has been well studied in the thermodynamic characterization [4] and electroviscous effect papers [7]. Due to the intermolecular counterion condensation, the number of charges or ionized acid groups present on the surface reduces thereby reducing its effective charge density. The surface tension results shown in Figure 2 can be fit using two linear fits to obtain the intersection point. The molar concentration at the intersection can be considered as the onset concentration for intermolecular counterion condensation. The interparticle distance at the onset concentration can be easily estimated using equation 8.

$$Inter-particle\ distance, IPD = \frac{1}{\sqrt[3]{n}},\ \ n = number\ conc.\ \ in\ m^{-3} \tag{8}$$

The number concentration, n, is the number of particles present in one cubic meter. When the interparticle distance at the onset concentration was plotted against charge density it indicated a linear behavior as shown in Figure 9. Having a higher charge density will increase the repulsive force between the particles and hence counterion condensation can be expected at lower concentrations. Low charge density particles must

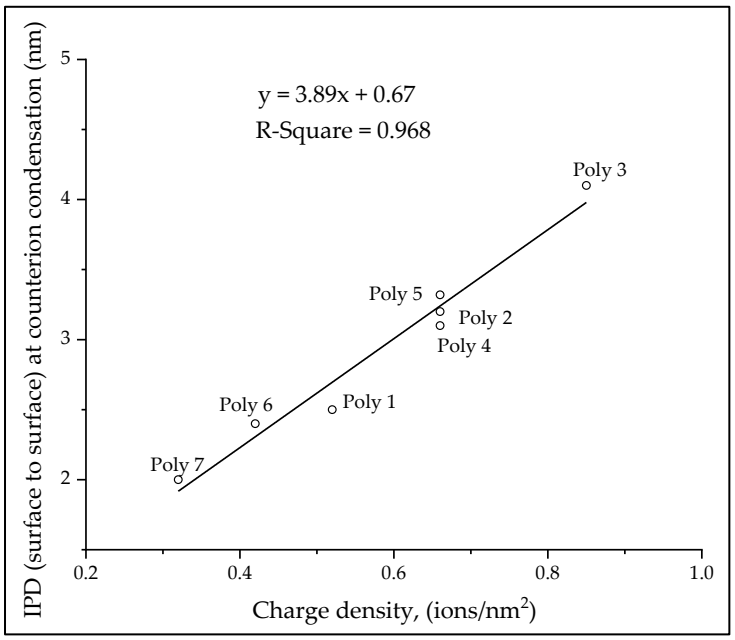

Figure 9. Interparticle distance (nm) at the onset concentration for counterion condensation against charge density (ions/nm^2) of the particle.

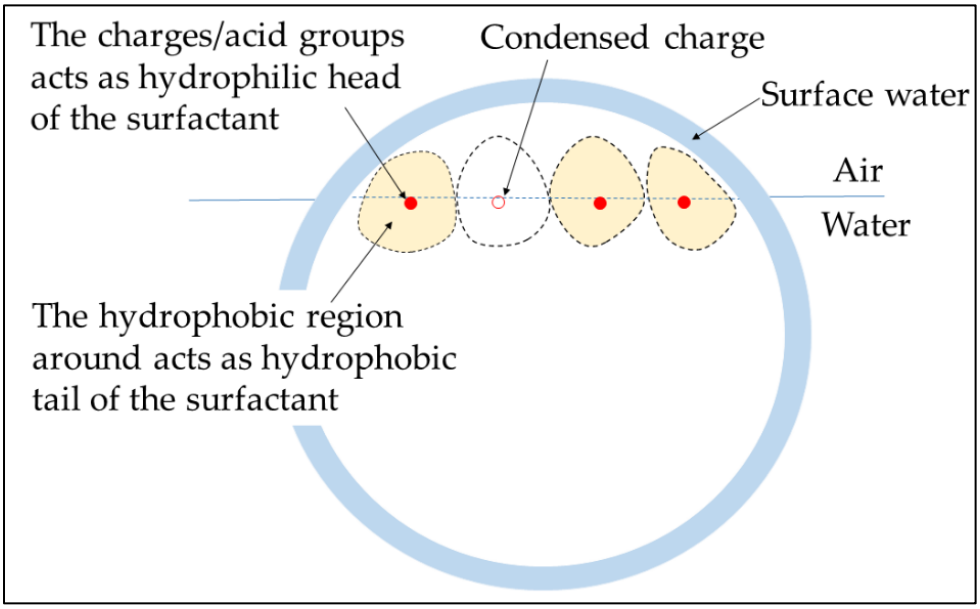

Figure 10. Charge condensation at high concentration reducing the number of charge groups present at the interfacial circumference.

come closer to each other for counterion condensation to take place. The surface tension becoming constant at high concentration can be explained by intermolecular counterion condensation. Counterion condensation reduces the overall number of charges present on the surface thereby reducing its charge density. This will reduce the number of charges present on the interfacial circumference, shown in Figure 10. The reduction in the number of interfacial charged groups will cause the surface tension to stay constant even when more CUP particles are being added to the solution.

3.7. DYNAMIC SURFACE TENSION BEHAVIOR

Polymers 1-5 were chosen due to their large $\Delta\gamma$ in the linear region (Figure 2) which was useful in understanding the effect of concentration by measuring the dynamic surface tension at three different concentrations along with understanding the effect of size and charge density on the dynamic surface tension. Figure 11 shows plots of dynamic surface tension for CUP solution of polymer 1-5 measured at three different concentrations for each. Surface age, defined as the time interval between the onset of bubble and moment of maximum pressure, was manipulated by changing the bubble rate. Slow bubble rate gives a longer surface age, therefore, giving more time for the CUP particle to reach the N_2 (bubble) -water interface. The dynamic data of surface tension (γ) vs surface age (t) for all the CUP polymers measured show an exponential fit by equation 9.

$$\gamma = \gamma_e + Ae^{-t/\tau} \tag{9}$$

where γ_e is the equilibrium surface tension and A (amplitude of the exponential curve, $\gamma_{t=0} - \gamma_e$) and τ (relaxation time) are the fitting parameters. Polymers used for the study

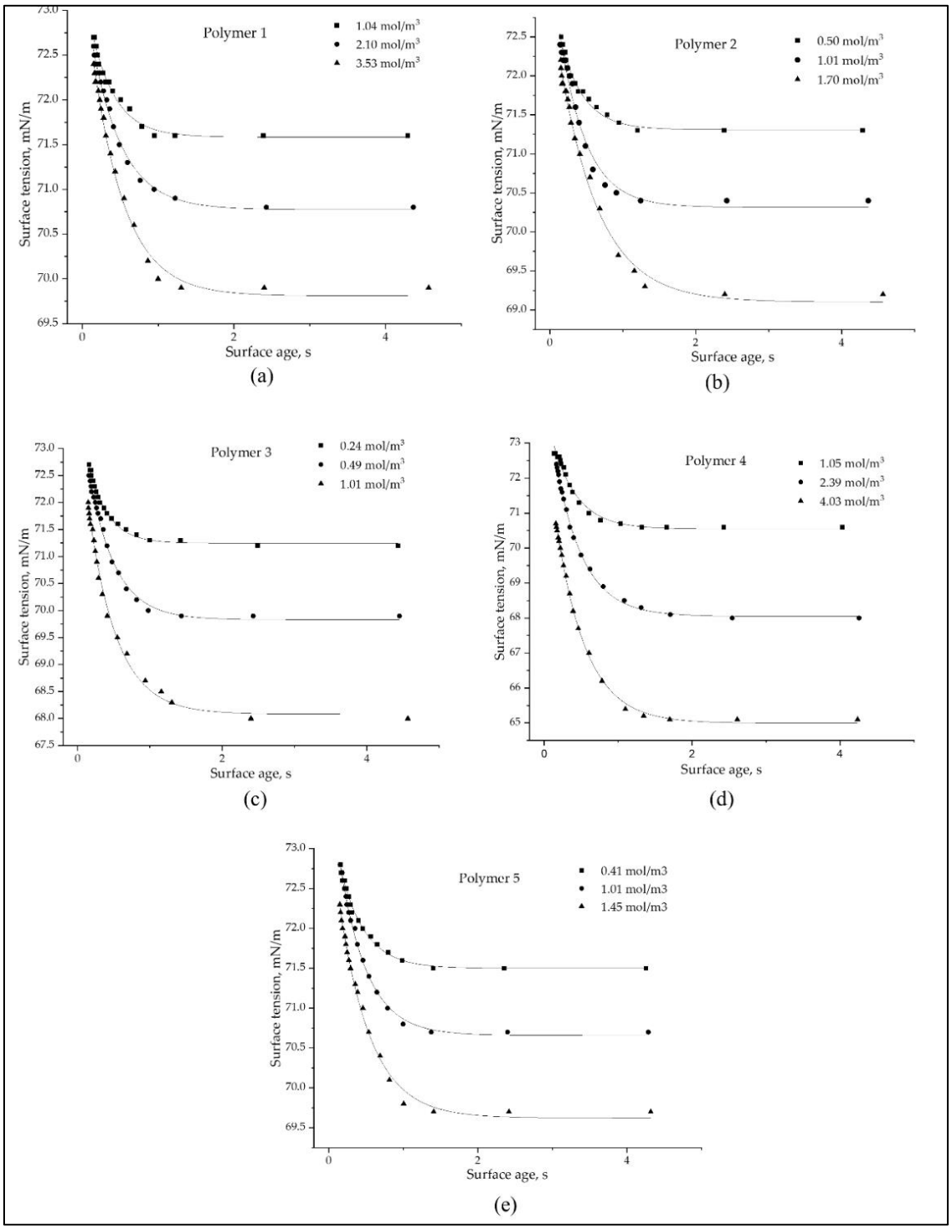

Figure 11. Dynamic surface tension (mN/m) at different concentration (mol/m^3) for CUP particles made from Polymer 1-5 (a-e).

Table 5. Relaxation time (τ) for the CUP particles of polymer 1-5 at different concentrations.

Sample ID	**Concentration, mol/m^3**	**γ_e, mN/m**	**τ, s**	**A**	**R^2**
Polymer 1	1.04	71.59	0.311	1.77	0.983
	2.10	70.77	0.401	2.57	0.993
	3.53	69.81	0.426	3.69	0.994
Polymer 2	0.50	71.31	0.315	1.84	0.984
	1.01	70.31	0.363	3.27	0.981
	1.70	69.10	0.543	3.99	0.993
Polymer 3	0.24	71.25	0.264	2.64	0.995
	0.49	69.83	0.360	4.22	0.994
	1.02	68.08	0.395	5.59	0.995
Polymer 4	1.05	70.55	0.331	2.63	0.994
	2.39	68.05	0.374	4.22	0.997
	4.03	64.99	0.406	5.59	0.995
Polymer 5	0.41	71.50	0.330	2.01	0.985
	1.02	70.66	0.361	3.28	0.998
	1.45	69.62	0.424	3.76	0.998

were of different molecular weights and charge density to understand the effects on the dynamic behavior. Relaxation time, τ, gives an indication of the rate at which the solution reaches equilibrium and therefore gives an idea of mobility of CUP particles. The

relaxation time, τ, values for all the CUP polymers measured at different concentrations are given in Table 5.

The particle size study with CUPs done by Van De Mark et. al [2] has shown that for accurate particle size measurement of CUP particles using DLS technique requires the viscosity of solvent to be replaced by the viscosity of solution to account for the increased viscosity due to the electroviscous effect. The collective diffusion coefficient of the spherical particles can be approximated from the generalized Stoke-Einstein equation (equation 10) which relates the diffusion coefficient (D_c) to the radius (r) of the particle measured using DLS, viscosity (η) of solution and temperature (T).

$$D_c = \frac{k_b \times T}{6 \times \pi \times \eta \times r} \tag{10}$$

As seen from the Table 5, the relaxation shows an increase with concentration for all the CUP polymers that were measured. This could be due to the lower diffusion coefficient of the particles at higher concentration. For a given CUP particle, as the concentration increases, it increases the solution viscosity which has an inverse relation to the diffusion coefficient as shown by the Stokes-Einstein.

Table 6 shows the relaxation time of the CUP polymers 1-5 measured at the same concentration of 1 mol/m^3. There are two variables affecting the diffusion of the CUP particle - particle size and charge density. Charge density gives rise to the electroviscous effect in the solution. Higher charge density leads to strong electroviscous behavior. The diffusion coefficients were calculated using equation 10, by measuring the viscosity at 1.03 mol/m^3 and the particles size on DLS at 22 °C. A plot of relaxation time against diffusion coefficient (Figure 12) show that as the diffusion coefficient increase the

relaxation time decreases. The particles can migrate faster to the newly created N_2-water interface (bubble).

Table 6. Particle size, Charge density, Relaxation time and Diffusion coefficient of the CUP polymers 1-5 measured at the average concentration of 1.03 ± 0.02 mol/m^3.

Sample ID	**Particle size, nm**	**Charge density, ions/nm^2**	**Relaxation time, τ**	**A**	**Diffusion coefficient 10^{-13} m^2/s**
Polymer 1	4.22	0.52	0.311	1.77	2.49
Polymer 2	5.38	0.66	0.363	3.27	1.35
Polymer 3	6.28	0.84	0.395	5.59	0.46
Polymer 4	4.04	0.66	0.331	2.63	2.30
Polymer 5	5.50	0.66	0.361	3.28	1.32

Figure 13 show the dynamic behavior of sodium dodecyl sulfate (SDS) at 2 mmol concentration [32]. The dynamic curve fits a double exponent equation.

$$\gamma = \gamma_e + A_d e^{-t/\tau_d} + A_k e^{-t/\tau_k} \quad (11)$$

where γ_e is the equilibrium surface tension and A_d and A_k (amplitude of the exponential curve, $\gamma_{t=0} - \gamma_e$) and τ_d and τ_k (relaxation time) are the diffusional and kinetic fitting parameters. In case of surfactants, the interface adsorption is dependent on diffusion at short surface age and on interfacial organization kinetic at long surface age. When a new surface is created, the interface is relatively empty and there is no barrier to adsorption at the interface. Hence, the time (τ_d) is governed by the diffusion rate of surfactant

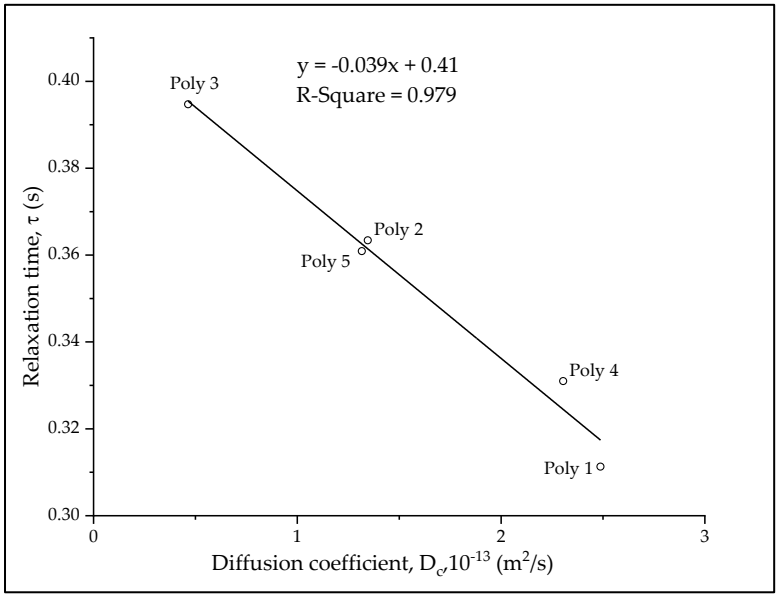

Figure 12. Relaxation time, τ_k (s) against diffusion coefficient, D_c (m^2/s) at 1 mol/m^3 concentration of CUP polymer 1-5.

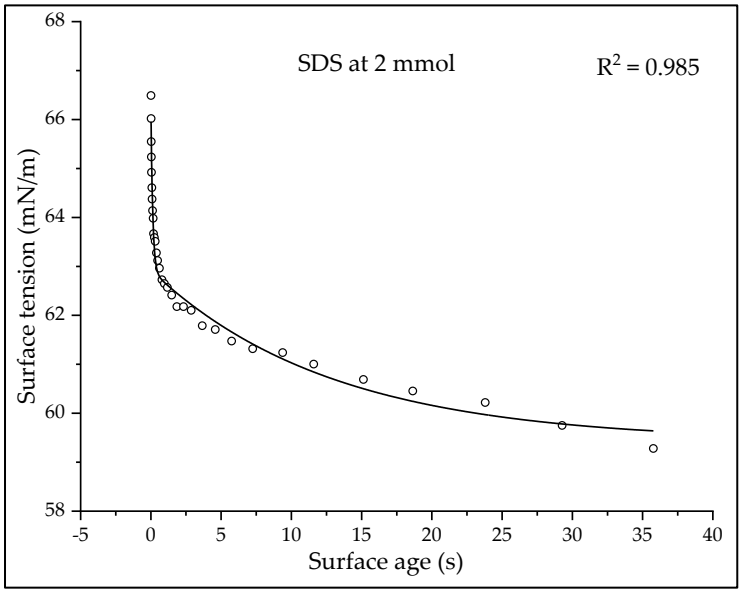

Figure 13. Dynamic curve of SDS at 2 mmol concentration. Reprinted (adapted) with permission from Christov, N. C., Danov, K. D., Kralchevsky, P. A., Ananthapadmanabhan, K. P., Lips, A. Maximum bubble pressure method: Universal surface age and transport mechanisms in surfactant solutions. *Langmuir*, **2006**, *22*, 7528-7542. Copyright 2019 American Chemical Society.

molecules to the interface. When the surface becomes older the concentration of surfactant molecules at the interface increases which creates an organizational barrier for the surfactant molecules that are moving to the interface. Hence, the time (τ_k) is governed by the organization kinetic of surfactant molecules at the interface. The diffusional and kinetic mechanisms are also observed in other surfactants [33]. For SDS, the τ_d and τ_k values are 0.133 and 12.85 s and the A_d and A_k values are 3.32 and 3.5 mN/m respectively.

All the CUP polymers have shown a single relaxation time (τ) at all the measured concentrations. All the τ values are relatively small. Polymer 1 at 2.1 mmol concentration show a $\tau = 0.401$ which is closer to the τ_d as compared to τ_k of SDS at similar concentration (2 mmol). Therefore, the relaxation time in CUPs is primarily a function of the rate of diffusion. The reestablishment of the charged particle distribution as the bubble grows into the solution is relatively rapid not dominated by any major structural organizational mechanism. The relaxation time, τ of all the CUPs (Polymer 1--5) measured is higher than the diffusion relaxation time, τ_d of SDS. This must be expected as CUP particles are larger in size as compared to SDS molecule and CUPs also exhibit the electroviscous behavior in solution which can further affect the diffusion rate.

4. CONCLUSIONS

Maximum bubble pressure tensiometer results on CUP particles provides a detail insight on the equilibrium and dynamic interfacial behavior of pure nanoscale size particles. The data from equilibrium surface tension combined with the evaporation

behavior gave a better model of particles present at the air-water interface. The model shows that the CUP particles were pushed out of the air-water interface which caused the surface charges to align at the air-water interface. The surface charges which then act as surfactants due to the hydrophobic region present around it. The magnitude of the surface tension was closer to sodium benzoate and sodium heptanoate although they are not good models for CUP solutions. At higher concentration, the surface tension becomes constant due to surface charge condensation. The surface charge condensation occurs at a longer distance when the CUP surface charge density is high. The charge condensation reduces the number of charges, which act as surfactants, present at the air-water interface. The dynamic surface tension behavior is mainly affected by the diffusion coefficient of the particle which is dependent on particle size and charge density. Slower particles show a longer relaxation time indicating the dynamic behavior to be influenced by rate of diffusion rather than a structure organization mechanism.

REFERENCES

1. Okubo, T. Surface tension of structured colloidal suspensions of polystyrene and silica spheres at the air-water interface. *J. Colloid Interface Sci.* **1995**, *171*, 55-62.

2. Riddles, C.; Zhao, W.; Hu, H.J.; Chen, M.; Van De Mark, M.R. Self-assembly of Water Insoluble Polymers into Colloidal Unimolecular Polymer (CUP) Particles of 3–9 nm. *Polymer* **2013**, *55*, 48–57.

3. Van De Mark, M.R.; Natu, A.; Gade, S.V.; Chen, M.; Hancock, C.; Riddles, C. Molecular Weight (Mn) and Functionality Effects on CUP Formation and Stability. *J. Coat. Technol. Res.* **2014**, *11*, 111–122.

4. Geng, P.; Zore, A.; Van De Mark, M.R. Thermodynamic Characterization of Free and Surface Water of Colloidal Unimolecular Polymer (CUP) Particles Utilizing DSC. *Polymers* **2020**, *12*, 1417.

5. Dawib, Y. A. NMR T1 studies of colloidal unimolecular polymer (CUP) surface water. Doctoral Thesis, Missouri University of Science and Technology, Rolla, 2015.

6. Chen, M.; Riddles, C.; Van De Mark, M. Gel point behavior of colloidal unimolecular polymer (CUP) particles. *Colloid Polym. Sci.* **2013**, *291,* 2893–2901.

7. Chen, M.; Riddles, C.J.; Van De Mark, M.R. Electroviscous contribution to the rheology of colloidal unimolecular polymer (CUP) particles in water. *Langmuir* **2013**, *29,* 14034–14043.

8. Mistry, J.K.; Van De Mark, M.R. Aziridine cure of acrylic colloidal unimolecular polymers (CUPs). *J. Coat. Technol. Res.* **2013**, *10,* 453-463.

9. Mistry, J.K.; Natu, A.M.; Van De Mark, M.R. Synthesis and application of acrylic colloidal unimolecular polymers as a melamine thermoset system. *J. Appl. Polym. Sci.* **2014**, *131,* 40916.

10. Natu, A. M. Synthesis, characterization and application of acrylic colloidal unimolecular polymer (CUP). Doctoral Thesis, Missouri University of Science and Technology, Rolla, 2015.

11. Natu, A.; Van De Mark, M.R. Synthesis and characterization of an acid catalyst for acrylic-melamine resin systems based on colloidal unimolecular polymer (CUP) particles of MMA-AMPS. *Prog. Org. Coat.* **2015**, *81,* 35–46.

12. Natu, A.M.; Wiggins, M.; Van De Mark, M.R. Synthesis and characterization of cationic colloidal unimolecular polymer (CUP) particles. *Colloid Polym. Sci.* **2015**, *293,* 1191–1204.

13. Gade, S. V. Application of Colloidal Unimolecular Polymer (CUP) particles in Coatings. Doctoral Thesis, Missouri University of Science and Technology, Rolla, 2015.

14. Okubo, T. Surface tension of synthetic polyelectrolyte solutions at the air-water interface. *J. Colloid Interface Sci.* **1988**, *125,* 386-398.

15. Millet, F.; Nedyalkov, M.; Renard, B.; Perrin, P.; Lafuma, F.; Benattar, J. Adsorption of Hydrophobically Modified Poly(acrylic acid) Sodium Salt at the Air/Water Interface by Combined Surface Tension and X-ray Reflectivity Measurements. *Langmuir* **1999**, *15,* 2112–2119.

16. Dong, L.; Johnson, D.T. The study of the surface tension of charge-stabilized colloidal dispersions. *J. Dispers. Sci. Technol.* **2005**, *25,* 575-583.

17. Dong, L.; Johnson, D. Surface tension of charge-stabilized colloidal suspensions at the water−air interface. *Langmuir* **2003**, *19*, 10205-10209.

18. Paunov, V.N.; Binks, B.P.; Ashby, N.P. Adsorption of charged colloid particles to charged liquid surfaces. *Langmuir* **2002**, *18*, 6946-6955.

19. Vafaei, S.; Purkayastha, A.; Jain, A.; Ramanath, G.; Borca-Tasciuc, T. The effect of nanoparticles on the liquid–gas surface tension of Bi_2Te_3 nanofluids. *Nanotechnology* **2009**, *20*, 185702.

20. Tanvir, S.; Qiao, L. Surface tension of nanofluid-type fuels containing suspended nanomaterials. *Nanoscale Res. Lett.* **2012**, *7*, 1-10.

21. Zore, A.; Van De Mark, M. Surface Tension Studies in Colloidal Unimolecular Polymers. *CoatingsTech* **2021**, *18*, 24-31.

22. Geng, P.; Zore, A.; Van De Mark, M.R. Investigation of the Evaporation Rate of Water from Colloidal Unimolecular Polymer (CUP) Systems by Isothermal TGA. *Polymers* **2020**, *12*, 2752.

23. Fainerman, V.B.; Miller R.; Aksenenko, E.V.; Makievski A.V. Equilibrium adsorption properties of single and mixed surfactant solutions. In *Surfactants: Chemistry, Interfacial Properties, Applications*, 1st ed.; Fainerman, V.B., Mobius, D., Miller R., Eds.; Elsevier, 2001; 189–286.

24. Le, T.T.Y.; Hussain, S.; Tsay, R.Y.; Noskov, B.A.; Akentiev, A.; Lin, S.Y. On the equilibrium surface tension of aqueous protein solutions–Bovine serum albumin. *J. Mol. Liq.* **2022**, *347*, 118305.

25. Lundberg, R. D.; Makowski, H. S. A Comparison of Sulfonate and Carboxylate Ionomers. In *Ions in Polymers*; Adi Eisenberg; ACS, 1980, 21–36.

26. Minofar, B.; Jungwirth, P.; Das, M.R.; Kunz, W.; Mahiuddin, S. Propensity of formate, acetate, benzoate, and phenolate for the aqueous solution/vapor interface: Surface tension measurements and molecular dynamics simulations. *J. Phys. Chem. C* **2007**, *111*, 8242-8247.

27. Long, F.A.; Nutting, G.C.; Harkins, W.D. The surface tension of aqueous soap solutions as a function of hydrogen ion (pH) and salt concentration. I. Sodium laurate and sodium nonylate. *J. Am. Chem. Soc.* **1937**, *59*(11), pp.2197-2203.

28. Dobrynin, A.V.; Rubinstein, M. Theory of polyelectrolytes in solutions and at surfaces. *Prog. Polym. Sci.* **2005**, *30*, 1049-1118.

29. Dobrynin, A.V.; Rubinstein, M.; Obukhov, S.P. Cascade of transitions of polyelectrolytes in poor solvents. *Macromolecules* **1996**, *29*, 2974-2979.

30. Peng, M.; Duignan, T.T.; Nguyen, C.V.; Nguyen, A.V. From Surface Tension to Molecular Distribution: Modeling Surfactant Adsorption at the Air–Water Interface. *Langmuir* **2021**, *37*, 2237-2255.

31. Sasaki, T.; Hattori, M.; Sasaki, J.; Nukina, K. Studies of aqueous sodium dodecyl sulfate solutions by activity measurements. *Bull. Chem. Soc. Jpn.* **1975,** *48*, 1397-1403.

32. Christov, N. C., Danov, K. D., Kralchevsky, P. A., Ananthapadmanabhan, K. P., Lips, A. Maximum bubble pressure method: Universal surface age and transport mechanisms in surfactant solutions. *Langmuir*, **2006**, *22*, 7528-7542.

33. Ritacco, H., Langevin, D., Diamant, H., Andelman, D. Dynamic surface tension of aqueous solutions of ionic surfactants: role of electrostatics. *Langmuir*, **2011**, *27*, 1009-1014.

III. DEFINING THE COLLAPSE POINT IN COLLOIDAL UNIMOLECULAR POLYMER (CUP) FORMATION

Ashish Zore, Peng Geng, and Michael R. Van De Mark

Department of Chemistry, Missouri University of Science and Technology, Rolla, MO 65409

ABSTRACT

Colloidal unimolecular polymer (CUP) particles were made using polymers with different ratios of hydrophobic and hydrophilic monomers via a self-organization process known as water reduction. The water reduction process and the collapse of the polymer chain to form a CUP was tracked using viscosity measurements as a function of composition. A vibration viscometer which allowed for viscosity measurement as the water was being added during the water reduction process was utilized. The protocol was optimized and tested for factors like temperature control, loss of material, measurement stability while stirring and changes in solution volume with water addition. The resulting viscosity curve provided the composition of THF and water mixture that triggers the collapse of polymer chain into a particle. Hansen parameters, as well as dielectric, were related to the polymer composition and % v/v of THF/water mixture at the collapse point.

Keywords: Colloidal Unimolecular Polymer (CUP), nanoparticle, chain collapse, vibration viscometer, Hansen parameters.

1. INTRODUCTION

Self-organization of amphiphilic polymers in aqueous solution is of high potential importance in a variety of applications such as paints, coatings, drug delivery, electronics, agriculture and personal goods. The conformational behavior of polymer chains in different regional environments can be explained using Flory-Huggin's theory. Flory [1] describes conformations of uncharged polymers in terms of the theta condition which could be a theta solvent or theta temperature. When a polymer chain is in the theta condition they behave as an ideal chain where polymer-polymer interactions are balanced with polymer-solvent interactions and the radius of gyration is equal to the random walk configuration. Any deviation from the theta condition can cause the radius Rg to change either due to swelling in a good solvent, greater than theta, or collapse in a poor solvent, less than theta. However, these conformational changes are more complex for charged polyelectrolytes in solution [2-5].

Colloidal unimolecular polymers or CUPs are nanoscale, charge stabilized, single chain nanoparticles made from a single polymer chain having a well-balanced number of hydrophobic and hydrophilic units [6]. The hydrophilic units can be anionic or cationic. The polymer chain is collapsed into a particle by a simple process called water reduction. Figure 1 shows the schematics of the water reduction process to form CUP particles. The water reduction process begins with dissolving the polymer in a low boiling, water-miscible solvent. The boiling point of the solvent should be less than that of water since the solvent will be stripped off at the end of the reduction process. THF, used in this

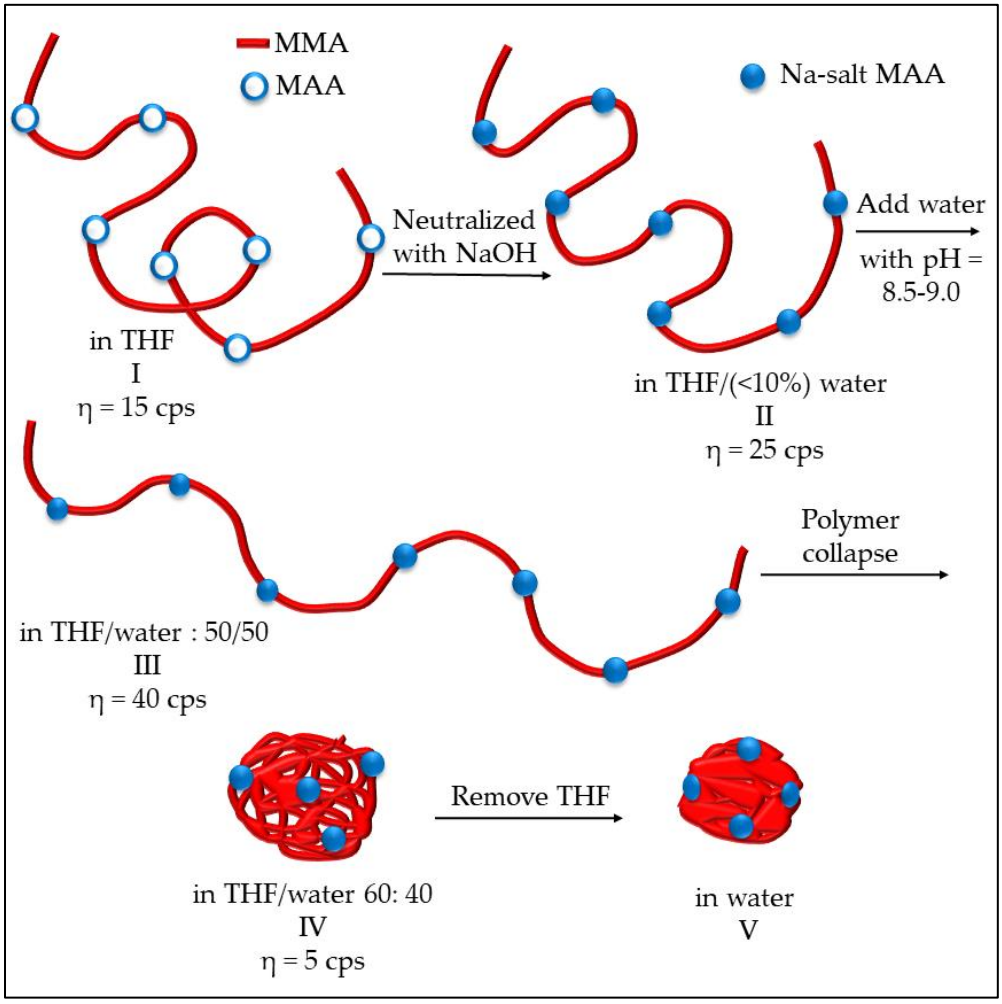

Figure 1. Schematics of the water reduction process and CUP formation.

study, is a good example of a water-miscible solvent that has good solubility for many polymers and has a low boiling point of 66 °C. The next step is to form the salt or ionic group. In this case by neutralizing the acid groups, carboxylic acids, using any base like sodium hydroxide, triethyl amine, ammonia, etc. The base should be added slowly, preferably, using a peristaltic pump. Due to the low dielectric of THF, the carboxylate anion and the sodium counterion exist as a tight or intimate ion pair. The repulsive force between the carboxylate anions on the polymer chain is negligible. The polymer chains

form inter-chain and intra-chain salt association, see Figure 2, via the sodium-carboxylate group which causes a small rise in viscosity. The next step is to add water very slowly (1.8 gm/min) with stirring to ensure homogenous composition of the solvent throughout the mixture. Water, being a poor solvent for the polymer, any localized spikes in concentration can cause the polymer to precipitate instead of a proper unimolecular collapse. As the water is being added, the dielectric of the solvent mixture increases as seen from Figure 3. The carboxylate anions start repelling each other stronger over a longer distance as the dielectric of the media increases. As a result, the polymer chain will become more elongated, and the viscosity will increase as more water is added. This trend will continue until the concentration of water in the solvent mixture reaches a point where it becomes a poor solvent for the polymer and the chain collapses into a spheroidal particle. Here, the transition from coil to globule is triggered by changing the dielectric and solubility parameter of the solvent. The changes in the thermodynamic quality of the solvent makes the polymer-polymer interactions stronger than polymer-solvent interactions which causes the chain to collapse into a globule. The collapse of the chain is such that the hydrophobic segments form the interior of the particle, and the charged groups are on the surface as shown in Figure 4. The self-organization of polymer chains into CUPs is similar to that of micelle formation in surfactants. CUPs have a lot of utility in the field of coatings due to its zero VOC content, low cost and easy synthesis. They can be used as a resin [8,9], an additive for freeze-thaw stability [10] or as a catalyst [11]. CUPs have also been extremely useful in studying properties of bound or surface water [12, 13], understanding the water evaporation behavior [14], electroviscous effect [15] and surface tension [16].

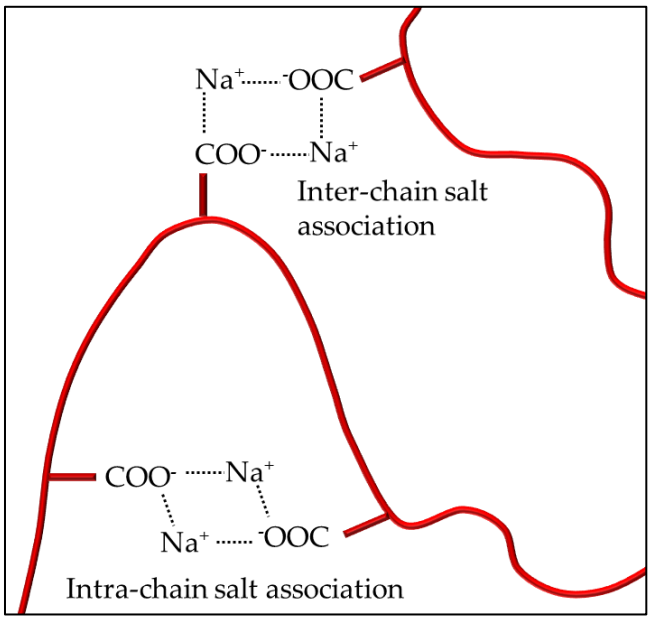

Figure 2. Inter and intra-chain salt associations in polymer.

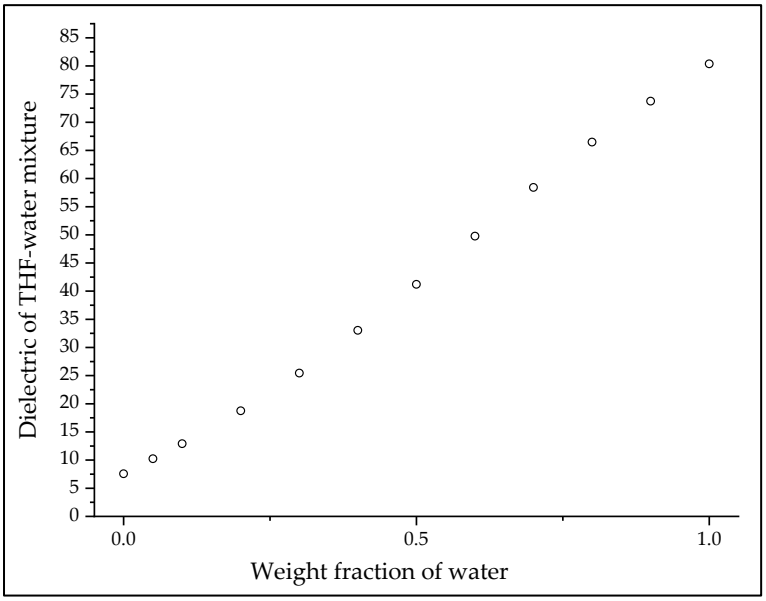

Figure 3. Dielectric of water-THF mixture [7].

A polyelectrolyte or a polymer chain containing several ionic groups can form many different conformations depending on the charge density on the chain and its

solvent environment. The conformations of polyelectrolytes have been modeled using an electrostatic blob and scaling theory which was first developed by DeGennes and Pfeuty and later reviewed by Dobrynin [17]. According to the theory, a neutral polymer in a poor solvent like water will collapse into a spheroidal globule. When charges are present on the chain, it collapses into an electrostatic blob, dumbbell or a pearl necklace depending on the fraction of charges present on the chain. Kirwan [2] observed conformational changes for polyvinyl amine in water at different pHs. At low pH =3, the polymer chain was highly charged and in an extended conformation. Increasing the pH, transitions the chain into a pearl necklace structure. Above pH 9, the polymer collapses to a globule due to attractive hydrophobic interactions between polymer segments in a poor solvent condition. Similar observations were made by DeMelo [3] using polyacrylic acid by going from high pH to low. The conformational behavior of polyelectrolytes allows the synthesis of polymers capable of forming a single chain nanoparticle. The coil to globule transition can be triggered by changing the temperature or by changing the solvent quality like solvent composition, dielectric, or pH.

Li [18] used hydrophobic blocks of the anticancer drug paclitaxel and grafted it onto blocks of polyether ester to produce a self-assembled multichain polymeric micelle as a drug delivery system. When the block co-polymer was placed in an aqueous environment with adjusted pH, the hydrophilic polyether ester oriented into the water phase leaving the hydrophobic paclitaxel oriented to the interior domain. Morishima reported micelle like behavior in single chain polyelectrolytes [19] using a random copolymer of 1:1 monomer ratio of hydrophilic and hydrophobic monomers. The chains are collapsed into unimolecular micelle by dissolving the polymer at very low

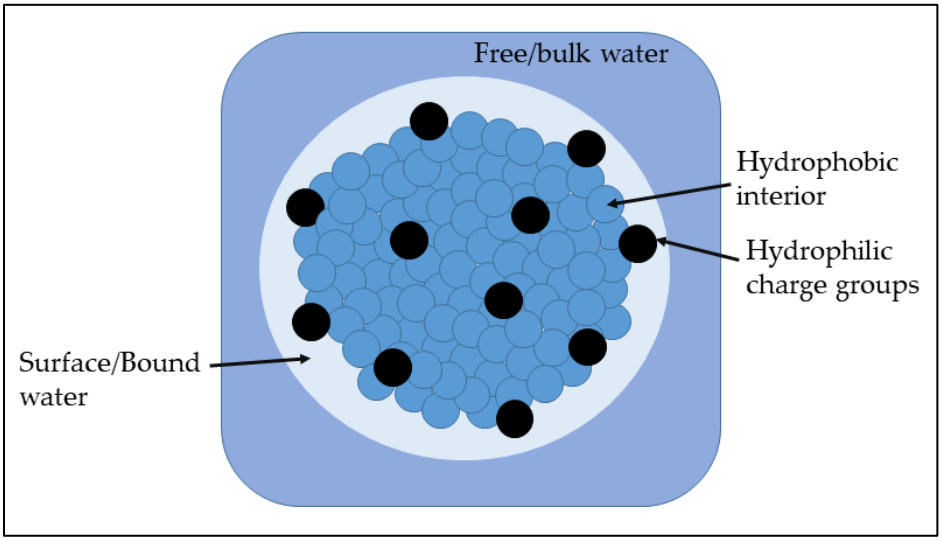

Figure 4. Structure of CUP particle suspended in water.

concentration in aqueous NaOH to obtain particles of 5.5 nm in diameter. The use of a change in solvent composition to achieve coil to globule transition like CUPs was reported by Aseyev [4]. In their work, polymethacryloyl ethyl trimethyl ammonium methyl sulfate (PMETMMS) was examined in a water acetone mixture where acetone was a non-solvent. Collapse of the polymer chains occurs at 0.80 mass fraction of acetone in aqueous solution as observed by decrease of the reduced viscosity, radius of gyration and hydrodynamic radius. In an earlier report on the synthesis of CUPs [6], viscosity was used to determine the composition of THF/water mixture required for coil to globule transition of MMA-MAA copolymer. Similar to Aseyev's observation, the viscosity of the solution drops when the polymer chains collapsed into CUP particles. The transition occurred at roughly 60% water and 40% THF composition for the CUP example. It should be noted that unlike other studies, in the CUP system the good solvent is removed

after the particle forms. This solvent removal secures the polymer's spheroidal conformation and removes all VOC.

Non-unimolecular collapse can also be observed in the case of polyurethane dispersions, which are used in the coating industry, where the polymer is synthesized in acetone and then followed by the addition of water. When the acetone is removed from the resin blend, the chain collapses into multi-chain aggregates/non-unimolecular particles with diameter of approximately 25 nm. For CUPs, the concentration of polymer in the solution is low enough to prevent chain overlapping or entangling thereby ensuring that the collapse is unimolecular/single chain. The unimolecular collapse was confirmed by measuring the particle size by dynamic light scattering (DLS) and overlapping its distribution with the particle size calculated from the absolute molecular weight measurements by GPC. For unimolecular collapse, the measured and calculated size distribution match [20, 6]. The addition of the non-solvent water will alter the dielectric and solubility parameters. The changing solvent composition will have an effect which will be highly dependent upon the polymer composition in terms of ionic groups and the size and number of hydrophobic groups. The point of collapse has both charge effects as well as solubility considerations.

The process of water reduction leading to the collapse of the polymer chain into a particle can be tracked by measuring the viscosity as water is being added to it. Figure 1 illustrates the conformational changes of a polymer and viscosity behavior during the water reduction process. The composition of water-THF mixture where the polymer chain transitions from a coil to globule is called the collapse point or collapse composition. In an earlier publication describing the synthesis of CUPs [6], preliminary

work for determination of collapse composition was done using a cone and plate viscometer (Brookfield). The method used was a batch process where the water reduction process was carried out in a separate vessel and small aliquots of sample were taken from that solution at regular intervals for viscosity measurement. As the measured sample was not returned to the solution, the concentration had to be corrected every time. Also, due to high volatility of THF, it was difficult to prevent evaporation loss despite the enclosure provided by the instrument. The amount of sample required to measure the viscosity on the instrument was very small (0.5 ml). Hence, even a small loss in THF would significantly change the composition of the solvent.

Due to the complexity, tediousness and high error margin of the cone and plate system, a new protocol was developed to measure viscosity continuously during the reduction using a different type of viscometer called the vibration viscometer. Furthermore, the effects of polymer chain composition on the solvent composition required for collapse was studied. The structure of the polymer was also changed by using different amounts and size of hydrophobic monomers and the type of base used for neutralizing the polymer was also investigated.

2. MATERIALS AND METHODS

2.1. MATERIALS AND SYNTHESIS

The method used for purification of materials, synthesis of polymers and reduction process to form CUP particles are reported elsewhere [12]. The molar quantities of monomers - methyl methacrylate (MMA), butyl methacrylate (BMA), ethyl

methacrylate (EMA) and methacrylic acid (MAA), initiator (AIBN) and chain transfer agent (1-dodecanethiol) used for synthesis of polymers made for this study are mentioned in Table 1. BMA and EMA were purified by passing through a basic alumina column. EMA was further purified by distilling at atmospheric pressure while BMA was distilled under reduced pressure.

Table 1. Molar quantities of monomers, initiator (AIBN) and chain transfer agent (1-dodecanethiol) used for synthesis of Polymer 1-6.

Polymer	**MMA (mol)**		**MAA (mol)**	**AIBN (mol)**	**1-Dodecanethiol (mol)**	**THF (mol)**
1[a]	0.912		0.101	$7.09* 10^{-4}$	$3.49* 10^{-3}$	2.77
2[a]	0.912		0.101	$7.09* 10^{-4}$	$1.45* 10^{-3}$	2.77
3	0.874		0.146	$7.14* 10^{-4}$	$1.46* 10^{-3}$	2.77
4[a]	0.953		0.053	$7.04* 10^{-4}$	$1.6* 10^{-3}$	2.77
	EMA (mol)	**BMA (mol)**	**MAA (mol)**			
5	0.279	0.446	0.056	$5.46* 10^{-4}$	$1.27* 10^{-3}$	2.77
6	0.330	0.413	0.040	$5.49* 10^{-4}$	$1.28* 10^{-3}$	2.77

a) Data were taken from Ref [12].

2.2. AFM IMAGING

The AFM images were obtained using the Bruker Dimension Icon instrument, Bruker, Billerica, MA, USA. For preparing the dry samples, 5 µL of 0.0002% Polymer 2 CUP solution was deposited onto freshly cleaved muscovite mica (Ted Pella, Inc.,

Redding, CA, USA) and air-dried for 3 min. The final traces of water were removed by drying with compressed air. Atomic force imaging was conducted by utilizing ScanAsyst mode in air, with ultrasharp 14 series (NSC 14) tips purchased from NANOANDMORE.

2.3. VISCOSITY MEASUREMENTS

Viscosity was measured using a tuning fork vibration viscometer SV 10A from A&D company Ltd. The instrument has two sensor plates in a tuning fork arrangement that vibrate at a natural (resonant) frequency of 30 Hz inside the sample fluid. Viscosity is then calculated based the amount of electric current required to drive and maintain the sensor plates at a constant vibration amplitude against the viscous resistance of the sample fluid. The instrument can record viscosity with time by using a computer software called RsVisco. The viscosity measurement for the determination of collapse point can be done by a batch process and continuous process. However, both methods were first tested for factors like temperature stability, loss of material, etc.

2.3.1. Testing the Batch Process for Loss of Solution. The batch process was tested using 60 ml of THF and water mixture (75/25 volume ratio) in a screw-top container covered with a lid. The sample was allowed to equilibrate to ambient temperature, which was between 22.5± 0.5 °C, before making measurements. The tuning forks were dipped into the sample for 10s to make each measurement. When the sample was removed from the tuning fork, a small amount of solution remains on them. The tuning forks were then immediately washed with DI water to remove the retained solution. The measurement and cleaning were repeated 35 times and the sample was

weighed at the end to determine the loss of sample during the entire process. The experiment was repeated three time to get the average loss of sample.

2.3.2. Testing the Continuous Process for Collapse Point Determination. The continuous process was tested by using 75/25 volume ratio of THF and water mixture. The container used for measurement was a 120 ml capacity polypropylene beaker with a lid. The lid had a slit big enough for inserting the tuning fork and temperature probe into the beaker and a small hole for inserting the tubing that will deliver water. The lid helped to reduce the evaporation of THF from the solution. Approximately 60 grams (exact amount should be known for concentration calculations) of stock solution was transferred into the container, a magnetic stirring bar was added and closed with the lid. The experimental setup is as shown in Figure 5. The beaker was placed in a water bath to keep the temperature constant. The CUP was then placed on a stirring plate with a piece of polystyrene foam placed to insulate the beaker from the heat of the stirring plate. Stirring was then initiated making sure that the stirring bar stays stable at a constant rotation speed. The stability of the viscosity reading was checked by measuring the base solution for a few seconds while stirring. When the readings stayed stable to ± 0.2 cps, the set-up was ready for the water addition. Water was added to the solution using a peristaltic pump at the rate of 1.8 gms/min. The tip of the pump tubing, when inserted in the beaker, was kept close to the stirring bar to ensure quick mixing of water into the solution. Viscosity measurement was initiated with viscosity and solution temperature being recorded at fixed regular time intervals of 20 seconds during the water addition process using RsVisco software. Based on the flow rate of the pump and time, the amount of water added was calculated which gave the % volume of water present in the

THF/water solvent composition. A plot of viscosity against % volume of water in the THF/water solvent composition was used for analysis.

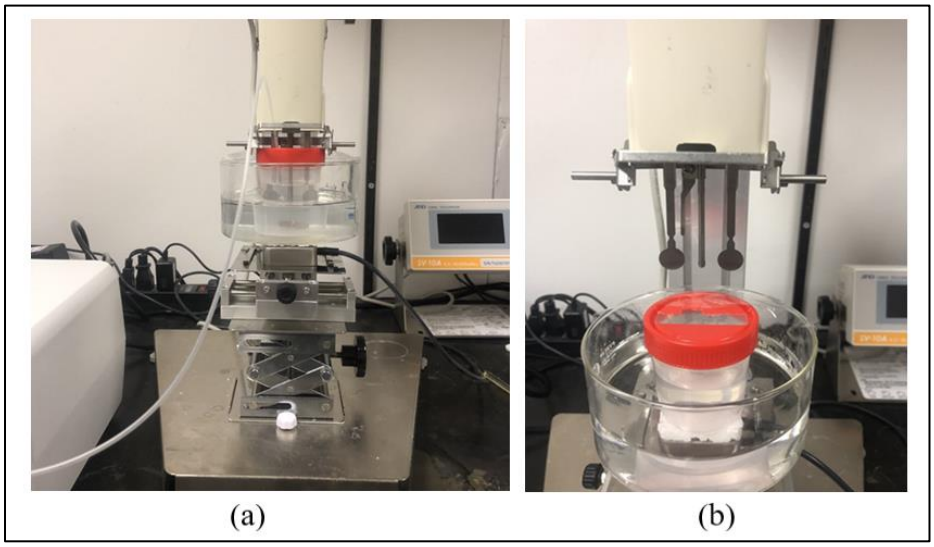

Figure 5. a) Experimental setup used for testing the continuous process for collapse point determination and for measuring the collapse point of CUP polymer. b) Picture of tuning forks on the vibration viscometer.

2.3.3. Collapse Point Determination of CUP Polymer by Continuous Process.

The experimental procedure used for collapse point determination of CUP polymer by continuous process was identical to batch process except for the use of a polymer stock solution instead of THF and water mixture (75/25 v/v). The polymer stock solution was prepared by dissolving the polymer in THF to make a 15% w/w solution. Then, 1M sodium hydroxide solution was added in an amount such that all the acid groups are neutralized, and the pH was 8.5-9. Finally, pH adjusted (pH= 8.5) deionized water was slowly added using a peristaltic pump at the rate of 1.8 gm/min. The amount water added was such that the final solvent composition in the polymer stock solution was 25% water

and 75% THF. The addition of water increased the temperature of the mixture and hence, before making viscosity measurements, the polymer stock solutions were equilibrated to 22.5 ± 0.5 °C for all the polymers measured. After temperature equilibration, the viscometer measurements were initiated, and the remainder of the water was added at 1.8 gms/min. The water addition was continued for 35 mins before ending the experiment. A plot of viscosity against % volume of water in the THF/water solvent composition was made to determine the collapse point or collapse composition.

3. RESULTS AND DISCUSSION

3.1. POLYMER SYNTHESIS AND CHARACTERISATION

To understand the effect of polymer composition, the polymers used in this study were made with different monomer ratios of hydrophobic (MMA, BMA, EMA) and hydrophilic (MAA) monomers. The use of BMA and EMA provides a larger size of hydrophobic group as compared to MMA. Table 2 shows the acid number, density and molecular weight of the copolymers used for this study. The molecular weight and density of the dry polymers are required for calculating the particle size.

3.2. PARTICLE SIZE ANALYSIS

The CUP samples were prepared by the method given in ref [12]. Table 3 shows the measured particle size for the copolymers and calculated particle size from absolute number average molecular weight. The diameter of the CUP particles was calculated from its molecular weight using equation 1.

$$d = \sqrt[3]{\frac{6M_w}{\pi N_A \rho_p}} \quad (1)$$

Where d is the diameter of the particle, M_W is the number average molecular weight of the CUPs, N_A is Avagadro's number and ρ_p is the density of the dry polymer. As seen from the results, the diameter of the CUP particle increases with increase in molecular weight. These results are consistent with our previous work and observations made with globular proteins [20, 21]. For a unimolecular collapse into a sphere, the particle size measured from DLS should be close to the particle size calculated from the molecular weight using equation 1 as shown in Table 3. The data shows excellent agreement of GPC and DLS diameters.

Table 2. Acid number, densities, and molecular weight of the copolymers.

Sample ID	**M_W (g/mol) [b]**	**Monomer ratio (MMA: MAA)**	**AN meas./calc. (mg KOH/g) [c]**	**Density dry, ρ_p (g/ml)**
Polymer 1[a]	28.9K	9:1	56.8/56.9	1.2246±0.0018
Polymer 2[a]	59.8K	9:1	57.0/56.9	1.2311±0.0014
Polymer 3	33.0K	6:1	81.3/81.7	1.2300±0.0012
Polymer 4[a]	45.4K	18:1	29.1/29.7	1.2390±0.0019
		(EMA:BMA:MAA)		
Polymer 5	51.1K	5:8:1	31.5/31.3	1.2370±0.0021
Polymer 6	47.1K	1:3.6:1	78.5/78.8	1.2353±0.0017

a) Data were taken from Ref [12].
b) Absolute number average molecular weight from GPC.
c) A.N. - Acid Number was measured using ASTM D974.

3.3. AFM IMAGE OF CUP PARTICLES

Imaging an isolated single CUP particle is difficult due to the formation of particle cluster or aggregation when drying the CUP solution. Figure 6 shows a dense

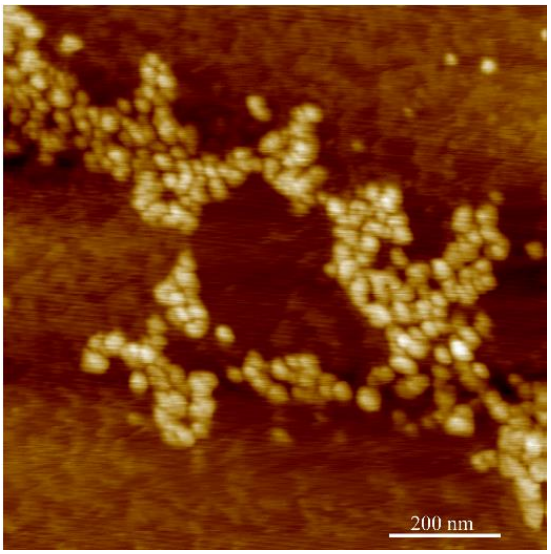

Figure 6. AFM-image showing Polymer 2 CUP particles in dense clusters or aggregates.

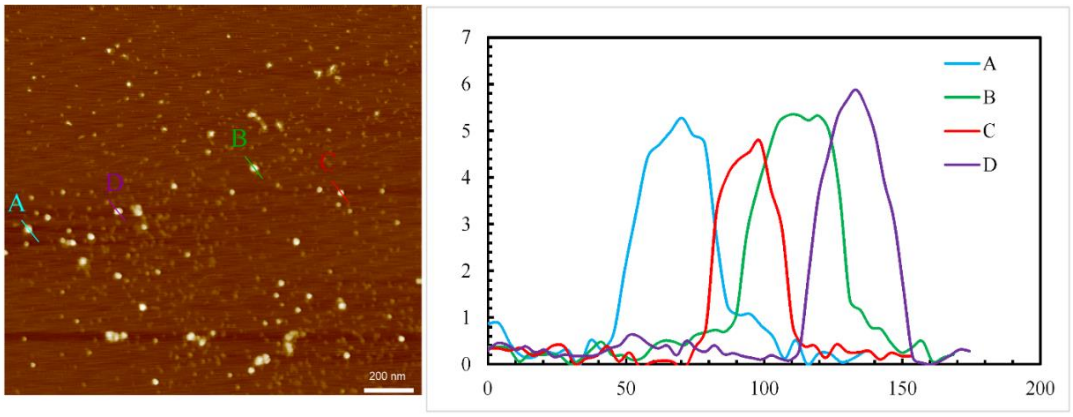

Figure 7. AFM image showing sparsely clustered or aggregated Polymer 2 CUP particles (left) and the height (nm—y axis) and width (nm—x axis) of the profile of the analyzed particles (A–D).

aggregation of Polymer 2 CUP particles, whereas Figure 7 shows sparsely aggregated Polymer 2 CUP particles. Based on the height analysis, the diameter of the particles was found to range from 4.8 to 5.9 nm. This is closer to the average diameter of 5.38 nm for Polymer 2 measured on a DLS instrument.

3.4. CHARGE DENSITY OF THE CUP PARTICLE

Charge density, ρ_v, i.e., number of charges per unit area (nm^2) on the CUP surface, can be calculated using equation 2.

$$\rho_v = \frac{M_W}{4\pi r^2 (n \times M_{H1} + m \times M_{H2} + \ldots\ldots\ldots + M_i)} \quad (2)$$

Table 3. Measured and calculated particle size (diameter) and charge density of the CUPs.

Sample ID	**d(DLS) [b] (nm)**	**d(GPC) [c] (nm)**	**charge density, ρ_v, (ions per nm^2)**
Polymer 1 [a]	4.22	4.25	0.52
Polymer 2 [a]	5.38	5.40	0.66
Polymer 3	4.38	4.42	0.80
Polymer 4 [a]	4.90	4.92	0.32
Polymer 5	5.12	5.10	0.35
Polymer 6	5.00	4.97	0.84

a) Data were taken from Ref [12].
b) Diameters are measured by dynamic light scattering (DLS) instrument.
c) Diameters are calculated from average molecular weight measured using gel permeation chromatography (GPC) using equation 1.

Where n and m are the number of hydrophobic monomer 1 and 2 for each unit of hydrophilic monomer in a repeat unit and is also mentioned as monomer ratio (e.g., n:1 of MMA: MAA) in Table 3, M_W is the molecular weight of the CUP, M_{H1} and M_{H2} is the molecular weight of hydrophobic monomer 1 and 2, M_i is the molecular weight of hydrophilic monomer, r is the radius of the CUP particle.

3.5. COLLAPSE POINT DETERMINATION USING VIBRATION VISCOMETER

Unlike a cone and plate viscometer, a vibration viscometer can be used to measure viscosity without removing a sample and can measure the viscosity with active stirring. The water reduction process and viscosity measurement can be done in the same vessel either through a batch or continuous measurement process.

3.5.1. Batch Process for Collapse Point Determination Using Vibration Viscometer.

Prior to using the batch process for measuring the collapse point of polymers, it was tested for stability of temperature, loss of material, etc. The measurement temperature in the batch process was easily controlled by allowing the sample to equilibrate to the required temperature before making measurements. However, the average loss of material measured by the test experiment was 4.5% by weight after the 35 measurements. The loss of THF due to evaporation can be assumed to be minimum because the sample is enclosed while equilibrating the temperature. Also, the measurements on the vibration viscometer are much faster (10s) which reduces the exposure to air and keeps the loss of THF to minimum. The major contributor for loss of material is the cleaning process of the tuning fork between each measurement. Any sample retained on the tuning fork is lost during the cleaning process. The loss material is

very difficult to account for due inconsistent loss every time and the tedious process of back-calculation. This method does have the advantage of giving accurate viscosity values since each measurement places the vibrating paddles at the correct depth. Due to the loss of material and labor-intensive nature, it was necessary to develop a continuous process for viscosity measurement.

3.5.2. Continuous Process for Collapse Point Determination Using Vibration Viscometer. In the continuous process, the viscosity measurements were made as water was added to the solution. The set up made for the continuous process for collapse point determination using the SV 10A vibration viscometer is shown in Figure 5. The set up was derived experimentally in order to optimize certain parameters involved in water reduction process and viscosity measurement. The test experiment performed to derive the set up and optimize the parameter is described in the experimental section 2.3.2. Figure 8 shows the results of the test experiment which is the plot of viscosity against % volume of water in the THF/water solvent composition during water addition of 75/25 v/v THF/water mixture and two curves that start with no water. Parameter optimization for continuous process:

3.5.2.1. Temperature control and heat of mixing. Temperature is one the key parameters that can change the viscosity of the solution. Hence, for our collapse point determination experiment that measures the changes in viscosity, control of temperature was very critical. One of the major sources of heat in the experiment was the heat of mixing evolved by adding water to THF. As water was being added during the water reduction experiment, the temperature of the solution rises. Figure 8 shows the temperature profile during water addition to THF. The plots were obtained by making

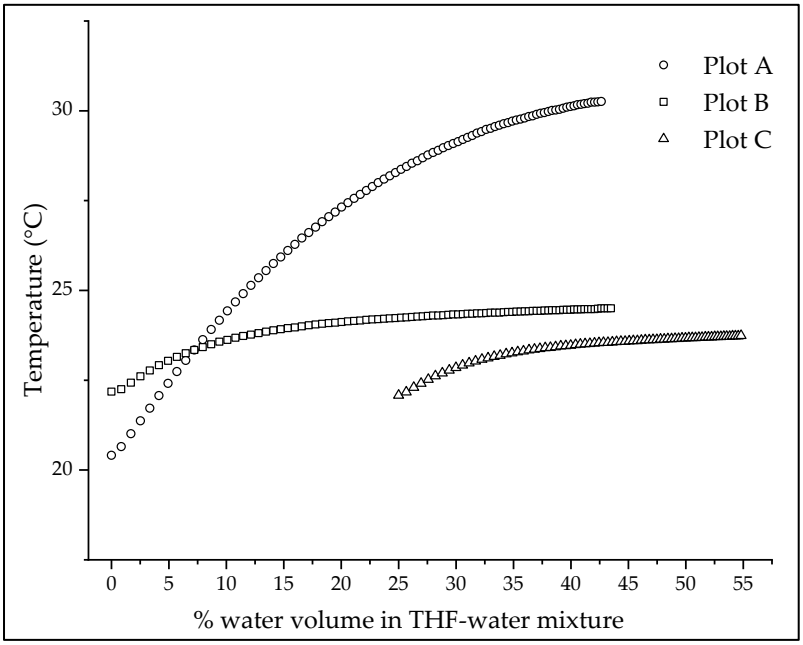

Figure 8. Temperature profile for water addition to pure THF measured on the set up in Figure 5 without using a water bath (Plot A), while using a water bath (Plot B) and water addition to THF/water mixture of 75/25 v/v composition (Plot C) using the set up.

three different changes to experimental setup are described in section 2.3.2. Plot A is the temperature curve for water addition to pure THF measured on the setup in Figure 5 without a water bath. Plot B and C are the temperature curves measured on the setup in Figure 5 for water addition to pure THF and THF/water mixture of 75/25 v/v composition respectively. The difference in the temperatures observed in plot A and B clearly demonstrates the control or mitigation of temperature rise provided by the water bath. It should be noted that the pump adds a small amount of heat to the system at a steady rate due to friction, about 0.5 degrees over thirty minutes. The plastic beaker is not a good conductor of heat, and the initial water addition shows a small rapid rise due to slow heat transfer regardless of initial water composition. The temperature profile of water addition to pure THF while using a water bath (Plot B) shows a temperature rise of 2.3 °C from

0.0% (22.2 °C) to 43.5% (24.5 °C). The temperature profile (Plot C) of the third method where the water is added to the THF/water mixture of 75/25 v/v composition while using a water bath shows a temperature rise of 1.6 °C from 25.0% (22.1 °C) to 54.8% (23.7 °C). The addition of 25% volume of water followed by equilibrating the temperature before beginning to measure the viscosity further helps in mitigating the rise in temperature by 0.7 °C. Another factor to consider is the stability of the temperature. Plot B shows the temperature reaching a plateau sooner than in Plot C. Plot C shows a stable temperature with a change of less than 0.5 °C from 40% onwards. For a collapse point measurement for the CUP polymers, which will be discussed in the later section, the critical data required for collapse point determination is from 40% and above as seen from Figure 9. Therefore, it was concluded that adding 25% volume of water and using a water bath gave a minimum rise in temperature and stable temperature with a change of less than 0.5 °C where the critical viscosity data is acquired. Hence a polymer stock solution by adding 25% volume of water as described in the experimental section 2.3.3 was prepared. The heat evolved during this stage was easily dissipated by allowing the polymer stock solution to equilibrate to a constant temperature. The steady temperature within 0.5 °C after 40% water volume mitigates the changes in viscosity caused by temperature variations. Another minor source of heat was from the stirring plate. The temperature of the stirring plate increases with time and was, therefore, higher toward the end of the experiment. The heat transfer from the stirring plate was avoided by placing a piece of insulating material, polystyrene foam, as shown in the experimental setup (Figure 5) and by allowing the heated stirring plate to cool before beginning the next run.

3.5.2.2. Loss of material and evaporation of THF. There was material lost during each measurement in the batch process, as described earlier, where the tuning fork retains a small amount of the solution. In the continuous process, however, there was no such material loss by this mechanism. The tuning fork was immersed once, and multiple measurements were made with time. Another source of material loss was due to evaporation of THF since the container is not completely sealed. To measure the loss of THF through evaporation the set up was tested by using a THF/water mixture of 75/25 v/v composition. A 60gm mixture was transferred to the beaker and was stirred for 40 mins which is the typical time for each run and then weighed again. The loss of mass after 40 mins was 1.2% which was assumed to be due to evaporation of mainly THF. The loss of material in the continuous process being less than that of the batch process, makes it a better choice for collapse point determination.

3.5.2.3. Measuring stability while stirring. The major benefit of using a tuning fork vibration viscometer SV 10A is the ability to mix or stir while making viscosity measurements. During the water reduction process, sufficient stirring is important to make the solution as homogenous as possible and to minimize localized concentration spikes. The vibration viscometer shows very stable viscosity measurement as seen from Figure 9 with minimum noise or fluctuations in values. The size of the magnetic stirring bar, size of stirring plate and RPM determination requires some trial-and-error. A simple test to determine the stability of the measurement can be done by using a sample like water and observing the fluctuations in the viscosity value. For the setup used in this work (Figure 5), a small size stirring plate (1.8 x 1.8 in., Cimarec^{TM} i micro stirrers by

Thermo Fisher Scientific) and a stirring bar of 1 cm in length was used. The observed noise in viscosity was about ± 0.02 cps on SV 10A instrument.

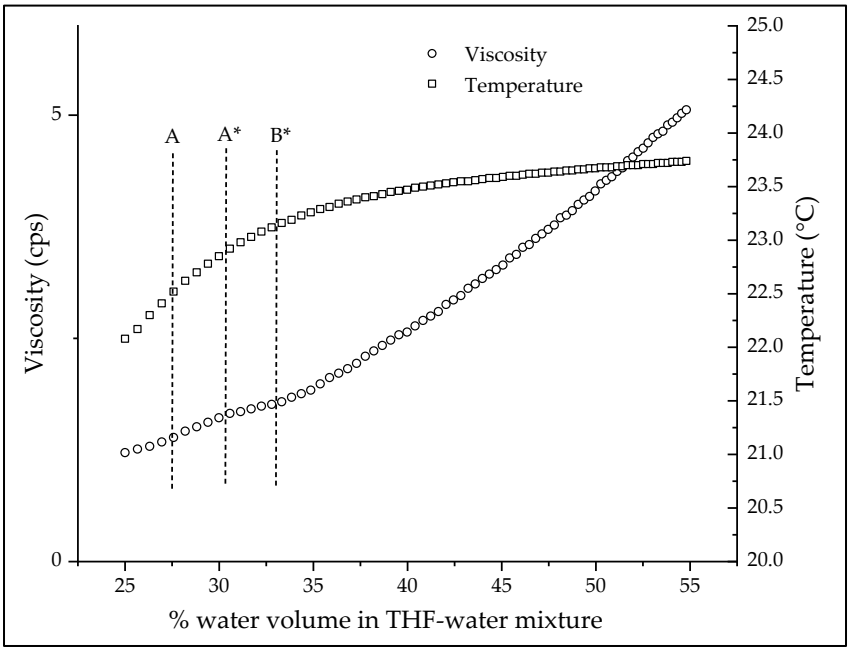

Figure 9. Viscosity against time for THF/water mixture of 75/25 v/v composition with water addition at different levels on tuning fork.

3.5.2.4. Changes in solution volume and real viscosity. Figure 10 shows the diagram of the tuning fork used in SV 10A instrument. For measuring the correct viscosity of a given sample, the tuning forks must be immersed into the solution such that the level is at the curved notch labelled as B (shown in Figure 10). If the solution level is at any other level along the tuning fork, the viscosity value is not the correct viscosity value. In the continuous measurement process, the water is added constantly and therefore the level of the solution rises over time. Therefore, the level of the solution cannot be maintained at point B while the water is being added. Hence, the viscosity

values measured during the water reduction process are not the correct values. Despite the incorrect viscosity, the overall plot of viscosity against time shows the trend or behavior of viscosity during the water reduction which is sufficient for determining the collapse point. The result of plotting viscosity against % water volume for a sample of THF/water mixture of 75/25 v/v composition is shown in Figure 9. Since no polymer is present in the sample, the change in viscosity was due to the increase in the amount of solution causing increasing levels of immersion of tuning fork. The viscosity shows an increase with time which is non-linear until point B* and then becomes almost linear. The viscometer is based on the principle of resistance to vibration of the tuning fork inside the sample. As the tuning fork is immersed deeper inside the sample, higher resistance to vibration can be expected due to the increase of the surface area of contact between the sample and the tuning fork. This should result in higher viscosity values as the tuning fork is immersed deeper into the sample as evident from the results (Figure 9). The changes in the dimensions of the submerged area of the tuning fork cause the non-linear increase in the beginning until point B*. Beyond point B*, the dimensions of the tuning fork remain constant and hence the increase in viscosity becomes linear. Knowing the behavior of the viscometer in the absence of any polymer, we can now test the actual polymer solution for its behavior.

3.5.3. Optimization of the Continuous Process and Measurement of Collapse Point for Polymer Samples. Based on the collapse point experiment in the previous paper [6], it was certain that the polymer will not collapse at a low concentration of water in the solvent mixture. This is another reason why, prior to making measurements, water was added to the neutralized polymer solution such that the composition of solvent

reaches 75/25 v/v of THF/water in order to create a polymer stock solution. The 25% water added upfront also reduced the total time of the collapse experiment carried out on the water reduction set up (Figure 5). Reducing the total experiment time will also keep the loss of THF via evaporation to a minimum. Moreover, the collapse occurs at higher concentration of water, so the initial measurements were not critical. The amount (25%) of water added prior to the measurements was also optimized for the small volume of the beaker used for the water reduction set up.

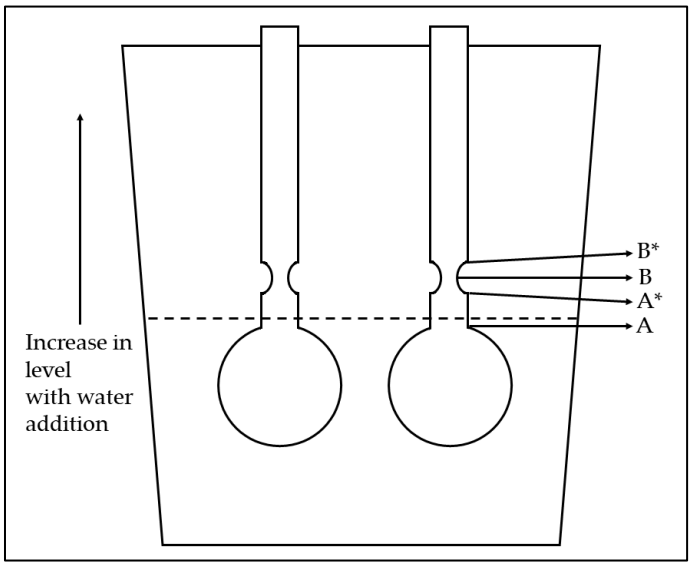

Figure 10. Depiction of solution levels and immersion of tuning forks.

The polymer stock solution must be charged into the set-up beaker in a known amount (which should be roughly 60 ml) such that the tuning fork is in the solution to approximately point A (Figure 10). Figure 11 shows the water reduction plot (viscosity against % volume of water present in the THF/water solvent composition) for Polymer 2

as it passes through different stages of the tuning fork (Figure 10). The initial level of solution for this run was slightly below the recommended point A which led to the

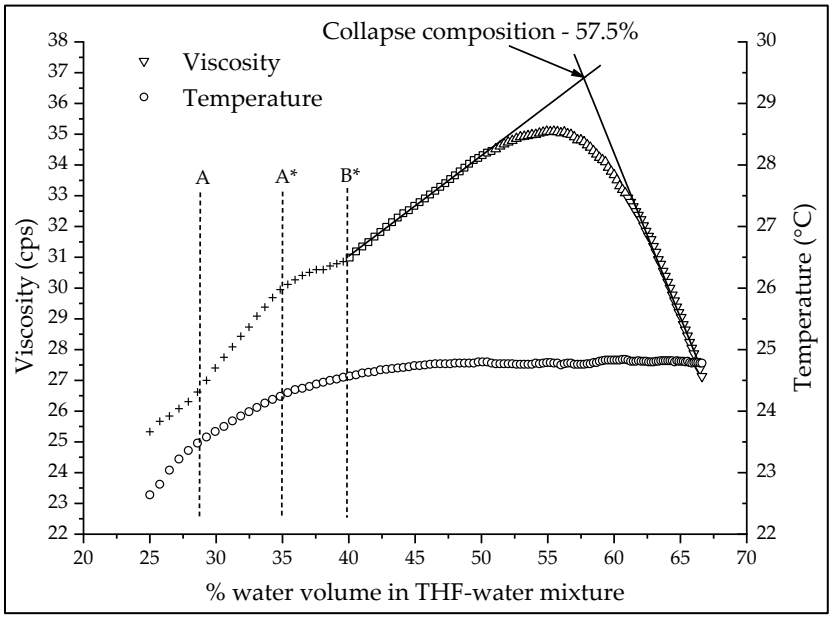

Figure 11. Water reduction (viscosity against % volume of water present in the THF/water solvent composition) plot for Polymer 2.

change in slope at point A. As expected at the beginning, the viscosity values are not linear which was due to the irregular shape of the tuning fork that begins from point A*. Beyond point B*, the shape of the tuning fork stays regular and consistent. When the solution level crossed Point B*, the viscosity increased in a linear trend for a while and then curved and later started to drop linearly. The amount of water (25%) added prior to the measurement and the initial solution level at point A are optimized such that the collapse happens roughly around midpoint between point B* and the full capacity of the beaker. The data in the non-linear region (before point B*) was not critical for our study. The data after point B* was used for collapse point determination. The increase in the

viscosity is due to the polymer chains expanding into a rod-like conformation. It is noteworthy that the viscosity increase occurs even though the concentration of the polymer in the solution is diluted by water addition. The drop in viscosity is due to the collapse of the polymer chain into a particle. The broadness of the curvature is due to two opposing effects happening at the same time. There is a decrease in viscosity due to the polymer chains beginning to collapse but at the same time, the water level is increasing and immersing the tuning forks deeper which increases the viscosity value. Later when the chains collapse completely the viscosity starts decreasing steadily. The linear rise and linear drop were fit to straight lines and the intersection of the lines was recorded as the collapse point or collapse composition for the given polymer.

3.6. COLLAPSE POINT BEHAVIOR OF DIFFERENT CUP POLYMERS

The collapse point composition measured for all the polymers used in this study are given in Table 4. Polymers 1 and 2 show the effect of size/molecular weight on the collapse composition. The collapse compositions for both polymers were very similar indicating that size has no major influence on collapse point and nor does the final charge density as long as the charges per repeat unit does not change. Polymers 3 and 4 are high and low charge density and differ in the amount of hydrophobic and hydrophilic groups present in the polymer chain. Polymer 3 (MMA:MAA::6:1) has more hydrophilic groups and shows collapse at higher % water volume concentration (59.34%) as compared to Polymer 1 & 2 (MMA:MAA::9:1). Polymer 4 (MMA:MAA::18:1) on the other hand has less hydrophilic groups and shows collapse at lower % water volume concentration (54.36%) as compared to polymer 1 & 2 (MMA:MAA::9:1). These results indicate that

hydrophobic and hydrophilic amounts in the polymer chain have a significant influence on the collapse composition. When the polymer chain has more hydrophilicity present, it requires more water in the solvent composition to trigger collapse. Polymer 5 & 6 validates the results observed using different hydrophobic monomers other than MMA. As expected, Polymer 5 which has a higher amount of hydrophobic unit, shows collapse at a lower % water volume composition (53.8 %). Similarly, Polymer 6 which has less of the hydrophobic units, shows collapse at a higher % water volume composition (56.62 %). Another way to change the structure of the polymer chain is by using a different base to neutralize the acid groups (hydrophilic groups). Polymer 2 was also neutralized with triethyl amine (Polymer 2*) instead of sodium hydroxide and then measured for collapse point. The use of triethyl amine shifts the % water volume composition (56.24 %) to the lower value as compared to the use of sodium hydroxide (57.49 %). This shift is because the triethyl amine quaternary counterion is solvated well by organic solvents like THF. The sodium ion requires more water to solvate, since each sodium ion can be associated with up to 6 water molecules [22]. The collapse point results from all the polymers indicate that the higher the hydrophobicity of the polymer chain or counter ion, the lower is the % water volume required to trigger the chain to collapse and vice versa. This behavior could be due to the differences in the solubility of polymer chain in the water THF mixture for different fractions of hydrophobic and hydrophilic units.

All the CUP polymers in this study collapse between 53 to 60% water. The dielectric of these solvent mixtures are between 45 to 50. The dielectric obviously plays an important role in determining the collapse point. When the polymer chain collapses the charges on the chains repel each other strongly to conform the chain into a spheroidal

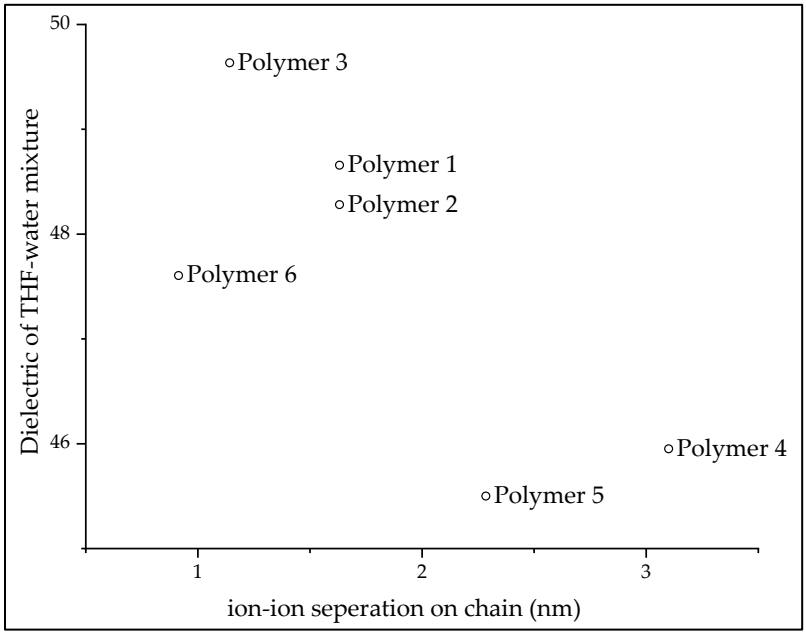

Figure 12. The dielectric of THF-water mixture at collapse points against ion-ion separation on the polymer chain.

particle. The strong repulsion is also responsible for an even surface charge distribution required for a stable particle. Hence, a minimum dielectric must be required to separate the ion pairs (acid groups and counter-ion) on the polymer chain enough that the charges repel each other strongly. Figure 12 shows the dielectric of the collapse concentration against distance between the charges on the polymer chain. Polymers 3 and 4 have distance of 1.14 nm and 3.1 nm respectively and show a dielectric of 49.6 and 45.9 for the mixture at collapse point respectively. Ionic repulsion between the charges is directly proportional to the dielectric and this is also evident from the viscosity curve in Figure 11 where the chain extends due to ion-ion repulsion as the dielectric increases. Hence, charges separated by short distance should require lower dielectric as compared to charges separated by long-distance to achieve similar ionic repulsion. If we assume the minimum dielectric required for strong ion-ion repulsion is reached at collapse point,

then polymer 3 where charge separation is shorter should have required a low dielectric as compared to polymer 4 where charge separation is longer. However, Figure 12 shows the opposite trend for all the polymers. Hence, it is very likely that the minimum dielectric required for strong ion-ion repulsion to provide a stable particle must be below the collapse point dielectric. At the collapse point, the polymer-polymer interactions becoming stronger than polymer-solvent interactions triggers the collapse.

Table 4. Collapse composition for polymers 1-6 and Hansen parameters of solvent composition at collapse.

Sample ID	**Volume composition at collapse point**		**δ_d**	**δ_p**	**δ_h**	**δ_T**	**Dielectric**
	% Water	**% THF**					
Polymer 1	58.0	42.0	16.1	11.7	27.9	34.3	48.7
Polymer 2	57.5	42.5	16.1	11.6	27.7	34.1	48.3
Polymer 3	59.3	40.7	16.1	11.8	28.3	34.7	49.6
Polymer 4	54.4	45.6	16.2	11.3	26.7	33.2	45.9
Polymer 5	53.8	46.2	16.2	11.2	26.5	33.0	45.5
Polymer 6	56.6	43.4	16.1	11.5	27.4	33.8	47.6
Polymer 2* [a]	56.2	43.8	16.1	11.5	27.3	33.7	47.3

a) *Polymer 2 was neutralized using triethyl amine instead of sodium hydroxide.

3.7. COMPARISON USING HANSEN SOLUBILITY PARAMETERS

Solubility parameters, also known as cohesion energy parameters, are derived from the energy required to convert a liquid to a gas state. The energy of vaporization is a direct measure of the total cohesive energy holding the liquid molecules in the liquid state. Hildebrand and Hansen solubility parameters are the two most widely used measures of solvent-polymer compatibility for determining whether a substance is a good solvent or nonsolvent for a given polymer. Hildebrand is a single parameter, δ, defined as the square root of the cohesive energy density,

$$\delta = (\frac{E}{V})^{1/2} \quad (3)$$

where V is the molar volume of the pure solvent and E is its (measurable) energy of vaporization. The Hansen solubility parameter splits the total cohesive energy E into three major intermolecular interactions: (nonpolar) dispersion forces, (polar) permanent dipole–permanent dipole forces, and (polar) hydrogen bonding. The nonpolar cohesive energy (E_d) is derived from induced dipole forces and is also referred to as atomic or dispersion interactions. The polar cohesion energy (E_p) results from inherent molecular interactions and is found in polar (non-centrosymmetric) molecules. The hydrogen bond cohesive energy (E_h) is the attractive interactions between a hydrogen atom from a molecule or a molecular fragment X–H in which X is more electronegative than H and an atom or a group of atoms in the same or a different molecule in which there is evidence of bond formation. The total cohesive energy E is the sum of the individual energies that make it up:

$$E = E_d + E_p + E_h \quad (4)$$

Dividing the cohesive energies by the molar volume gives the square of the total (or Hildebrand) solubility parameter as the sum of the squares of Hansen components:

$$\frac{E}{V} = \frac{E_d}{V} + \frac{E_p}{V} + \frac{E_h}{V} \quad (5)$$

$$\delta^2 = \delta_d^2 + \delta_p^2 + \delta_h^2 \quad (6)$$

The Hansen parameters (δ_d, δ_p, δ_h, δ_T) for water and THF are 15.6, 16.0, 42.3, 47.8 and 16.8, 5.7, 8.0, 19.4 respectively [23]. For a mixture of solvents, the Hansen parameters can be calculated based on the volume fractions (ϕ_1 and ϕ_2) of the solvent present in the mix using equations 6, 7, 8, and 9. The Hansen parameters calculated for solvent composition at the collapse point for Polymer 1-6 are shown in table 4.

$$\delta_d = \delta_{d1}\phi_1 + \delta_{d2}\phi_2 \quad (7)$$

$$\delta_p = \delta_{p1}\phi_1 + \delta_{p2}\phi_2 \quad (8)$$

$$\delta_h = \delta_{h1}\phi_1 + \delta_{h2}\phi_2 \quad (9)$$

The Hansen parameters and the interaction radius (R_0) for the homopolymers shown in Table 5 are experimentally measured and taken from ref [23]. The interaction radius (R_0) (Figure 10) is the extent of solubility sphere encompassing the good solvents and excluding the bad ones. The Hansen parameters for a copolymer shown in Table 6 were calculated based on the weight fraction (w_1 and w_2) of each monomer present in the copolymer chain and individual homopolymer Hansen parameters [24, 25] using equation 10. The interaction radius (R_0) of the copolymer was also calculated as the weighted average of individual homopolymers. The calculated Hansen parameters and interaction radius for Polymers 1-6 are shown in Table 6.

$$\delta_{block-copolymer} = w_1\delta_1 + w_2\delta_2 \quad (10)$$

Table 5. Hansen parameters and the interaction radius (R_0) for the homopolymers [23].

Homopolymer	**δ_d**	**δ_p**	**δ_h**	**δ_T**	**Interaction radius, R_0**
Poly methyl methacrylate (PMMA)	19.1	11.3	4.1	22.6	10.3
Poly ethyl methacrylate (PEMA)	19.0	9.0	8.0	22.5	11.0
Poly n-Butyl methacrylate PnBMA	16.0	6.2	6.6	18.4	9.5
Poly methacrylic acid (PMAA)	25.6	11.2	19.6	34.1	20.3

Table 6. Hansen parameters, interaction radius (R_0) and the distance (D_{S-P}) at collapse composition for Polymer 1-6.

Co-polymer	**δ_d**	**δ_p**	**δ_h**	**δ_T**	**Interaction radius, R_0**	**Distance D_{S-P}**
Polymer 1	19.7	11.3	5.5	23.3	11.2	23.4
Polymer 2	19.7	11.3	5.5	23.3	11.2	23.6
Polymer 3	19.9	11.3	6.0	23.7	11.6	23.6
Polymer 4	19.4	11.3	4.8	23.0	10.8	22.8
Polymer 5	17.4	7.3	7.7	20.4	10.5	19.4
Polymer 6	17.6	7.3	8.4	20.8	11.0	19.7

For a polymer, its solubility in a solvent or solvent blend depends on the Hansen solubility parameters of solvent being within the solubility sphere of the polymer (Figure 13). The distance (D_{S-P}) of the solvent from the center of the solubility sphere can be calculated using equation 11.

$$D_{S-P} = \left[4\left(\delta_{ds} - \delta_{dp}\right)^2 + \left(\delta_{ps} - \delta_{pp}\right)^2 + \left(\delta_{hs} - \delta_{hp}\right)^2\right] \quad (11)$$

Where δ_{xs} is the Hansen component parameter for solvent composition THF-water at the collapse point and δ_{xp} is the Hansen component parameter for the polymer. If the distance ($D_{S\text{-}P}$) is less than the interaction radius, then polymer is expected to dissolve in the solvent. A recent study [26] shows that the predictive accuracy of Hansen parameters is limited and is found to be 67% for solvent and 76% for non-solvents.

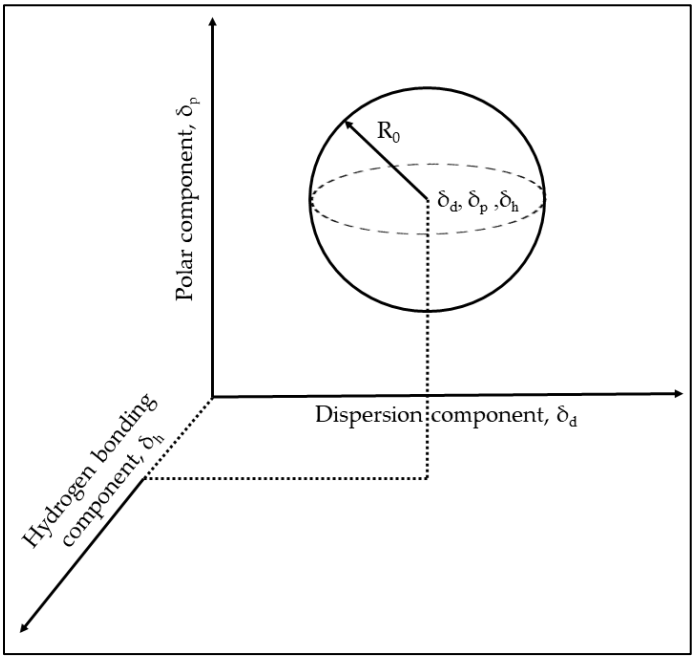

Figure 13. The Hansen volume of solubility for a polymer is depicted with a 3-D model of solubility sphere with center at (δ_d, δ_p, δ_h) and radius of interaction (R_0). Liquids whose parameters lie within the volume of the solubility sphere are active solvents for that polymer. "Reprinted (adapted) with permission from Venkatram, S.; Kim, C.; Chandrasekaran, A.; Ramprasad, R. Critical assessment of the Hildebrand and Hansen solubility parameters for polymers. J. Chem. Inf. Model. 2019, 59, 4188-4194. Copyright 2019 American Chemical Society.

The distance (D_{S-P}) calculated using equation 11 for the water-THF solvent composition at the collapse point for Polymers 1-6 is shown in Table 6. The distance is higher than the interaction radius for all the copolymers. This indicates that the solvent mixture is a non-solvent for the polymer which results in its collapse. The interaction radius of the copolymers gives a close but not a true picture of the solubility behavior. This is due to the Hansen parameters and the interaction radius of the copolymer calculated using polymethacrylic acid. However, the copolymer during the water reduction process is ionized and the carboxylic acid groups are present as sodium salt or triethyl amine quaternary salt. But the Hansen parameters for polymethacrylic acid sodium salt or any other polyelectrolyte type polymers or copolymers have not been reported in any publications. The total Hansen parameter (δ_T) for the water-THF solvent composition at the collapse point for all the polymers is shown in Table 4. For polymers with low charge density (Polymer 4), the δ_T value of the solvent composition is lower than that of a polymer with high charge density (Polymer 3). Increasing the hydrophobicity in the polymer chain, therefore, affects the Hansen parameters required for the solvent composition which in this case becomes lower. Similar observations can be seen in Polymer 5 & 6 which is made using different monomers and in the case of Polymer 2* when it is neutralized using a hydrophobic base like triethylamine. The major contribution to the variation in δ_T of different polymer structures is due to the hydrogen bonding (δ_h) component of the Hansen parameter as compared to the polar (δ_p) component. The dispersive component shows the least variation due to changes in hydrophobic-hydrophilic balance of the polymer. This observed trend is not surprising as adding more ionic groups in the polymer chain will increase the affinity of the polymer

towards aqueous system since the carboxylate anions on the polymer chain can hydrogen bond with water. When comparing Polymer 3 & 4 against Polymer 5 & 6, we can see the effect of using different types of hydrophobic monomers on the Hansen parameters. For low charge density (high hydrophobicity), Polymer 4 made using MMA and MAA monomers has δ_T = 33.15 at collapse composition whereas Polymer 5 made using BMA, EMA and MAA has lower δ_T = 32.97. This is also observed in high charge density polymers made using the same monomers (Polymer 3 & 6). The small difference due to incorporation of butyl methacrylate monomer can be attributed to the different Hansen parameters of PnBMA and PMMA shown in Table 5. PnBMA has a lower δ_T value than PMMA.

4. CONCLUSIONS

The collapse composition of water-THF mixture was successfully determined using viscosity measurements. The use of a vibration viscometer for continuous viscosity measurements during water addition made it possible to get reproducible collapse points with less effort and better accuracy. The vibration viscometer was an ideal tool for this study since it provides stable viscosity values with minimum noise even when the solution was under constant stirring. The viscosity of the CUP polymer shows a steady rise in viscosity with addition of water until it reaches the collapse composition. The rise in viscosity overcomes the dilution effect caused by the water addition. After reaching the collapse composition, the viscosity drops which is due to the polymer transforming from an extended coil to a spheroidal particle. The composition of water-THF mixture at

collapse changes as the co-polymer structure is varied. Adding more hydrophobicity to the copolymer reduced the amount of water required to trigger the collapse. The dielectric of the solvent mixture plays an important role in separating the ion pair so that charges are felt over a longer distance. Altering the copolymer structure, changes its Hansen solubility parameter. This changes the composition of the solvent mix where it is a poor solvent for the polymer thereby leading to collapse.

REFERENCES

1. Flory, P. J. Thermodynamics of dilute solutions of high polymers. *J. Chem. Phys*. **1945** *13*, 453-465.

2. Kirwan, L. J.; Papastavrou, G.; Borkovec, M.; Behrens, S. H. (2004). Imaging the coil-to-globule conformational transition of a weak polyelectrolyte by tuning the polyelectrolyte charge density. *Nano lett***. 2004**, *4*, 149-152.

3. Seixas de Melo, J.; Costa, T.; Miguel, M. D. G.; Lindman, B.; Schillén, K. Time-resolved and steady-state fluorescence studies of hydrophobically modified water-soluble polymers. *J Phys. Chem. B*, **2003**, *107*, 12605-12621.

4. Aseyev, V. O.; Tenhu, H.; Klenin, S. I. Contraction of a Polyelectrolyte upon Dilution. Light-Scattering Studies on a Polycation in Saltless Water− Acetone Mixtures. *Macromolecules*. **1998**, *31*, 7717-7722.

5. Kulkarni, P.; Rajagopalan, K.; Yeater, D.; Getzenberg, R. H. Protein folding and the order/disorder paradox. *J. Cell. Biochem*. **2011**, *112*, 1949-1952.

6. Riddles, C.; Zhao, W.; Hu, H.J.; Chen, M.; Van De Mark, M.R. Self-assembly of Water Insoluble Polymers into Colloidal Unimolecular Polymer (CUP) Particles of 3–9 nm. *Polymer* **2013**, *55*, 48–57.

7. Critchfield, F. E.; Gibson Jr, J. A.; Hall, J. L. Dielectric constant and refractive index from 20 to 35° and density at 25° for the system tetrahydrofuran—Water. *J. Am. Chem. Soc.* **1953**, *75*, 6044-6045.

8. Mistry, J.K.; Van De Mark, M.R. Aziridine cure of acrylic colloidal unimolecular polymers (CUPs). *J. Coat. Technol. Res.* **2013**, *10,* 453-463.

9. Mistry, J.K.; Natu, A.M.; Van De Mark, M.R. Synthesis and application of acrylic colloidal unimolecular polymers as a melamine thermoset system. *J. Appl. Polym. Sci.* **2014**, *131,* 40916.

10. Gade, S. V. Application of Colloidal Unimolecular Polymer (CUP) particles in Coatings. Doctoral Thesis, Missouri University of Science and Technology, Rolla, 2015.

11. Natu, A.; Van De Mark, M.R. Synthesis and characterization of an acid catalyst for acrylic-melamine resin systems based on colloidal unimolecular polymer (CUP) particles of MMA-AMPS. *Prog. Org. Coat.* **2015**, *81,* 35–46.

12. Geng, P.; Zore, A.; Van De Mark, M.R. Thermodynamic Characterization of Free and Surface Water of Colloidal Unimolecular Polymer (CUP) Particles Utilizing DSC. *Polymers* **2020**, *12*, 1417.

13. Chen, M.; Riddles, C.; Van De Mark, M. Gel point behavior of colloidal unimolecular polymer (CUP) particles. *Colloid Polym. Sci.* **2013**, *291,* 2893–2901.

14. Geng, P.; Zore, A.; Van De Mark, M.R. Investigation of the Evaporation Rate of Water from Colloidal Unimolecular Polymer (CUP) Systems by Isothermal TGA. *Polymers* **2020**, *12*, 2752.

15. Chen, M.; Riddles, C.J.; Van De Mark, M.R. Electroviscous contribution to the rheology of colloidal unimolecular polymer (CUP) particles in water. *Langmuir* **2013**, *29,* 14034–14043.

16. Zore, A.; Van De Mark, M. Surface Tension Studies in Colloidal Unimolecular Polymers. *CoatingsTech* **2021**, *18,* 24-31.

17. Dobrynin, A.V.; Rubinstein, M. Theory of polyelectrolytes in solutions and at surfaces. *Prog. Polym. Sci.* **2005**, *30,* 1049-1118.

18. Li, G.; Liu, J.; Pang, Y.; Wang, R.; Mao, L.; Yan, D.; Zhu, X.; Sun, J. Polymeric micelles with water-insoluble drug as hydrophobic moiety for drug delivery. *Biomacromolecules*. **2011**, *12,* 2016-2026.

19. Morishima, Y.; Nomura, S.; Ikeda, T.; Seki, M.; Kamachi, M. Characterization of unimolecular micelles of random copolymers of sodium 2-(acrylamido)-2-methylpropanesulfonate and methacrylamides bearing bulky hydrophobic substituents. *Macromolecules*, **1995**, *28*, 2874-2881.

20. Van De Mark, M.R.; Natu, A.; Gade, S.V.; Chen, M.; Hancock, C.; Riddles, C. Molecular Weight (Mn) and Functionality Effects on CUP Formation and Stability. *J. Coat. Technol. Res.* **2014**, *11*, 111–122.

21. Erickson, H. P. Size and shape of protein molecules at the nanometer level determined by sedimentation, gel filtration, and electron microscopy. *Biol. Proced. online* **2009**, *11*, 32-51.

22. Wang, P.; Shi, R.; Su, Y.; Tang, L.; Huang, X.; Zhao, J. Hydrated Sodium Ion Clusters [Na+(H2O)n (*n* = 1-6)]: An *ab initio* Study on Structures and Non-covalent Interaction. *Front. Chem.* **2019**, *7*, 624.

23. Hansen, C. M. *Hansen solubility parameters: a user's handbook*, 2nd ed.; CRC press: Boca Raton, USA, 2007.

24. Camacho, J.; Díez, E.; Díaz, I.; Ovejero, G. Hansen solubility parameter: From polyethylene and poly (vinyl acetate) homopolymers to ethylene–vinyl acetate copolymers. *Polym. Int.* **2017**, *66*, 1013-1020.

25. Pospiech, D.; Gottwald, A.; Jehnichen, D.; Friedel, P.; John, A.; Harnisch, C.; Voigt D.; Khimich G.; Bilibin, A. Y. Determination of interaction parameters of block copolymers containing aromatic polyesters from solubility parameters obtained from solution viscosities. *Colloid Polym. Sci.* **2002**, *280*, 1027-1037.

26. Venkatram, S.; Kim, C.; Chandrasekaran, A.; Ramprasad, R. Critical assessment of the Hildebrand and Hansen solubility parameters for polymers. *J. Chem. Inf. Model.* **2019**, *59*, 4188-4194.

IV. SYNTHESIS AND WATER REDUCTION OPTIMIZATION OF COLLOIDAL UNIMOLECULAR POLYMERS (CUP)

Ashish Zore, Peng Geng, and Michael R. Van De Mark

Department of Chemistry, Missouri University of Science and Technology, Rolla, MO 65409

ABSTRACT

Colloidal unimolecular polymer (CUP) particles are a new type of single chain nanoparticles made by self-folding of amphiphilic co-polymers having a well-balanced amount of hydrophobic and hydrophilic units. CUP particles have a spheroidal conformation and diameter ranging from 3-9 nm. The conformation and the stability of the CUP particles was dependent on the number charges per unit surface area of the particle or charge density (ions/nm^2). It was found having a charge density between 0.32 to 0.85 ions/nm^2 was required for formation of stable and spheroidal CUP particles. Increasing the charge density above 0.85 ions/nm^2, resulted in a non-spheroidal conformation (such as dumbbell, pearl necklace, etc.) whereas charge density below 0.32 ions/nm^2 resulted in aggregation and poor stability. Using the charge density range, a set of rules were developed for designing the polymer, for making CUP, using any type and size of hydrophobic monomer and carboxylate based hydrophilic monomer. The water reduction process was optimized by defining the maximum initial concentration that can be used for achieving unimolecular collapse.

Keywords: Colloidal Unimolecular Polymer (CUP), single chain polymer nanoparticle, charge density, spheroidal conformation, optimization.

1. INTRODUCTION

Recently, research in single chain nanoparticles (SCNPs) has received a lot of attention due to its potential for applications in drug delivery, MRI, fluorescence imaging, etc [1-3]. These particles made from a single polymer chain, either through self-crosslinking or self-folding, are of a true nanoscale size, below 10 nm. Colloidal unimolecular polymer, CUP, is one such single chain polymer nanoparticle made by a process of self-folding or self-assembly of the polymer chain to form a particle. The self-assembly [4] of the polymer chain can be explained using Flory-Huggin's theory where a polymer chain in a good solvent collapse due to the addition of a poor solvent. For uncharged polymers, the theory describes a theta condition [5], theta solvent or theta temperature, where the polymer behaves as an ideal chain and the polymer-polymer interactions are balanced by polymer solvent interaction. At the theta condition, the radius of gyration Rg is equal to a random walk configuration. When the polymer is above the theta condition, i.e. in good solvent, it swells whereas below the theta condition, i.e. in a poor solvent, it collapses. This behavior in polyelectrolytes was also observed by Morishima [6] where a random copolymer consisting of 50/50 monomer ratio of hydrophilic and hydrophobic monomer undergoes self-assembly/collapse in a poor solvent. The chains collapsed into a particle of a diameter of 5.5 nm. The self-assembly observed in Morishima's work [6] and in the formation of CUP particles [4] is analogous to that of micelle formation. Surfactants undergo micelle formation through self- assembly such that the hydrophobic tails are in the interior and the hydrophilic head groups are on outside surface of the micelle.

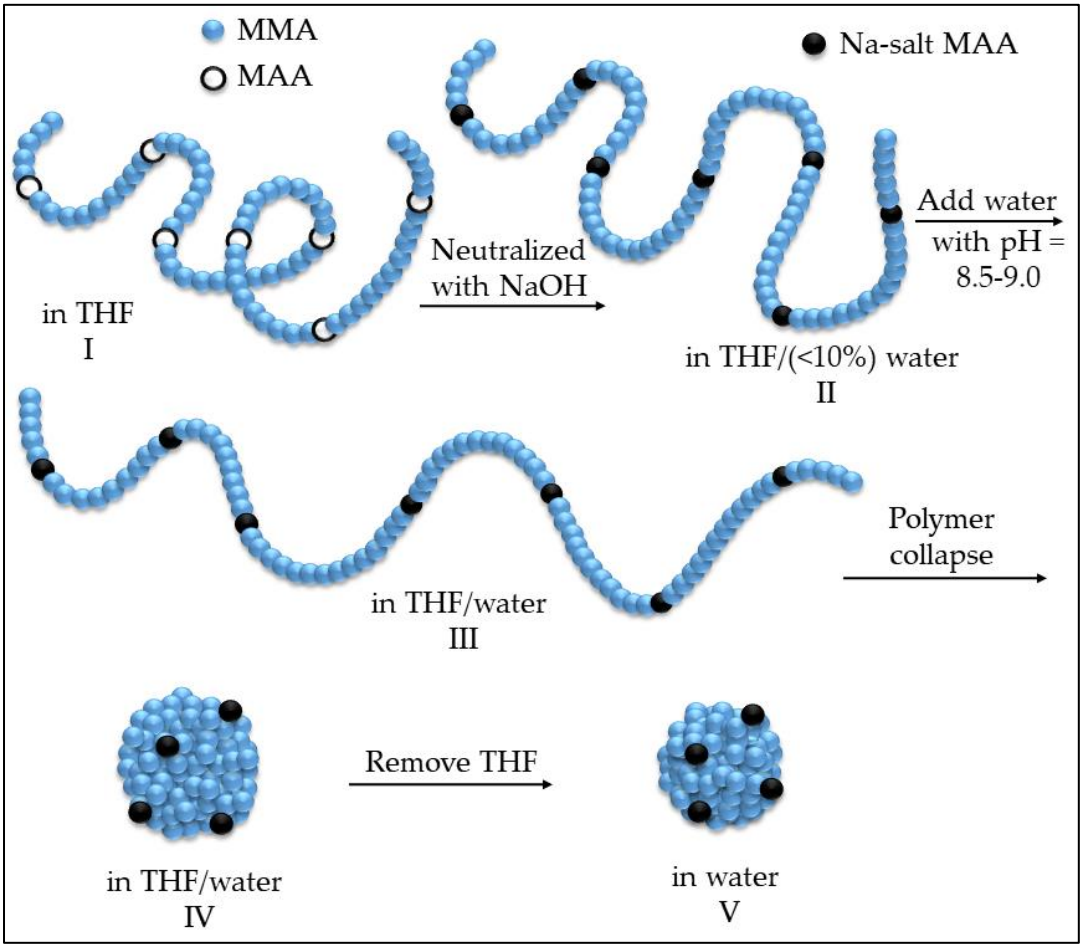

Figure 1. Schematics of the water reduction process for CUP formation.

Colloidal unimolecular polymers or CUPs particles are made from a random or statistical copolymer having both hydrophobic as well hydrophilic monomers through a process known as water reduction (Figure 1). Stage I show a random copolymer consisting of methyl methacrylate as the hydrophobic monomers, shown as a green line, and methacrylic acid as an ionizable carboxylic functional hydrophilic monomer, shown as a red circle. At this stage, the carboxylic acid is not ionized, and the polymer chain exists in a random coil configuration in the good solvent, tetrahydrofuran (THF). At stage II, a base such as sodium hydroxide in water is added slowly to the polymer solution to

neutralize all the carboxylic acids and form carboxylate salts. A slight excess of base solution is added to raise the pH to 8.5. The polymer chains have a very weak charge repulsion between the ionized groups due to the low dielectric constant of THF. The carboxylate anion and the sodium counterion exist as a tight or intimate ion pair. However, there is a small rise in viscosity caused by inter-chain and intra-chain salt association formed by the polymer chains via the sodium-carboxylate group as shown in Figure 2. At stage III, pH adjusted water (pH = 8.5) is slowly added to the polymer solution which increases the repulsion between the charges (i.e. carboxylate ions). The polymer starts extending into a rod-like conformation thereby increasing the viscosity of the solution. The increased charge repulsion is because the dielectric of the solvent is raised by the addition of water. As more water is added, the charge repulsion and consequently the viscosity increases steadily until the polymer collapses as shown in Stage IV. This polymer collapse is driven by polymer-polymer interaction becoming greater than polymer-solvent interaction due to the addition of a poor solvent, water. Similar to the process of micelle formation, the polymer chain collapsing into a CUP particle is also entropically favored by release of water. After the collapse, the low boiling THF is stripped off from the solution to obtain a pure, VOC-free CUP solution. The polymer collapses such that all the charged groups are distributed on the surface of the particle and the hydrophobic group forms the interior. The charges distribute evenly on the surface to minimize or prevent charge repulsion between them which creates a spheroidal shape in the process. The charges provide stability by electrostatic repulsion and prevent aggregation. Once formed, CUPs are thermodynamically stable in water as long as the pH is maintained basic. CUPs made using a non-volatile base for

neutralization like sodium hydroxide or potassium hydroxide are stable even after drying the CUP solution to a powder. The dry powder can be easily dissolved back into water to re-form the CUP solution provided the glass transition temperature, T_g, is above the ambient temperature. Other hydrophilic groups like sulfonates [7] or quaternary ammonium salts [8] can also be used instead of carboxylates.

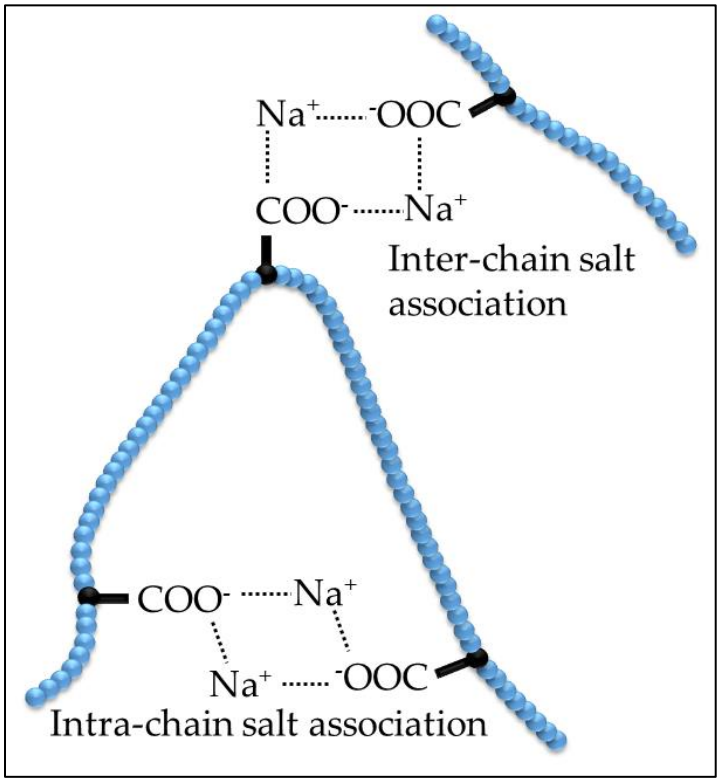

Figure 2. Inter and intra-chain salt associations in polymer at stage II.

The self–assembly or collapse observed in CUP formation also occurs in water-borne urethanes (PUDs) and other water-reducible systems. Water reducible resins are dissolved in a water-miscible solvent like acetone followed by addition of water. Further, removal of acetone from the mixture results in collapse of polymer chains into particles

with diameter of approximately 25 nm [9]. Unlike CUPs, the polymer chain collapse is non-unimolecular which results in larger particle diameters. CUPs have most of its charges on the surface and is, therefore, an ideal candidate to study the charge effects on properties like surface water [10, 11], evaporation rate [12], electroviscous effect [11], etc. Unlike latex, CUPs are free of surfactants and additives and are zero VOC, making them an ideal model for fundamental scientific studies. CUPs are inexpensive and easy to synthesize and can be used as resins in coatings [13, 14], an additive for freeze-thaw stability [15] or as a catalyst [7].

Designing a CUPs particle to meet one's requirements is extremely easy due to the flexibility and variability it offers in terms of size and charge density, number of charges per unit area on the surface, as well as the type of hydrophobic and hydrophilic monomers. Since each polymer chain collapses into a single particle, the size can be easily controlled by manipulating the molecular weight of the polymer [16. The size distribution of the particles can be made broad or narrow by using free radical polymerization or controlled/living free-radical polymerization like ATRP, RAFT, etc. Since all the charges end up on the surface, it is easy to design a CUP particle of a known charge density by varying the ratio of hydrophobic and hydrophilic monomer or by varying the size or both. The choice of hydrophobic monomers to make CUPs is large and is only limited by the reactivity ratios since a random copolymer is necessary or at least having charges distributed on the chain. The hydrophilic groups can be positively or negatively charged. CUPS makes an ideal model for understanding proteins and micelles which are limited by size, functionality, shape, availability, etc. Like proteins, CUPs are surrounded by layer of bound water which is non-freezable [17-21] at 0° C like bulk

water. Properties of bound water like the thickness of the water layer, density, specific heat capacity have been extensively studied, using differential scanning calorimetry, densitometry, and rheology, for CUPs of different size, charge density, functionality, etc. [8,10].

The polymers used for CUP synthesis are charged polymers (polyelectrolytes) which unlike the uncharged polymers as discussed in Flory-Huggins's theory, can form more complex conformations in solution [22]. These conformations depend on the charge density of the polyelectrolyte. Studies have shown that anionic or cationic homopolymers undergo conformational changes from a coil to globule transition when there was a change in the solvent dielectric [22]. Changes in pH can also trigger a change from coil to expanded chain conformation as observed by de Melo [23]. Kirwan was able to observe the extended coil and pearl necklace conformation of poly(vinylamine) using atomic force microscopy [24]. However, smaller conformational changes like elongated blob or a dumbbell shape are difficult to observe. Poly(vinylamine) was transitioned from extended chain to pearl necklace and then to a globule by change in pH. Changing the pH of a poly(vinylamine) introduces ionized groups in the polymer and affects the charge density. Proteins also show conformational changes due to change in pH where the shape of the protein molecule depends on the sequence of the amino acids but when the pH is shifted unfolding or denaturing of the proteins can occur [25].

The name 'Colloidal Unimolecular Polymer or CUPs', in the present work and previous work, is used to define a spheroidal conformation of the polyelectrolyte in an aqueous solution. For a polyelectrolyte to form a CUP i.e., spheroidal conformation, the balance between the hydrophobic and hydrophilic group is very critical. If there are not

enough charges, it can result in precipitation or aggregation of the chains due to poor stability from electrostatic repulsion. Too many charges can cause a conformational change from a sphere to a dumbbell or pearl necklace or extended coil. In order to define the limits or range of charges on the chain that can form CUP, a parameter called charge density or the number of charges per unit area on the surface of the particle is used.

This study describes the key aspects of CUP polymer synthesis and CUP particle formation. The design of the polymer structure was simplified by defining the limits of charge density for sphere conformation for a carboxylate-based hydrophilic group and any type and size of hydrophobic group. The charge density limits defined in this study may be different for different hydrophilic groups like sulfonates, QUATs, etc. However, the type of hydrophobic group does not affect the limits of the CUP formation. A charge density range for MMA-MAA copolymer will be the same as BMA-MAA or any other copolymer. The water reduction process for making the CUP particles is simplified by defining the dissolution time and initial concentration of polymer in THF required for unimolecular collapse.

2. MATERIALS AND METHODS

2.1. MATERIALS AND SYNTHESIS

The method used for synthesis of polymers 1-13 followed by its reduction into CUP particles are reported elsewhere [10]. The methodology and procedure for characterization of polymer 1-13 (molecular weight, acid number and dry polymer density) and particle size measurement (DLS) of the corresponding CUP particles are

also reported in our previous work [12]. The molar quantities of monomers - methyl methacrylate (MMA), butyl methacrylate (BMA), ethyl methacrylate (EMA), and methacrylic acid (MAA), initiator (AIBN) and chain transfer agent (1-dodecanethiol) used for synthesis of polymers 7-13 made for this study are mentioned in Table 1. BMA and EMA were purified by passing through a basic alumina column. EMA was further purified by distilling at atmospheric pressure and BMA was vacuum distilled. The initiator (AIBN) and chain transfer (1-dodecanethiol) were purchased from Sigma Aldrich.

Table 1. Molar quantities of monomers, initiator (AIBN) and chain transfer agent (1-dodecanethiol) used for synthesis of polymer 7,8, 10-13.

Polymer	**MMA (mol)**		**MAA (mol)**	**AIBN (mol)**	**1-Dodecanethiol (mol)**	**THF (mol)**
7	0.953		0.053	7.04 × 10-4	1.60 × 10-3	2.77
8	0.852		0.170	7.16 × 10-4	1.60 × 10-3	2.77
	EMA (mol)	**BMA (mol)**	**MAA (mol)**			
10	0.330	0.413	0.040	5.49 × 10-4	1.28 × 10-3	2.77
11	0.279	0.446	0.056	5.46 × 10-4	1.27 × 10-3	2.77
12	0.330	0.413	0.040	5.49 × 10-4	1.28 × 10-3	2.77
13	0.330	0.413	0.040	5.49 × 10-4	1.28 × 10-3	2.77

2.2. DSC MEASUREMENTS

The heat of fusion and melting point depression was measured using a differential scanning calorimeter from TA instruments Q2000. Tzero hermetic pan from DSC consumables Inc. was loaded with 30 mg of sample and sealed properly. The temperature was dropped to 233.15 K and maintained at isothermal for 10 mins. The sample was then heated to 313.15 K at a rate of 3 K/min. The weight of the sample was measured before and after each run to ensure that no weight was lost during the measurement due to pan leaks. The results were considered valid if the mass difference was smaller than 0.001 mg.

2.3. ABSOLUTE AND SPECIFIC VISCOSITY MEASUREMENTS

The absolute viscosity of the CUP solution was measured using an Ubbelohde capillary viscometer. The measurements were done in a constant temperature water bath at 25.0 ± 0.1 °C. The solution was equilibrated for 20 min before making measurements. Elution time was measured using a stopwatch with 0.01 s precision. The absolute viscosity (cPs) was calculated using equation 1.

$$\eta = t \times \rho_s \times k \tag{1}$$

Where t, ρ_s and k are the elution time in secs, density of the solution in g/ml and the constant for the Ubbelohde capillary viscometer in mm^2/s^2 respectively.

The specific viscosity of the CUP polymer 1-7,11 and 12 in 50/50 %v/v of water/THF was measured using an Ubbelohde capillary viscometer. The measurements were done in a constant temperature water bath at 25.0 ± 0.1 °C. The solution was

equilibrated for 20 min before making measurements. Elution time was measured using a stopwatch with 0.01 s precision. The specific viscosity was calculated using equation 2.

$$\eta_{sp} = \frac{t \times \rho_s}{t_0 \times \rho_{solv}} - 1 \quad (2)$$

Where t and t_0 are the elution time in secs for polymer solution and solvent and ρ_s and ρ_{solv} are the density of the solution and solvent in g/ml. The densities were measured using a pycnometer at 25.0 ± 0.1 °C.

3. RESULTS AND DISCUSSION

3.1. POLYMER SYNTHESIS AND CHARACTERISATION

Polymers 1-3 were made with the same monomer ratio but increasing molecular weights to illustrate effects of molecular weight on CUP formation. Polymers 2, 4 & 5 have the same charge density whereas polymers 2, 6, 7 and 8 have similar molecular weights but different charge densities. Polymer 7 has the lowest charge density and polymer 8 has the highest charge density. All the polymers mentioned below covers the workable range of charge density values. Polymers 10-13 were made using a different hydrophobic monomer (BMA and EMA) other than MMA to verify the charge density limits for CUP formation. Table 2 shows the acid number, density and molecular weight of the copolymers used for this study.

Table 2. Acid number, densities, and molecular weight of the copolymers.

Sample ID	**M_W (g/mol)** [b]	**Monomer ratio (MMA: MAA)**	**AN meas. (mg KOH/g)** [c]	**Density dry, ρ_p (g/ml)**
Polymer 1 [a]	28.9K	9:1	56.8	1.2246±0.0018
Polymer 2 [a]	59.8K	9:1	57.0	1.2311±0.0014
Polymer 3 [a]	122.5K	9:1	56.9	1.2342±0.0018
Polymer 4 [a]	25.4K	6.8:1	73.2	1.2243±0.0018
Polymer 5 [a]	73.5K	9.8:1	52.6	1.2320±0.0018
Polymer 6 [a]	49.7K	14:1	37.7	1.2307±0.0016
Polymer 7	45.4K	18:1	29.1	1.2390±0.0019
Polymer 8	50.1K	5:1	95.8	1.2300±0.0012
Polymer 9	22.7K	19:1	28.2	1.2240±0.0018
		(EMA:BMA:MAA)		
Polymer 10	50.0K	8:10:1	23.2	1.2343±0.0012
Polymer 11	51.1K	5:8:1	31.5	1.2371±0.0021
Polymer 12	47.1K	1:3.6:1	78.8	1.2353±0.0017
Polymer 13	48.3K	0.5:3:1	98.5	1.2313±0.0020

a) Data were taken from Ref [10].
b) Absolute number average molecular weight from GPC.
c) A.N. - Acid Number was measured using ASTM D974.

3.2. PARTICLE SIZE ANALYSIS

Table 3 shows the measured particle size for the copolymers and the calculated particle size from molecular weight. The diameter of the CUP particles was calculated from its molecular weight using equation 3

$$d = \sqrt[3]{\frac{6M_w}{\pi N_A \rho_p}} \quad (3)$$

Where d is the diameter of the particle, M_W is the number average molecular weight of the CUPs, N_A is the Avogadro's number and ρ_p is the density of the dry polymer. As expected, the diameter of the CUP particle increases with an increase in molecular weight. These results are consistent with the size dependence of globular proteins on their molecular weight and our previous work [16, 26]. The distribution of the molecular weight of the polymer gives a distribution to the particle size of the CUPs. For a unimolecular collapse into a sphere, the measured size from DLS should be close to that calculated from the molecular weight as shown in Table 3. It is obvious that Polymers 8, 9, 10 and 13 have deviation from this and will be discussed later.

3.3. CHARGE DENSITY OF THE CUP PARTICLE

Charge density, ρ_v, i.e., n umber of charges per unit area (nm^2) is the parameter that will be used to define the workable monomer compositional range of CUP formation since the charge density can be easily applied to any monomer system.

$$charge\ density, \rho_v = \frac{Total\ number\ of\ charges\ in\ a\ CUP\ particles\ (N)}{Surface\ area\ of\ the\ CUP\ particle\ (A)} \quad (4)$$

Since CUPs are spherical in shape the surface area is $A=4\pi r^2$. The radius r can be measured from DLS or calculated from the molecular weight using equation 3. If the

charge density exceeds that needed to form CUPs, as discussed later in this study, it may form a dumbbell. For a dumbbell shape particle, the area is $8\pi r^2$ and r is the radius of one

Table 3. Measured and calculated particle size (diameter) and charge density of the CUPs.

Sample ID	**d(DLS) [b] (nm)**	**d(GPC) [c] (nm)**	**charge density, ρ_v, (ions per nm^2)**
Polymer 1 [a]	4.22	4.25	0.52
Polymer 2 [a]	5.38	5.40	0.66
Polymer 3 [a]	6.83	6.80	0.85
Polymer 4 [a]	4.04	4.05	0.66
Polymer 5 [a]	5.76	5.80	0.66
Polymer 6 [a]	5.06	5.08	0.42
Polymer 7	4.90	4.92	0.32
Polymer 8	5.94	5.08	1.04 [d], 0.83 [e]
Polymer 9	13.20	3.90	0.24
Polymer 10	12.00	5.10	0.25
Polymer 11	5.12	5.07	0.35
Polymer 12	5.00	4.97	0.85
Polymer 13	5.80	5.00	1.06 [d], 0.85 [e]

a) Data were taken from Ref [10].
b) Diameters are measured by dynamic light scattering (DLS) instrument.
c) Diameters are calculated from average molecular weight measured using gel permeation chromatography (GPC) using equation 1.
d) Charge density calculated assuming sphere conformation.
e) Charge density calculated assuming dumbbell conformation.

of the two spheres forming the dumbbell. The total number of charges depends on the molecular weight and size of the repeat unit. The random copolymers used for making CUPs have a composition consisting of several hydrophobic monomers (n) (e.g. MMA) to a single hydrophilic monomer (e.g. MAA) as shown in Figure 3. The number of repeat units 'z' is also equal to the total number of charges N. It should be noted that these are random copolymers, and the repeat unit is the average repeat unit of the carboxylate, z.

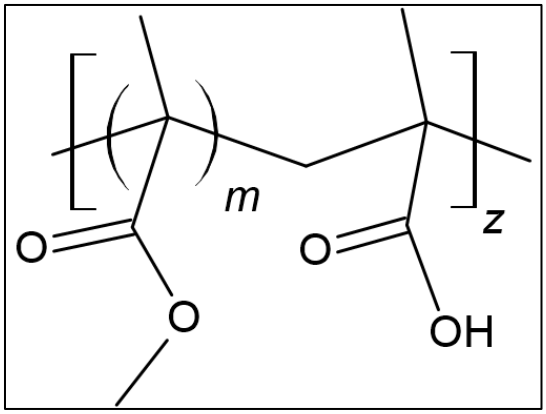

Figure 3. Structure of a random copolymer of MMA-MAA.

The number of charges can be calculated using equation 5,

$$Total\ number\ of\ charges = N = \frac{M_W}{n \times M_{H1} + m \times M_{H2} \ldots\ldots + M_{CM}} \quad (5)$$

where n, m is the number of hydrophobic monomers in a repeat unit and is also mentioned as monomer ratio (e.g. n:1 of MMA:MAA) in Table 2, M_W is the number average molecular weight of the CUP, M_{H1} is the molecular weight of hydrophobic monomer 1, M_{H2} is the molecular weight of hydrophobic monomer 2, M_{CM} is the molecular weight of hydrophilic monomer. Combining Equations 4 and 5 along with the surface area, we get the equation of charge density for a CUP particle as

$$\rho_v = \frac{M_W}{4\pi r^2(n\times M_{H1}+m\times M_{H2}\ldots\ldots+M_{CM})} \quad (6)$$

Equation 6 shows that for a given monomer combination, the charge density can be manipulated using molecular weight or radius and the monomer ratio n:m:1.

3.4. UPPER AND LOWER LIMITS OF CHARGE DENSITY FOR CUP FORMATION

Polymer 1-9 covers a range of charge density using MMA-MAA monomer combination. For polymer 1-7, the particle size measured on DLS matches the particle size calculated from average molecular weight as shown in Table 3. This indicates a unimolecular collapse and spheroidal shape of the CUP particles. Polymers 8 and 9, with higher and lower charge density respectively, show the measured particle size on DLS to be higher than the calculated size from average molecular weight. This could be due to either a change in conformation or aggregation of chains. The upper limit of charge density is when the CUP particles changes it conformation from spheroidal to a non-spheroidal conformation. The lower limit of charge density is when the particle does not have enough charges on the surface to provide stability which then leads to aggregation. Polymers 10-13 validates the extreme ranges of charge density using a different monomer combination, BMA-EMA-MAA. Polymers 10 and 13 also show the measured particle size on DLS to be higher than the calculated size from average molecular weight.

3.4.1. Model for Conformation of Polyelectrolytes. A widely accepted theoretical model based on an electrostatic bob and scaling theory [27] shows that a polyelectrolyte can form several conformations from electrostatic blob to a dumbbell shape and then to a pearl necklace of three or more pearls depending upon the number of

charges on the chain. A polymer with a few or no charges in poor solvent (like water) will collapse into a spheroid globule. As more charges are added it forms an elongated electrostatic blob followed by a dumbbell and later into a pearl necklace. The model [28] predicts that for a polyelectrolyte of a uniform charge having a degree of polymerization N=200 and fraction of charged monomer f in a solvent having dielectric ε, the conformation should be a spherical globule at f=0.00, dumbbell shape at f=0.125 and pearl necklace with three beads at f=0.150. The CUP particles are designed to be on the lower edge of the theoretical model, to keep them spheroidal in conformation. Increasing the charge density beyond the upper limit will cause a change in conformation from spheroid to a dumbbell and so on. However, if there is insufficient charges on the surface the particles will not be stable in water and aggregation is likely.

3.4.2. Conformation of Particle Based on Particle Size Measurements. If the polymer collapses into a spherical conformation, the measured particles size should be very close to the calculated diameters. A collapse into a different conformation like dumbbell or pearl necklace should cause an increase in the diameter of the particle, due to the length of the dumbbell or necklace as depicted in Figure 4, D1>D2.

Polymers 1-7 have the measured particles size very close to the calculated diameters (see Table 3) which suggests a spherical conformation. Polymer 8, on the other hand, shows particles size larger than the calculated diameter for a spherical conformation. Assuming, that the Polymer 8 (50K) collapses into a dumbbell conformation with each blob of size 25K as shown in Figure 4, the average size can be calculated to be 6nm which is close to the measured particle size of 5.94 nm. The size measurements suggest the conformation to be an elongated blob or a dumbbell shape.

Polymer 13 also validates the chain collapse to dumbbell conformation at high charge density as demonstrated by the measured particle size of 5.80 nm being close to the calculated size of 5.93 nm assuming a dumbbell conformation.

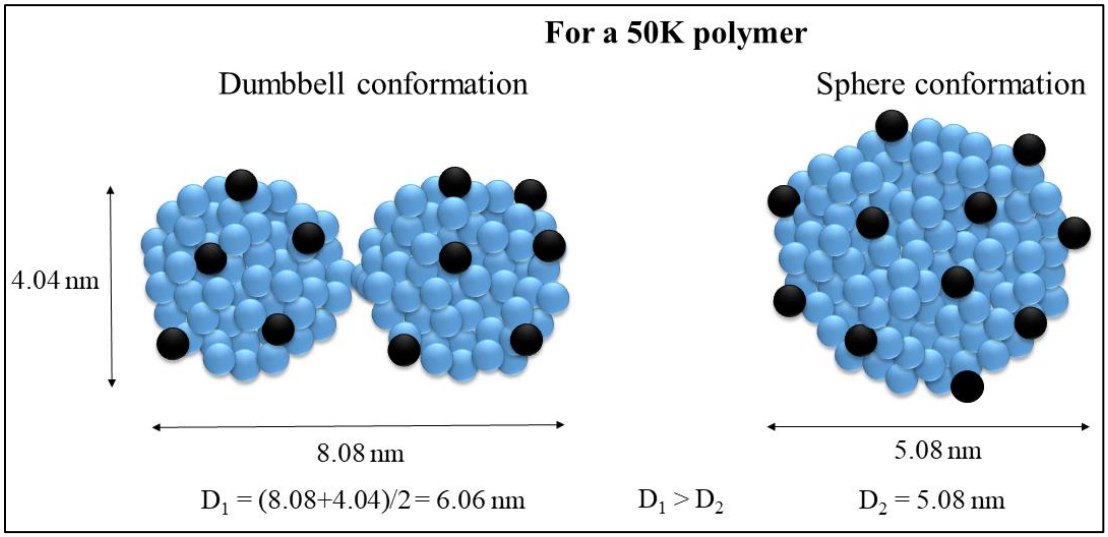

Figure 4. Size comparison of sphere and dumbbell conformation with 50K polymer.

3.4.3. Conformation of Particle Based on Viscosity Measurements. The intrinsic viscosity of a polymer solution depends on the molecular weight of the polymer and its conformation. This relation is defined by the Mark-Houwink equation 7 [29, 30] –

$$[\eta] = KM^a \quad (7)$$

where [η] is the intrinsic viscosity, M is the viscosity-average molecular weight, and K and a, are the constants for a given solute–solvent system. The constant 'a' is a function of the shape of the polymer in the given solvent. For theta solvents a=0.5, for a good solvent a=0.8, for a hard-sphere a=0 and for a rigid rod a=1.8-2.0. Since the CUP particles are spherical in shape, we can assume that the value of constant 'a' will be very

close to that of zero. Therefore, the effect of molecular weight on the viscosity is almost negligible for a hard-sphere. The other factor affecting the viscosity of the CUP particles is the electroviscous effect [11]. There are three different types of electroviscous effect: primary, secondary, and tertiary. The primary electroviscous effect is due to additional energy dissipation under shear caused by the distortion of the electrical double layer around the charged particles. The secondary electroviscous effect is the increase in viscosity due to the electrical repulsion between the electrical double layers as the particles approach each other. The tertiary electroviscous effect is due to the expansion and contraction of particles because of a change in conformation, especially in case of polyelectrolytes. In the case of CUP, the electroviscous effect can be assumed as the major cause for the increase in viscosity. Figure 5 shows the measured viscosity against the charge density at a concentration of 5% by weight. The increase in the viscosity is linear and can be attributed to the electroviscous effect. However, polymers 8 and 13 shows a deviation from the linear behavior towards higher viscosity. This increase can be due to the change of conformation from sphere to a dumbbell. A dumbbell conformation will have a higher value for the constant ‘a’ of the Mark-Houwink equation as compared to the sphere. This will result in an additional increase in viscosity along with the electroviscous effect.

3.4.4. Conformation of Particle Based on Melting Point Depression Method. Studies on the depression of melting point using DSC have shown the number and size of the acid and ester groups present on the surface of the CUP particles [10]. It is well known that adding a non-volatile solute to a liquid reduces it melting point. In the case of CUPs, each acid and ester group present on the surface contributes to the reduction in

melting point. For an ideal solution, the freezing/melting point depression can be described by using Equation 8.

$$\Delta T_F = K_F \times m \times i \quad (8)$$

where ΔT_F is the melting point depression in K, K_F is cryoscopic constant (1.853 K.kg/mol), i is van't Hoff constant, m is the molality of solute in mol/kg.

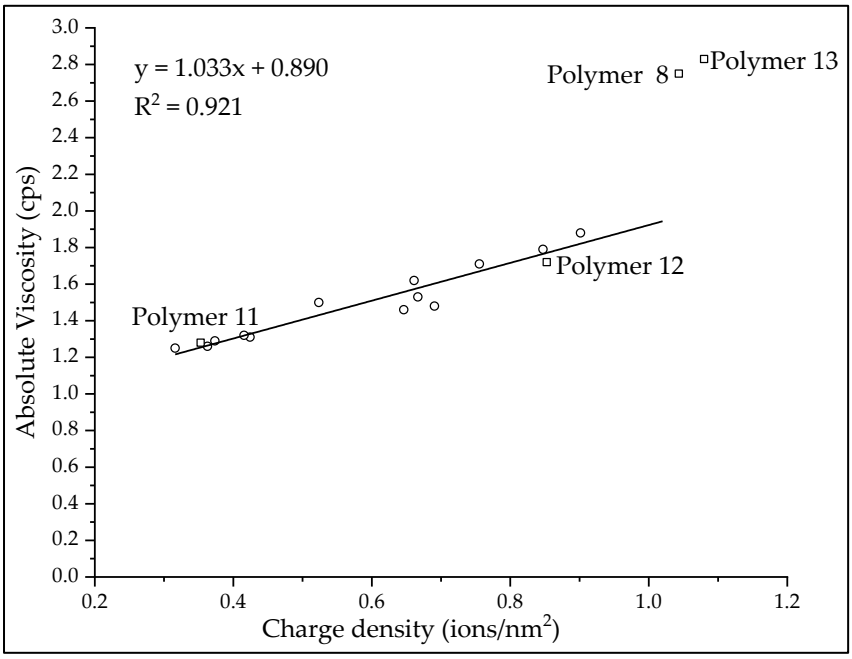

Figure 5. Viscosity of Polymers 1-8 was measured. Other viscosity values were taken from Ref [16].

The CUP solution is maintained at pH =8.5 and therefore has Na^+ ions that can contribute to the melting point depression. However, as mentioned in the DSC study, the effect of these excess sodium ions on the melting point depression was calculated to be 1.1755×10^{-5}, which is negligible. The molality of the CUP particles can be calculated from Equation 9,

$$m_{CUP} = \frac{X_{CUP}}{(1-X_{CUP})\times M_W} \quad (9)$$

where m_{CUP} is the molality of CUP particle, M_W is the molecular weight of CUP, X_{CUP} is the weight fraction of CUP. ΔT values were measured for Polymer 7, 8, 11, 12 and 13 at molality of 0.001mol/kg and the van't Hoff factor 'i' was calculated using equation 7. For each CUP particle, the number of repeat units can be calculated using Equation 10.

$$n_{rep} = \frac{M_W}{n\times M_{MMA}+M_{MAA}} \quad (10)$$

Where n_{rep} is the number of repeat units in one CUP particle, M_{MMA} is the molecular weight of MMA monomer, M_{MAA} is the molecular weight of MAA monomer, n is the molar ratio of monomer MMA/MAA.

The effective number of groups (n_{eff}) that contributed to van't Hoff factor can be expressed as Equation 11.

$$n_{eff} = \frac{i}{n_{rep}} \quad (11)$$

n_{eff} represents the size of a repeat unit on the surface and consists of an acid group and a several ester groups. The number of esters in each repeat unit on the surface can be calculated using Equation 12.

$$n_{ester} = n_{eff} - 2 \times n_c \quad (12)$$

where n_c is the number of carboxylate groups in each repeat unit, which is equal to 1, n_{ester} is the number of ester groups in each repeat unit. Each carboxylate consists of COO- and Na+ counter ion, hence the number 2 in equation 12. In the previous study on freezing point depression of CUPs, the calculated average area of the carboxylate group was 0.287 nm^2 and the average area of the ester group was 0.374 nm^2. Knowing the n_{ester}

and the area of carboxylate group (A_c) and ester group (A_{ester}) [10], the total area of CUP particle can be calculated using Equation 13.

$$A_{CUP} = n_{rep}(A_c + n_{ester} \times A_{ester}) \quad (13)$$

where A_c is the average area of one carboxylate group occupied on CUP surface, A_{ester} is the average area of one ester group occupied on CUP surface. The area calculated for Polymers 7, 8, 11, 12 and 13 using equation 13 are mentioned in Table 4. The areas for polymers 7, 11 and 12 are very close to the areas calculated assuming a spherical shape ($A=4\pi r^2$, where r is the radius of the CUP particle) which indicates the sphere conformation. However, the area for Polymer 8 and 13 was higher than the area calculated assuming a sphere shape but slightly lower than assuming a dumbbell shape. The surface area calculated from freezing point measurements provide strong evidence for the conformation of the Polymer 8 CUP particle to be close to a dumbbell shape rather than a sphere.

Table 4. Freezing point measured at m_{cup} (molality) = 0.001.

Sample ID	**dT (°C)**	**i**	**n_{rep}**	**n_{eff}**	**n_{est}**	**A_{cup}**	**Calculated area (nm^2)**
Polymer 7	0.420	226.7	23.83	9.52	7.52	73.93	75.39 [a]
Polymer 8	0.690	372.4	85.30	4.36	2.36	99.96	81.67 [a], 102.5 [b]
Polymer 11	0.467	252.0	28.48	8.85	6.85	81.27	80.71 [a]
Polymer 12	0.551	297.4	68.81	4.32	2.32	79.51	77.56 [a]
Polymer 13	0.674	363.7	83.37	4.36	2.36	97.63	77.56 [a], 97.98 [b]

a) Area calculated assuming a sphere.
b) Area calculated assuming a dumbbell.

3.4.5. Surface Water Thickness. The DSC measurement for freezing point depression also provides the heat of fusion of the freezable water which can be used to get the weight fraction of surface water (X_{SW}) using Equation 14.

$$X_{SW} = 1 - X_{CUP} - \left(\frac{\Delta H_{FW}}{\Delta H_W}\right) \quad (14)$$

where X_{CUP} is the weight fraction of CUPs, ΔH_{FW} is the heat of fusion of freezable water and ΔH_W is the heat of fusion of water, 333.5 J/g. Knowing the weight fraction of surface water, the thickness of the water layer can be calculated for a spherical particle using Equation 15 and a dumbbell-shaped particle using Equation 16.

$$\frac{4}{3}\pi(\lambda + \frac{d}{2})^3 - \frac{4}{3}\pi\left(\frac{d}{2}\right)^3 = \frac{X_{SW} \times M_W}{X_{CUP} \times N_A \times \rho_{SW}} \quad For\ sphere \quad (15)$$

Where λ is the thickness of surface water, d is the diameter of CUP particle, X_{SW} is the weight fraction of surface water, X_{CUP} is the weight fraction of CUP particle, M_W is the molecular weight of CUP, N_A is Avogadro constant, ρ_{SW} is the density of surface water.

$$\frac{8}{3}\pi(\lambda + \frac{d}{2})^3 - \frac{8}{3}\pi\left(\frac{d}{2}\right)^3 = \frac{X_{SW} \times M_W}{X_{CUP} \times N_A \times \rho_{SW}} \quad For\ dumbbell \quad (16)$$

The diameter d for a dumbbell is the size of one of the two spheres forming a dumbbell. The values of surface water thickness for polymer 7, 11, and 12 assuming a sphere and Polymer 8 and 13 assuming a dumbbell are shown in figure 6. The surface water thickness increases linearly with charge density until the charge density becomes too high and the thickness starts to plateau. Polymers 7 and 11 follow the linear behavior. However, Polymers 3, 8, 12, and 13 show a deviation from linearity for the surface water thickness.

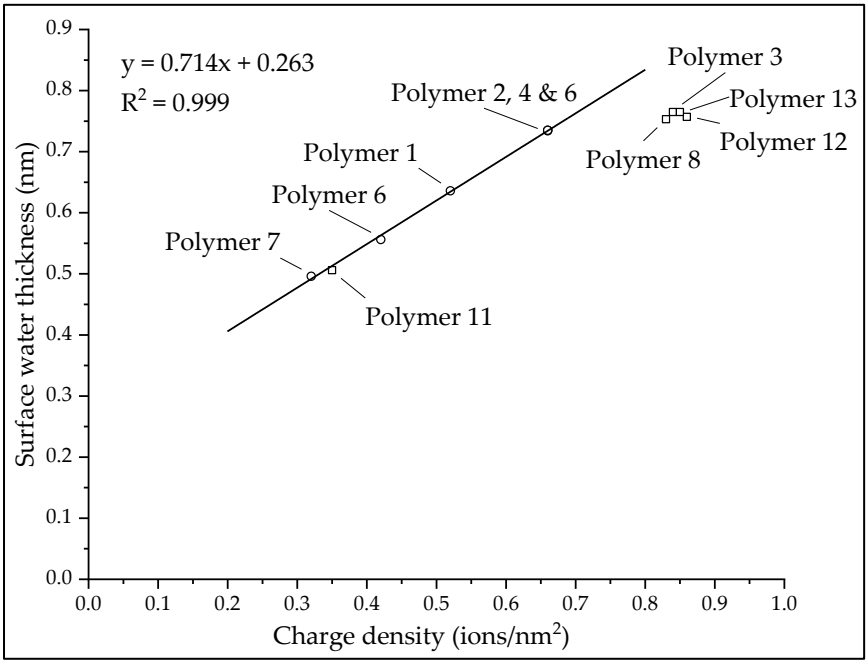

Figure 6. Surface water thickness on each CUP particle vs surface charge density of the CUP particle.

There are two possible reasons for the surface water thickness to plateau, intra-molecular counterion condensation and change in conformation, both of which reduces the charge density. The DLS measurements and freezing point depression indicates the conformation for Polymer 3 and 12 to be spherical. Since there is no significant change in conformation, the most probable cause is counterion condensation. Polymers 8 and 13, on the other hand, show a significant change in conformation along with some counterion condensation. To better understand counterion condensation, it is necessary to look at the distribution of charges and size/molecular weight of a polymer chain. Even though polymers are synthesized using a mole ratio of for e.g., 9 to 1, not all charges will distribute along the same ratio in a polymer chain. Some may be greater than 9 to 1 while some may be smaller like 7 to1 or less. The charges that are very close to each other will

undergo condensation as they are forced to conform into a sphere because their numbers are too low to cause a shape change. Similar behavior is expected for a 5 to 1 ratio where most of the charges are close enough to trigger a conformation change to a dumbbell shape while fewer charges that are closer will be forced to undergo counterion condensation. The effect of size can be understood from Polymers 1, 2 and 3 that have the same molar ratio of 9 to 1 but have different molecular weight which results in different charge densities. For the same molar ratio, higher molecular weight gives higher charge density. All the polymers used for this study are made by free radical polymerization which unlike living polymerization, gives a broader distribution of molecular weights/particle size. For e.g., Polymer 3 has average molecular weight of 122K and diameter of 6.83 but the DLS data shows a distribution of size ranging from minimum diameter of 5.86 to maximum diameter of 9.09 nm. When calculated for charge density using equation 6, the values range from 0.73 to 1.09 ions/nm2. The higher charge density can cause counterion condensation and may also possibly result in minor conformation changes from sphere to a slightly elongated blob. Polymer 3 can be assumed to be a borderline case where conformation changes might just begin to occur. For polymers that have lower charge density shows negligible counterion condensation since they have enough room to accommodate the charges that are distributed closer to each other.

3.5. LOWER LIMIT OF CHARGE DENSITY FOR CUP FORMATION

The lower limit of charge density is when the CUP particles aggregate and lead to a collapsed particle that is not unimolecular. This aggregation happens because there are

not enough charges present on the particle to provide electrostatic stabilization. Due to aggregation, the particle size becomes larger than the theoretical value and can lead to a hazy solution. As seen from Figure 7, polymer 9 CUP solution has a bluish hazy color, and its measured particle size is 13.2 nm which is larger than its calculated particle size of 3.9 nm. Similar observations were made with Polymer 11 where its measured particle size is 12.0 nm is larger than its calculated particle size of 5.1 nm. The charge density of Polymer 9 and 11 is below the lower limit that is required for stability.

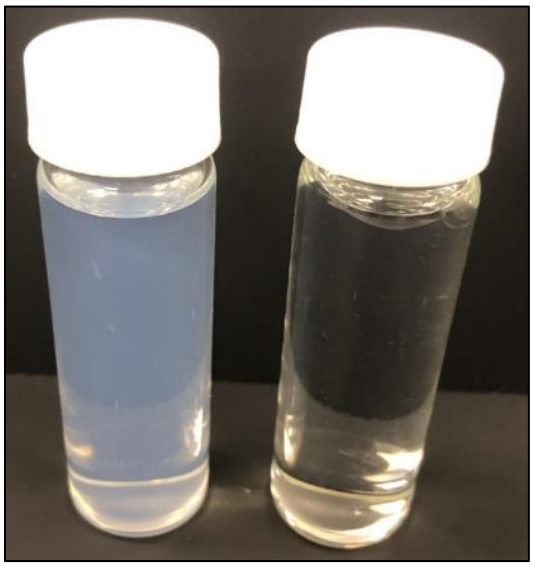

Figure 7. Polymer 9 (left) CUPs having unstable CUP formation after the water reduction process is shown in comparison to a stable CUP solution of Polymer 2 (right).

3.6. DEFINING THE CHARGE DENSITY RANGE FOR CUP FORMATION

The conformation study based on size, viscosity and freezing point measurement indicated a dumbbell conformation for polymer 8. The higher charge density (1.04, assuming a sphere) of polymer 8 result in charge-charge repulsion which prevent its collapse into a sphere. The polymer chains, instead, reduces the charge repulsion between

them by distortion into a dumbbell which also reduces the charge density (0.83, assuming a dumbbell). Of all the polymers used in this study, Polymer 3 has the highest charge density (0.85) while having a spheroidal conformation. The upper limit for charge density for CUP formation can, therefore, be assumed to be at 0.85. Polymer 3, however, does show counterion condensation on its surface. For a CUP particle without counterion condensation, the upper limit of charge density is 0.72, which can be obtained by extrapolating as shown in Figure 6.

In the lower limits, Polymer 9 (0.24) fails to form CUPs due to aggregation. Hence, Polymer 7 (0.32) with the lowest charge density to form CUPs becomes the lower limit value.

Based on the results of polymer 1-9, for a carboxylate-based polymer to form CUPs, the charge density must be between 0.32 to 0.85 ions/nm^2. For CUPs, without counterion condensation, the charge density limits are 0.32 to 0.72 ions/nm^2. This range is defined for a carboxylate-based polymer and changing to sulfonates, QUATs or any other hydrophilic group may change the workable range.

3.7. RULES FOR DESIGNING CUPS

Defining the workable range of charge density, it is now easy to design CUPs using any hydrophobic monomer and carboxylate based hydrophilic monomer by following these steps:

1. Select the hydrophobic and hydrophilic monomer and use the Fox equation to set the T_g for the required application. These may require adjustment to optimize the charge density.

2. Set the desired size of the particle or the molecular weight of the polymer as needed. Since the size and molecular weight are related by, $d = \sqrt[3]{\frac{6M_w}{\pi N_A \rho_p}}$, either one of the two can be fixed.
3. Set the required charged density within the workable range based on the application.
4. Finally, using the set size/molecular weight and charge density we can calculate the molar quantities of the monomers from equation 6.

Table 5. Examples of some CUP polymers.

MMA:MAA [4]	**Mol. Wt.**	**Diameter (nm)**	**charge density, ρ_v, (ions per nm^2)**
9:1	13.0K	3.4	0.36
9:1	15.0K	3.6	0.37
9:1	20.0K	3.9	0.42
9:1	72.0K	5.8	0.69
9:1	90.0K	6.2	0.76
EA:AAZ [15]			
9:1	11.1K	3.0	0.38
9:1	39.1K	4.5	0.60
EA:AA			
9:1	31.0K	4.4	0.52

Table 5. Examples of some CUP polymers (cont.).

EA:BMA:MAA [13]			
2.5:5.5:1	19.0K	3.7	0.38
2.5:5.5:1	50.0K	5.1	0.53
EA:BMA:2-EHMA:MAA	**Mol. Wt.**	**Diameter (nm)**	**charge density, ρ_v, (ions per nm^2)**
1.5:4:1.5:1	21.0K	3.8	0.42
1.5:4:1.5:1	51.0K	5.1	0.57
MMA:BA:TFEMA:MAA			
6.33:2.5:0.33:1	26.0K	4.6	0.36
MMA:QUAT (Quaternary) [8]			
9:1	29.0K	4.3	0.45
9:1	65.0K	5.6	0.60
9:1	93.0K	6.3	0.67
MMA:AMPS (Sulfonates) [7]			
9:1	28.0K	4.2	0.46
9:1	56.0K	5.3	0.57
9:1	80.0K	5.9	0.66

MMA: methyl methacrylate, MAA: methacrylic acid, EA: ethyl acrylate, AAZ: aziridine adduct , AA: acrylic acid, EMA: ethyl methacrylate, BMA: ethyl methacrylate, 2-EHMA: 2- ethyl hexyl methacrylate, BA: butyl acrylate, TFEMA: 2,2,2-trifluoroethyl methacrylate, QUAT: 2-(methacryloyloxy)ethyl]trimethylammonium chloride , AMPS:2-acrylamido-2-methylpropane sulfonic acid.

As seen from equation 6, multiple monomers can be used for making the polymer and to obtain CUP particles with desired properties. Table 5 shows examples of some additional polymers made in previous studies. These polymers have charge densities within the workable limits and therefore form CUPs. The table also shows a few examples of sulphonates and QUATs, although, the complete range for these systems is yet to be determined.

3.8. RULES FOR WATER REDUCTION PROCESS AND CONCENTRATION DEPENDENCE

The process of water reduction begins with dissolving the polymer in a low boiling and water-miscible solvent. The solvent chosen should have boiling point lower than that of water since after the completion of water reduction process the solvent must be removed. THF, used in this study, is water-miscible and has a boiling point of 66° C which makes THF an ideal solvent for water reduction process. In THF, the polymer chain has a random walk conformation. The concentration at which the polymer is dissolved in THF at the beginning of the water reduction process is crucial for CUP formation and is discussed later in the paper. After the solid polymer dissolved in THF, it must be stirred for at least one hour before proceeding to the next step. The anionic polymer is then neutralized with any base of choice like sodium hydroxide, potassium hydroxide, ammonia, etc. The base used here was sodium hydroxide. After neutralizing, water is added slowly at rate of 1.8 gm/min. It is crucial that water should be added in a slow gradient during reduction to avoid significant localized solvent compositional changes. The water should also be devoid of any polyvalent cations like calcium or magnesium which can bind to the carboxylates and result in aggregation of particles [14].

The addition of water increases the dielectric of the solvent mixture almost linearly [31]. As the dielectric of the mixture increases, the charges start to repel each other strongly and the chains start to elongate. When the mixture composition reaches roughly, 55% water and 45% THF, which is referred to as collapse point, the polymer chains collapse into a unimolecular colloidal sphere [32].

When chains collapse into a particle, there should not be any chain entanglement as it could cause multiple chains to collapse into a single particle thereby leading to a non-unimolecular particle. For the same polymer, the entanglement of the chains depends on the concentration where the entanglement occurs when the concentration is high. The concentration at which the entanglement begins depends on factors like molecular weight of the polymer and charge-charge separation on the chain. The higher the molecular weight of the polymer, the larger is the size or radius of gyration of the chain, the lower is the concentration at which entanglement begins. Shorter charge-charge separation on the polymer chain leads to a stronger repulsion between them and more chain elongation. This causes the size or the radius of gyration to be larger compared to a polymer chain of same molecular weight with longer charge-charge separation. For a polymer with same molecular weight, shorter charge-charge separation on the chain should show entanglement at lower concentration as compared to longer charge-charge separation.

The entanglement concentration for a regular polymer as well as polyelectrolytes can be determined by measuring the specific viscosity at increasing concentration [33-36]. Studies done with sodium poly (2-acrylamido-2-methylpropane sulfonate and sodium poly (styrene sulfonate) in water show the entanglement concentration determined by measuring the specific viscosity (η_{sp}). In a previous publication [32] on

collapse point, the composition of water and THF mixture, at which the CUP polymer collapses from an open chain to particle, was determined by viscosity measurement. The study showed that the collapse composition ranged from a lowest value of 53.8/46.2 %v/v of water/THF for polymer 11 with charge density - 0.35 to the highest value of 59.3/40.7 %v/v of water/THF for polymer (see ref [32]) with charge density - 0.80. Based on this range we can assume that Polymers 1-7,11 and 12 reaches closer to its maximum extended open-chain conformation at about 50/50 %v/v of water/THF. The solvent composition of 50/50 %v/v of water/THF was used to study the CUP in its open-chain conformation just prior to its collapse. For a proper unimolecular collapse of the CUP polymer, the concentration of the chains should be such that there is no entanglement at the collapse composition. The entanglement concentration of a CUP polymer prior to the collapse can be determined by measuring the specific viscosity of the CUP polymer in a 50/50 %v/v of water/THF mixture.

Figure 8 show the plot of $\ln(\eta_{sp})$ against the ln(c) in % weight for polymer 1-7,11 and 12 at 50/50 %v/v of water/THF. The concentration (c_e) where the slope changes, as shown by the intersection of the two linear plots in figure 9, is the on-set of chain entanglement. From the entanglement concentration (c_e) at 50/50 %v/v of water/THF, the initial concentration of the CUP polymer can be calculated as $2*c_e$. Table 6 shows the particle size results for CUP polymers 1-7,11 and 12 when the water reduction process is performed at initial concentration above and below $2*c_e$. When the water reduction of the CUP polymer is done at concentration in THF above $2*c_e$, it shows the measured particle size to be higher than the calculated size from the molecular weight. When reduced at concentration of 1% below $2*c_e$, the measured particle size to match the calculated size

from the molecular weight. The measurement of entanglement concentration in 50/50 %v/v of water/THF simplifies the determination of the CUP polymer concentration in

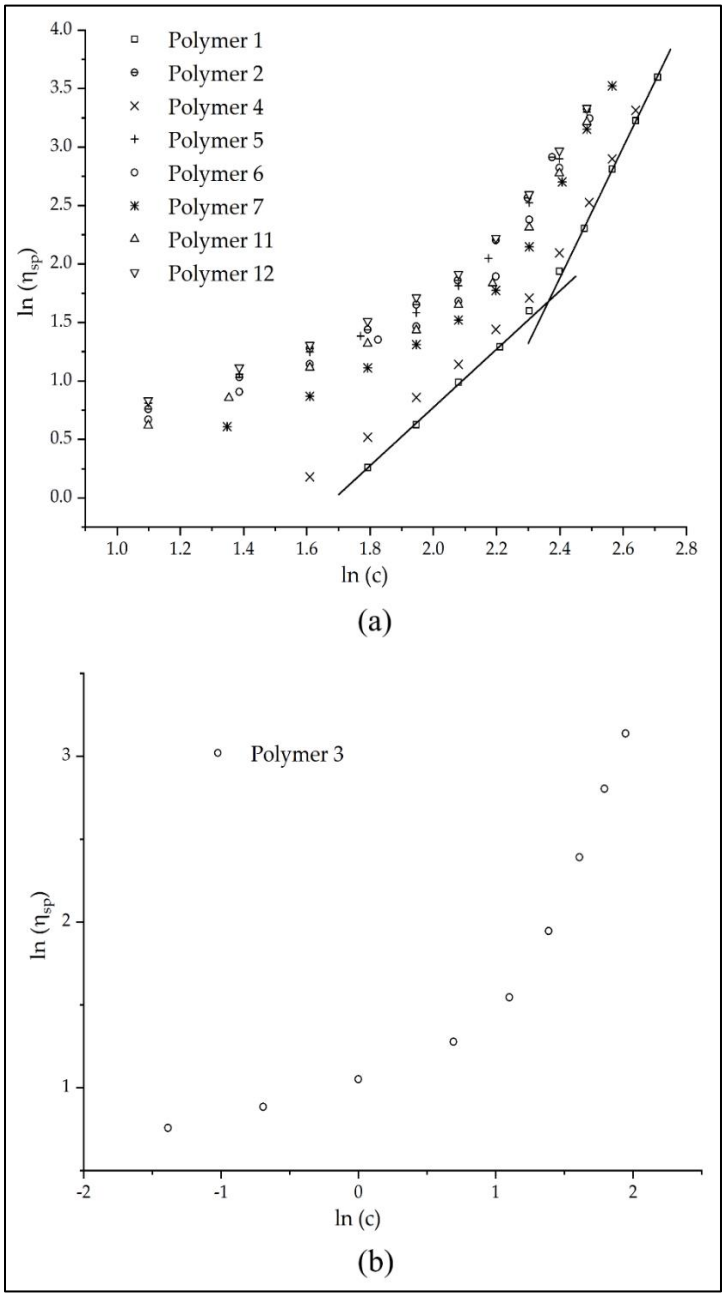

Figure 8. Viscosity behavior of polymer 1-7,11 and 12 in 50/50 %v/v of water/THF at different concentrations. The intersection of the two linear fits gives the entanglement concentration.

Table 6. Entanglement concentration (c_e), $2*c_e$ and particles size measurement for water reduction done above and below $2*c_e$.

Sample ID	**c_e (%wt)**	**$2*c_e$ (%wt)**	**Above $2*c_e$**		**Below $2*c_e$**	
			c (%wt)	**d(DLS)' (nm)**	**c (%wt)**	**d(DLS) (nm)**
Polymer 1	10.63	21.26	22.00	5.15	20.00	4.22
Polymer 2	8.00	16.00	17.00	6.12	15.00	5.38
Polymer 3	2.93	5.86	7.00	8.35	5.00	6.83
Polymer 4	9.98	19.97	21.00	4.96	19.00	4.04
Polymer 5	7.99	15.99	17.00	6.30	15.00	5.76
Polymer 6	8.54	17.08	18.00	5.73	16.00	5.06
Polymer 7	8.98	17.97	19.00	6.00	17.00	4.90
Polymer 11	8.65	17.31	18.00	6.08	16.00	5.12
Polymer 12	8.08	16.15	17.00	5.85	15.00	5.00

THF required for a proper unimolecular collapse. This greatly reduces the trial experiment required for setting the initial concentration for any given polymer and eliminates guesswork. This method for setting the initial concentration should apply to polymers made using any hydrophobic and hydrophilic monomer.

4. CONCLUSIONS

The design of the co-polymer structure required for formation of CUP was optimized by defining the balance of hydrophobic and hydrophilic groups using the charge density parameter. For the formation of stable and spheroidal CUP particles the charge density must be between 0.32 to 0.85 ions/nm^2. Non-spheroidal conformation (like a dumbbell, pearl necklace, etc.) was observed at charged density higher than 0.85 ions/nm^2 and aggregation due to poor stability was observed when the charged density was than 0.32 ions/nm^2. The surface water thickness results showed the occurrence of intramolecular counter ion condensation at charge density above 0.72 ions/nm^2. The designing of the CUP polymer, using any type and size of hydrophobic monomer and carboxylate-based hydrophilic monomer, was simplified by defining a fixed set of rules. The rules greatly increase the flexibility with respect to monomer choice, size of the particles and amount surface charges which will allows CUPs to be tailor-made for desired purpose. The entanglement concentration for the CUP polymer, determined by viscosity measurements, was critical to the unimolecular collapse required for the CUP formation. The maximum possible initial concentration of polymer in THF at the beginning of the water reduction process can be set from the entanglement concentration. This optimizes the water reduction process to save time by prepare highest possible concentration of CUP solution while avoiding aggregated collapse. The optimized synthesis and water reduction process opens door for other academic and industrial researcher to customize and prepare CUP particles, as per their need, easily and precisely.

REFERENCES

1. Van De Mark, M.R.; Zore, A.; Geng, P.; Zheng, F. Colloidal Unimolecular Polymer Particles: CUP. In *Single-Chain Polymer Nanoparticles*; Pomposo, J.A., Ed.; Wiley-VCH: Weinheim, Germany, **2017**; pp.259–312..

2. Gonzalez-Burgos, M.; Latorre-Sanchez, A.; Pomposo, J. A. Advances in single chain technology. *Chem. Soc. Rev*. **2015**, *44*, 6122-6142.

3. Kröger, A. P. P.; Paulusse; J. M. Single-chain polymer nanoparticles in controlled drug delivery and targeted imaging. *J. control. release* **2018**, *286*, 326-347.

4. Riddles, C.; Zhao, W.; Hu, H.J.; Chen, M.; Van De Mark, M.R. Self-assembly of Water Insoluble Polymers into Colloidal Unimolecular Polymer (CUP) Particles of 3–9 nm. *Polymer* **2013**, *55*, 48–57.

5. Flory, P. J. Thermodynamics of dilute solutions of high polymers. *J. Chem. Phys*. **1945** *13*, 453-465.

6. Morishima, Y.; Nomura, S.; Ikeda, T.; Seki, M.; Kamachi, M. Characterization of unimolecular micelles of random copolymers of sodium 2-(acrylamido)-2-methylpropanesulfonate and methacrylamides bearing bulky hydrophobic substituents. *Macromolecules*, **1995**, *28*, 2874-2881.

7. Natu, A.; Van De Mark, M.R. Synthesis and characterization of an acid catalyst for acrylic-melamine resin systems based on colloidal unimolecular polymer (CUP) particles of MMA-AMPS. *Prog. Org. Coat.* **2015**, *81*, 35–46.

8. Natu, A.M.; Wiggins, M.; Van De Mark, M.R. Synthesis and characterization of cationic colloidal unimolecular polymer (CUP) particles. *Colloid Polym. Sci.* **2015**, *293,* 1191–1204.

9. Rosthauser, J. W.; Nachtkamp, K. (1986). Waterborne polyurethanes. *J. coat. Fabr.* **1986** *16*, 39-79.

10. Geng, P.; Zore, A.; Van De Mark, M.R. Thermodynamic Characterization of Free and Surface Water of Colloidal Unimolecular Polymer (CUP) Particles Utilizing DSC. *Polymers* **2020**, *12*, 1417.

11. Chen, M.; Riddles, C.J.; Van De Mark, M.R. Electroviscous contribution to the rheology of colloidal unimolecular polymer (CUP) particles in water. *Langmuir* **2013**, *29,* 14034–14043.

12. Geng, P.; Zore, A.; Van De Mark, M.R. Investigation of the Evaporation Rate of Water from Colloidal Unimolecular Polymer (CUP) Systems by Isothermal TGA. *Polymers* **2020**, *12*, 2752.

13. Mistry, J.K.; Van De Mark, M.R. Aziridine cure of acrylic colloidal unimolecular polymers (CUPs). *J. Coat. Technol. Res.* **2013**, *10*, 453-463.

14. Mistry, J.K.; Natu, A.M.; Van De Mark, M.R. Synthesis and application of acrylic colloidal unimolecular polymers as a melamine thermoset system. *J. Appl. Polym. Sci.* **2014**, *131*, 40916.

15. Gade, S. V. Application of Colloidal Unimolecular Polymer (CUP) particles in Coatings. Doctoral Thesis, Missouri University of Science and Technology, Rolla, 2015.

16. Van De Mark, M.R.; Natu, A.; Gade, S.V.; Chen, M.; Hancock, C.; Riddles, C. Molecular Weight (Mn) and Functionality Effects on CUP Formation and Stability. *J. Coat. Technol. Res.* **2014**, *11*, 111–122.

17. Oncley, J.L. Evidence from Physical Chemistry Regarding the Size and Shape of Protein Molecules from Ultra-centrifugation, Diffusion, Viscosity, Dielectric Dispersion, and Double Refraction of Flow. Ann. N. Y. Acad. Sci. 1941, 41, 121–150.

18. Pammenter, N.W.; Vertucci, C.W.; Berjak, P. Homeohydrous (Recalcitrant) Seeds: Dehydration, the State of Water and Viability Characteristics in Landolphiakirkii. Plant Physiol. 1991, 96, 1093–1098.

19. Yaghmur, A.; Aserin, A.; Tiunova, I.; Garti, N. Sub-zero temperature behaviour of non-ionic microemulsions in the presence of propylene glycol by DSC. J. Therm. Anal. Calorim. 2002, 69, 163–177.

20. Jahnert, S.; Vaca, C.F.; Schaumann, G.E.; Schreiber, A.; Schonhoff, M.; Findenegg, G.H. Melting and freezing of water in cylindrical silica nanopores. Phys. Chem. Chem. Phys. 2008, 10, 6039–6051.

21. Findenegg, G.H.; Jahnert, S.; Akcakayiran, D.; Schreiber, A. Freezing and Melting of Water Confined in Silica Nanopores. Chem. Phys. Chem. 2008, 9, 2651–2659.

22. Aseyev, V. O.; Tenhu, H.; Klenin, S. I. Contraction of a Polyelectrolyte upon Dilution. Light-Scattering Studies on a Polycation in Saltless Water− Acetone Mixtures. *Macromolecules*. **1998**, *31*, 7717-7722.

23. Seixas de Melo, J.; Costa, T.; Miguel, M. D. G.; Lindman, B.; Schillén, K. Time-resolved and steady-state fluorescence studies of hydrophobically modified water-soluble polymers. *J Phys. Chem. B*, **2003**, *107*, 12605-12621.

24. Kirwan, L. J.; Papastavrou, G.; Borkovec, M.; Behrens, S. H.. Imaging the coil-to-globule conformational transition of a weak polyelectrolyte by tuning the polyelectrolyte charge density. *Nano lett***. 2004**, *4*, 149-152.

25. Kulkarni, P.; Rajagopalan, K.; Yeater, D.; Getzenberg, R. H. Protein folding and the order/disorder paradox. *J. Cell. Biochem*. **2011**, *112*, 1949-1952.

26. Erickson, H. P. Size and shape of protein molecules at the nanometer level determined by sedimentation, gel filtration, and electron microscopy. *Biol. Proced. online* **2009**, *11*, 32-51.

27. Dobrynin, A.V.; Rubinstein, M. Theory of polyelectrolytes in solutions and at surfaces. *Prog. Polym. Sci.* **2005**, *30*, 1049-1118.

28. Dobrynin, A.V.; Rubinstein, M.; Obukhov, S.P. Cascade of transitions of polyelectrolytes in poor solvents. *Macromolecules* **1996**, *29*, 2974-2979.

29. Flory, P. J. Principles of polymer chemistry. Ithaca, NY: Cornell University Press, 1953, pp. 266–316.

30. Tanford, C. Physical chemistry of macromolecules. New York: John Wiley Press, 1961, pp. 390–412.

31. Critchfield, F. E.; Gibson Jr, J. A.; Hall, J. L. Dielectric constant and refractive index from 20 to 35° and density at 25° for the system tetrahydrofuran—Water. *J. Am. Chem. Soc.* **1953**, *75*, 6044-6045.

32. Zore, A.; Geng, P.; Van De Mark, M.R. Defining the Collaspe Point in Colloidal Unimolecular Polymer (CUP) Formation. (Submitted to) *Polymers*, **2022**

33. Colby, R. H. Structure, and linear viscoelasticity of flexible polymer solutions: comparison of polyelectrolyte and neutral polymer solutions. *Rheologica acta*, **2010**, *49*, 425-442.

34. Boris, D. C.; Colby, R. H. Rheology of sulfonated polystyrene solutions. *Macromolecules*, **1998**, *31*, 5746-5755.

35. Han, A.; Colby, R. H. Rheology of entangled polyelectrolyte solutions. *Macromolecules*, **2021**, *54*, 1375-1387.

36. Krause, W. E.; Bellomo, E. G.; Colby, R. H. Rheology of sodium hyaluronate under physiological conditions. *Biomacromolecules*, **2001**, *2*, 65-69.

V. SURFACE TENSION STUDIES IN COLLOIDAL UNIMOLECULAR POLYMERS

Ashish Zore and Michael R. Van De Mark

Department of Chemistry, Missouri University of Science and Technology, Rolla, MO 65409

1. INTRODUCTION

Colloidal unimolecular polymer particles, or CUPs, are true nanoscale charged particles of size less than 10 nm that are made by a simple and easy method, which allows for preparation of additive-free, zero-volatile organic content (VOC) and stable dispersions.1 These CUP particles are made from a single polymer chain containing a well-balanced number of hydrophobic and hydrophilic units (Figure 1). The polymer chain is transformed into a CUP particle because the polymer-polymer interaction exceeds polymer-solvent interaction during the addition of water to the polymer in dilute solution in a low-boiling, water-loving solvent, resulting in collapse of the chain to form a particle.

This process is similar to formation of micelles, or the water reduction process in water-reducible coatings [1]. The charged groups on the surface of the particles provide stability and prevent aggregation due to ionic repulsion. The CUP suspension is free of any additives or surfactants as it contains only charged particles, water, and counterions. Due to the process simplicity, it is easy to control the particle size, charge density on the surface, and composition of these particles [2]. CUP particles can also be a good model

material for study of protein due to similarities in their size. They can also have potential applications in the field of coatings, drug delivery, catalyst matrix, etc.

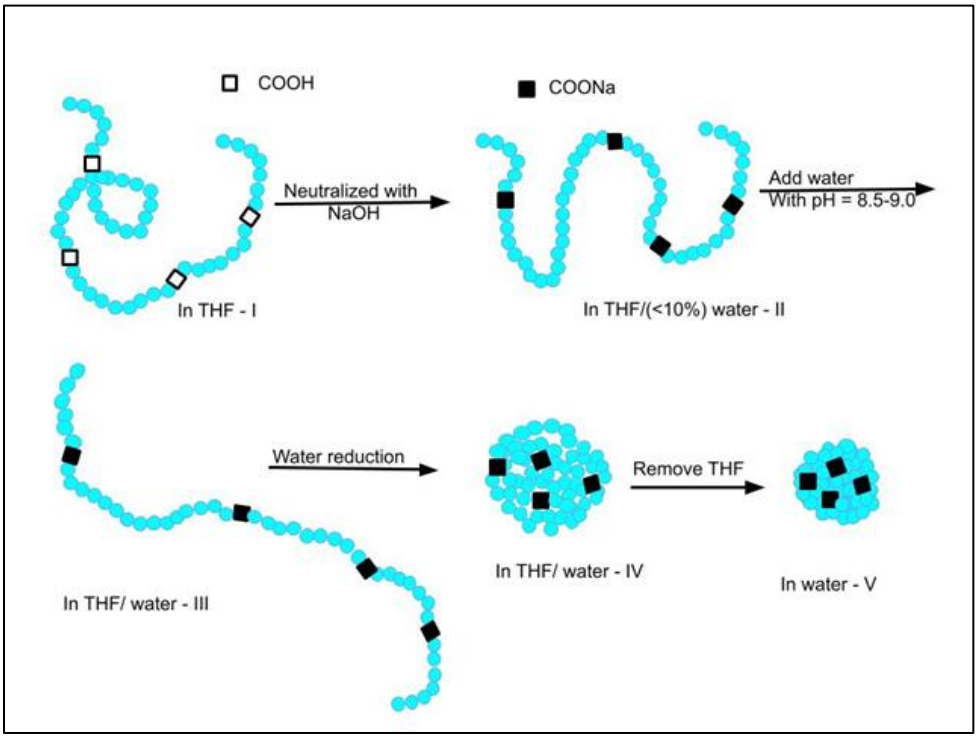

Figure 1. Formation of CUPs

CUPs have a great potential in the field of coatings as demonstrated in several publications by Van De Mark et.al. They can be used as coating resin in conjunction with latex and polyurethane dispersions (PUDs) and can be cured with an aziridine [3] or a melamine crosslinker [4]. CUPs with sulfonic acids as the charged stabilizing group can be used as a catalyst for waterborne curing such as acrylic-melamine systems.[5] CUPs with amine functional group have been synthesized and used as a crosslinker for waterborne epoxy coatings [6]. The CUP particles are hydrated with a layer of water around them, often referred to as surface or bound water, which is non-freezable.

Due to the presence of non-freezable water, CUP particles can now be used as additives for freeze-thaw stability and wet edge retention [6]. Surface tension is very important in paints, and surfactants have long been used to reduce the surface tension of liquid/solvents to improve wetting of pigments and substrate. Like surfactants, CUP particles also have an ability to alter interfacial tension, and it is important to study their interfacial behavior and compare its influence to that of other resin systems that have an excellent history in coatings, such as latex or PUDs.

The surface behavior of small-charge, stabilized particles like silica [7], polystyrene [7], and titanium dioxide [8] have been widely studied. Paunov [9] has developed a thermodynamic model and relationship for adsorption of charged colloidal particles at the air-water interface. These studies describe the adsorption behavior of the charged particles at the air-water interface, but the particle size of these suspensions are more than 30 nm in diameter. Surface tension studies of truly nanoscale (particle size less than 10 nm) charge-stabilized particles have been rarely reported. This is due to difficulties in making stable suspensions containing only nanoparticles without any other ingredients. Some nanoscale dispersions that have been successfully studied include inorganic particles like silica [7,10], bismuth telluride [11], and fullerene [12], dispersed in toluene

In this present work, the surface tension behavior of CUP particles of different sizes, charge densities and different charge stabilizing groups will be studied. The paper will look at the equilibrium as well as the dynamic surface tension behavior of the CUP suspension using a maximum bubble pressure tensiometer. The interfacial behavior of the CUPs will be compared with latex and PUDs, which are the common resins used in the

waterborne coatings. In equilibrium surface tension, there is enough time for surfactant to reach equilibrium at the air-water interface during the measurement. This is achieved by using very slow bubble rate. In dynamic measurement, the bubble rate is varied from slow to fast, and surface tension is measured for each bubble rate. This gives a surface tension vs surface age (related to bubble rate) profile with information about the migration and diffusion behavior of the surfactant, or in this case, CUP particles. The surface tension was measured using the maximum bubble pressure method, which allows both dynamic and equilibrium surface tensions to be measured without the effects of humidity, air turbulence, and contamination of carbon dioxide. Other common methods are the Du Noüy ring method, oscillating jet method and drop methods.

2. EXPERIMENTAL

2.1. SYNTHESIS OF POLYMER AND WATER REDUCTION

The carboxylate (anionic) functional polymers (Polymer 1 and 2) were synthesized and reduced using procedure mentioned in reference (1). The monomer ratio of methyl methacrylate (MMA) to methacrylic acid (MAA) was 9:1 for both the polymers. The amounts of 1-dodecanethiol used was 0.82 g and 0.33 g for 28K and 60K polymer, respectively. The sulfonate (anionic) functional polymer (Polymer 3) was synthesized and reduced using procedure mentioned in reference (5). The monomer ratio of MMA to AMPS (2-acrylamido-2-methylpropane sulfonic acid) was 9:1. The molecular weights of the polymers were controlled by using chain transfer agent n-butanethiol (0.14 g). The QUAT (cationic) functional polymer (Polymer 4) was

synthesized and reduced using the procedure mentioned in reference (13). The monomer ratio of MMA to QUAT ([2-(methacryloyloxy) ethyl] trimethylammonium chloride) was 9:1. The latex and PUDs used in this study were obtained from commercial sources. The latex was diluted to 24% solids using water before making measurements. Two PUDs were used for this study: PUD1 has no solvents or surfactant, while PUD2 contains coalescing aid (N-methylpyrrolidone, or NMP). Both the PUDs were diluted to 24% using water. The PUD2 has 12.9% NMP at resin concentration of 24% solids.

2.2. CHARACTERIZATION

The absolute molecular weights and distribution of the copolymers were measured by gel permeation chromatography (GPC) using a Viscotek model 305 from Malvern Corp. The GPC instrument was equipped with a triple detector array (refractive index detector, low- and right-angle light scattering detector, and intrinsic viscosity detector), thus yielding absolute molecular weight. The flow rate of tetrahydrofuran was 0.5 ml/min, and the injection volume was 100 µl. The acid numbers of copolymers were measured by the titration method found in ASTM D 974 that was modified by using potassium hydrogen phthalate (KHP) instead of hydrochloric acid, and phenolphthalein instead of methyl orange. The titration was performed in tetrahydrofuran as the solvent for carboxylate copolymer and in methanol for sulfonate copolymer.

The CUP suspensions were dried at 50° C under vacuum in presence of solid sodium hydroxide to absorb carbon dioxide. The clear crystal-like material was then heated at 110° C until constant weight was obtained. The density of the CUP was measured by a gas displacement pycnometer, Micrometrics AccuPycII 1340. Equilibrium

flow rate of Helium gas is 0.005 psig/min, and temperature was controlled at 25.89 ± 0.04° C. Twenty-five readings were made for each sample, and the results were reported by its average and standard deviation. The particle size of the CUPs was measured by dynamic light-scattering (DLS) technique using the Microtrac Nanotrac 250. The viscosity of the suspension was used instead of water viscosity in order to compensate for the change in diffusion coefficient due to viscosity increase caused by the charged groups on the surface of CUP particles [1]. The particle size of latex and PUDs was measured using the regular procedure (i.e., using the viscosity of water).

Sensadyne PC-500 LV was used to measure the surface tension of CUP suspensions. Suspensions were equilibrated in a constant temperature water bath at 25 ± 0.1° C. The tensiometer was calibrated with analytical reagent 100% absolute ethanol and Milli-Q ultrapure water. Flow rate of nitrogen gas was 40 ml/min and flow pressure was maintained at 25 psi. An average of three readings with less than 0.1 dyne/cm difference was reported. The surface age used for measuring the equilibrium surface tension was 3 sec. For dynamic surface tension, the maximum and minimum bubble rate were determined as the rate beyond which the surface tension did not change.

3. RESULTS AND DISCUSSION

3.1. CHARACTERIZATION OF POLYMERS

Table 1 shows the acid number, density, and molecular weight of the copolymers. There is an increase in the density of the dry CUPs as the molecular weight increases due to decrease in the weight fraction of the end groups with increasing molecular weight

[14]. The density observation was consistent with the molecular dynamic simulation result of a Leonard-Jones model with fixed bond length reported by Leporini et al [15]. The molecular weights of Polymer 1 and Polymer 2 were measured using gel permeation chromatography (GPC) technique. The molecular weights of Polymer 3 and Polymer 4 were calculated from the particle size of the CUPs using the equation relating molecular weight and particle size of globular proteins, assuming a perfect sphere shape for the CUP particles. The equation was expressed as:

$$MW = \frac{\pi d^3 \rho_p N_A}{6} \quad (1)$$

where N_A=Avogadro's number and ρ_p is the CUP density.

3.2. PARTICLE SIZE ANALYSIS

The CUP suspensions were filtered through a 0.45-μm Millipore membrane filter before performing particle size measurement. Table 2 shows the measured particle size for the copolymers, calculated particle size from molecular weight for Polymers 1 and 2, and calculated molecular weight from particle size for Polymers 3 and 4. The diameter of the CUP particles was calculated from its molecular weight using Equation 1. These results are consistent with size dependence of globular proteins on their molecular weight [16] and our previous work [2]. The distribution of molecular weight of the polymer gives the same distribution to the particle size of the CUP.

Table 1. Acid number, densities, and molecular weights of the copolymers.

SAMPLE ID	**MONOMER RATIO**	**MEASURED ACID VALUE [a]**	**ρ_p [b]**	**Mn [c]**	**Mw/ Mn**
Polymer 1 (Carboxylate functional)	MMA:MAA = 9:1	56.8	1.2250 ± 0.0018	28,900	1.83
Polymer 2 (Carboxylate functional)	MMA:MAA = 9:1	57.0	1.2310 ± 0.0014	59,800	1.73
Polymer 3 (Sulphonate functional)	MMA:AMPS = 9:1	46.9	1.2016 ± 0.0020	56,000	
Polymer 4 (QUAT functional)	MMA:QUAT = 9:1	N.A.	1.1751 ± 0.0012	55,000	

a) Acid number from ASTM D 974 , mg KOH/g ; Calculated acid number for polymer 1 and 2 is 56.9 mg KOH/g ; calculated acid number for polymer 3 is 46.8 mg KOH/g
b) Density of dry CUPs (g/cc) at 25.89 ± 0.04 °C except Polymer 1 at 24.38 ± 0.03 °C.
c) Molecular weights of Polymers 1 and 2 were measured using GPC. Molecular weights of Polymers 3 and 4 were calculated from particle size measurements (d = diameter) using Equation 1.

Table 2. Molecular weights and particle size of the CUPs.

SAMPLE ID	**Mn [a]**	**Mw/Mn**	**d(DLS) [b] (nm)**	**d(GPC) [c] (nm)**
Polymer 1	28,900	1.83	3.4	3.5
Polymer 2	59,800	1.73	4.2	4.2
Polymer 3	56,000		5.3	
Polymer 4	55,000		5.6	
Latex			140.0	
PUD1			30.0	
PUD2			24.6	

a) Molecular weights of Polymers 1 and 2 were measured using GPC. Molecular weights of Polymers 3 and 4 were calculated from particle size measurements [d(DLS) = diameter] using Equation 1.
b) Diameters are measured by dynamic light scattering (DLS) instrument.
c) Diameters calculated from average molecular weight measured using gel permeation chromatography (GPC)

3.3. EQUILIBRIUM SURFACE TENSION BEHAVIOR

Latex and PUDs often contain additives, surfactants, coalescing aid, or cosolvents, which makes it difficult to study the properties of the nanoparticle by itself. In order to purify them, complicated and lengthy procedures like dialysis need to be done. These additives can also show interfacial behavior along with the nanoparticle. Figure 2 shows the surface tension behavior of pure PUD resin (PUD1) containing no solvents or surfactants (solid circles ●) as well as PUD resin (PUD2) containing a coalescing aid NMP (N-methyl pyrrolidone) (solid triangles ▲) at different concentration prepared by diluting with DI water. Comparing the two plots, one can see the difference in the slopes of the curves, especially at lower percent solids. This is because small amount of NMP

can cause large reduction in surface tension of water. The surface tension behavior of water-NMP mixture is not linear and is more pronounced at lower weight fractions. The pure PUD resin at highest dilution of 0.5% solids has surface tension of 71 dyne/cm, which is close to that of water, 72.2 dyne/cm, and with any further dilution the surface tension will approach that of water. However, the PUD resin with NMP at 0.5% solids shows much lower surface tension (i.e., 62.2, which is far from that of water). Even at much lower concentration of 0.125% solids, the surface tension (68.5 dyne/cm) does not approach that of water. This behavior is due to the presence of NMP, which has significant effect on surface tension of water even at low concentrations. Another approach to study the behavior of a PUD resin having NMP or other cosolvents is to dilute the resin such that the concentration of NMP is the same at different concentration of PUD. This is shown in the Figure 2 (solid squares ■), where the different percent solids of PUD resin (PUD2) were prepared by diluting with 12.9% of NMP-water mixture instead of regular DI water. The PUD resin (PUD2) at 24% resin solids had 12.9% NMP in it, which was kept constant by diluting it with NMP-water mixture of same concentration. The curve (solid squares ■), therefore, shows the behavior of PUD2 at different concentrations by eliminating the effect of NMP. The surface tension values at low percent solids seems to approach that of 12.9% NMP-water mixture (62.1 dyne/cm) as expected. However, this method is not ideal because the concentration of free NMP present in the water is dependent on the percent solids of PUD present. NMP is a coalescing aid and should therefore partition inside the PUD particles. This will reduce the amount of free NMP present in water that can influence the surface tension. One

needs to know the partitioning behavior at all concentration to be able to eliminate the effect of NMP.

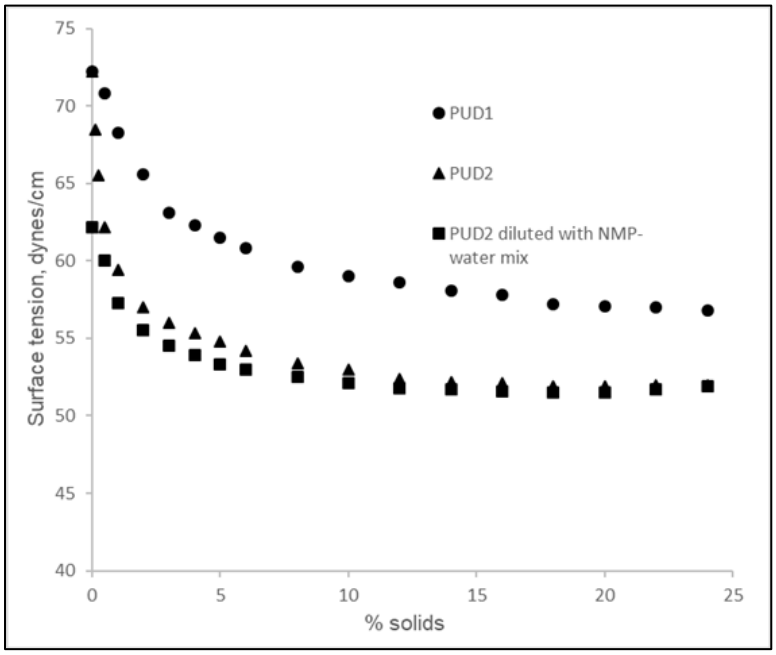

Figure 2. Surface tension vs Concentration behavior for PUD1 (solid circles ●), PUD2 (solid triangles ▲) and PUD2 (solid squares ■) diluted to different concentration using 12.9% NMP- water mixture instead of water.

Figure 3 shows the surface tension behavior of latex, pure PUD, and CUPs. The latex used has not been purified to remove the impurities, which could have influenced the surface tension behavior of the system. The latex and PUD show lower surface tension values than CUPs at all concentration, whereas PUD has higher values from 4% solids onwards and similar values at lower concentrations. In general, these differences can be related to the particle size of the three systems. The higher the particle size, greater is the reduction in surface tension. The similar values between latex and PUDs can be explained by the presence of impurities in the latex, which include residual surfactant and

additives. Without the knowledge of the type of impurities and their amounts, it is difficult to explain the behavior of latex. CUPs, on the other hand, are free of additives, and their behavior, shown in Figure 3, is entirely due to the effect of particles present at air-water interface.

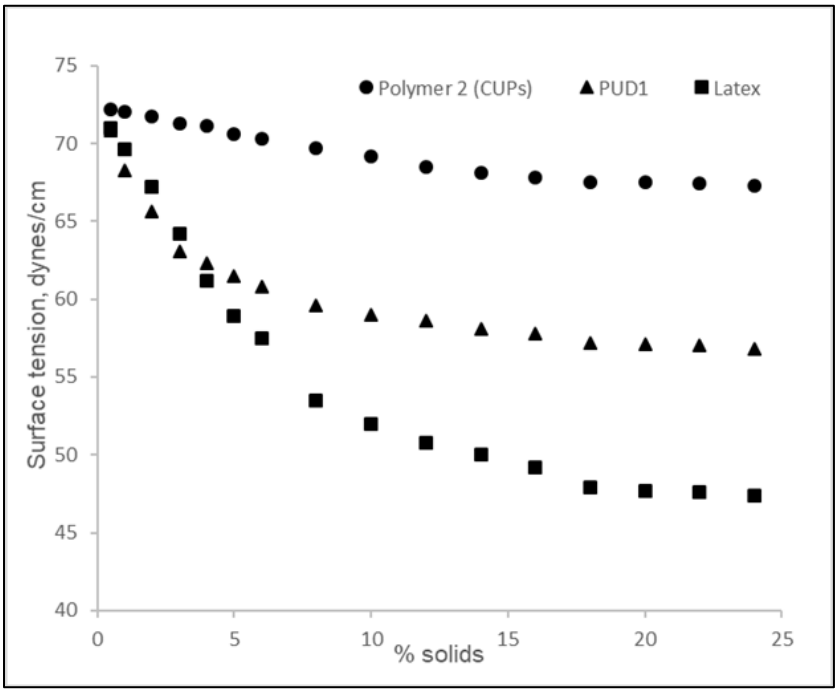

Figure 3. Surface tension vs Concentration behavior for Polymer 2 (CUPs) (solid circles ●), PUD1 (solid triangles ▲) and latex (solid squares ■).

The equilibrium surface tension of the carboxylate CUPs, sulfonate CUPs and QUAT-CUPs decreases at low concentrations linearly with increasing concentration as seen from Figure 4. This behavior of reduction in surface tension with increasing concentration is also observed for typical surfactants. Increasing the CUP concentration increases the concentration of counterions and leads to Manning condensation (i.e., condensation of counterions on the CUP surface). The phenomenon of counterion

condensation causes the reduction of effective surface charge making it lower than the bare surface charge. The reduced surface charge allows a greater number of CUP particles with a better packing at the air-water interface thereby increasing the total number of charged groups at the air-water interface since only a small fraction of the charged group undergo Manning condensation. This leads to increased electrostatic repulsion at the interface, which reduces surface energy of the system.

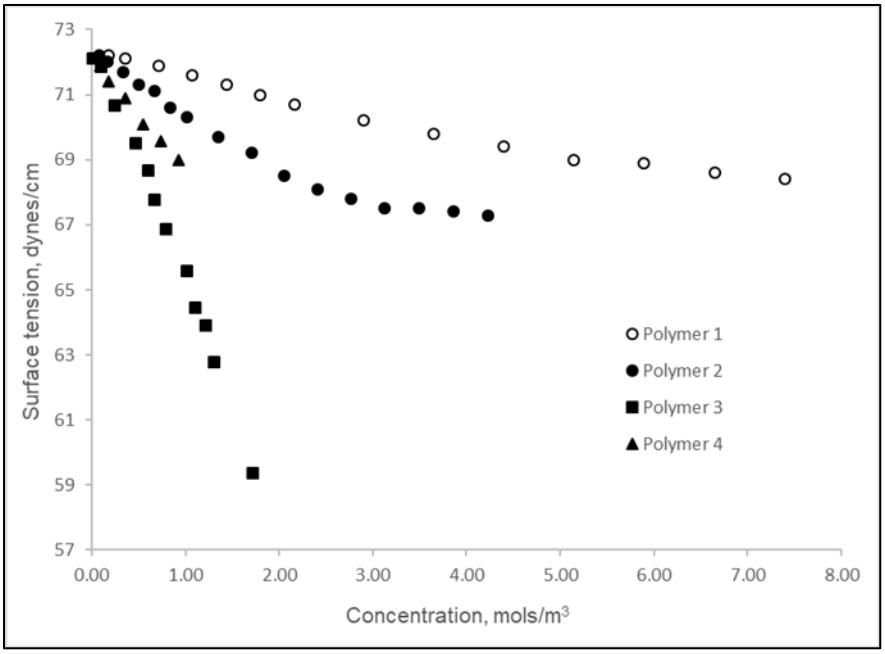

Figure 4. Equilibrium surface tension of the carboxylate CUPs (Polymer 1 and 2), sulfonate CUPs (Polymer 3) and QUAT-CUPs (Polymer 4) [13].

The equilibrium surface tension of the carboxylate CUPs decreases with increasing the molecular weight (size) from 28K (Polymer 1 – 4.2 nm) to 60K (Polymer 2 – 5.4 nm). Similar behavior has been observed by Okubo [7], where the surface activity of methyl polyethylenimine increased with increasing molecular weight. Okubo

attributed this behavior to the increase in hydrophobicity of the backbone with increasing molecular weight. In the case of CUPs, reduction of surface tension with increasing molecular weight could be due to an increase in the number of charged groups on the surface of the CUP particles with increasing molecular weight. The individual polymer chain is composed of 9:1 ratio of MMA (Mw = 100): MAA (Mw = 86.06) for the carboxylate Polymers 1 and 2. There is one carboxylate group every 986 Da of polymer. Therefore, the number of charged groups present per particle for Polymer 1 is 28 and Polymer 2 is 61. The charge density can be calculated for CUP particles made from Polymer 1 and 2 using equation 2. The charge density (in ions/nm^2) for CUP particles made from Polymer 1 and 2 is 0.52 and 0.66, respectively. The change in the surface energy caused by particles at the interface can be due to attractive (van der Waals) or repulsive (electrostatic) forces between them. When the van der Waals force increases, there is an increase in the surface energy and consequently an increase in surface tension since more work is required to distort the surface. CUP particles have charged groups, either anionic (carboxylates and sulfonates) or cationic (QUAT), that repel each other when adsorbed at the air-water interface and can possibly reduce the surface energy of the system, therefore lowering the surface tension. CUP particles with higher molecular weight have lower surface tension because of higher electrorepulsion due to the presence of more charged groups per unit area on the surface.

$$\sigma = \frac{M_{CUP}}{4\pi r^2 (n \times M_{MMA} + M_{MAA})} \quad (2)$$

σ is the charge density in ions/nm^2, r is the radius of the CUP, n is the monomer ratio (n:1 of MMA:MAA), M_{CUP} is the molecular weight of the CUP, M_{MMA} is the molecular weight of MMA, M_{MAA} is the molecular weight of MAA.

The effect of size on surface tension is also observed in latex and PUDs, as discussed earlier. But it is difficult to relate the behavior to charge density because, in the case of latex and PUDs, it is not possible to determine the number of charges present on each particle. The CUP particle was designed such that when the polymer collapses, it forms a particle from a single chain and the hydrophobic groups to fold in and form the interior of the particle, leaving the hydrophilic groups on the surface. It is therefore possible to calculate the number of charges present on the surface of the particle. The PUDs are large in size and are formed by collapse of multiple polymer chains to a particle. Many of the hydrophilic groups on the polymer chain get buried inside the particle, and the number of groups present on the surface is unknown. This makes it harder to calculate the charge density of the particle.

The sulfonate CUPs show greater reduction in surface tension as compared to carboxylate CUPs and QUAT-CUPs. This can be explained by contact angle reduction due to particles at the interface. As the surface tension is reduced, the contact angle of the adsorbed particles at the interface also decreases [17,18]. The work of Okkema and Cooper [19] have shown that the sulfonate group, being more polar and hydrophilic than the carboxylate, gave lower contact angle at the air-water interface. The QUAT CUPs shows similar reduction in surface tension as the carboxylate CUPs, which is due to similar polarities of the hydrophilic quaternary ammonium group and carboxylate group.

3.4. DYNAMIC SURFACE TENSION BEHAVIOR

Figure 5 shows the dynamic surface tension behavior of the latex, PUD1, and CUPs by plotting the surface tension against the surface age at concentration of 3%

solids. Surface age is defined as the time interval between the onset of bubble growth and the moment of maximum pressure. When there is an increase in surface age, the bubble rate is slow, which gives the CUP particles more time to reach the air (bubble)- water interface. The time to reach equilibrium is the longest for latex, which is then followed by PUDs and then by CUPs. The kinetically limited adsorption (KLA) model reported by Diamant and Andelman [20] explains such exponential relaxation of surface tension. According to Andelman et al., the kinetic relaxation time τ_k was indicative of electrostatic potential at the surface, which gave rise to electrostatic repulsion. As seen from the values in Table 3, the τ_k increases with increasing molecular weight which indicates a barrier to surface adsorption via electrostatic repulsion, thus slowing the adsorption of CUP particles to the interface.

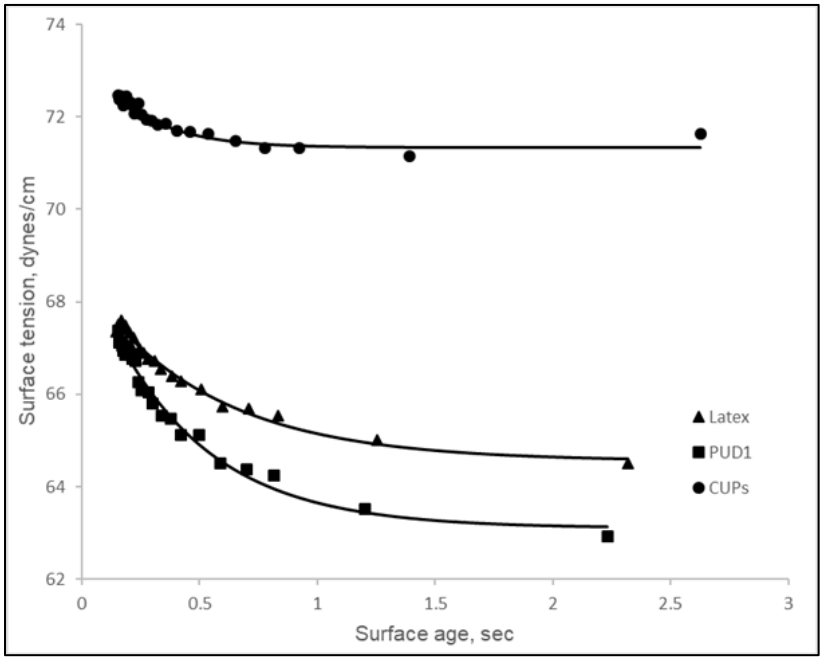

Figure 5. Dynamic surface tension behavior of the Latex, PUD1 and CUPs at different surface ages at 3% solids.

The data has an exponential fit represented by equation 3. The fitting parameters are shown in Table 3.

$$\gamma - \gamma_e = A \times exp\,(\frac{-t}{\tau_k}) \quad (3)$$

Where γ_e is the equilibrium surface tension and A and τ_k are fitting parameters.

Table 3. Fitting parameters for dynamic surface tension vs surface age at 0.5 mol/m^3 and diffusion coefficient (D_c) at 25° C.

SAMPLE ID	**γ_e**	**A**	**τ_k**	**ADJ. R^2**	**D_c (10^{-6} cm^2/s)**
Latex	64.55	3.93	0.53	0.984	0.03
PUD1	63.11	5.88	0.42	0.927	0.12
Polymer 2	71.34	2.22	0.23	0.984	0.51
Polymer 3	69.56	7.52	0.13	0.985	0.66
Polymer 4	70.27	3.32	0.21	0.95	0.45

Accurate particle size of the CUP particles can be measured using DLS method while replacing the solvent viscosity with the solution viscosity to compensate for increased viscosity due to electroviscous effect. For latex and PUD, viscosity of water is used and not viscosity of solution. The collective diffusion coefficient can be calculated from the generalized Stokes-Einstein model for the diffusion of spherical particles expressed as equation 4, which relates the collective diffusion coefficient to the radius of the particle (r) measured using DLS and the viscosity of the solution (η) at 25° C.

$$D_c = \frac{k_b \times T}{6 \times \pi \times \eta \times r} \quad (4)$$

Where k_b is the Boltzmann constant, and T is the absolute temperature of the solution. The diffusion coefficients at 25° C calculated (each at a volume fraction of 0.05) for the CUP polymers, latex, and PUD1 are mentioned in Table 3. The values of diffusion are very low for latex and PUDs due to their large size. This explains the longer time taken by them to reach equilibrium surface tension since they diffuse slowly to the air-water interface.

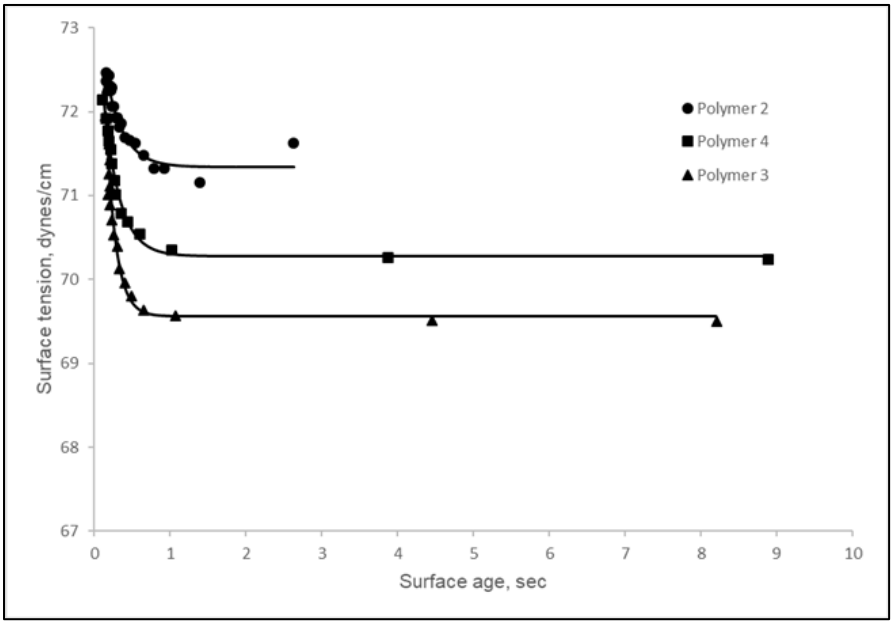

Figure 6. Dynamic surface tension behavior of the carboxylate (Polymer 2), sulfonate (Polymer 3) and QUAT (Polymer 4) CUPs at different surface ages.

Figure 6 shows the dynamic surface tension behavior of carboxylate, sulfonate, and QUAT CUPs by plotting the surface tension against the surface age at concentration of 0.5 mol/m^3. Both QUATs and carboxylates require a similar amount of time to reach equilibrium surface tension. They both reach equilibrium surface tension at surface age of 1.5 sec. This could be because they have similar diffusion coefficients and similar

polarities of their hydrophilic groups. Sulfonates show much faster relaxation time, which could be due to higher polarity of its hydrophilic group.

4. CONCLUSIONS

Colloidal unimolecular polymers with anionic (carboxylates and sulphonates) and cationic group on surface were successfully made and studied to understand their equilibrium and dynamic behavior. These CUP suspensions had a true nanoscale size (3-9 nm) and zero-VOC due to complete removal of solvent. The CUP particles have surface water associated with them as do the latex and PUDs. However, the CUPs have a higher volume fraction of surface water associated with it than PUDs and latex. In the case of CUPs, the thickness of the water layer is comparable to the radius of the CUP particles, whereas for latex and PUDs, the thickness is much smaller compared to the radius. Due the presence of this thick bound water layer, the CUP particles behave as a larger particle than their actual size. The equilibrium surface tensions of latex, PUDs and CUPs show that the surface tensions decrease as the size increases at a fixed concentration. The presence of impurities and cosolvents can affect the surface tension behavior as shown in the case of PUD resin containing NMP (PUD2). The sulfonate CUPs show lower surface tension than QUATs and carboxylates due to differences in the polarities of the hydrophilic groups. CUPs show an increase in surface tension with increase in size, which could be attributed to the increase in surface charge density. The dynamic surface tension reveals the effect of size on the time required to equilibrium surface tension. As the size increases, the diffusion becomes slower, and more time is

required to reach the equilibrium surface tension. Further study of CUPs with different molecular weight but same charge density would elucidate impact of charge density on the surface tension. The effect on surface tension as the charge density increases, and also the effect of concentration where Manning condensation (i.e., counterion condensation) begins needs to be investigated.

REFERENCES

1. Riddles, Cynthia J.; Zhao, Wei; Hu, Hua-Jung; Chen, Minghang; and M. R. Van De Mark. Self-assembly of Water Insoluble Polymers into Colloidal Unimolecular Polymer (CUP) Particles of 3–9 nm, Polymer, 2014, 55:1, 2014, 48-57.

2. Van De Mark, M. R.; Natu, A. M.; Gade, S. V.; Chen, M.; Hancock, C.; and C. J. Riddles. J. Coat. Technol. Res., 2014, 11:2, 111-122.

3. Mistry, Jigar, and M. R. Van De Mark. J. Coat. Technol. Res., 2013, 10:4, 453–463.

4. Mistry, J. K.; Natu, A. M.; and M. R. Van De Mark. Synthesis and Application of Acrylic Colloidal Unimolecular Polymers as a Melamine Thermoset System. J. Appl. Polym. Sci., 2014, 131, 40916.

5. Natu, A. M., and M. R. Van De Mark. Progress in Organic Coatings, 2015, 81, 35–46.

6. Gade, Sagar Vijay. Application of Colloidal Unimolecular Polymer (CUP) Particles in Coatings. Doctoral Dissertations. 2015. Paper 2446.

7. Okubo, T. Journal of Colloid and Interface Science, 1995, 171, 55-62.

8. Dong, L., and D. T. Johnson. Journal of Dispersion Science and Technology, 2005, 25:5, 575-583.

9. Paunov, V. N.; Binks, B. P.; and N. P. Ashby. Langmuir, 2002, 18:18, 6946-6955.

10. Ravera, F.; Santini, E.; Loglio, G.; Ferrari, M.; and L. Liggieri. J. Phys. Chem. B, 2006, 110:39, 19543-19551.

11. Vafaei, S.; Purkayastha, A.; Jain, A.; Ramanath, G.; and T. Borca-Tasciuc. Nanotechnology, 2009, 20:18, 185702.

12. Xu, Q.; Liu, X.; Frisch, H. L.; and W. E. Broderick. J. Chem. Phys. 1993, 98, 7648-7650.

13. Natu, A. M.; Wiggins, M.; and M. R. Van De Mark, Colloid Polym. Sci., 2015, 293, 1191–1204.

14. East, G. C.; Margerison, D.; and E. Pulat. Trans Faraday Soc., 1966, 62, 1301–1307.

15. Barbieri, A.; Prevosto, D.; Lucchesi, M.; and D. Leporini. J. Phys. Condens. Matter, 2004, 16:36, 6609–6618.

16. Erickson, H. P. Biol. Proced. Online, 2009, 11:1, 32–51.

17. Chaudhuri, R. G., and S. Paria. J. Colloid. Interf. Sci., 2009, 337, 555-562.

18. Bernett, M. K., and W. A. Zisman. J. Phys. Chem., 1959, 63, 1911-1916.

19. Okkema, A. Z., and S. L. Cooper. Biomaterials, 1991, 12, 668-676.

20. Diamant, H., and H. D. Andelman. J. Phys. Chem., 1996, 100:32, 13732–13742.

SECTION

2. CONCLUSIONS

This dissertation discusses the air-water interface behavior, collapse point analysis and synthesis, and water reduction optimization of the aqueous colloidal single chain polymer nanoparticles called Colloidal unimolecular polymers (CUPs).

Paper I show the CUP particle formation from an amphiphilic copolymer having a balanced amount of hydrophobic and hydrophilic units. It reviews all the previous work with CUPs related to the synthesis, and studies of properties like electroviscous effect, gel point, and surface tension. It shows the CUP formation using different hydrophilic groups like sulfonates and QUATs and analyses the properties and thickness of non-freezable (at 0 °C) surface water. CUPs have shown to be useful in the field of coating as resins and crosslinkers due to their near-zero VOC and as a freeze-thaw and wet edge retention additive for latex paint due to the presence of non-freezable (at 0 °C) surface water.

In Paper II, the air-water interfacial behavior of CUP particles was studied by measuring the equilibrium and dynamic surface tension of CUP using a maximum bubble pressure tensiometer. CUP particles with different sizes and surface charge density were measured for equilibrium and dynamic surface tension. The equilibrium surface tension showed a strong dependence on the surface charge density where a higher charge density showed a higher reduction in surface tension. This was further attributed to the charges present at the air-water and CUP interface acting like surfactant molecules thereby

causing the surface tension reduction. The dynamic surface tension was shown to be dominated by the diffusion of the particle at the air-water interface and the effect of the interfacial organizational mechanism was negligible or minimum.

In Paper III, the transformation of the polymer chain into a collapsed particle was studied using viscosity measurements. The water reduction process was tracked by continuous measurement of viscosity which allowed the rapid and precise determination of the transition of the polymer chain to a particle or the collapse point. The continuous viscosity measurement during the water reduction process was made possible using a vibration viscometer which allows for stable viscosity measurement while stirring. The collapse point study showed that increasing the hydrophobicity of the polymer chain decreases the amount of water required to trigger the chain to particle collapse. The dielectric of the solution is also critical for the formation of the particle however, the minimum required dielectric for a stable particle is reached before the collapse point.

In Paper IV, the design of the CUP polymer and the water reduction process was optimized and simplified. The design of the CUP polymer was simplified by defining the charge density range for CUP formation. Based on the observation of polymers made with a range of charge density, it was found that having the charge density (ions/nm^2) of the CUP particle between 0.32 to 0.85 provides a stable and spheroidal particle. Exceeding the charge density above 0.85 gives a non-spheroidal (dumbbell or pearl necklace conformation) and reducing charge density below 0.32 results in aggregation of particles due to poor electrostatic repulsion. This simplified the design of CUP particles using any type and size of hydrophobic monomer and carboxylate-based hydrophilic monomer. The water reduction process was optimized by determining the maximum

possible concentration while avoiding chain entanglement, of CUP polymer in THF at the beginning of the water reduction process. This makes the preparation of the CUP solution efficient, faster and saves time.

In Paper V, the surface tension of CUPs with different types of surface charges was studied and compared against large size particles like latex and PUDs. CUP particles with sulfonate have shown lower surface tension than QUATs and carboxylates which was attributed to the differences in the polarities of the hydrophilic groups. The effect of slow diffusion due to the large size of the latex and PUDs can be seen from the dynamic surface tension behavior which shows a higher relaxation time than CUP particles.

The simplification of the design and preparation of CUP should make this technology commercially attractive given the numerous applications of CUP particles.

BIBLIOGRAPHY

1. Gonzalez-Burgos, M., Latorre-Sanchez, A., & Pomposo, J. A. (2015). Advances in single chain technology. *Chemical Society Reviews*, *44*(17), 6122-6142.

2. Van De Mark, M. R., Zore, A., Geng, P., & Zheng, F. (2017). Colloidal Unimolecular Polymer Particles: CUP. *Single-Chain Polymer Nanoparticles: Synthesis, Characterization, Simulations, and Applications*, 209.

3. Aiertza, M. K., Odriozola, I., Cabañero, G., Grande, H. J., & Loinaz, I. (2012). Single-chain polymer nanoparticles. *Cellular and Molecular Life Sciences*, *69*(3), 337-346.

4. Mecerreyes, D., Lee, V., Hawker, C. J., Hedrick, J. L., Wursch, A., Volksen, W., Miller, R. D. (2001). A novel approach to functionalized nanoparticles: self-crosslinking of macromolecules in ultradilute solution. *Advanced Materials*, *13*(3), 204-208.

5. Harth, E., Horn, B. V., Lee, V. Y., Germack, D. S., Gonzales, C. P., Miller, R. D., & Hawker, C. J. (2002). A facile approach to architecturally defined nanoparticles via intramolecular chain collapse. *Journal of the American Chemical Society*, *124*(29), 8653-8660.

6. Cherian, A. E., Sun, F. C., Sheiko, S. S., & Coates, G. W. (2007). Formation of nanoparticles by intramolecular cross-linking: following the reaction progress of single polymer chains by atomic force microscopy. *Journal of the American Chemical Society*, *129*(37), 11350-11351.

7. Adkins, C. T., Muchalski, H., & Harth, E. (2009). Nanoparticles with individual site-isolated semiconducting polymers from intramolecular chain collapse processes. *Macromolecules*, *42*(15), 5786-5792.

8. Oria, L., Aguado, R., Pomposo, J. A., & Colmenero, J. (2010). A versatile “click” chemistry precursor of functional polystyrene nanoparticles. *Advanced Materials*, *22*(28), 3038-3041.

9. Radu, J. É. F., Novak, L., Hartmann, J. F., Beheshti, N., Kjøniksen, A. L., Nyström, B., & Borbély, J. (2008). Structural and dynamical characterization of poly-gamma-glutamic acid-based cross-linked nanoparticles. *Colloid and Polymer Science*, *286*(4), 365-376.

10. Beck, J. B., Killops, K. L., Kang, T., Sivanandan, K., Bayles, A., Mackay, M. E., ... & Hawker, C. J. (2009). Facile preparation of nanoparticles by intramolecular cross-linking of isocyanate functionalized copolymers. *Macromolecules*, *42*(15), 5629-5635.

11. Wang, P., Pu, H., & Jin, M. (2011). Single-chain nanoparticles with well-defined structure via intramolecular crosslinking of linear polymers with pendant benzoxazine groups. *Journal of Polymer Science Part A: Polymer Chemistry*, *49*(24), 5133-5141.

12. Zhu, B., Ma, J., Li, Z., Hou, J., Cheng, X., Qian, G., ... & Hu, A. (2011). Formation of polymeric nanoparticles via Bergman cyclization mediated intramolecular chain collapse. *Journal of Materials Chemistry*, *21*(8), 2679-2683.

13. Jiang, X., Pu, H., & Wang, P. (2011). Polymer nanoparticles via intramolecular crosslinking of sulfonyl azide functionalized polymers. *Polymer*, *52*(16), 3597-3602.

14. Sanchez-Sanchez, A., Asenjo-Sanz, I., Buruaga, L., & Pomposo, J. A. (2012). Naked and self-clickable propargylic-decorated single-chain nanoparticle precursors via redox-initiated RAFT polymerization. *Macromolecular rapid communications*, *33*(15), 1262-1267.

15. Dirlam, P. T., Kim, H. J., Arrington, K. J., Chung, W. J., Sahoo, R., Hill, L. J., ... & Pyun, J. (2013). Single chain polymer nanoparticles via sequential ATRP and oxidative polymerization. *Polymer Chemistry*, *4*(13), 3765-3773.

16. Chao, D., Jia, X., Tuten, B., Wang, C., & Berda, E. B. (2013). Controlled folding of a novel electroactive polyolefin via multiple sequential orthogonal intra-chain interactions. *Chemical Communications*, *49*(39), 4178-4180.

17. Sanchez-Sanchez, A., Akbari, S., Etxeberria, A., Arbe, A., Gasser, U., Moreno, A. J., Colmenero, J & Pomposo, J. A. (2013). “Michael” nanocarriers mimicking transient-binding disordered proteins. *ACS Macro Letters*, *2*(6), 491-495.

18. Huerta, E., Stals, P. J., Meijer, E. W., & Palmans, A. R. (2013). Consequences of folding a water-soluble polymer around an organo-catalyst. *Angewandte Chemie*, *125*(10), 2978-2982.

19. Hansell, C. F., Lu, A., Patterson, J. P., & O'Reilly, R. K. (2014). Exploiting the tetrazine–norbornene reaction for single polymer chain collapse. *Nanoscale*, *6*(8), 4102-4107.

20. Willenbacher, J., Wuest, K. N., Mueller, J. O., Kaupp, M., Wagenknecht, H. A., & Barner-Kowollik, C. (2014). Photochemical design of functional fluorescent single-chain nanoparticles. *ACS Macro Letters*, *3*(6), 574-579.

21. Perez-Baena, I., Asenjo-Sanz, I., Arbe, A., Moreno, A. J., Lo Verso, F., Colmenero, J., & Pomposo, J. A. (2014). Efficient route to compact single-chain nanoparticles: photoactivated synthesis via thiol–yne coupling reaction. *Macromolecules*, *47*(23), 8270-8280.

22. Li, G., Liu, J., Pang, Y., Wang, R., Mao, L., Yan, D., ... & Sun, J. (2011). Polymeric micelles with water-insoluble drug as hydrophobic moiety for drug delivery. *Biomacromolecules*, *12*(6), 2016-2026.

23. Terashima, T., Sugita, T., Fukae, K., & Sawamoto, M. (2014). Synthesis and single chain folding of amphiphilic random copolymers in water. *Macromolecules*, *47*(2), 589-600.

24. Morishima, Y., Nomura, S., Ikeda, T., Seki, M., & Kamachi, M. (1995). Characterization of unimolecular micelles of random copolymers of sodium 2-(acrylamido)-2-methylpropanesulfonate and methacrylamides bearing bulky hydrophobic substituents. *Macromolecules*, *28*(8), 2874-2881.

25. Riddles, C. J., Zhao, W., Hu, H. J., Chen, M., & Van De Mark, M. R. (2014). Self-assembly of water insoluble polymers into Colloidal Unimolecular Polymer (CUP) particles of 3–9 nm. *Polymer*, *55*(1), 48-57.

26. Geng, P., Zore, A., & Van De Mark, M. R. (2020). Thermodynamic characterization of free and surface water of colloidal unimolecular polymer (CUP) particles utilizing DSC. *Polymers*, *12*(6), 1417.

27. Dawib, Yousef Abobaker, "NMR T1 studies of colloidal unimolecular polymer (CUP) surface water" (2015). Doctoral Dissertations. Paper 2406.

28. Mistry, J. K., & Van De Mark, M. R. (2013). Aziridine cure of acrylic colloidal unimolecular polymers (CUPs). *Journal of Coatings Technology and Research*, *10*(4), 453-463.

29. Mistry, J. K., Natu, A. M., & Van De Mark, M. R. (2014). Synthesis and application of acrylic colloidal unimolecular polymers as a melamine thermoset system. *Journal of Applied Polymer Science*, *131*(20).

30. Gade, Sagar Vijay, "Application of colloidal unimolecular polymer (CUP) particles in coatings" (2015). Doctoral Dissertations. Paper 2446.

31. Natu, A. M., & Van De Mark, M. R. (2015). Synthesis and characterization of an acid catalyst for acrylic-melamine resin systems based on colloidal unimolecular polymer (CUP) particles of MMA-AMPS. *Progress in Organic Coatings*, *81*, 35-46.

32. Aseyev, V. O., Tenhu, H., & Klenin, S. I. (1998). Contraction of a Polyelectrolyte upon Dilution. Light-Scattering Studies on a Polycation in Saltless Water− Acetone Mixtures. *Macromolecules*, *31*(22), 7717-7722.

33. Rosthauser, J. W., & Nachtkamp, K. (1986). Waterborne polyurethanes. *Journal of coated Fabrics*, *16*(1), 39-79.

34. Okubo, T. (1995). Surface tension of structured colloidal suspensions of polystyrene and silica spheres at the air-water interface. *Journal of colloid and interface science*, *171*(1), 55-62.

35. Dong, L., & Johnson, D. T. (2005). The study of the surface tension of charge-stabilized colloidal dispersions. *Journal of dispersion science and technology*, *25*(5), 575-583.

36. Dong, L., & Johnson, D. (2003). Surface tension of charge-stabilized colloidal suspensions at the water− air interface. *Langmuir*, *19*(24), 10205-10209.

37. Zore, A., & Van De Mark, M. (2021). Surface Tension Studies in Colloidal Unimolecular Polymers. *COATINGSTECH*, *18*(2), 24-31.

VITA

Ashish Shantaram Zore was born in Mumbai, India. He received his Bachelor's degree in Surface Coating technology in May 2013 from the Institute of Chemical Technology in Mumbai, India. Ashish joined research and development in Pidilite Industries ltd. in 2013. In September 2015, He began his doctoral studies in Chemistry under the guidance of Dr. Michael R. Van De Mark at the Missouri University of Science & Technology. During the course of his Ph.D. work, Ashish has published two peer-reviewed papers, submitted one paper for publication in a peer-reviewed journal, and presented his research work at one ACS annual meeting (2021) and one American Coating Conference (April 2022). Ashish received his Doctor of Philosophy in Chemistry in July 2022.